Cape Peninsula University of Technology

THE EFFECT OF GYPSUM PHASE COMPONENTS ON THE RHEOKINETICS OF CEMENT PASTE

by

WILLY MBASHA MIGABO
M.Tech: Civil Engineering
B.Tech: Civil Engineering (Structural)

Thesis submitted in fulfilment of the requirements for the degree

Doctor of Engineering in Civil Engineering

in the Faculty of Engineering

at the Cape Peninsula University of Technology

Supervisor: Prof. Rainer Haldenwang
Co-supervisor: Dr. Nicolas Roussel & Prof. Irina Masalova

Cape Town

20 June 2018

Declaration

I, Willy Mbasha Migabo, declare that the contents of this thesis represent my own unaided work, and that the thesis has not previously been submitted for academic examination towards any qualification. Furthermore, it represents my own opinions and not necessarily those of the Cape Peninsula University of Technology.

(Signature)

Signed in Cape Town this 20th day of June 2018

Abstract

Rheological properties of most ordinary Portland cements are dictated by the hydration reactions that their different phases experience. Cement clinker has four main phases with aluminate being the most reactive. Once in contact with water, the aluminate phase reacts rapidly and generally impedes the early hydration of other cement compounds such as calcium silicates that are responsible for the strength of cement systems. Consequently, the obtained matrix is stiff without much strength. Alternatively, calcium sulphate bearing materials are added within the clinker as set regulators of the aluminate phase hydration. For this purpose, natural gypsum is moslty gound with cement clinker as a source of sufficient sulphate, thereby keeping the cement paste plastic for a certain amount of time, allowing the hydration of silicate phases that are responsible for the early and later strength.

However, the heat generated within the mill during the grinding process of clinker and gypsum causes a partial dehydration of natural gypsum into hemihydrate. The final ground cement product is thus comprised of two unexpected types of calcium sulphate bearing materials in an unpredictable proportion. Due to the difference in their solubility, the hydration of the aluminate phase can variably be altered which consequently affects the rheokinetics of the cement paste. Currently, the effect of the available amount of hemihydrate and natural gypsum in the cement sulphate phase, on both the hydration and rheology of ordinary Portland cements (OPC), are not well-understood.

An ordinary Portland cement clinker was sampled during the production process of CEM I under stable kiln operations at a local cement plant. This was ground without any form of calcium sulphate bearing material and the final product was considered as relatively pure cement clinker. The degree of natural gypsum degeneration was achieved by partially replacing fractions of hemihydrate with those of natural gypsum. Firstly, the individual effect of these calcium sulphate bearing materials on the hydration kinetics was studied by varying their concentrations from 2-7% within the cement system. Secondly, the effect of their mix proportions at an optimum calcium sulphate concentration on cement paste rheokinetics was investigated.

This research confirmed the findings of previous investigations relative to the effect of calcium sulphate on the hydration kinetic , giving new insight on the rheokinetics of cement paste with mix proportions of various calcium bearing materials. Results showed that the reaction rates of cement systems with hemihydrate were faster than those with natural gypsum and generally tended to decrease with the increase in their concentrations. Cements with hemihydrate experiencing shorter dormant durations than those with natural gypsum, likely due to the fact that

the consumption rate of calcium sulphate was higher in cement systems with hemihydrate than those with natural gypsum. Consequently, before the exhaustion of sulphate ions, cement systems with hemihydrate had higher degrees of hydration and became almost similar thereafter. More ettringite and portlandite were formed in cement systems with hemihydrate as compared to those with natural gypsum. The amount of ettringite increased with the increase in calcium sulphate concentration up to 4% and thereafter remained constant. Conversely, the amount of portlandite decreased with the increase in calcium sulphate and also remained unchanged after 4%. The strength development of the cement microstructure depended on the concentration of hemihydrate within the suspension. The rigidification of the newly formed network was affected at higher hemihydrate fractions. Rheological parameters were more pronounced when the concentration of hemihydrate exceeded 50%. Below this hemihydrate concentration, cements had almost similar flow properties as those with only natural gypsum. Large changes in yield stress values and variation in plastic viscosity values of approximately 50% were observed. The trend of mixes dynamic yield stress were similar to their corresponding strength rate developments. This rheological behaviour was primarily attributed to the morphology change of ettringite that was triggered by the presence of a higher hemihydrate concentration. It was also noticed that physical performances of cement systems depended on their respective microstructure developments.

I can do all this through him who gives me strength.

Philippians 4:13

Dedication

To my dearest parents: Innocent Mbasha Muhamiriza and Sophie Cizungu Rhulinabo

To Patrice Kasigwa Nyenyezi and Marthe Cizungu Tabu

To Reverend Bishop Tshalo Katshunga and Reverend Beatrice Katshunga

Acknowledgements

I would like to express my utmost gratitude to my advisors, **Professor Rainer Haldenwang, Dr Nicolas Roussel** and **Professor Irina Masalova,** for their guidance throughout my Master's degree studies at the Cape Peninsula University of Technology. As their insightful advice has been absolutely priceless, I am fortunate to have them as mentors.

I would also like to thank **Professor Veruscha Fester, Mr Tshepo Motau, Mr Martin Lombaard** and **Mr Nazeem George** for technical assistance during the course of this project.

I would like to express my sincerest gratitude to **Madam Myriam Boeglin** and **Maria Mater Misericordae Foundation** for supporting my studies.

Most importantly, I must express my deepest gratitude to **PPC Cement,** especially **Mr Eduardo Auger**, **Mr Walter Wirth** and **Mr Frans Scheurwater,** for supporting this project, both financially and technically.

I thank my friends, **Dr Steve Tshilumbu Nsenda, Dr Mahabubur Rahman Chowdhury Fahaad**, **Mr John Shamu Tafadzwa**, **Mr Buyisile Kholisa, Mrs Zintle Ntshoko** and **Ms Whitney Heuwel,** for their encouragement and support in my hardest times. I appreciate everything they have done for me.

And I express my deepest gratitude to my future wife, **Ms Rachel Ciebwe Ndumbi,** for her support, advice and affection thoughout this journey.

Publications and Conferences

Peer reviewed publications

Mbasha, W., Masalova, I., Haldenwang, R. & Malkin, A.Y. 2015. The yiled stress of cement pastes as obtained by different rheological approaches. *Applied Rheology*, 25(5): 53517.

Elmakki, R., Masalova, I., Haldenwang, R. & Mbasha, W. 2016. Effect of limestone on the cement paste hydration in the presence of polycarboxylate superplasticiser. *Appl. Rheol*, 26(2): 25122.

Masalova, I., Mbasha, W., Haldenwang, R. & Malkin, A.Y. 2018. Rheokinetics of cement paste hydration during the dormant phase. *Appl. Rheol*, 28: 15452.

Almuwbber, O., Haldenwang, R., Mbasha, W. & Masalova, I. 2018. The influence of variation in cement characteristics on workability and strength of SCC with fly ash and slag additions. *Construction and Building Materials*, 160: 258–267.

Mbasha, W., Haldenwang, R., Roussel, N., Bessaies-Bey, H. & Masalova, I. 2018. The influence of sulphate availability on the packing properties and rheology of fresh cement paste. *(Under review)*.

Oral conference

Mbasha, W., Haldenwang, R. & Masalova, I. 2014. The effect of different cements and superplasticiser on the rheology of cement paste. In *5th Rheology conference presented by SASOR*. Stellenbosch, South Africa: Southern Africa Society Of Rheology: 14–18.

Mbasha, W., Haldenwang, R. & Masalova, I. 2016. Effect of hydration kinetics on cement paste microstructure using rheological approach. In *8th International RILEM symposium on Self-compacting concrete*. Washington State: RILEM Publications SARL: 573.

Mbasha, W., Haldenwang, R., Masalova, I. & Roussel, N. 2016. The effect of fly ash on the rheokinetics of cement paste. In *6th Rheology conference presented by SASOR*. Johannesburg, South Africa: Southern Africa Society Of Rheology: 26–30.

Mbasha, W., Haldenwang, R., Masalova, I. & Roussel, N. 2017. The effect of hydration temperature on the rheokinetics of fly ash blended cement paste. In *Knowledge Exchange for Young Scientist*. Johannesburg, South Africa: KEYS Symposium: 57.

Research Project currently heading/ Involved

Effect of gypsum component phases on the rheokinetics of cement paste during hydration

Numerical optimization of mineral and chemical admixture for self-compacting concrete

Effect of superplasticiser on the yield stress development of cement paste

Optimisation of soil hydraulic conductivity for wetland filtrate system

Effect of surfactant on soil hydraulic conductivity

The effect of rheological parameters on static segregation of self-compacting concrete mortar

Effect of polycarboxylate superplasticiser on the adsorption and rheology of self-compacting cement paste

Effect of recycled plastics particles on the fresh and hardened properties of self-compacting concrete

Use of silica fume and nano silica fume for rubber treatment in concrete

Effect of silica fume and fly ash on the mechanical properties of concrete.

Table of Contents

Page

Declaration ii
Abstract iii
Acknowledgements vii
Publications and Conferences viii
Table of Contents x
List of Figures xiii
List of Tables xviii
Nomenclature xix
Terms and concepts xxi
Chapter 1 Introduction 1
1.1 Background and motivation 1
1.2 Research problem 3
1.3 Research questions 3
1.4 Objectives and outcomes 3
1.5 Significance 4
1.6 Delineation 4
1.7 Assumptions 5
1.8 Methodology 5
1.9 Organisation of research 6
Chapter 2 Literature review and theory 8
2.1 Introduction 8
2.2 Cement history 8
2.3 Cement manufacturing process 10
2.3.1 Raw materials preparation 10
2.3.2 Clinker production 11
2.3.3 Cement clinker oxides 14
2.3.4 Cement grinding process 14
2.3.5 Classification of cement 17
2.3.6 Cement chemical nomenclature 19
2.4 The environmental impact of cement production 20
2.5 Cement paste hydration 21
2.5.1 Chemical interactions within poly-phase cement systems 21
2.5.2 Effects of hydration on cement paste microstructure 27
2.5.3 Chemical interactions within mono-phase cement systems 31

2.5.4 Effect of gypsum phases on the hydration of poly phase cement systems..... 41
2.6 Rheokinetics of cement paste..... 43
2.6.1 Fundamentals of rheology..... 44
2.6.2 Physical interactions within cement hydrating systems..... 51
2.7 Overview of cement hydration measurements..... 61
2.7.1 Thermodynamic..... 61
2.7.2 Spectroscopy..... 61
2.7.3 Microscopy..... 62
2.7.4 Rheometry..... 62
2.8 Conclusion..... 62
Chapter 3 Research methodology..... 65
3.1 Introduction..... 65
3.2 Rheokinetics measurements of cement paste..... 65
3.3 Cement hydration kinetics measurements..... 66
3.4 Cement hydrate phases estimation..... 66
3.5 Research design..... 67
3.6 Research methodology..... 67
3.6.1 Experimental project matrix..... 67
3.6.2 Physical and chemical interactions for cement microstructure development..... 68
3.6.3 Ionic activity within cement suspensions..... 70
3.6.4 Collection and analysis of data..... 72
3.6.5 Research instruments..... 80
3.6.6 Material used..... 82
3.6.7 Sample preparations and measurements..... 83
3.7 Conclusion..... 86
Chapter 4 Effect of natural gypsum and hemihydrate on cement paste hydration kinetics..... 88
4.1 Introduction..... 88
4.2 Hydration kinetics of cement systems..... 88
4.3 Reactivity induced within cement systems..... 92
4.4 Early hydrate products: ettringite (Aft) and portlandite (CH)..... 94
4.5 Effect of calcium sulphate bearing materials on physical and mechanical properties of cement paste..... 101
4.6 Conclusion..... 104
Chapter 5 Rheokinetics of cement paste with mix proportion of natural gypsum and hemihydrate..... 107
5.1 Introduction..... 107

5.2 Effect of natural gypsum and hemihydrate on the viscoelastic properties of cement paste 107
5.3 Effect of natural gypsum and hemihydrate on the flow properties of cement paste 111
5.4 Early hydration cement products: ettringite and portlandite 112
5.4.1 Ettringite and cement paste rheological properties 116
5.4.2 Ettringite and cement paste microstructure 117
5.5 Effect of mix proportion of natural gypsum and hemihydrate on the initial and final setting times 121
5.6 Conclusion 122
Chapter 6 Conclusions and recommendations 124
6.1 Effect of natural gypsum and hemihydrate on the hydration kinetics 124
6.2 Effect of natural gypsum and hemihydrate on the microstructure 124
6.3 Effect of hemihydrate and natural gypsum on the mechanical and physical properties of cement 125
6.4 Effect of mix proportion of natural gypsum and hemihydrate on the rheokinetics of cement paste 125
6.5 Effect of ettringite morphology on the flow properties of cement paste 126
6.6 Recommendations for further research 127
References 128
Appendices 140
Appendix A. Heat flow rate profiles 140
Appendix B. Reaction rate and total heat of reaction 141
Appendix C. Thermogravimetric analysis and differential scanning calorimetric 142
Appendix D. Compressive strength readings of cement mortar 144
Appendix E. Flow curves of cement pastes 145
Appendix F. X-ray diffraction patterns of hydrated cement paste 146

List of Figures

Page

Body

Figure 2.1: Typical rotary kiln for the cement clinkering process (Jennings & Thomas, n.d.)... 11
Figure 2.2: Reactions within the kiln for the formation of Portland cement clinker phases (Newman & Choo, 2003)... 13
Figure 2.3: Closed circuit ball mill for cement grinding process (Newman & Choo, 2003)... 15
Figure 2.4: Typical cement hydration stages describing the heat flux curve (Newman & Choo, 2003) ... 22
Figure 2.5: Formation of hydrate phases during cement hydration (Odler, 1998)... 25
Figure 2.6: Regions of sulphate depletion and the second dissolution of C_3A during hydration (Aïtcin & Flatt, 2016) ... 26
Figure 2.7: The C-S-H morphology of a mature cement paste (Stutzman, 2004)... 28
Figure 2.8: The morphology of other cement hydrate products: portlandite, monosulfoaluminate and ettringite (D'Ayala & Fodde, 2008) ... 30
Figure 2.9: Contribution of main cement phases to the strength development of cement paste at 20 ^oC with w/c=0.45 (Hewlett, 2001) ... 31
Figure 2.10: Hydration kinetics of β-hemihydrate investigated by the means of an ultrasonic velocity method (Yu & Brouwers, 2011) ... 34
Figure 2.11: Optimization of sulphate additions from different gypsum phase types (hemihydrate, natural gypsum) (Barnes & Bensted, 2002)... 37
Figure 2.12: Heat flow rate and conductivity of the C_3A hydration process in the presence of gypsum (Minard *et al.*, 2007)... 39
Figure 2.13: Dissolution rate of different type of calcium sulphates (Zhang *et al.*, 1996)... 42
Figure 2.14: Parallel plate model constitutes with two planes of identical areas A, away from each other of h distance filled with a sheared liquid. A force F is applied to the upper plate and moves at velocity v. (Barnes *et al.*, 1989) ... 45
Figure 2.15: Deformation of materials according to Hooke's law ... 46
Figure 2.16: Illustration of flow properties: (1) Newtonian flow; (2a) general non-Newtonian with shear thickening; (2b) general non-Newtonian with shear thinning; (3a) viscosity non-Newtonian with shear thinning; (3b) viscosity non-Newtonian Bingham plastic; and (3c) viscosity non-Newtonian Bingham plastic non-ideal (Hanehara & Yamada, 2008) ... 48

Figure 2.17: The relationship between applied stress and resulting strain within a viscoelastic material (Eirich, 1958) 50
Figure 2.18: Relative importance of the interaction forces in cementitious materials at different concrete scale (particle size in the suspension) (Flatt, 2004) 52
Figure 2.19: Effect of particle density of a typical cementitious material on the yield stress values (Bentz *et al.*, 2012) 59
Figure 3.1: Experimental project matrix for each concentration of individual calcium bearing material (phase I) and their mix proportions (phase II) 68
Figure 3.2: Typical electrical conductivity of cement with natural gypsum and hemihydrate at different concentrations 71
Figure 3.3: Shear rate variation within the measuring time for cement paste yield stress and plastic viscosity assessments 73
Figure 3.4: Generic heat flow rate of cement with 3% of natural gypsum: (A) pre-induction zone; (B) dormant phase; (C) acceleration zone; and (D) deceleration zone 75
Figure 3.5: Typical thermogravimetric and differential thermal profile of cement (Monteagudo *et al.*, 2014) 77
Figure 3.6: Typical energy dispersive X-ray spectra on a spot area of cement paste sample with only hemihydrate as set regulator after 1 hour of hydration time 78
Figure 3.7: Typical atomic ratio of Si/Ca vs Al/Ca for cement paste with only hemihydrate as set regulator hydrated for 1 h 79
Figure 4.1: Influence of natural gypsum concentration on the hydration kinetics of cement paste 89
Figure 4.2: Influence of hemihydrate concentration on the hydration kinetics of cement paste 89
Figure 4.3: Cumulative heat flow of cement with natural gypsum (a) and hemihydrate (b) at different concentrations 90
Figure 4.4: Comparison of reaction rates and cumulative heat flow of cement with hemihydrate (HH) and natural gypsum (NG) at 3%, 4% and 5% concentrations 91
Figure 4.5: Comparison of dormant phase duration of cement systems with natural gysum and hemihydrate at different concentrations 92
Figure 4.6: Consumption rate of calcium sulphate per gram of cement with hemihydrate (HH) and natural gypsum (NG) at different concentrations 93
Figure 4.7: Degree of hydration of cement system with different calcium bearing material at variant concentrations (a) at the exhaustion of $CaSO_4^{-2}$; (b) after $CaSO_4^{-2}$ depletion at 24 hours 94
Figure 4.8: Typical thermogravimetric analysis and differential scanning calorimetry profiles after calcium sulphate depletion within cement systems with hemihydrate (HH) and natural gypsum (NG) at 2%, 4% and 7% concentrations 95

Figure 4.9: Amount of ettringite formed after 12 hours of hydration for cement clinker with different calcium sulphate types at different concentrations 97
Figure 4.10: Amount of portlandite formed after 12 hours of hydration for cement clinker with different calcium sulphate types at different concentrations 98
Figure 4.11: Cumulated heat flow at the time of sulphate exhaustion against the initial added quantity of sulphate per gram of cement 99
Figure 4.12: SEM-BSE of cement system hydrated for 30 min of (A) hemihydrate; and (B) natural gypsum at a concentration of 4% 101
Figure 4.13: Compressive strength of cement mortar with natural gypsum and hemihydrate at different concentrations hydrated during 1 day..... 102
Figure 4.14: Final and Initial setting times of cement paste with natural gypsum and hemihydrate at different concentrations..... 103
Figure 5.1: Evolution of storage modulus (a) and corresponding phase angle (b) during the early hydration of cement with different proportions of natural gypsum and hemihydrate set at 4% calcium sulphate cement content 108
Figure 5.2: Time required for the microstructural network percolation occurrence with respect to the inclusion of hemihydrate in the gypsum phase 109
Figure 5.3: Maximum storage modulus of hydrate cement (at 20 ^{o}C) with different fractions of hemihydrate within the gypsum phase set at 4% cement content 110
Figure 5.4: Strength rate development of cement paste with different fractions of hemihydrate within the gypsum phase set at 4% cement content..... 110
Figure 5.5: Typical flow curves of cement pastes with different proportions of natural gypsum and hemihydrate within gypsum cement phase..... 111
Figure 5.6: Effect of hemihydrate fraction within gypsum cement phase on (a) the yield stress and (b) plastic viscosity..... 112
Figure 5.7:Thermogravimetric analysis and differential scanning calorimetry of one hour hydrated cement pastes with different proportions of natural gypsum and hemihydrate within the gypsum phase set at 4%: (a) cement with hemihydrate 0/100; (b) cement with natural gypsum 100/0; (c) cement with 70/30 proportion; (d) cement with 60/40 proportion; (e) cement with 50/50 proportion; and (f) cement with 40/60 113
Figure 5.8: Amount of hydrate products precipitated after 1 hour of cement hydration with different fractions of hemihydrate within the gypsum phase set at 4%: (a) ettringite and (b) portlandite..... 114
Figure 5.9: Calcium sulphate consumption rate per gram of cement with different proportions of natural gypsum and hemihydrate within the 4% calcium sulphate cement phase 115

Figure 5.10: SEM-BSE images of mixes with different proportions of natural gypsum and hemihydrate within the gypsum cement phase hydrate sfter 1 hour of hydration117
Figure 5.11: Typical x-ray difraction patterns of one hour hydrated cement with different proportion of natural gypsum and hemihydrate within 4% cement calcium sulphate phase..... 118
Figure 5.12: Effect of hemihydrate fraction within cement gypsum phase on cement paste packing 119
Figure 5.13: SEM-BSE images of cement surface hydrated for 1 hour and prepared with (A) natural gypsum and (B) hemihydrate 120
Figure 5.14: Initial and final setting times of cement with different hemihydrate fractions with the gypsum phase set at 4% cement content..... 122

Appendices

Figure A.1: Heat flow rate of cement paste with different concentrations of natural gypsum . 140
Figure A.2: Heat flow rate of cement paste with different concentrations of hemihydrate 140
Figure A.3: Heat flow rate of cement paste with different proportions of natural gypsum and hemihydrate at 4% calcium sulphate cement phase 140
Figure B.1: Comparison of reaction rate and cumulative heat flow of cement with hemihydrate (HH) and natural gypsum (NG) at 2%, 6% and 7% 141
Figure C.1: Typical thermogravimetric analysis and differential scanning calorimetry profiles after calcium sulphate depletion within cement systems with hemihydrate (HH) and natural gypsum (NG) at 3%, 5% and 6% 142
Figure C.2: Thermogravimetric analysis and differential scanning calorimetry profiles of 4 hours hydrated cement with different proportion of hemihydrate and natural gypsum within the calcium sulphate phase set at 4% concentration 143
Figure E.1: Rheological parameters fitted by Bingham model of cement pastes with different natural and hemihydrate proportions within the calcium sulphate cement phase set at 4% 145

List of Tables

Page

Body

Table 2.1: Different ordinary Portland cement type and their applications (Taylor, 2003)..... 18
Table 2.2: Chemical composition ranges for ordinary Portland cements (Taylor, 2003)..... 20
Table 3.1: Chemical and phase composition of clinker and calcium sulphate 83
Table 3.2: Concentration of SO_3 as provided by the initially added amount of natural gypsum and hemihydrate in the clinker 84
Table 3.3: Total SO_3 concentration within the clinker with 4% calcium sulphate provided by the mixture of natural gypsum (NG) and hemihydrate (HH) in different proportions.. 84
Table 3.4: Particle size distribution of the clinker and cement clinker with different proportion of NG and HH at 4% calcium sulphate within the system 85
Table 4.1: Mass loss of cement with natural gypsum (NG) at different concentrations 2%-7% within temperature ranges of cement phase decomposition 96
Table 4.2: Mass loss of cement with hemihydrate at different concentrations 2%-7% within temperature ranges of cement phase decomposition 96
Table 5.1: Mass loss of 1 hour hydrated cement with mix proportions of natural gypsum and hemihydrate within the calcium phase set at 4% 114
Table 6.1: 1 day compressive strength of cement mortar with natural gypsum and hemihydrate at different concentrations 144

Nomenclature

Constants, subscripts and superscripts

a_i	Regression coefficient
a^*	Radius curvature
A	Area *(m^2)*
A_0	Hamaker constant
h	Height or thickness of the material (m)
H	Surface to surface seperation
F	Force (N)
v	Velocity (m/s)
dv/dh	Velocity gradient (1/s)
s	Strain
G'	Storage modulus (Pa)
G''	Loss modulus (Pa)
G^*	Complex modulus (Pa)
k	Consistency, Boltzmann constant
η	Power law index
t	Time (s)
d	Particle size
$d_{\min}$	Small dimeter of particles
$d_{\max}$	Maximum diameter of particles
T	Absolute Temperature
N_r	Relative magnitude of particles interactions with the suspension
m_1	Volume mean particle size parameter
Δw	Weight loss of sample
ΔW_{dx}	Weight loss of a cement sample within the dehydroxylation interval
ΔW_{dc}	Weight loss of a cement sample within the decarbonation interval
ΔW_{dh}	Weight loss of a cement sample within the dehydration interval
w_B	Chemically bound water
M_{hp}^{H2O}	Molecular weight of a cement hydrate phase
M_{hp}	Molecular weight of the decomposed a cement hydrate phase
$P(\%)$	Amount of a cement hydrate phase

Greek letters

α	Degree of hydration
φ	Particle density
φ_c	Percolation threshold
ξ	Inter-particle bond
β	Critical percolation
η	Apparent viscosity (Pa.s)
η_c	Liquid phase apparent viscosity
γ	Strain rate (%)
γ_0	Strain amplitude
γ_c	Critical strain
ω	Angular frequency (*rad/s)*
μ	Plastic viscosity
δ	Phase angle or phase lag,
ϕ	Porosity, Packing fraction
ϕ_c	Critical packing fraction
$\phi_{\max}$	Maximum packing fraction
ϕ_0	Energy potential
τ	Shear stress (Pa)
τ_y	Yield stress (Pa)
$\dot{\gamma}$	Shear rate (1/s)

Terms and concepts

AFm	Monosulpho-aluminate
AFR	Alternative Fuels and Raw materials
AFt	Ettringite
Agglomeration	Process wherein colloids come out of suspsension in the form of floc
ASTM	American Society to Testing and Materials
Attrition	Reduction in size
Binder	A cementitious material, either hydrated cement or a product of cement and supplementary cement material for joining aggregates together
BL	Designation for white cement
C_2S	Dicalcium silicate
C_3A	Tricalcium aluminate
C_3S	Tricalcium silicate
C_4AF	Ferrite
CAC	Calcium Aluminate Cement
CAH	Calcium aluminate hydrate
Calcination	Thermal treatement process in the absence or limited supply of air or oxygen
CEM	Designation of ordinary Portland cement type
CH	Portlandite, calcium hydroxyl
Clay	Finely grained natural soil material that combines more minerals with possible traces of quartz, metal oxides and organic matter
Clinker	A partially fused product of a kiln, which is ground for use in cement
Clinkering	The process of manufacturing cement clinker
Colloidal	Particles of small size that float in a medium of one of three substances: solid, liquid or gas
Comminution	Reduction of solid materials from one average particle size to a smaller average particle size, by crushing, grinding, cutting, vibrating or other process
C-S-H	Calcium silicate hydrate
Dehydration	Removal of water from any substance
Diffusion	Net movement of molecules from a region of high concentration to a region of low concentration as a result f random motion
Dihydrate	Chemical compound containing two molecules of water
Fineness	A measure of particle size distribution
Flocculation	Process by which fine particles are caused to clump together into a flooc
Gypsum	A soft material consisting of a hydrated calcium sulphate used as set retarder
Hemihydrate	A crystalline hydrate containing one molecule of water for every two molecules of the compound in question

Hydration	chemical reaction between water and cement powder
Hydraulic binder	Binder that sets and hardens by the chemical interaction with water and its capable of doing so under water
Hydrolysis	Chemical breakdown of a compound due to reaction with water
Hygroscopic	Substance with tendency to absorb water
IP	Inner part of calcium silicate hydrate
Kiln	Furnace or oven for calcining lime
Limestone	Hard sedimentary rock, composed mainly of calcium carbonate or dolomite
Microstructure	The very small scale structure of a material defined as the structure of a prepared surface of material as revealed by a microscope
Network	System of interconected cement particles
Nucleation	The very first step in the formation of a hydrate phase
Nuclei	Characteristic and stable complex of atoms or groups in a molecules
OK	A type of vertical mill
OP	Outer part of calcium silicate hydrate
OPC	Ordinary Portland cement
Paste	The mixture of water and cement powder
Percolation	Describes the phenomenon of connected clusters in a random graph
Porosity	A measure of the void, spaces in a material, a fraction of volume of voids over the total volume
Pozzolana	A natural siliceous or siliceous and aluminous material which reacts within calcium hydroxide in the presence of water at room temperature
PSD	Particle size distribution
Rigidification	The process of becoming rigid, stiff or inflexible
Rheokinetics	Rheological changes that occur within the fresh cement paste
SCM	Supplementary cementitious material
SCP	Small capillary pores
Shear rate	The rate of change of velocity at which one layer of fluid passes over an adjacent layer
Shear strain	The displacement of the surface that is in direct contact with the applied shear stress from its original position
Soundness	Ability of cement paste to harden while retaining its volume after setting without delayed destructive expansion
SSA	Specific surface area
Stress	Force tending to cause deformation of a material by slippage along a plane or planes parallel to the imposed stress
Suspension	Heterogeneous mixture that contains solid particles sedimentation
Thixotropy	The decrease of a fluid viscosity when subjected to an applied stress

w/c	Water to cement ratio
Hydrogarnet	A group of minerals where the silicon oxide tetrahedra are partially or completely replaced by hydroxide
LVD	Linear viscoelastic domain
Flow curve	A graph relating the shear stress and shear rate experienced by a material
Yield stress	The stress needed to initiate the flow
Flow	Breakage of the internal structure of a material or move of a fluid
Deformation	Change in an object's shape or form due to the application of a force
BSE	Backscatter electron
SEM	Scanning electron microscopy
EDS	Energy dispersive spectroscopy
XRD	X-ray diffraction
TEM	Transmission electron microscopy
TGA	Thermogravimetric analysis
SAO	Small amplitude oscillation
SAOS	Small amplitude oscillatory shear
HH	Hemihydrate
NG	Natural gypsum
Cdt	Conductivity
DTA	Differential thermal analysis
DSC	Differential scanning calorimetry

Chapter 1 Introduction

Gypsum is a calcium sulphate bearing material that can be quarried or synthetised, commercially available in different forms based on its combined water fraction. Natural gypsum or gypsum dihydrate is usually added into cement clinker for Portland cement production. Cement has arguably become the second most consumed substances after water on this planet, to a point where many cannot conceive of a world without its derivative products (Potgieter, 2012). Cement is the binding agent in concrete (an artificial conglomerate, essentially a mix of fine and coarse aggregates, water and cement) and mortar (primarily a mix of sand, water and cement used in masonry-type construction) and therefore a key component of construction sector in most countries. It is thus imperative that special attention be paid to the cement system. Furthermore, sustainability, innovation and quality improvement of cement are mostly achieved by considering its manufacturing process and revising specifications that guide the design and regulate the use of most cementitious materials. This research work focuses mainly on the performance of the fresh cement paste with respect to its calcium sulphate phase.

1.1 Background and motivation

The performance of concrete in its fresh and hardened state depends strongly on the early hydration of cement. This chemical and physical process influences the workability during concrete processing as well as the strength of the final product. This reaction is predominantly exothermic, with the amount of heat emitted depending on the fragmentation of the cement phase composition, type and concentrations within the cement system. Correlations between the 28 days' concrete strength and the amount of heat liberated during cement hydration have been successfully established (Baran & Pichniarczyk, 2017).

Although it is difficult to quantitatively predict the performance of concrete based on that of the cement paste phase, the success of most numerical prediction techniques (mesoscale model) of concrete's mechanical and physical properties relies on the contribution of cement paste hydration (Contrafatto *et al.*, 2016).

It is also agreed that concrete hydration reactions occur mostly at the cement paste scale since coarse aggregates are regarded as inert materials. Hence, the optimization of most reactive concrete additives is preferably done on cement paste scale (López *et al.*, 2009). The understanding of cement paste hydration kinetics is therefore essential in controlling the flow behaviour of concrete.

Ordinary Portland cement consists of finely ground clinker which itself is a multi-phase inorganic material comprised of four major phases: alite (C_3S), belite (C_2S), aluminate (C_3A), and ferrite (C_4AF). These constitute the main compounds of pure cement clinker and are formed through the burning of limestone and other materials in a kiln at high temperatures. A large amount of scientific research has been devoted to the effects of the content of these cement clinker phases to the rheological properties of cement paste. There exists a linear or exponential correlation between these clinker phases and the flow resistance of cement paste (Vikan *et al.*, 2007).

Enough knowledge has been gathered on the hydration kinetics of these individual cement phases owing to a number of studies that have been conducted on cement mono-phase. However, this approach seems rather dissatisfactory in trying to characterize the hydration kinetics of cement paste, since cement hydration is not the summation of the individual hydrations of its phases that are interdependent and occurs at different rates and times (Quennoz & Scrivener, 2013a).

The exothermic reaction of these compounds in the presence of water releases a large amount of heat, rendering the matrix stiff with no chance of being remixed. The early stage of this reaction is dominated more by the dissolution of C_3A. Thus, the yielded hydration products do not contribute to the matrix strength and generally impede the early hydration of other cement compounds such as calcium silicates (C_3S, C_2S) that are responsible for the strength of cement systems. To overcome this phenomenon, calcium sulphate bearing materials are added within the clinker as set regulators of aluminate phase hydration. Calcium sulphate dihydrate or natural gypsum ($CaSO_4.2H_2O$) is mostly ground with clinker as a source of sufficient sulphate which is able to control the hydration of C_3A. This addition is of great importance because it allows the cement paste to remain plastic for a certain amount of time, prolonging the workability time and also allowing the hydration of calcium silicate phases responsible for the early and later strength of concretes.

The heat generated within the mill during the grinding process of clinker and gypsum causes a partial dehydration of natural gypsum into hemihydrate ($CaSO_4.0.5H_2O$). The final ground cement product thus comprises two unexpected types of calcium sulphate bearing materials (CSBM) in an unpredictable proportion. Due to the difference in their solubility, the hydration of the aluminate phase can variably be altered; consequently, this affects the rheokinetics of the cement paste.

1.2 Research problem

The effects of the available amount of hemihydrate and natural gypsum in the cement sulphate phase on both the hydration and rheology of ordinary Portland cements (OPC) are not currently well-understood.

1.3 Research questions

What is the impact of the concentration of dihydrate (natural gypsum) and hemihydrate on the early hydration reaction of cement paste?

What is the influence of the concentration of these cement gypsum phase components on the rheological behaviour of cement paste?

1.4 Objectives and outcomes

The aim of this research is to evaluate the effect of the concentration of dihydrate and hemihydrate contained in the cement gypsum phase on the hydration kinetic of cement paste.

The answer to these questions necessitated the following objectives:

- To evaluate the effect of hemihydrate and natural gypsum concentrations in a multi-phase cement system on early hydration reactions;
- To identify and quantify the hydrate products induced by these gypsum phase components during hydration;
- To analyse the microstructural changes of cement paste due to the concentrations of the gypsum phase components;
- To determine and evaluate the effect of the gypsum phase components on cement paste flow and viscoelastic properties; and
- To evaluate the rheological behaviour of cement matrix with respect to their hydration kinetics.

The expected outcomes were as follows:

- The reactivity induced by the gypsum components in the cement paste hydration based on calorimetric profiles and storage modulus developments.
- The x-ray diffraction patterns of cement with different mix proportions of natural gypsum and hemihydrate collected after different hydration times.
- Different scanned images of cement matrix collected after specific hydration times (30 min and 1 hour).
- The yield stress value and viscosity evolutions of cement paste with different proportions of gypsum phase components.

- A qualitative description of the influence of the microstructure development on the rheological properties of the cement paste matrix.

1.5 Significance

The grinding process of cement clinker during cement production is important, mainly because the targeted fineness of the finished cement is one of the main factors that dictates the early strength development of the cement. Generally the energy consumption during grinding has been proven to be linear up to a Blaine of approximately 300 m^2/kg (Peray, 1979). Above this fineness, the energy consumption increases progressively in the cement mill and a higher amount of energy is lost in heat, inferring that there is more heat generated in the cement mill for commercial cements which target higher finesses. Techniques to mitigate this problem are available, for instance, by optimizing the cement mill technology and using different grinding aids such as triethanolamines and many other polyol based cement grinding aids (Engelsen, 2009), though the partial dehydration of natural gypsum seems inevitable during this process due to the rise of ambient temperature within the mill caused by the dissipation of excessive heat. The current work contributes to the present knowledge about cement by providing relevant information concerning the impact of the degree of natural gypsum dehydration during grinding operations on the kinetics of hydration and the rheology of cement paste.

Despite the fact that the effect of calcium sulphate on cement hydration is known due to the progress made in cement chemistry and its wide use in construction globally, knowledge of the effect of using the mix of two different calcium bearing materials on the hydration process of cement paste is still limited. This study contributed to the understanding of the hydration of cement pastes with different types of calcium sulphate and their effects on the rheology of cement paste.

1.6 Delineation

This research focused solely on the effect of the concentration of both dihydrate and hemihydrate on the hydration reaction of ordinary Portland cement paste in a multi-phase system. It considered a realistic model of cement with all its phases at constant concentrations, including the gypsum phase that was the object of this study. The proportions of dihydrate and hemihydrate were the only variables in the constant gypsum phase of the cement system. In addition, only the early hydration of the cement matrix was studied. The other physical properties of cement paste, such as resistance to environmental sulphate attack, the late ettringite formation, water permeability and resistance to carbonation, were not part of this study.

It is true that the presence of admixtures within cement pastes alters their hydration tremendously even with constant phases. However, these alterations were not investigated in this study since there was no admixture used.

1.7 Assumptions

A few assumptions were made concerning the material used and the techniques applied in this research. A comprehensive study of cement paste hydration requires a congruent use of different scientific disciplines owing to the fact that many physicochemical phenomena happen during hydration. Therefore, for this work, cement suspensions were assumed to be colloidal materials with spherical solids suspended in a liquid phase of water. Furthermore, all the theories developed for these types of suspensions were applied during the investigations by considering the presence of internal forces and their interactions due to physical and chemical properties inherent in cementitious materials. With relatively same mixes in terms of the clinker purity and experimental measurement conditions, the only variable responsible for any changes observed either in hydration or rheological behaviour was the type and amount of calcium sulphate bearing materials used.

1.8 Methodology

The rheokinetics of cement paste is directly related to the microstructural changes that occur during cement hydration. It is agreed that the early hydration of cement paste is predominated by the reaction of the aluminate phase. In the presence of calcium sulphate, calcium aluminate hydrates are yielded. These hydrate products are responsible for the rigidification of the newly formed internal structure and dictate the rheological behaviour of the fresh cement paste. This research aims to correlate the microstructural changes induced by the presence of hemihydrate in the gypsum cement phase and the rheokinetics of cement paste during the early hydration. Experimental and comparative research designs were conducted for the achievement of this purpose. Different techniques were employed, such as calorimetry, thermal analysis, spectroscopy, imaging and rheometry. The hydration kinetics were evaluated by isothermal calorimetry while the quantification of the hydrate phases was done by thermogravimetric analysis (TGA) and x-ray diffraction (XRD). The microstructure of cement pastes was identified by scanning electron microscopy (SEM) using backscatter electron (BSE) and energy dispersive spectroscopy (EDS). The dynamic mode (small oscillatory amplitude sweep) and the shear mode were used to characterize the rheological properties of the cement paste. The experiments were conducted in various facilities depending on the availability of the required equipment. The physics and chemistry laboratories of PPC Cement Ltd at Jupiter Plant, the Flow Process and Rheology Centre (FPRC) at Cape Peninsula University of Technology and the laboratory of the

Department of Physics at the University of Western Cape (UWC) were used for the described experiments.

1.9 Organisation of research

This research entails a full understanding of the effects of calcium sulphate type and concentration on the rheokinetics of cement paste. Various experimental tests have been conducted to shed light on the problem stated. This current research is subdivided into six chapters, including the *Introduction (Chapter 1)*.

Literature review (Chapter 2): Different publications and investigations are reviewed and relevant theories pertaining to cementitious materials are considered. A brief presentation of cement production lines is presented with an overview of their impact on the environment and sustainability. Various stages that occur during cement hydration are discussed depending on the cement system of interest (multi-phase cement system or mono-phase cement systems). Focus is given mostly to physical and chemical interactions that occur during this process. Applications of rheology to cement paste are also presented and different measurement techinques to estimate the hydration/rheological knietics are reviewed.

Research methodolgy (Chapter 3): Experimental methods with descriptive procedures for data collection and analysis of cement hydration and microstructural kinetics are introduced. Subsequently, a rheological approach to evaluate the effect of calcium bearing material on cement paste microstructural development is explained and the characterization of the heat flow rate curves are presented. Quantitative estimation of hydrate products and techniques to investigate the microstructural changes of cement paste are discussed.

Results and discussion were presented in two different chapters:

Effect of hemihydrate and natural gypsum on the hydration kinetics of cement paste (Chapter 4): The individual effects of these calcium sulphate bearing materials on the hydration kinetics and subsequent hydrate products are investigated with respect to their concentrations. Mechanical and physical performances of cement systems are also considered with respect to each calcium sulphate bearing material and their concentrations.

Rheokinetics of cement paste with mix proportion of natural gypsum and hemihydrate (Chapter 5): The effect of mix proportions of natural gypsum and hemihydrate at an optimum calcium sulphate concentration on cement paste rheological properties is assessed. The hydration

kinetics and physical performances of cement mixes are evaluated. A link between the rheokinetics, the hydration kinetics and physcal properties of cement systems is established.

Conclusion (Chapter 6): A general conclusion related to the observation of the hydration and rheological kinetics of cement systems in the presence of natural gypsum and hemihydrate is drawn. Relevant recommendations are suggested for further research and the contributions of this study in the field of interest are presented

Chapter 2 Literature review and theory

Portland cement is the most important hydraulic cement in the construction industry. As it is the most consumed construction material on earth, with 3.6 billion tonnes of production worldwide, it is predicted to grow by 1.2% per annum in the immediate future (Stafford *et al.*, 2015).The term *cement* is restricted to the material that is able to bond different elements such as stones, sand, bricks and building bricks to form a composite material. Portland cement is referred to as hydraulic cement because it has the property of setting and hardening when mixed with water by virtue of a chemical reaction referred to as hydration (Peray, 1979).

Thanks to perpetual research conducted within the field of fundamental knowledge required for cementitious materials, the cement industry has experienced continuous innovations that improve the production process and the quality of cement.

The following section introduces relevant theory based on actual publications and investigations pertaining to cement materials. Different stages involved in cement production lines are briefly presented with an overview of their impact on the environment and sustainability. Thereafter, stages that occur during cement hydration are discussed, firstly in a multi-phase cement system and secondly, in mono-phase cement systems. Physical and chemical interactions that occur during this process are also reviewed in detail.

2.1 Introduction

The current review is subdivided into three main parts: first, the relative development in the art of cement making is highlighted for suitable classification of cements; next, the kinetics of cement hydration are presented with a specific emphasis on the microstructure changes that occur during this chemical interactions; and finally, the rheological behaviours of cement pastes as a response to contact and non-contact interactions between cement particles within the suspension are addressed.

2.2 Cement history

The use of cement originates from ancient civilizations. Despite the fact that earlier structures were composed of earth raised in the form of walls or domes by ramming successive layers of stone blocks set one above another without the assistance of any adhesion, the stability of these structures has always given place to masonry erected with the aid of some plastic materials. For instance, Egyptians raised their walls with dried bricks joined together with a moist layer of Nile mud or loam. The Babylonians and Assyrians used burnt bricks and alabaster slabs connected together with bitumen. According to Blezard (1998), the idea of using materials similar to

cementitious materials was found in their massive masonry constructions. The Egyptian mortar generally consisted of burnt lime and sand, with its technological property largely attributed to the Romans (Lucas, 1933). Also, the Greeks mixed volcanic ash with lime and sand to produce a mortar with both superior strength and resistance to severe environmental attacks. The corresponding material for Roman builders was volcanic tuff found in the surroundings of Pozzuoli, near the Bay of Naples, and the material was referred to as Pozzolana. This designation has been extended to the entire class of mineral materials of similar properties. In the absence of volcanic tuff, Romans used other powders such as tiles and pottery powders which produced a similar effect. It is known that the word *cement* was first used to appropriately designate such materials classified now as artificial pozzolanas.

The need to improve the performance of these materials dates hundreds of years back. In 1756, John Smeaton conducted an investigation to select the best building materials for the construction of a new lighthouse on the Eddystone Rock (Reid, 1877). When comparing the performance of mortars made of limes mined from different origins, he found that the proportions of clay in these limes were the main factors responsible for the mechanical performance of mortars. It was only in 1796 that the possibility of making hydraulic lime by the calcination of argillaceous limestone nodules was discovered (Patent granted to James Parker, 1811). Due to its hydraulic properties (quick setting), the final product was referred to as *Roman cement*, not to be mistaken for Roman mortar (Thurston, 1938). The interest in developing “cement” with better hydraulic properties has taken place around the world ever since. However, Roman cement continued to be used in much construction until 1850 after which it was gradually replaced by Portland cement.

Portland cement was first made in England in the early part of the 19th century, its name derived from its similarity in colour and quality to a stone in Portland. Many people have claimed to have been the first to make Portland cement, but it is generally accepted that it was first manufactured by William Aspdin in Northfleet, England in about 1842. The name *Portland cement* was given by Joseph Aspdin, suspected to be a British bricklayer. He was granted the patent for a process of making cement as early as 1824. This patent of the cement manufacturing process was a precursor to the modern Portland cement. It is assumed that William Aspdin did bring some improvements (clinkered or over burning materials, synthesising calcium silicate) to the existing process established by his father Joseph Aspdin (Ludwig & Zhang, 2015; Fathi, 2012).

It is remarkable that up to this stage, innovation in the cement industry was dominated by the search for the strongest construction materials by improving techniques and using different materials to produce cement. It is therefore important to differentiate the different stages that took

place in the history of the Portland cement development based on the mineralogical assemblage and the kiln technology.

In its initial stage, referred to as proto-Portland cement, the cement is essentially a calcined mixture of limestone and clay with inappreciable evidence of the $CaO\text{-}SiO_2$ interaction due to a low burning temperature. The following stage is referred to as Meso-Portland cement. At this level, the cement is simply a heterogeneous material with evidence of a $CaO\text{-}SiO_2$ interaction that favours the formation of C_2S and C_3S and poorly defined flux phases, achieved by cooling the feed from the shaft kiln slowly. The final stage is the same as the normal Portland cement that is used nowadays. This is a calcareous cement manufactured in a rotary kiln

2.3 Cement manufacturing process

The most significant event that took place in the history of Portland cement is probably the replacement of the shaft kiln by the rotary kiln (Blezard, 1998) as this made it possible for cement production to shift from a batch process to a continuous manufacturing process.

Generally, the cement manufacturing process consists of three major stages (Salas *et al.*, 2016): raw meal preparation, clinker production and cement preparation. And these manufacturing stages can typically be processed in two different ways: dry process or wet process (UNIDO & MITI, 1994).

2.3.1 Raw materials preparation

Contrary to other industrial products, the raw materials that are required in the manufacturing process of Portland cement are found and exploited in nearly all parts of the world. This is a significant reason for its worldwide importance as a construction material (Fathi, 2012).

There are four major raw materials involved in cement production: limestone, clay or shale, sand and iron ore. These materials are preferentially mined from quarries near to the plant (Ishak & Hashim, 2015) and undergo a series of crushing. Initially, raw materials most often in the form of stones are sized and reduced to fragments of approximately 125 mm on primary crushing. Afterwards, with the help of mechanical conveyors, these fragments are carried on to secondary crushing where they are reduced to grains of about 19 or 20 mm. It is at the plant where these grains are mixed and proportioned to attain the requirements of a cement with specific chemical compositions (Salas *et al.*, 2016).

2.3.2 Clinker production

The proportioned raw materials, or the raw mix, is thereafter fed into a rotary kiln, a long cylindrical shaft that slopes downward and rotates slowly as illustrated in Figure 2.1.The purpose at this stage is to convert the raw mix into granular materials referred to as *cement clinker*. This single process requires maximum temperatures that are high enough to partially melt the raw mix. The latter is constantly agitated to ensure the homogenisation of the chemical composition within the clinker.

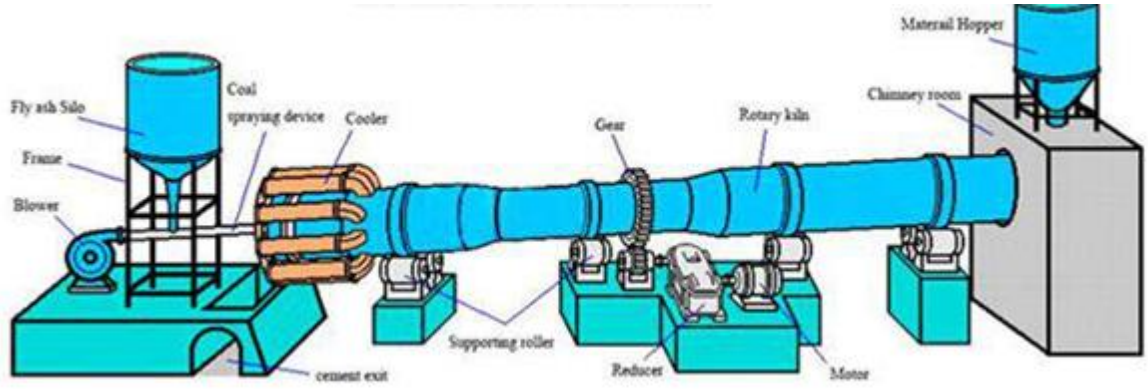

Figure 2.1: Typical rotary kiln for the cement clinkering process (Jennings & Thomas, n.d.)

Generally, the raw mix enters at the upper end of the kiln and moves slowly downward to the hottest area of the kiln within a couple of hours (60-90 minutes). Materials undergo different chemical reactions as they gradually approach the end of the kiln, a progressive allowing each reaction to be completed at its appropriate temperature. However, it is difficult to reach these designated temperatures for each specific reaction due to their endothermicity properties. This is the reason why it is challenging to bring a reaction at a particular zone in the kiln to its completion. In fact, there are four different reaction zones that can be found in the kiln depending on the prevailing temperature (Jennings & Thomas, n.d.).

First thermic zone

This zone in the kiln is referred to as the *dehydration section* with ambient temperatures of up to 450 ^{o}C. The aim of this zone is simply to allow for the evaporation and removal of free water since, regardless of the selected process (dry or wet process), adsorbed moisture can be found in the raw mix. The time and energy needed for this task depend on the moisture content of the raw mix. However, this moisture is only partially removed due to the fact that the ambient temperatures in this zone are not high enough to accomplish this work. In the wet process, this zone takes half of the kiln length, whereas in the dry process only short distances are required.

Second thermic zone

This is the *calcination zone.* The ambient temperatures in this region vary between 450-900 ^{o}C. Normally, at around 600 ^{o}C, the bound water is driven out of the clay while the decomposition of limestone or calcium carbonate occurs at about 900 ^{o}C and carbon dioxide is released. At the end of this zone, the mix consists mostly of oxides of the four main raw materials. At this stage, the mix is still a free-flowing powder since calcination does not involve melting.

Third thermic zone

This zone is referred to as the *solid-state zone* with ambient temperatures between 900-1300 ^{o}C. This region sometimes overlaps with the calcination zone since the onset of the solid-state reactions occurs at 900 ^{o}C. Calcium oxides (CaO) combine with reactive silica and form small crystals of dicalcium silicate (C_2S). In the same way, the formation of intermediate calcium aluminates and calcium ferrites takes place. These chemical compounds are very important in the clinkering process because they play the role of fluxing agent and can melt at relatively low temperature of about 1300 ^{o}C, increasing the reaction rate and aiding the formation of calcium silicate cement compounds. As the mix goes through this zone, adjacent particles tend to fuse together and the products become quite sticky.

Fourth thermic zone

This constitutes the *clinkering zone,* the hottest zone of the kiln with ambient temperatures varying between approximately 1300-1500 ^{o}C. The formation of tricalcium silicate (C_3S) occurs in this zone. The beginning of this zone is characterized by the melting of the intermediate calcium aluminate and ferrite phases. These melt phases activate the agglomeration of the mix into large nodules that consist of many small solid particles joined together by a thin liquid layer. Inside this liquid phase, the reaction between C_2S crystal and CaO takes place and C_3S is formed. As the process evolves, the crystals of solid C_3S grow within the liquid while those of C_2S decrease in number but grow in size. The clinkering process is completed when all the silica is in the C_3S and C_2S crystals and the amount of free lime, CaO, is reduced to a minimal level, normally below an admissible value of 1%.

A schematic illustration of these reactions within the kiln are shown in Figure 2.2.

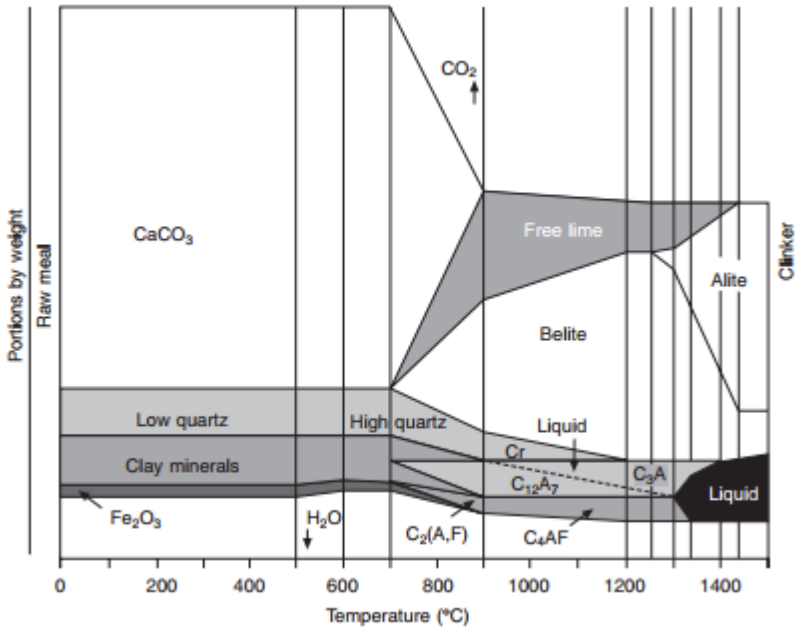

Figure 2.2: Reactions within the kiln for the formation of Portland cement clinker phases (Newman & Choo, 2003)

The cooling zone

This region is located at the bottom part of the kiln behind the heating source. As the mix moves past this hot point, the temperature drops rapidly and the liquid phase solidifies, allowing the complete formation of C_3A and C_4AF. The dissolved sulphate and alkalis (K and Na) in the liquid phase also combine to form K_2SO_4 and Na_2SO_4. The final products, the nodules formed, are hard after being through this zone. The reactivity of the cement in the future depends strongly on the actual rate of cooling of the clinker. Rapid cooling has been found to provide a more reactive cement, which is why the clinker is rapidly cooled down by either air blowing or water spraying as it exists the kiln (Shafeek *et al.*, 2017). Without this rapid cooling, the prevailing temperature in the cooling zone (1100 ^oC) can cause the C_3S to degenerate back into C_2S and CaO.

In modern cement plants, there is another section placed at the upper end of the kiln and referred to as suspension preheaters or calciners. In fact, the reaction that happens inside the kiln is mostly endothermic. This suggests that the raw mix particles will require a consistent and permanent input of energy for the completion of a particular reaction at a specific zone. This is difficult to achieve as the raw mix piles up in the kiln. Consequently, the rate at which the heat can be transferred into a large mass of particles decreases and the rate of reaction will be limited. A remedy to this issue is to use suspension preheaters that allow the hot gas from the kiln to enter from the bottom, moving upward, thereby dehydrating and partially calcining the mix particles as they enter and settle in the kiln in less than a minute. Similarly, some plants can have precalciners

in which some of the fuel is burnt directly and completely calcine the mix particles as they enter the kiln.

2.3.3 Cement clinker oxides

The major oxide components of a cement clinker include CaO (Lime), SiO_2 (Silica), Al_2O_3 (Aluminium oxide), Fe_2O_3 (Iron oxide) and MgO (Periclase) (Macphee & Lachowski, 2003). CaO, the most important oxide of cement clinker, comes from the calcination of the limestone. The reactivity of this oxide in the presence of water depends on the previous calcination temperature. This decreases with increasing temperatures that diminish the active surface area of lime by sintering.

The SiO_2 generally comes from aluminosilicate minerals in the shale and clay components of the kiln. It can exist within the clinker in different states. Most of the time, it is present in its pure state under different crystalline polymorphs such as quartz, cristobalite and tridymite. In its impure state, it is poorly crystallised and amorphous. Silica oxides combine with those of lime during clinkering to give calcium silicates (alite and belite) which comprise the bulk of the hydraulic active materials in Portland cement.

The periclase, MgO, is introduced within the clinker as an impurity in the raw materials either in limestone, clay or shale sources. The acceptable content of this oxide is limited to a value below 1%, since its slow hydration is deleterious and causes unsoundness.

Aluminium oxides arise in the kiln on heating bauxite and clays at temperatures close to 900 ^oC. Iron oxides derive from the clay in the kiln and shale feeds.

There are also unavoidably minor oxides such as Na_2O, K_2O, SO_3 and P_2O_5 that come mostly from the fuel used during clinkering (Ludwig & Zhang, 2015). The presence of these trace elements influences the clinker formation and the cement properties (e.g. cement reactivity) depending on their doping level in the clinker phase. Li *et al.* (2014), studying the effect of some of these oxides on the alite polymorphisms using the ex-situ XRD, found that the silicate phases content in the clinker were linearly proportional to the SO_3/MgO ratio. This is because MgO enhances the formation of C_3S, while SO_3 hinders its formation. The presence of MgO and SO_3 can also increase the amount of C_4AF and C_3A in the clinker.

2.3.4 Cement grinding process

The purpose of this process is mainly to provide cement with the required fineness for achieving a particular reactivity. Gypsum is added to the clinker and inter-ground together to control the

early hydration of cement at the time of its use. The particle size distribution (PSD) of cement is a very important parameter since most of the cement quality and concrete properties depend on it. There is a correlation between the specific surface area (SSA) and the PSD of a given cement. The Blaine of a cement can be predicted based on a measured PSD (Jankovic *et al.*, 2004).

Cement grinding mill

The size of the clinker nodules, of which 80% lie between 10-20 mm, is normally reduced to 90 µm during this process. The grinding is generally done in a mill that can either be a ball mill (tube mill) or a vertical mill, as shown in Figure 2.3 (Joergensen, 2016).

The ball mill allows the comminution to take place by impact and attrition. This happens in two compartments of different lengths. The first compartment consists of larger balls of 80-50 mm that are used to grind coarse clinker. The second compartment is used to grind the ground clinker from the previous compartment using smaller balls of about 25 mm.These two compartments are separated by a diaphragm that allows only particles of a specific size to pass through to the second chamber. The ground material is collected in an air classifier where the fine fraction is air-swept out of the mill while coarse materials return to the mill.

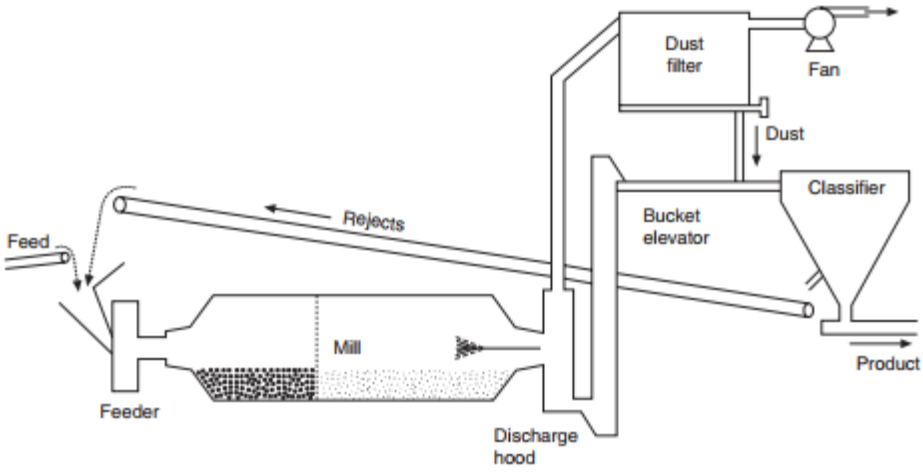

Figure 2.3: Closed circuit ball mill for cement grinding process (Newman & Choo, 2003)

The vertical mill allows the comminution to occur by exposing a bed of material to a pressure that is high enough to cause the fracturing of particles using rollers. This requires that a stable and consistent grinding bed be formed between the rollers and the geared table of the vertical mill. This has, however, been a challenge in cement grinding due to the disproportion in size of the ground cement and the feed material. Although more improvements have been made on the vertical mill by implementing newer technologies such as the vertical mill (OK mill), the ball mill is preferred to the vertical one.

The efficiency of the grinding systems cannot only be limited to the fineness, the specific surface or Blaine of the cement achieved. Its effects on the eventual performance of the ground cement are more complex and should be considered. Liu *et al.* (2015) discovered a numbers of factors that can significantly affect the performance of the cement due to the grinding process (e.g the dehydration degree of the added gypsum).

The effect of the grinding system on the dehydration of cement

Cement Grinding Office (2016) has reported that only 5% of the total energy supplied to the mill systems is used effectively, while the rest is converted into heat; energy that is generated heats up the ground cement in the mill and can cause the ambient mill temperature to rise up to 120 ^{o}C, depending on the initial temperature of the clinker and the characteristics of the mill (Nowack, 2015). Cement manufacturers pay special attention to the prevailing temperatures inside the mill. In the interest of minimizing issues related to setting (false or flash setting) and stiffening, these temperatures are limited to certain maxima by cooling the mill with water or fresh air. At temperatures within the range of 90-120 ^{o}C, the water of crystallisation of the added gypsum will partially be lost. Papageorgiou *et al.* (2005) confirmed that temperatures below 120 ^{o}C are considered to avoid excessive or complete dehydration of gypsum, generally achieved by spraying water into the interior of the mill. Under these conditions, the natural gypsum partially dehydrates into hemihydrate by losing half of its crystallisation water (Smallwood & Wall, 1981; Dunn *et al.*, 1987; Svinning *et al.*, 2008).

To a certain extent, the dehydration of natural gypsum is favourable for both cement hydration and storage as it increases the solubility of the calcium sulphate during cement hydration. This makes the gypsum more effective in controlling and retarding the hydration of the aluminate phase, thus improving the cement strength. The partial dehydration of gypsum is also desirable since its crystal water may cause cement particles to adhere or form lumps during cement storage. Moreover, the formation of these lumps increases in the presence of potassium sulphate that reacts with gypsum and yields syngenite during cement storage (Taylor, 2003).

Due to economic and environmental reasons, modern cement plants attempt to use less energy during grinding and shorten the retention time of the ground cement in the mill, without compromising the required cement fineness. However, this does not always allow the adequate dehydration of gypsum. Therefore, as a remedy, either more gypsum is added within the limit of SO_3 cement recommendations or more heat is supplied to the mill system to increase the gypsum dehydration or a more reactive form of gypsum is added such as hemihydrates (Joergensen, 2016).

2.3.5 Classification of cement

Based on the proportion of these chemical compounds and the physical properties achieved during grinding, the American Society for Testing and Materials (ASTM) designation C150 provides eight types of Portland cement.

Ordinary Portland cement

This type of cement consists of Portland cement clinker ground with a specified amount of gypsum. Table 2.1 describes different types of ordinary Portland cement and their applications.

Table 2.1: Different ordinary Portland cement type and their applications (Taylor, 2003)

Ordinary Portland cement type (OPC)	Application
CEM I	Suitable for all uses where the special properties of other types are not required. To be used where mortar or concrete is not exposed to sulphate attack from soil or water or objectionable temperature rise due to heat generated by hydration. Can be used for reinforced concrete building, bridges, pavements, reservoirs, tanks, railway structures and masonry units.
CEM II	Generates low heat of hydration. Can therefore be used in structures of considerable mass such as large piers, heavy abutments and heavy retaining walls. Suitable in moderate sulphate attack environments and where concrete is placed in warm weather.
CEM III	High early strength Portland cements. To be used when formworks are to be removed as soon as possible or when structure must be put into service quickly.
CEM IA, IIA, IIIA	These cements are similar to the corresponding CEM I, II and III types in terms of composition, except that small quantities of air-entraining materials are inter-ground with the clinker during manufacture to produce small well distributed air bubbles. Suitable for freeze-thaw action.
CEM IV	Low heat of hydration cement advisable for construction where the rate and amount of heat generated must be minimized, such as large gravity dams.
CEM V	Sulfate-resisting cement to be used only in concrete exposed to severe sulphate action.

Other Portland cements

White Portland cement (BL): This cement is made from raw materials containing very little iron and magnesium oxides. Its manufacturing requires higher firing temperatures since there are not enough iron elements. Unlike ordinary Portland, this cement has lower C_4AF contents, lower specific gravity and lower strength; however, its fineness is higher than that of ordinary Portland.

Calcium aluminate cement (CAC/R): The clinker is mostly constituted of calcium aluminate from aluminous and calcareous raw materials. These are very fast-hardening cements that can be used in pre-stressed concrete.

Blended hydraulic cement: These cements are produced by uniformly blending the Portland cement and the by-product materials such as blast-furnace slag, fly ash, silica fume and other pozzolans (e.g. Portland blast-furnace slag cement).

The potential mineral compounds of these cements are given in Table 2.2.

2.3.6 Cement chemical nomenclature

The oxides of cement clinker are preferentially designated by capital letters for technical and industrial purposes (Nelson *et al.*, 1990):

A: Al_2O_3

C: CaO

F: Fe_2O_3

S: SiO_2

M: MgO

H: H_2O

$\overline{S}$: SO_3

$\overline{C}$: CO_2

The anhydrous phases of ground cement are abbreviated (Zhang *et al.*, 2010; Hall, 2009) by:

$C_3S = Ca_2SiO_5$: Tricalcium silicate or alite

$C_2S = Ca_2SiO_4$: Dicalcium silicate or belite

$C_3A = Ca_3Al_2O_3$: Tricalcium aluminate or aluminate

$C_4AF = Ca_4Al_2Fe_2O_{10}$: Tetracalciumalumino ferrite or ferrite

Table 2.2 gives the required amount of these phases within ground cements with respect to each type of cement.

Table 2.2: Chemical composition ranges for ordinary Portland cements (Taylor, 2003)

	Phase							
	C_3S [%]		C_2S [%]		C_3A [%]		C_4AF[%]	
Type	Min	Max	Min	Max	Min	Max	Min	Max
CEM I	40	63	9	31	6	14	5	13
CEM II	37	68	6	32	2	8	7	15
CEM III	46	71	4	27	0	13	4	14
CEM IV	37	49	27	36	3	4	11	18
CEM V	43	70	11	31	0	5	10	19
White	51	72	9	25	5	13	1	2

2.4 The environmental impact of cement production

The increase of cement production has been assumed to be parallel with the evolution of modern societies, considering the cost and strength that it provides to all type of infrastructures, buildings and houses. Although this growth is ostensibly a positive factor for the economy and social development, its environmental impact is an issue deserving of special attention.

The cement manufacturing process not only requires a significant amount of raw materials but also a large amount of fuel as the heating source. As far as climate change is concerned, the cement industry has been reported as among the major contributors of carbon dioxide (CO_2) emission (Lin & Zhang, 2016). In fact, the cement industry sector is responsible for approximately 5% of the global CO_2 emission. Vargas and Halog (2015), conducting extensive research on the reduction of carbon emissions within the cement industry, confirmed that for every ton of cement produced, a ton of carbon dioxide is ejected into the atmosphere. Due to the population increase and the need for more efficient infrastructures, cement consumption has also drastically increased over recent decades and according to analysts, will further increase in the near future (Gao *et al.*, 2015).

In recent years, more attention has been given to the environmental aspects of material conversion. This has significantly affected the research towards possible modifications of ordinary Portland cement (OPC) to meet all possible demands for sustainability in the concrete industry. Consequently, strategies have been established to reduce the carbon emission in the cement industry around the world (Potgieter, 2012). Although there are many technologies available for CO_2 abatement, such as the utilization of alternative fuels and raw materials (AFR), the use of supplementary cementitious materials (SCMs) is still preferable due to their economical and engineering benefits (Vargas & Halog, 2015; Ishak & Hashim, 2015). SCMs are used to replace the clinker in ground cement during the cement manufacturing process or cement in concrete during concrete production. This underlines the fact that the emission of carbon is mitigated by

producing or using less cement. Fly ash, burnt furnace slag, limestone, silica fume and other pozzolanic materials have been used successfully for this purpose. These are mostly industrial by-products or wastes, the utilization of which assumes no additional emissions (Ataie & Riding, 2016).

2.5 Cement paste hydration

Hydration is referred to as a process that involves the contact of water and cement powder, and implies the transformation of cement paste from a fluid suspension to a porous solid after a few hours, progressively developing strength over days or months (Juilland *et al.*, 2010). The kinetics of cement paste hydration comprise numerous and simultaneous phenomena with specific mechanisms, including chemical and physical phenomena.

This section reviews the hydration of cement paste by considering firstly, the reactions that take place in poly-phase systems and secondly, those that occur in mono-phase systems. The latter consideration emphasises the reaction kinetics in the aluminate and gypsum phases since the early hydration of cement paste is predominantly controlled by their reactivity.

2.5.1 Chemical interactions within poly-phase cement systems

Chemical interactions within poly-phase cement systems include the dissolution, diffusion, growth, nucleation, complexation and adsorption of ions during the cement hydration process.

Dissolution mechanisms involve the disunion of molecular units from the surface of a solid in contact with water. Wang *et al.* (2016) confirmed that during cement hydration this mechanism is more characterized by the dissociation of Ca^{+} and $Al(OH)^{-}_{4}$ ions. Bisschop and Kurlov (2013) have reviewed and researched intensively on the dissolution of the main cement phases such as alite and belite, whereas, the dissolution of gypsum in the early hydration of cement paste has been studied by Burgos-Cara *et al.* (2016). Diffusion mechanisms define the transport of solution components through the pore volume of cement paste or along the surface of solids in the adsorption layer.

Nucleation and growth activities involve both the precipitation of solids (either heterogeneously or homogeneously) on the solid surfaces and the incorporation of these molecular units into a crystalline or amorphous solid within the solution (Bullard *et al.*, 2011; Bishnoi & Scrivener, 2009). Complexation and adsorption relate to the reaction that occurs between ions to form complex ions or molecules and accumulate on the surface of solid particles.

It has been observed in many experimental works that these mechanisms can occur in series, in parallel or in some complex combination. They also happen at different stages and rates during hydration. This makes the investigation of these mechanisms individually difficult. In addition, they cannot be observed directly due to the fact that they occur on a microscopic scale (Bishnoi, 2008). Consequently, scholars have used different techniques in combination to study the Portland cement hydration process, techniques that involve the determination of the amount of non-reacted clinker minerals and calcium sulphate and/or by determining the amount of the formed hydrate phases over time (Odler, 1998).

Since the hydration of cement is an exothermic reaction, the thermodynamic approach is the primary approach for identifying this process. The chemical processes that occur over the course of cement hydration can therefore be associated with the heat flow curves, as presented in Figure 2.4 (Salvador *et al.*, 2016). Jolicoeur and Simard (1998) subdivided this process into five parts corresponding to the hydration stages: initial hydration, induction period, acceleration and set, deceleration and hardening, and finally, curing.

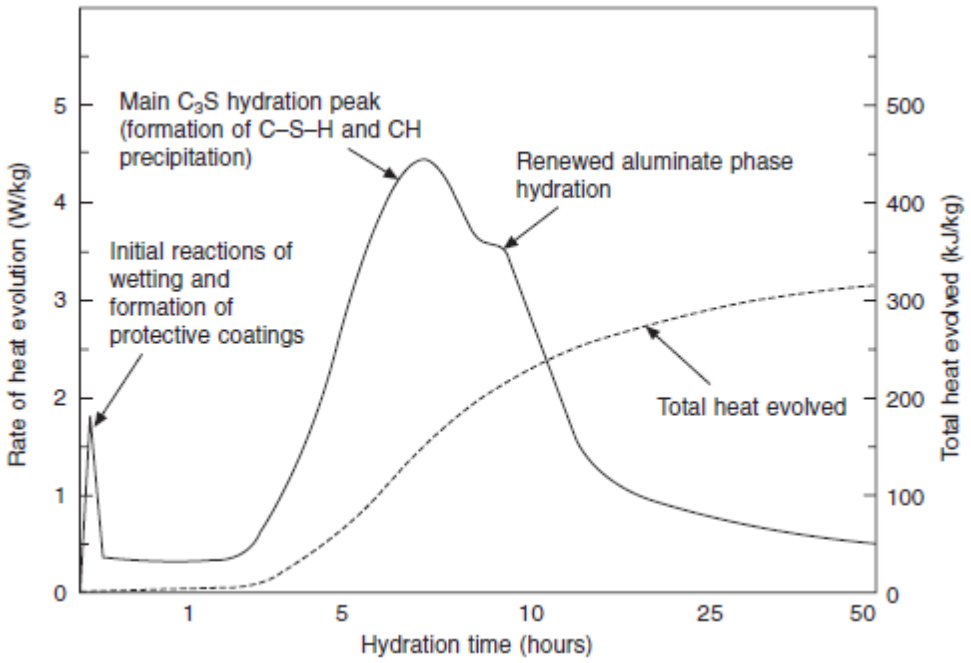

Figure 2.4: Typical cement hydration stages describing the heat flux curve (Newman & Choo, 2003)

First stage: Initial hydration

During this period, the easily soluble phases such as alkali $NaSO_4$, KSO_4 and gypsum components dissolve into the aqueous solution. Simultaneously, the hydrolysis of aluminate and silicate releases Ca^{2+} and OH^- ions from their surfaces. The concentration of soluble alkali in the

solution influences the dissolution of aluminate and silicate phases, thereby increasing their solution concentration with increase in pH. It is clear that in this stage of the hydration, water plays the role of wetting the highly hygroscopic cement compounds, causing the hydrolysis of their surfaces. This degradation leads to the formation of a gel-like thin layer which consists mostly of aluminate hydrates. Tricalcium silicate dissolves congruently and C-S-H gels also form rapidly around the C_3S particles during this period. This has been demonstrated by Roussel *et al.* (2012) and furher discussed by Juilland *et al.* (2010). Odler (1998) reported that the fraction of C_3S hydrated in this period remains low and was estimated at around 2-10%.

Besides the dissolution process, nucleation and growth mechanisms take place as well during this period. For instance, calcium sulfoaluminates are one of the most important hydration products that nucleate and grow from the interaction of Ca^{2+}, SO_4^{2-} and the $Al(OH)_4^-$ ions during this stage. The rate of these mechanisms depends on the concentration of the precipitated ions, the availability of water to the reaction sites and the activation energy for the formation of molecular units (Jolicoeur & Simard, 1998).

The occurrences of all these mechanisms are not the only contributors to the rapid heat evolution observed during this stage. The type of calcium sulphate (i.e hemihydrate) has also been identified by Kumar *et al.* (2012) as another factor influencing the heat liberation during OPC hydration.

Second stage: Induction period

After about 15 minutes, the rate of heat evolution drops drastically and becomes constant. In literature, this is referred to as the *dormant period.* It is worth clarifying that the hydration process does not stop during this period, but occurs at a very low rate. Processes that started in the previous period continue in the dormant phase. The very beginning of this stage is dominated by the reaction of aluminate C_3A. During the course of this period, different ions available in the suspension arrange themselves in a regular way and form nuclei. The formation and disintegration of these nuclei continue until they reach critical sizes (Kumar *et al.*, 2012).

A number of phenomena are observed during this stage: the growth of ettringite (mostly of needle like shape), the gradual thickening of the gel layer on the cement particles surface, disproportional nucleation and growth of both calcium aluminate hydrate (CAH) and gypsum crystals depending on the concentration of SO_4^{2-}. A low concentration of these ions allows the development of CAH, while higher concentrations favour the formation of gypsum crystals. In this case, flash set has to be distinguished from false set, the latter taking place at high concentrations of sulphate ions available in the suspension, whereas the former occurs at lower concentrations.

It has been proven that the presence of hemihydrate and alkali sulphate increases the concentration of sulphate ions. When there are enough sulphate ions in the aqueous phase, numerous reactions take place yielding phases that contribute to the rigidification process of cement paste systems. For instance, ettringite crystals grow continuously, the increase in production of C-S-H gel, accretion of Ca^{2+} and OH^- concentrations in the suspension and transformation of ettringite (AFt) to monosulfoaluminate (AFm) when the present sulphate has been completely consumed. Jolicoeur and Simard (1998) assured that most of cementitious material properties, such as setting time and flow behaviours, depend actively on the development of these reactions.

Third stage: Acceleration period

There are a number of hypotheses that have been suggested by various researchers intending to explain the essence of the slowing down of the hydration during the dormant phase and the onset of the acceleration period. The rate of heat liberation sharply increases during the third stage of hydration attesting to a significant augmentation in the number and energy of the physical and chemical interactions between the growing cement phases. The rate of heat evolution reaches its maximum after a few hours of hydration.

There have been various views regarding the cement phase responsible for this hydration period. Kumar *et al.* (2012) observed that this period is mostly due to the hydration of C_3S phase in the cement. Aïtcin and Flatt (2016) confirmed that the hydration of C_3A and C_3S does not happen simultaneously. In particular, Barnes and Bensted (2002) specified that after the induction period, only 2% of the total amount of C_3S hydrated, and only around 10% of the same amount would hydrate at the end of the acceleration period. They also attributed the peak identified in this period to the hydration of the main cement phase, C_3S. Scrivener *et al.* (2015), after extensively reviewing the different mechanisms controlling the hydration of Portland cement, reported that the rate controlling the acceleration period or the heat evolution peak was related to the growth of C-S-H.

It is also accepted that during this period, the calcium hydroxide (CH) precipitates from the liquid phase and, together with the concentration of Ca^{2+}, gradually declines. The SO_4^{2-} completely dissolves and its concentration in the pore solution begins declining due to the formation of AFt phase and adsorption on the formed C-S-H phase. The evolution of the hydrates formed during this period has been estimated by Odler (1998), as given in Figure 2.5.

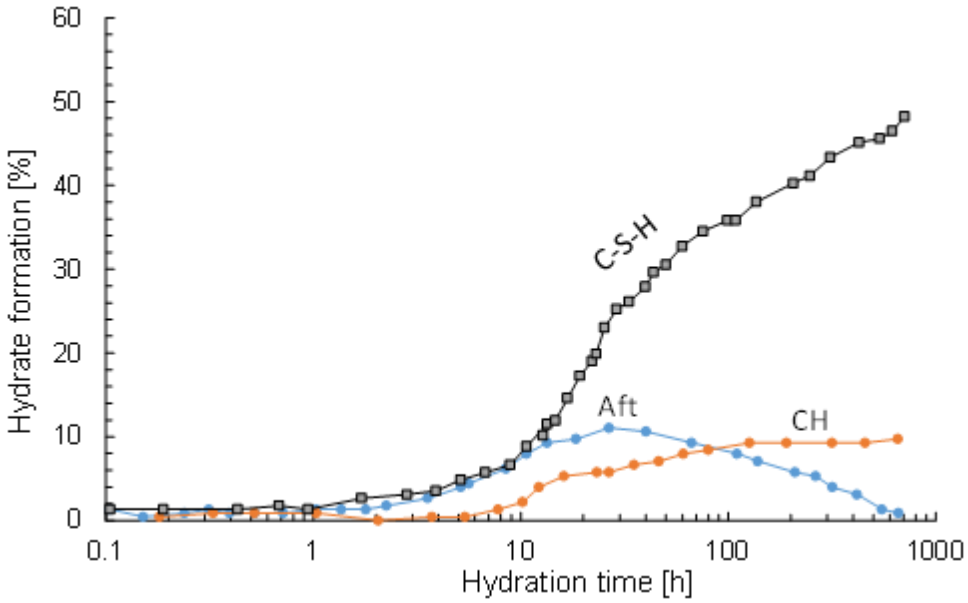

Figure 2.5: Formation of hydrate phases during cement hydration (Odler, 1998)

Bellmann *et al.* (2015) have recently focused on the dissolution rate of alite in the presence of other cement compounds, while Bullard *et al.* (2011) studied the interaction of Alite and aluminate during cement hydration and found that, although C_3S is the main cement compound that controls the mechanism of cement hydration during the acceleration stage, C_3A governed the early hydration depending on the amount of calcium sulphate available in the system for the formation of the AFt phase.

Fourth and Fifth stage: Deceleration period

Immediately after the second heat evolution has reached its peak, the hydration continuously decreases. This stage is referred to as the *deceleration period*. In this stage the reaction is more controlled and dominated by the diffusion mechanism due to the formation of a significant amount of hydrate products (Kumar *et al.*, 2012). Hesse *et al.* (2011) discovered that, due to the rapid growth of hydrate products in the previous period, the amount of water available within the suspension is reduced and the rate of dissolution of the cement compounds decreases. Consequently, the precipitation of hydrate products slows down until the reaction becomes diffusion controlled.

Beside the decrease in water quantity, Bullard *et al.* (2011) suggested other factors that may contribute to the deceleration of heat evolution, including the particle size distribution of the solid phase in the system and the lack of space. They attested that the effect of PSD is as important during the main peak of hydration as it is in the post peak stage. In fact, smaller particles are consumed quicker and leave only larger ones to react. For instance in cement systems, particles

of about 3 µm are completely consumed after 10 hours, while those below 7 µm after 24 h. Therefore, the researchers investigated the mechanisms that control this period of hydration, finding that diffusion was not the only mechanism prevailing during this stage. They demonstrated that although diffusion mechanisms control most of this period, its onset is dominated by nucleation and growth mechanisms that favour the yielding of considerable amounts of hydrate products. The progress of these activities reduces the available surface for the next products in the system, so that the rate of hydration shifts from accelerating to deceleration defined by the diffusion mechanism at the later stage.

The formation of hydrate products during this hydration phase was evidenced by Kumar *et al.* (2012) who noticed an imperceptible peak (on the heat flow rate curve) adjacent to the main peak that is generally difficult to distinguish from one another in poly-phase cement systems. They attributed this maximum to the depletion of sulphate, characterized by the renewal of C_3A dissolution. Clarity between the depletion of sulphate and the second dissolution of C_3A was ascribed by Aïtcin and Flatt (2016) and distinguished as demonstrated in Figure 2.6.

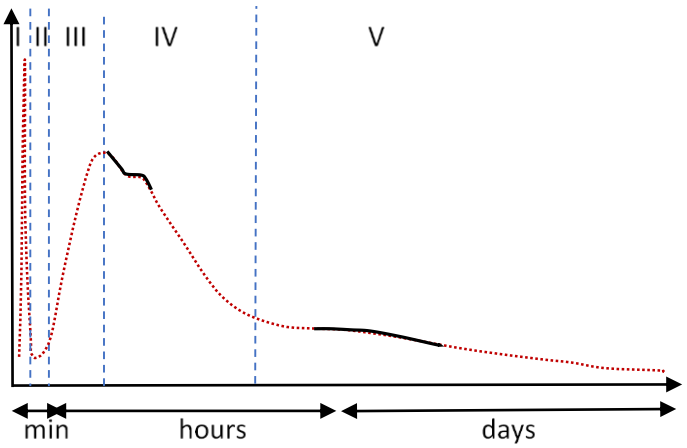

Figure 2.6: Regions of sulphate depletion and the second dissolution of C_3A during hydration (Aïtcin & Flatt, 2016)

The main peak between phase III and IV corresponds to the main hydration of C_3S. The small peak (shoulder) observed during the fourth stage (IV) was attributed to the depletion of sulphate leading to a more massive C_3A hydration. The hump in phase V defined the conversion of ettringite to monosulfoaluminate. This was concluded by confirming the interdependence of the aluminate and alite phases during cement hydration.

Finally, it is clear that the heat of hydration is primarily influenced by the proportion of alite and aluminate in the cement system. However, it is true that the water-cement ratio, fineness of

cement grains and the curing temperature also affect the liberation of heat during hydration. Variation in these factors will cause change in the heat of hydration and thus the kinetics of cement paste hydration.

2.5.2 Effects of hydration on cement paste microstructure

The microstructure of cement paste is strongly affected by the evolution of the hydration process, which explains why cement systems are known as “living structures” and as such, are time and temperature dependent materials (Nehdi & Al Martini, 2009; Saleh Ahari *et al.*, 2015).

The microstructure of cement paste can be defined by considering different parameters such as pore size distribution, porosity, number of hydrated compounds and strength development of the system. All these properties depend firmly on the hydration products of various cement phases. For instance, Ma *et al.* (2015) and Kamali and Ghahremaninezhad (2016) studied the effect of some admixtures on the microstructure of Portland cement focusing solely on the pore size distribution and the porosity changes in the hydrated cement systems. Similarly, Yu and Brouwers (2011) studied the effect of β-hemihydrate on the strength growth of calcium sulphate based materials by investigating the microstructure development of the hydrated systems.

Morphology of main cement hydrates

Several investigations on the cement paste microstructure have reported a number of changes that occur on the main hydration products, such as calcium aluminate hydrate (CAH), portlandite (CH) and calcium silicate hydrate (C-S-H) (Rossen *et al.*, 2015). These changes affect and define the flow and mechanical properties of cement paste.

Ciach and Swenson (1971) followed the hydration of C_3A in different systems. They firstly observed it in a pure phase, discovering that the very first hydration products were dominated by C_2AH_8 in hexagonal form of semicrystalline foils and plates. After 1 hour of hydration, the cubic hydrogarnet phase of 1 μm crystal size appeared in the hexagonal phase and only became dominant after 1 day. Secondly, they considered the pure phase of C_3A in the presence of the gypsum phase, observing in the first few minutes of hydration some partly rolled, semicrystalline foils and rods in the form of flower-like aggregates on the surfaces of gypsum crystals. After one day of hydration, the main hydration product became dominated by ettringite, short and rod-like particles of the sulphate form of CAH. At the onset of setting, the hydration products became a loose and amorphous mass covered by ettringite of a coin-in-coin type. After the cement paste had set, the microstructure was similar to that of a loose structure made up of unoriented thin hexagonal plates.

Richardson (2000) and other scholars such as Goñi *et al.* (2012) acknowledge the fact that cement paste properties depend strongly on the characteristics of the C-S-H and CH phases. They have very complex structures that exhibit different shapes at specific scales (Constantinides & Ulm, 2004). On the atomic scale, their structure is described as a hydrate with layers arranged in a disorderly manner, whereas at nanoscale, they have been observed as gel-like materials with properties similar to those of a colloidal (Fonseca & Jennings, 2010).

Although there are various models that have been used to characterize the C-S-H morphology (Jennings, 2008), all agree on a few aspects pertaining to its structure. For example, C-S-H is determined by the inside and outside parts. These sides are referred to as the inner (IP) and outer (OP) hydrate products, respectively defining the products that lie inside and outside the cement particles (Powers, 1958). Two types of C-S-H morphology can therefore be observed based on these defined entities of its hydrate products, as illustrated in Figure 2.7. The OP corresponds to the C-S-H gel of a less dense morphology, mostly found in the space originally filled by water, while the IP coincides with C-S-H gel of denser morphology that is generally found in the space occupied by the cement particles (Hu *et al.*, 2016; Tennis & Jennings, 2000).

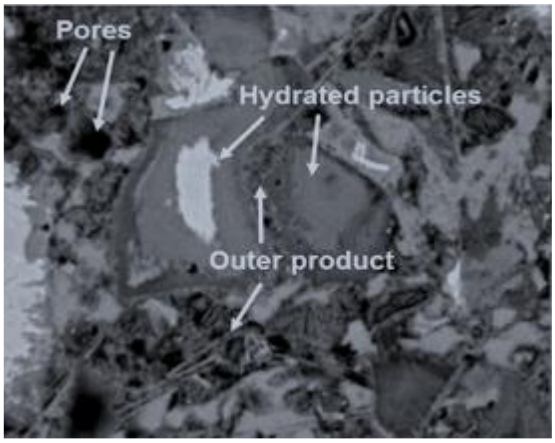

Figure 2.7: The C-S-H morphology of a mature cement paste (Stutzman, 2004)

Garrault *et al.* (2006) reported that during cement hydration, the low-density C-S-H is formed exclusively in the early stage while the high-density C-S-H is most abundant in the later stage of hydration. Fonseca and Jennings (2010), studying the effect of hydration on the morphology of C-S-H, found that at each stage of hydration, C-S-H presented a specific morphology that could be affected by more than one parameter, such as water to cement ratio (w/c), temperature of curing and ambient relative humidity. Moreover, they observed that C-S-H can possess more than one shape in the early stage of hydration. The OPs of some young pastes were fibrous, similar to partly rolled sheets of 0.5 to 2 µm in length. In other pastes, their OPs were either an interlocking structure comparable to a reticular network or they consisted of an equant grain morphology.

However, at a later stage, the structure of C-S-H was dominated by the OP with a more stable structure.

Ma *et al.* (2015), investigating the effect of the w/c ratio on the C-S-H structure, revealed that the capillary pores that prevail in the vicinity of the OP are quite small, with their porosity depending on both the degree of hydration and the w/c ratio. They therefore established a relationship between the hydrate porosity and the w/c, based on the degree of hydration as defined by Equation (2.1):

$$\phi_{SCP}^{CSH} = \frac{0.63w/c - 0.226\alpha}{0.852w/c - 0.09\alpha} \tag{2.1}$$

With ϕ_{SCP}^{CSH} the porosity of outer C-S-H product with small capillary pores (SCP); *w/c* water cement ratio; and α the degree of hydration.

This equation is a more meaningful relationship than a purely empirical one. It implies that in cement paste, the porosity of the outer C-S-H structure will decrease with the increase in the degree of hydration, thereby promoting the strength development of the cement paste.

Although C-S-H remains the main hydrate product in poly-phase cement systems, there are other hydrate products that develop in the available space of the C-S-H gel, including portlandite (CH), ettringite (Aft) and monosulfoaluminate (AFm) (Richardson, 2000; Hu *et al.*, 2016). These hydrates may affect the features of the C-S-H structure (defined by the presence of calcium and oxygen on the central layer which is flanked on both sides by tetrahedral chains of silicate) by increasing its Ca/Si ratio (Trapote-Barreira *et al.*, 2014). Several values of Ca/Si atomic ratio characterizing the structure of C-S-H have been suggested in literature, but doubt still remains as to the value over 1.50 (Rossen *et al.*, 2015).

Conversely, other hydrate products have well-defined crystalline structures, as shown in Figure 2.8. CH or portlandite has a penny-shaped structure and can be modelled as oblate. Ettringite has prismatic needles or sometimes flower like-aggregates, whereas monosulfoaluminate has a shape similar to that of CH, but with a smaller size (Hu *et al.*, 2016; Richardson, 2000).

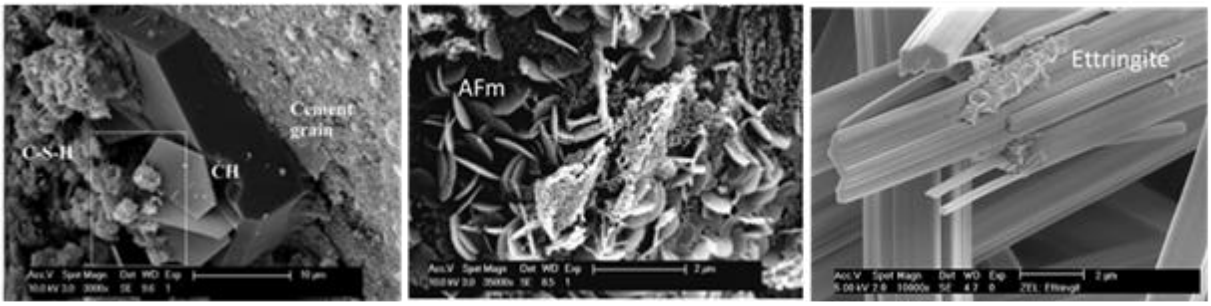

Figure 2.8: The morphology of other cement hydrate products: portlandite, monosulfoaluminate and ettringite (D'Ayala & Fodde, 2008)

Mechanical properties

The physical properties of cement paste depend on the changes that occur on the structure of the hydrate products, changes which include the increase in specific surface area, the decrease in the pore size distribution and the continual rigidification of the cement paste system (Thomas & Jennings, 2006). Constantinides and Ulm (2004) evidenced this by using the nanoindentation technique, showing that the macroscopic elastic properties of cement paste can be predicted accurately by the intrinsic properties of C-H-S. Subsequently, the mechanical properties of cement paste depend strongly on the hydration of the available cement phase contents. Their contributions to the overall strength development of cement systems are very different, as illustrated in Figure 2.9.

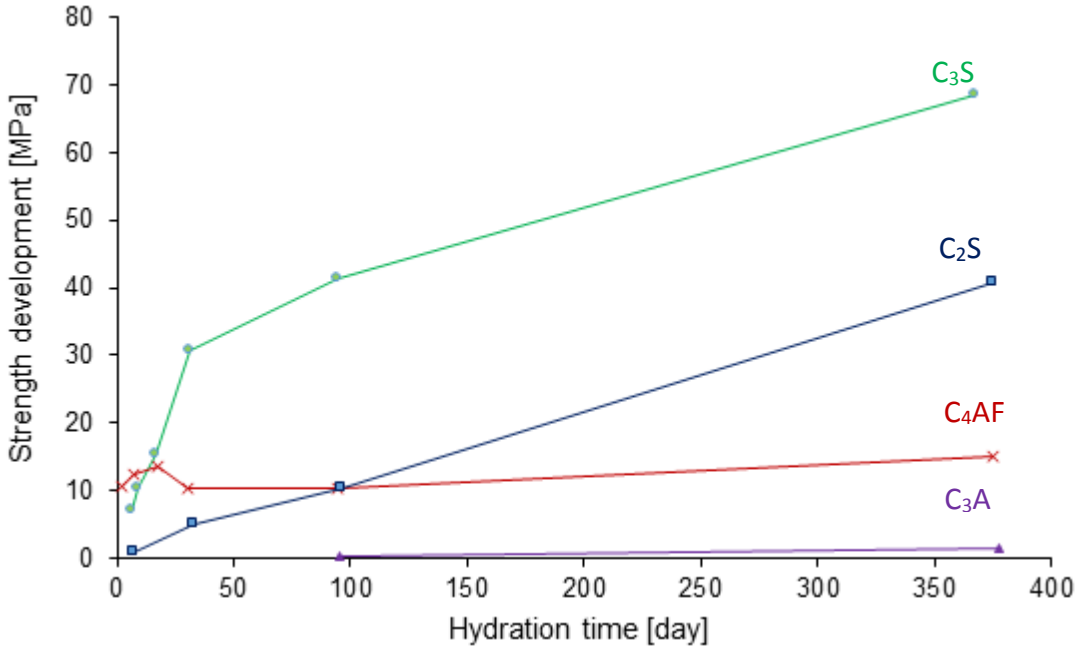

Figure 2.9: Contribution of main cement phases to the strength development of cement paste at 20 °C with w/c=0.45 (Hewlett, 2001)

It is worth noting that, although all cement phases contribute to the strength development of the cement paste at different times with distinct magnitudes, the overall strength of the cement system at a specific time cannot be considered as an additive function of the individual cement phase strength. Certainly, for a cement composition with a constant amount of gypsum and a well-specified fineness, relationship can be established between the strength and the cement phase provided that regression coefficients be determined correctly, as suggested by Hewlett (2001) in Equation (2.2):

$$\sigma = a_o + a_1 C_3S + a_2 C_2S + a_3 C_3A + a_4 C_4AF \quad (2.2)$$

With $a_0,\ a_1, \ldots . a_4$ regression coefficients whose magnitudes depend on the hydration time and approached testing method.

Besides these cement clinker main phases, the presence of minor oxides such as alkali oxides (Na_2O and K_2O) and SO_3 also affect the strength of the cement paste. In fact, the exact amount of calcium sulphate that yields the highest strength depends on the composition of the clinker, cement fineness and the form of added sulphate.

2.5.3 Chemical interactions within mono-phase cement systems

The early hydration of cement is governed mostly by the reactions of the most reactive clinker phase, such as aluminate compounds C_3A, with the added gypsum phase. It is thus important to

understand the fundamentals of their interactions within the cement systems. This section introduces first of all the absolute hydration of the gypsum phases; thereafter, it discloses the role of gypsum in cement systems; finally, it addresses the C_3A-gypsum phase interactions during the early hydration of cement.

Hydration of gypsum phases

Gypsum is actually a sulphate dihydrate that can be found in many countries across the world with widespread use. It can be used either in its natural or burnt form. The latter produces hemihydrate and is used mostly in buildings, ceramic and medical industries, while the former is used in agriculture and in Portland cement. However, gypsum in its burned form is the most readily available product on the market because the majority of gypsum production is burnt. Almost 30% of the global gypsum production is utilized in the cement industry, while only 11% is used in agriculture (Yu & Brouwers, 2011; Camarini & De Milito, 2011).

Gypsum-based binders owe their reactivity to the dehydration of the dihydrate part of gypsum $CaSO_4.2H_2O$. The dehydration of gypsum depends on many factors, including the temperature, the vapour pressure and the heat inside the furnace, as well as the fineness and density of the raw materials (sulphate dehydrate) (Camarini & De Milito, 2011).

Gypsum dehydrates and yields different products depending on the temperature that it has been exposed to, as given in Equations (2.3) through (2.5). Hence, β-hemihydrate ($CaSO_4.0.5H_2O$) is formed when gypsum is heated at temperatures between 100-180 ^oC. Anhydrite III ($CaSO_4.\varepsilon H_2O$, with ε ranging between 0.06 and 0.11) is obtained when gypsum is heated at temperatures below 300 ^oC. Anhydrite II ($CaSO_4$) is obtained when gypsum is heated at temperatures over 300 ^oC (Camarini & De Milito, 2011; Pan *et al.*, 2013).

$$CaSO_4.2H_2O \xrightarrow{<180^oC} CaSO_4.O.5H_2O + 1.5H_2O \quad (2.3)$$

$$CaSO_4.2H_2O \xrightarrow{<300^oC} CaSO_4.\varepsilon H_2O + (2-\varepsilon)H_2O \quad (2.4)$$

$$CaSO_4.2H_2O \xrightarrow{>300^oC} CaSO_4 + 1.5H_2O \quad (2.5)$$

Hemihydrate and anhydrite III, when they react with water at room temperature, produce dehydrate. Yu and Brouwers (2011) confirmed that the properties of gypsum are mainly influenced by the hydration kinetics of the hemihydrate phase. This reaction is followed by the

formation of a network of gypsum crystals that are reported by Camarini and De Milito (2011) as the main factors of gypsum based materials properties.

Yu and Brouwers (2011) have investigated the hydration of hemihydrate and subdivided this reaction into two distinct steps: firstly, the material dissolved quickly just after mixing it with water and the reaction was described, as per Equation (2.6); secondly, the generated dehydrate precipitates from the solution, as shown in Equation (2.7).

$$CaSO_4.0.5H_2O \rightarrow Ca^{+2} + SO_4^{-2} + 0.5H_2O \quad (2.6)$$

$$Ca^{+2} + SO_4^{-2} \rightarrow CaSO_4.2H_2O \quad (2.7)$$

These researchers, studying the microstructure of the hemihydrate phase based on the defined chemical reactions that occur during its hydration, concluded that the total volume of the hydrate product was formed primarily by a significant fraction of gypsum, a small portion of remaining hemihydrate and a fraction of void spaces that presumably contain air or water. Using the ultrasonic wave method, Yu and Brouwers (2011) observed two important regions that characterized the hydration kinetics of this gypsum phase, as illustrated in Figure 2.10. First and foremost, they recorded low constant values of velocity at the beginning of hydration, evidencing the early formation of a stable microstructure within the system. During this period, the nucleation and progressive growth of gypsum crystals take place until they saturate the suspension. Afterwards, the ultrasonic velocity rapidly increase due to the changes that occur in the voids fraction and physical properties of the hydrating system. This indicated the generation and precipitation of gypsum crystals. Finally, the rate of the ultrasonic velocity gradually decreased until it reached a plateau, essentially due to the reduction of free ions within the suspension after the precipitation of sufficient amounts of gypsum crystals.

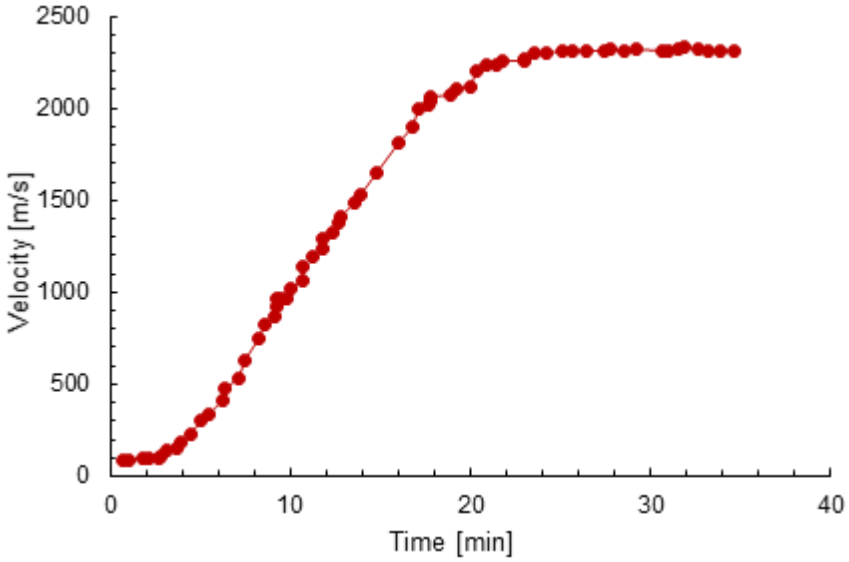

Figure 2.10: Hydration kinetics of β-hemihydrate investigated by the means of an ultrasonic velocity method (Yu & Brouwers, 2011)

The duration of these zones depended largely on the quantity of the liquid phase. From this, they therefore suggested that the hydration of gypsum-based materials is water dependent, highlighting the sensitivity of the β-hemihydrate microstructure to the initial amount of water used during hydration. The singularity in the hydration kinetics of the gypsum phases has already been pointed out by Maksoud and Ashour (1981) who researched the hydration of gypsum based systems, focusing on the theoretical prediction of heat released during the reactions. They demonstrated through standard heat formation methods that the heat released by the type of gypsum increased depending on the available molecule of crystal water in that gypsum phase. Consequently, hemihydrate had less heat released (5 Kcal/g) as compared to anhydrite, with 29 Kcal/g.

Some studies have also shown that kinetics are influenced once exposed to foreign ions. Lewry and Williamson (1994) and other scholars such as Singh and Middendorf (2007), Bobby and Singamneni (2014) and Zhou *et al.* (2016) studied the hydration of hemihydrate in the presence of various anions. They observed that the hydration of hemihydrate was accelerated when dihydrate was added to the hydrating hemihydrate systems. This was mostly due to the enhancement of nucleation sites that depend on the surface area and the amount of gypsum added in the system. However, it was found that hemihydrate in the presence of alkali sulphate (Na_2SO_4, K_2SO_4) reacted faster as compared to other anions and cations by increasing the rate of hemihydrate dissolution.

The role of gypsum phase in cement systems

It was stated already in section 2.3.4 that gypsum is added to the ground clinker as set regulator of ordinary Portland cement. This addition is of great importance because it allows the cement paste to remain plastic for a certain duration, so the workability of the fresh cement paste is therefore extended. With no gypsum phase in the ground clinker, the hydrating system experiences flash set phenomena and within a few minutes becomes stiff and difficult to handle. This is the reason why there is no commercial Portland cement without gypsum.

Undoubtedly, without the gypsum phase, the C_3A phase yields calcium aluminate hydrates (CAH) by realising profuse exothermic heat with respect to Equation (2.8), rendering the matrix stiff with no chance of being remixed. The yielded CAH in this condition does not contribute to the matrix strength and impedes the early hydration of other cement phases such as calcium silicate (Bhanumathidas & Kalidas, 2004).

$$3CaSO_4.Al_2O_3 + nH_2O \rightarrow CAH + \text{significant exothermic heat} \quad (2.8)$$

It is therefore imperative to find ways to control the C_3A reaction. This was made possible by the use of sulphate salts. Since aluminates and sulphates tend to attract each other naturally, aluminate readily reacts with sulphate once in the solution, thus preventing the reaction of C_3A and water. Eventually, gypsum was identified as the most effective source of sulphate to supply to C_3A hydration, as described in Equation (2.9):

$$3CaSO_4.Al_2O_3 + 3CaSO_4.2H_2O + nH_2O \rightarrow 3CaO.Al_2O_3.3CaSO_4.32H_2O + \text{moderate exothermic heat} \quad (2.9)$$

Natural gypsum has been used since as a set regulator in cement matrixes. However, the potential ability of gypsum-based materials to act as set accelerators has been neglected by many investigators. This lack in knowledge has misled many, supposing that the more gypsum is added to the ground clinker OPC, the more additional retardation in setting occurs. This is absolutely not true, due to the fact that if the formation of ettringite surpasses a certain limit, the hardening process of the matrix is accelerated and consequently hastens strength at early ages resulting in false set (Bhanumathidas & Kalidas, 2004).

Barnes and Bensted (2002) have studied a number of setting abnormalities that might occur depending on the availability and quality of calcium sulphate within the cement paste. Setting has been considered as the first physical consequence of the chemical interactions that happen within

the paste. It is therefore defined as the transformation of a workable plastic cement paste into a rigid material (Hildago *et al.*, 2008). Generally, the setting of cement paste depends on the relative rate at which the ions are released from the cement phases into the liquid phase and their reactions to form initial hydrate products responsible for the rigidification of the cement paste. In most instances, abnormal setting phenomena can be traced to the chemical reaction of the aluminate and gypsum phases. A false set causes a rapid increase in paste rigidity without excessive heat evolution and can be dispelled by mixing to regain the lost plasticity. This is frequently due to a rapid crystallization of gypsum from the liquid medium, as a consequence of excessive dissolutions of the hemihydrate phase present in cement paste.

Flash set, however, causes a severe and irreversible stiffening of the paste followed by a strong heat evolution induced by the excessive reaction of the C_3A cement phase with the liquid phase in the earliest stage of hydration. The AFm phase is consequently formed as a result of the high dissolution rate of aluminate phases relative to the rate at which sulphate and calcium ions are being transported to the reacting aluminate surfaces. During cement storage, pack set can also occur. This is defined as warehouse or silo set and is characterized by a decrease in flowability of the unhydrated cement powder. Pack set is directly related to the dehydration of natural gypsum during cement grinding and to silo ambient temperatures. Although this set happens during storage rather than after mixing cement with water, pack set can alter the whole course of cement hydration reactions (Barnes & Bensted, 2002).

In view of this behaviour, the amount of SO_3 in OPC is limited and varies from one country to the other. For instance, the European code recommends an amount of SO_3 in some cements to be between 3.5 to 4%. The Indian specifications limit the content of sulphate to a maximum of 2.5% for cements which have a C_3A content of less than 5% and a maximum of 3% for cements with C_3A content more than 5%. However, for blended cements, especially with fly ash and slag, the resultant calcium aluminate is more than what is generally available in OPC. Therefore, these threshold levels of gypsum are increased in order to overcome the weakness of strengths at early ages (Bhanumathidas & Kalidas, 2004).

It is clear that gypsum is not only used in cement as a set regulator but also influences the strength rate development of cement paste by either accelerating or decelerating the hydration of the alite phase. It is therefore required that an optimum content of gypsum be selected as the amount of gypsum that favours normal setting, maximizes strength rate development and maintains the volume stability of the cement paste. Barnes and Bensted (2002) have reported a few factors that influence the optimum gypsum content within the ground cement, including specimen age, type

of gypsum phase (as illustrated in Figure 2.11), temperature of curing, the amount and reactivity of C_3A phase and the w/c ratio.

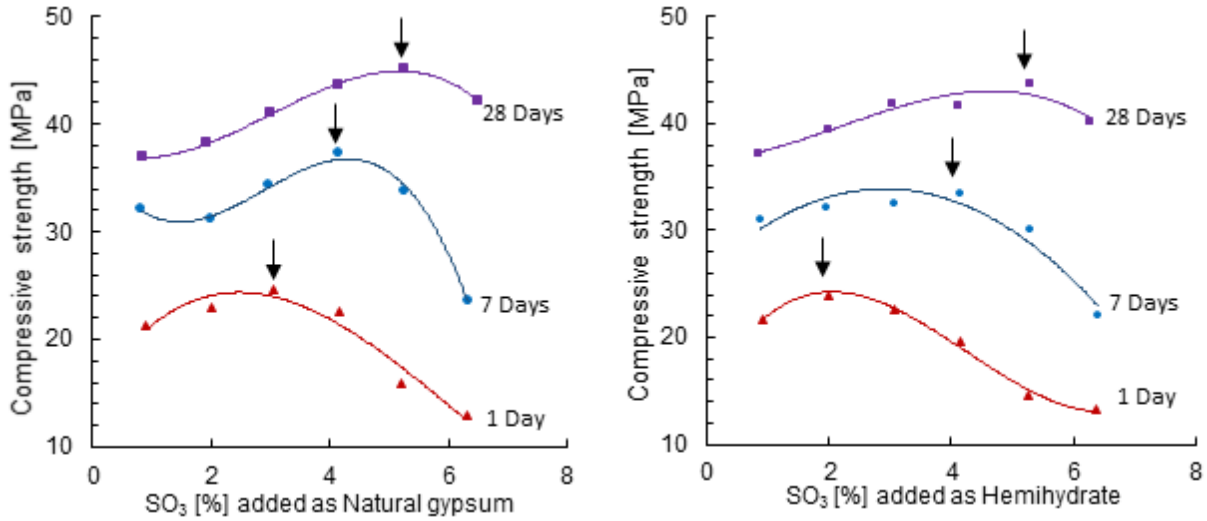

Figure 2.11: Optimization of sulphate additions from different gypsum phase types (hemihydrate, natural gypsum) (Barnes & Bensted, 2002)

Hydration of cement aluminate phase in the presence of gypsum phase

The chemical reaction of C_3A and calcium sulphate in water is important to understand as it affects the early hydration of cement pastes (Danner *et al.*, 2016). When cement comes in contact with water, C_3A immediately reacts with gypsum and yields ettringite (AFt) as the first stable hydration product. The production of ettringite will continue as long as there are enough sulphate ions in the suspension. When all the available gypsum is consumed, ettringite becomes unstable and starts reacting with the remaining C_3A amount to produce monosulpho-aluminate hydrate (AFm) phases.

Ettringites are formed around the C_3A cement grains, preventing them from further rapid hydration. This is referred to as C_3A retardation in the literature. The precipitation of ettringite plays a major role in controlling the hydration rate of C_3A and thus assures the plasticity of the fresh cement paste (Scholtzová *et al.*, 2015). Numerous studies have investigated the effect of ettringite formation and the deceleration of cement paste hydration. Two important theories around this subject have been suggested.

The first hypothesis states that during cement hydration, the yielded ettringite precipitates and forms a layer around the cement particle, preventing water from reaching the unhydrated C_3A phase (Havlica *et al.*, 1993). Consequently, the hydration slows down until this layer is broken. The second hypothesis stipulates that the adsorption of calcium and sulphate ions on active

dissolution sites of C_3A would be the main cause of the slowdown of cement hydration (Quennoz & Scrivener, 2012).

Much evidence has been provided to validate these hypotheses. Quennoz and Scrivener (2012) reported the ambiguity of the first theory based on previous works and showed that in the early hydration, the morphology of the formed ettringite is unlikely to provide a substantial barrier around cement particles. In addition, Minard *et al.* (2007), studying the mechanisms of retardation of C_3A hydration in the presence of gypsum, have also questioned the possibility of the formation of a layer around the cement particles as the origin of the slowdown of the hydration process.
Two setups consisting of controlled and uncontrolled C_3A hydrations were investigated. It was observed that during early hydration where C_3A was not controlled, hydroaluminate or hydroxyl AFm phases precipitated from the suspension without stopping the C_3A hydration. When C_3A hydration was controlled using hemihydrate as calcium sulphate source, it was observed that the dissolution rate of C_3A was so high even after all sulphate ions were consumed. Therefore, it was concluded that neither ettringite nor AFm precipitations could be at the origin of the slowing down of C_3A hydrations. Alternatively, they attributed this phenomenon to the specific adsorption of Ca^{+2} and/or SO_4^{-2} ions on the surface grains of C_3A which block the dissolution sites of C_3A. This prodived enough evidence to explain the high C_3A dissolution rate which was observed after the sulphate depletion within the system.

The mechanisms of C_3A hydration in the presence of gypsum has been studied extensively by Minard *et al.* (2007) who, in considering various parameters including the ionic concentration evolutions of aluminium, sulphate and calcium, the granularity of C_3A grain and the amount of C_3A consumed during the C_3A-gypsum hydration, found that the hydration of C_3A in the presence of gypsum could be divided into two periods, as illustrated in Figure 2.12.

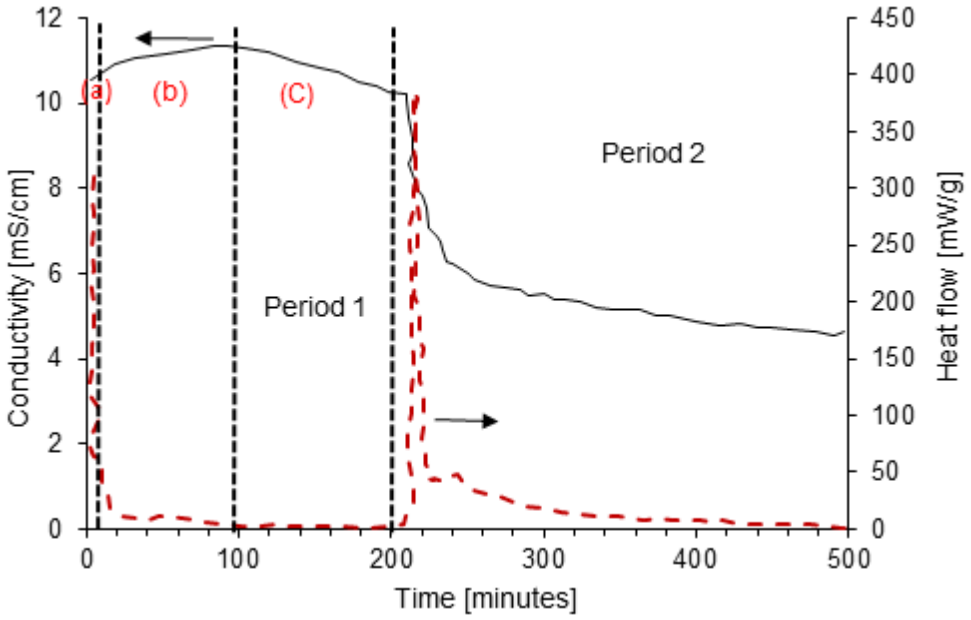

Figure 2.12: Heat flow rate and conductivity of the C_3A hydration process in the presence of gypsum (Minard *et al.*, 2007)

The first period (period 1) corresponded to the consumption of calcium sulphate followed by the formation of ettringite. Three different stages characterized this period: Stage (a) coincided with the first five minutes of the hydration presenting a short and very intense exothermic peak. In this stage, C_3A grains hydrate and their surfaces are covered by two types of hydrates with different morphology such as ettringite (needle-like) and sheets of hydroxyl-aluminate phases (AFm). Stage (b) correlated to the period during which the concentration of sulphate increased though consumed for the formation of ettringite. Consequently, a quasi-stationary state was observed as all the sulphate ions consumed for ettringite formation were replaced by the dissolution of an equivalent amount of gypsum. Therefore, at this stage, there is always a remaining amount of solid gypsum that is in equilibrium with the solution. Stage (c) was characterized by a significant decrease in the sulphate concentration until it completely disappeared. At the end of this stage, the ettringite is the dominant hydrated phase in the suspension.

The second period (period 2), starting after the exhaustion of the sulphate ions, corresponded to a new thermal activity. This period is initiated by a very fast exothermic reaction that causes the occurrence of a second peak on the heat flow rate curve. During this period, the sulphate ions are exhausted while those of calcium increase.

There was not much known about the second period of C_3A - gypsum hydration systems until the Quennoz and Scrivener (2012) investigations. They confirmed that the first period of this process is controlled by the dissolution of C_3A, whose duration depends on the initial amount of gypsum

available in the paste. They also stated that the adsorption of sulphate ions and the specific surface area of C_3A grains in cement paste were the main factors governing the dissolution of C_3A. They ascribed the second sharp exothermic peak to a high speed reaction of the remaining C_3A and ettringite yielding monosulfoaluminate (AFm). The acceleration rate of this reaction (on left side of the peak) was shown to be influenced by the remaining surface area of the reacting C_3A particles and the nucleation and growth of AFm phases on it. The deceleration part of the reaction (the right side of the peak) was due to the incursion of AFm crystals on the surface of the C_3A particles. This reduced its active space and consequently the reaction rate was limited and decreased.

The reaction of C_3A in the presence of other calcium sulphate bearing materials has been scrutinized by Tzouvalas *et al.* (2004) who studied the effect of anhydrite on the hydrating cement system. They found that this gypsum phase could be used efficiently as a set retarder without changing the physical and mechanical properties of the matrix. Lagosz and Malolepszy (2003), examining the effect of hemihydrate on the C_3A hydration, observed that hemihydrate accelerated the hydration of C_3A and calcium monosulphate aluminate in the form of hexagonal plates precipitated from the suspension. However, the speed of the reaction was affected by slowing down when calcium hydroxide was added into the suspension.

Similarly, Radwan and Heikal (2005) inspected the influence of phosphogypsum (by-product of phosphatic fertilizer and chemical industries) on the hydration of the C_3A -hemihydrate systems, reporting that phosphogypsum enhances the rate of hydration and consequently improves the cement paste workability. They further observed that by increasing the amount of phosphogypsum at the expense of hemihydrate, the rate of tricalcium aluminate hydration was decreased in the early stage. Furthermore, they noticed that the presence of certain impurities in the mix such as fluoride (F^-) and P_2O_5 activated the formation of ettringite. Since hemihydrate has a high solubility (García-Maté *et al.*, 2015), Radwan and Heikal (2005) expected that the hydration of C_3A and phosphogypsum would proceed at a much lower rate than that of C_3A and hemihydrate. They found, however, that due to the presence of these aforementioned impurities in the phosphogypsum, both calcium sulphate materials had similar hydration behaviour in the presence of C_3A.

Papageorgiou *et al.* (2005) advised that phosphogypsum may not be used in the production of high aluminate cements as a source of calcium sulphate, due to the eventual retardation effect that these impurities can exhibit. Singh (2000) suggested that this effect could be offset by blending phosphogypsum used with a certain amount of natural gypsum. Likewise, Danner *et al.* (2016) reported that the reactivity and the crystal structure of C_3A is modified when exposed to

certain impurities such as alkali (Na^+, K^+), showing that Na-doped C_3A changes the crystal structure completely from cubic to an orthorhombic or monoclinic structure depending on the concentration of Na^+.

2.5.4 Effect of gypsum phases on the hydration of poly phase cement systems

The dual effect of the gypsum phase on C_3A hydration has been highlighted previously in section 2.5.3. The same behaviour has been reported by Tzouvalas *et al.* (2004) within poly-phase cement systems. Exceeding certain limits in the addition of calcium sulphate bearing materials within cement matrixes can lead to abnormal sets and the substantial expansion of the cement paste. Many cement standards frequently set the required amount of gypsum phase based on the C_3A, alkali contents and the fineness of the ground cement (Papageorgiou *et al.*, 2005). This practice allows for obtaining normal settings since available sulphates combine exclusively with the hydrating portion of C_3A to give sufficient ettringite (Roller, 1934).

Taylor (2003) discussed the fact that the adsorption of sulphate ions on the C_3A sites not only depends on their concentration but also on their physical and chemical nature. More SO_4^{2-} ions are supplied within the suspension when gypsum is inter-ground rather than blended with cement clinker. This is due to the achievement of an improved homogenous PSD of calcium sulphates within the clinker by grinding. Zhang *et al.* (1996) also observed that the strength growth behaviour of cement pastes depends on the type of calcium sulphate available within the cement system because each form of calcium sulphate has a particular solubility different from one another. For instance, it is agreed that natural gypsum dissolves faster and is more stable than anhydrite and that only at higher calcium sulphate-water ratios, anhydrite will dissolve faster than the natural gypsum, as shown in Figure 2.13. Higher solubility rates result in higher concentrations of SO_4^{2-} which may accelerate the C_3A hydration, raising the Ca^{2+} concentrations.

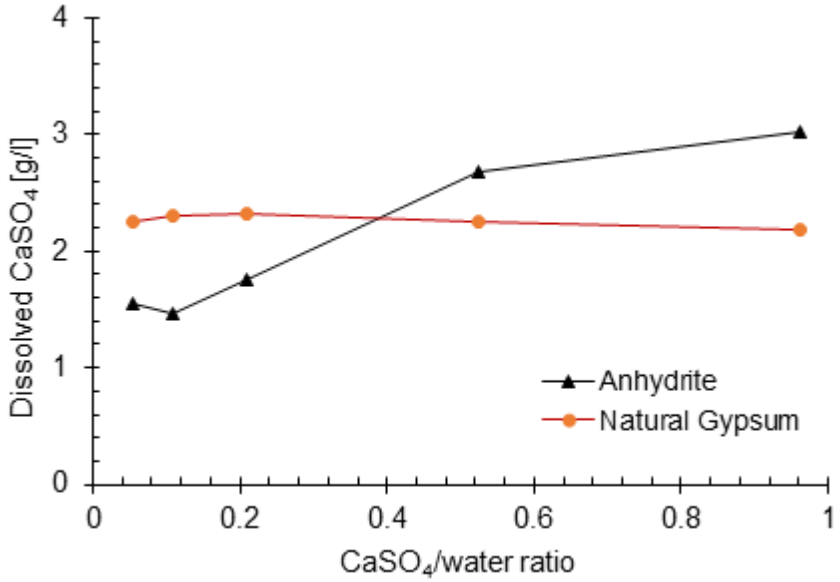

Figure 2.13: Dissolution rate of different type of calcium sulphates (Zhang *et al.*, 1996)

The effect of gypsum phases on the mechanical properties of the hydrating cement systems was investigated by Garrault *et al.* (2006) who reported that in the presence of portlandite (CH), the suspension is enriched with Ca^{+2} ions a few hours after the addition of water with respect to Equation (2.10).

$$Ca(OH)_2 \Leftrightarrow Ca^{+2} + 2OH^- \tag{2.10}$$

In this case, the concentration of OH^- decreases, as there are more Ca^{2+} ions within the system. Consequently, ettringite formation occurs at a distance far from the surface of the solid phase, accelerating the hydration of calcium silicate. However, in the absence of portlandite, the concentration of OH^- does not change with the increase in Ca^{2+} concentration.

Similarly, Mota *et al.* (2015), investigating the influence of gypsums within hydrating cement systems in the presence of some sodium salts, found that the addition of gypsum slightly lengthened the induction period and increased both the rate of hydration and amplitude of the main peak in the acceleration period. However, the presence of alkali lowered the concentration of Ca^{+2} ions in the suspension and increased the under-saturation of alite phase and its dissolution, while the presence of aluminium within the sulphate cement based systems showed a negligible effect.

Tzouvalas *et al.* (2004) determined that at an optimum percentage of SO_3 in cements, those with anhydrite set faster as compared to those with gypsum. They also discovered that decreasing the

amount of natural gypsum in the anhydrite-natural gypsum mixtures resulted in less available soluble SO_3 for the ettringite formation and consequently lowered the setting time. In the same way, high compressive strengths were obtained with cements with anhydrite as a calcium sulphate source because cement with anhydrite hydrated faster and accelerated the precipitation of more C-S-H responsible for cement system strength development.

Research conducted by Mardani-Aghabaglou *et al.* (2016) ascertained that hemihydrate hydrated faster than anhydrite in such a way that the amount of ettringite formed after one day of hydration was lower in mortar containing anhydrite, thereby exhibiting a lower strength development. After a thorough comparison between different types of calcium sulphate bearing materials, they reported that there were some gypsums that could retard the setting time without affecting the strength of the cement depending on the degree of dehydration of some calcium sulphates.

The influences of gypsum phases on the fresh properties of cement paste were intensively studied by Mardani-Aghabaglou *et al.* (2016). They discovered that the funnel flow times of cements with hemihydrate were higher than those of cements with natural gypsums. Apparently, mini-slump values of gypsum dihydrate mixtures were higher than those of hemihydrate mixtures. Besides, their results from XRD measurements revealed that there were more ettringite and monosulfoaluninate formed in the early hydration for cement with hemihydrate than those with natural gypsum. This, according to Mardani-Aghabaglou *et al.* (2016), was due to some intrinsic properties of gypsum phases, including the high solubility of hemihydrate estimated at approximately 6.2-8.2 g/l (three times more than that of natural gypsum) and the rapid precipitation of ettringite and sulfoaluminate hydrate phases with respect to a significant production of SO_3 in cements with hemihydrate.

2.6 Rheokinetics of cement paste

Most physical and mechanical properties of cement paste are a result of an explicit response of the physicochemical mechanisms that occur during the hydration process. These phenomena are complex and their understanding requires the intervention of more than one discipline. The effect of cement microstructure on cement paste properties has been highlighted previously in section 2.5.2. The formation of this structure is a consequence of internal interactions between hydrating cement particles (Gauffinet-Garrault, 2011).

In general, it is difficult to directly study the structure of most suspension materials. Subsequently, indirect techniques are used to obtain information related to the strength and stability of particles network within the formed structure (Eriksson *et al.*, 2009). Rheology has been applied

extensively as an indirect method to study particle interactions and network structures of colloidal suspensions in many investigations (Chong *et al.*, 1971; Han, 2007).

The growth rate of rheological parameters can be assessed to give an indication of the time dependence of cement paste microstructure (Mostafa & Yahia, 2017). The macroscopic behaviour of concrete also depends on the degree of microstructural build-up of cement paste (Baldino *et al.*, 2014; Mostafa & Yahia, 2017). Rheology has recently become an essential tool in the investigation of cement-based materials because it is able to relate macroscopic properties to material structures and it is able to bring solutions to different issues related to their productions.

Moreover, rheology has been promising in the implementation of 3D-printing in the concrete industry in providing understanding of the kinetics of the internal network strength of cement paste. For instance, cement paste with faster microstructure build-up rate results in high internal shear strength of the first cast layer. This makes it difficult for second layer stresses to induce flow in the first one, thus causing issues related to cold joints in concrete structures. On the other hand, cement with a high build-up microstructure is preferred for casting tall wall elements for the reduction of lateral pressure exerted on formwork (Mostafa & Yahia, 2016).

2.6.1 Fundamentals of rheology

The interest in understanding the flow and deformation of different materials once subjected to a range of stresses started in 17th century with Robert Hooke and Isaac Newton. Focused on solids, in 1678 with his true theory of elasticity, Robert Hooke suggested that “the power of any spring is in the same proportion with the tension thereof”. He observed that if you double the tension within the spring, its extension doubles accordingly. Separately, Isaac Newton gave attention to liquids and after conducting his experiment (illustrated in Figure 2.14), observed that other things being equal, the resistance to flow offered by adjacent layers of the liquid is proportional to the velocity with which these layers are separated from one another (Barnes *et al.*, 1989).

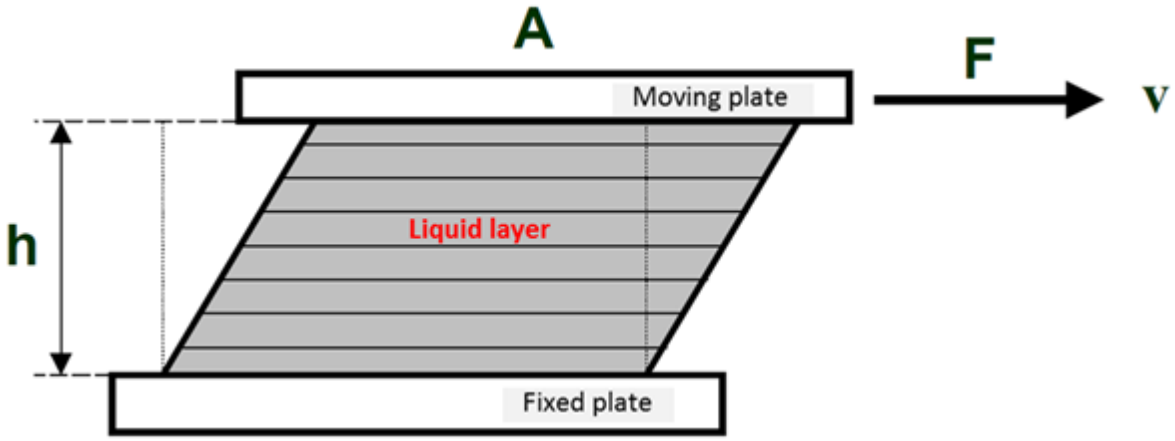

Figure 2.14: Parallel plate model constitutes with two planes of identical areas A, away from each other of h distance filled with a sheared liquid. A force F is applied to the upper plate and moves at velocity v. (Barnes *et al.*, 1989)

In the seating committee of the American Society of Rheology, founded in 1929, rheology was for the first time defined in terms that could encompass a range of materials from Hookean solids or ideal solids to Newtonian liquids or ideal liquids. *Rheology*, as a word, was suggested by Professor Bingham and was accepted in this seating as defined as the study of the deformation and flow of matter (Barnes *et al.*, 1989; Mezger, 2006).

Hooke's and Newton's laws

Ideal solids, or elastic materials, are defined as materials that are able to store energy due to an imposed deformation and fully recover their initial state once the imposed stress is released. This underscores the fact that these materials experience an instantaneous deformation when subjected to a shear stress, as shown in Figure 2.15. They keep their deformed state as long as the stress is applied. On the other hand, *ideal liquids* are defined as materials that are not able to store energy due to the deformation undergone. This means that, to the contrary, these materials will keep flowing as long as they are under stress. The energy gained is dissipated as heat during the flow process. Rheological characterization of these materials under some circumstances of flow is quite easy and can be described by simple relationships, as described in Equation (2.12) (Tattersall & Banfill, 1983).

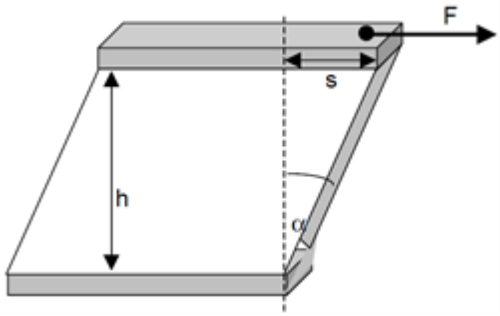

Figure 2.15: Deformation of materials according to Hooke's law

For a Newtonian liquid (see Figure 2.14), the material experiences a velocity gradient (dv/dh) along its thickness upon the application of a shear stress (τ). The latter is proportional to the described velocity gradient with respect to the resistance to flow (η) exhibited by the liquid's layers.

$$\tau = \frac{F}{A} \tag{2.11}$$

$$\tau = \eta \frac{dv}{dh} \tag{2.12}$$

The velocity gradient is referred to as the shear rate and is noted by $\dot{\gamma} = dv/dh$, while the constant of proportionality (η) is the viscosity of the material and quantitatively describes the resistance to flow.

On the other extreme, a Hooke's solid (see Figure 2.15) experiences a strain (γ) along its edge length (h) according to Equation (2.13).

$$\gamma = \frac{s}{h} = \tan\alpha \tag{2.13}$$

This strain is also proportional to the applied stress and depends on the stiffness of the material known as modulus (G). The shear modulus is therefore defined as per Equation (2.14).

$$G = \frac{\tau}{\gamma} \tag{2.14}$$

These laws were used for more than three hundred years to characterize the flow behaviour of different materials, up until the 19th century when scientists began noticing inconsistencies when applied to some materials.
In practice, in fact, it is very difficult to find materials that behave according to these defined linear laws. Most industrial materials behave differently, exhibiting much more complex behaviour. As they are partly liquid, or *viscous*, and partly solid, or *elastic,* they are able to store some of the deformation energy and lose some when under stress. These are referred to as *viscoelastic materials* and do not fully recover their initial state upon stress being released (Whorlow, 1992; Barnes *et al.,* 1989; Ferguson & Kemblowski, 1991).

Although viscoelastic materials describe a non-linear behaviour, they also exhibit a restrictive linear framework in which a range of rheological behaviour can be accommodated. The range of stress over which viscoelastic materials behave linearly is invariably limited. This underlines that the rigidity modulus and viscosity can change either instantaneously or over a long period of time when a high stress is applied to the material.

Flow properties – rheological constitutive equations

A range of non-linear behaviours can be established when relating applied stresses to the induced deformations within a material (shear rate or strain rate). Difficulties can therefore arise when attempting to label a given material. Rheological behaviours are classified using mathematical descriptions (Chhabra & Richardson, 1999) that define material flow behaviour based on intrinsic parameters or rheological parameters. Flow curve is used for this purpose; Figure 2.16 illustrates possible flow behaviours characterizing a variety of materials.

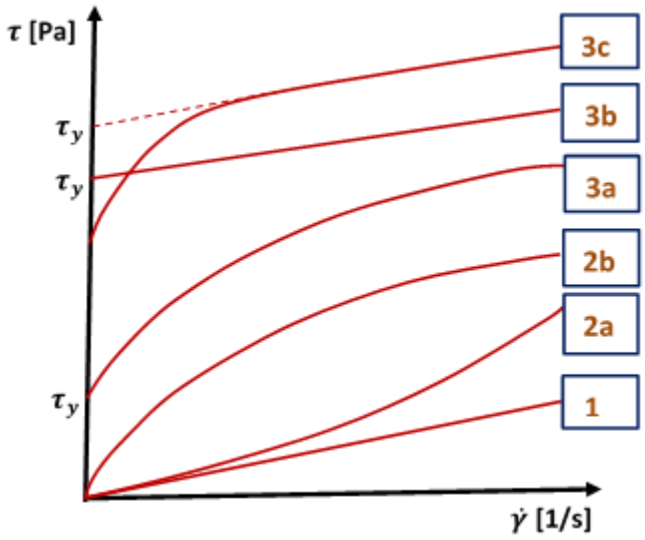

Figure 2.16: Illustration of flow properties: (1) Newtonian flow; (2a) general non-Newtonian with shear thickening; (2b) general non-Newtonian with shear thinning; (3a) viscosity non-Newtonian with shear thinning; (3b) viscosity non-Newtonian Bingham plastic; and (3c) viscosity non-Newtonian Bingham plastic non-ideal (Hanehara & Yamada, 2008)

The flow curve in Figure 2.16 shows the indisputability that the slopes and intercepts of curves with the y-axis are the fingerprints of the materials' rheological behaviour. There are materials that, before flowing, their shearing stress should absolutely exceed a limit shearing stress (τ_y), referred to as *yield stress.* In the same way, increasing the shear rate, the slope of the curve (defining the viscosity of the material), either remains unchanged or increases or decreases. Materials that maintain a linear relationship between the shearing stress and shearing rate (i.e. constant viscosity) after the yield stress has been reached are called Bingham fluids, as in Equation (2.15), whereas, materials in which a nonlinear relationship is confirmed after the yield stress are referred to as non-Bingham fluids. Physically, cementitious materials correspond to non-Bingham fluids, characterized by the Herschel Buckley model, as shown in Equation (2.16). But most often, rheological analysis is applied by assuming them to be Bingham fluids (Wallevik & Wallevik, 2011).

$$\tau = \tau_y + \mu\dot{\gamma} \tag{2.15}$$

$$\tau = \tau_y + k\dot{\gamma}^n \tag{2.16}$$

With τ_y the yield stress parameter; μ the plastic viscosity; k the consistency of the fluid; and n the power law index.

Viscoelastic properties of materials

As mentioned previously, the deformation of viscoelastic materials is not proportional to the applied force due to the energy dissipation within the system. The dynamic approach is therefore relevant in determining the extent of this energy dissipation, making it possible to distinguish and classify materials based on their elastic and viscous properties. In this context, the shear modulus inducing the mechanical energy within the system has two distinct components defining the stored energy in deformation and the dissipated energy in other forms. The shear modulus (G^*) or the modulus of rigidity can be expressed in a complex format, as given in Equation (2.17) and is referred to as *complex modulus.*

$$G^* = \frac{\tau}{\gamma} = G' + iG'' \tag{2.17}$$

G' is the storage modulus representing the energy stored or the elastic behaviour of the material; and G'' is the loss modulus designating the viscous behaviour, or the energy dissipation of the material.

In practice, these determinations are done by subjecting the material to a stress (strain) varying sinusoidally with time at a certain frequency, as per Equation (2.18).

$$\gamma(\omega, t) = \gamma_0 \sin(\omega t) \tag{2.18}$$

Where ω is the angular frequency; γ_0 is the strain amplitude; and t is the time.

A phase lag (δ) is noticed between this applied stress and the corresponding strain (Eirich, 1958), as described in Figure 2.17.

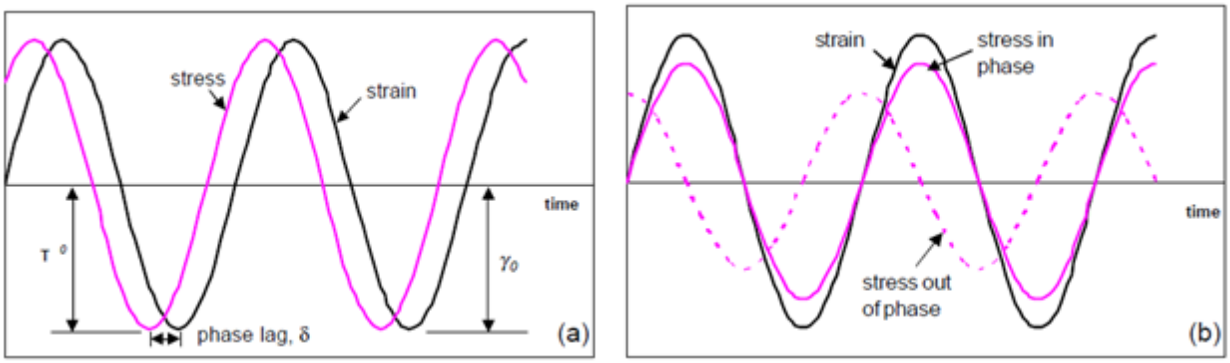

Figure 2.17: The relationship between applied stress and resulting strain within a viscoelastic material (Eirich, 1958)

From Equation (2.17), it can be seen that the storage modulus is in phase with the strain while the loss modulus is $\frac{\pi}{2}$ out of phase such as:

$$G' = \frac{\tau_0}{\gamma_0}\cos\delta \tag{2.19}$$

$$G'' = \frac{\tau_0}{\gamma_0}\sin\delta \tag{2.20}$$

The phase lag (δ) between strain and stress changes within [0, $\frac{\pi}{2}$] and can also be used to describe the material behaviour, according to Equation (2.21). Ideal elastic materials have a phase angle equal to zero, while ideal viscous materials have δ equal to $\frac{\pi}{2}$.

$$\tan(\delta) = \frac{G''}{G'} \tag{2.21}$$

Generally speaking, the elastic moduli of a viscoelastic material are time dependent. However, there exists a region under which these moduli are independent of time, the amplitude of the applied stress (strain) and the frequency at which the stress (strain) is being applied to the material. This region is referred as to linear viscoelastic domain (LVED) and the loading and unloading trajectories within this zone are identical. The determination of this region for a given material requires that both critical strain and frequency be found (Ching *et al.*, 2016). The critical

strain marks the end of the linear stress-strain relation and indicates the limit strain of the LVD beyond which loading and unloading the material describes different trajectories with a residual stress within the system. The critical frequency of the applied strain is related to the relaxation of the material structure. In fact, the microstructure of the material needs sufficient time to relax and release residual energy from oscillating stress (strain), as this allows the particles to elastically recover to their equilibrium status. In this context, the applied frequency has to be low enough to avoid any residual energy within the system (Sun *et al.*, 2006).

2.6.2 Physical interactions within cement hydrating systems

Cement paste is viewed as a suspension with poly-dispersed particles ranging from $1\,\mu m$ to $100\,\mu m$ in a continuous fluid phase. It is assumed therefore that colloidal interactions such as Brownian forces, hydrodynamic forces and various other contact forces may be present in the cement suspension. The magnitude of these interactions and their predominance within the paste depends on the size, the volume fraction of the cement particles and the applied stress or strain rate (Flatt, 2004). For instance, in the colloidal range, where the characteristic diameter is in the order of a few nanometres, dispersion electrostatic, Brownian and viscous drag interactions will dominate. Figure 2.18 shows the importance of these interactions within a specific suspension with typical particle size. In Figure 2.18, all the forces are normalized in terms of the gravity force. It is remarkable that when dealing with cement paste, for example, colloidal, viscous and gravity forces are all quite important. This implies that the prevention of segregation in the cement paste will require the paste to exhibit a high plastic viscosity or a sufficient yield stress.

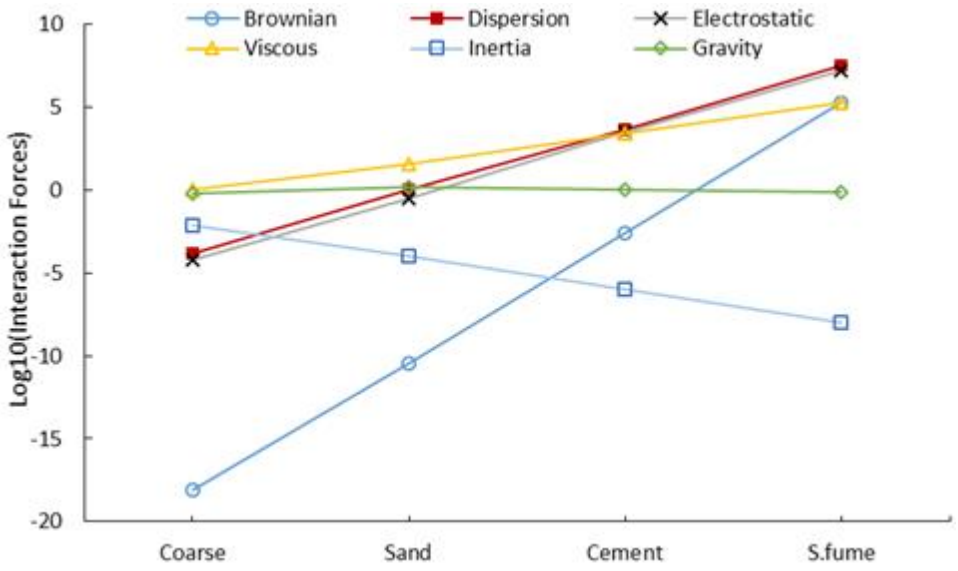

Figure 2.18: Relative importance of the interaction forces in cementitious materials at different concrete scale (particle size in the suspension) (Flatt, 2004)

Flatt (2004) confirmed that rheological properties of cement paste can be used to characterize its macroscopic response under a defined stress.

Cement paste critical strains

According to the work of Roussel *et al.* (2012), macroscopic flow is achieved once the stress applied overcomes the yield stress which is the stress that the network of interacting particles within the material can withstand. The workability of cement paste is directly related to this stress. The yield stress of cement paste is dictated by the structure and the strength of the internal network of interacting cement particles. Once at rest, it has been proven that the yield stress of the cement paste continuously increases during the dormant phase of hydration (Roussel *et al.*, 2012). This internal network can only be modified once its structure has been subjected to a critical strain γ_c (Maloney & Lemaître, 2006). This strain is therefore related to the yield stress, as given in Equation (2.22).

$$\tau_0 = G\gamma_c \tag{2.22}$$

With the shear elastic modulus *G* defined within the LVD.

The values of this critical strain have been a subject of many controversies in the literature. Some researchers suggested values of several percentages while others estimate it to be up to few hundred percent. A fresh cement paste experiences two critical strain values simultaneously: the smallest and the largest strains are both related to different phenomena that occur during cement

hydration. The smallest critical strain is associated with the breakage of the early hydrates which form preferentially at the contact points between flocculated cement grains, while the largest critical strain is related to the breakage of the colloidal network of interacting cement particles. The smallest critical strain can be observed at a small strain below 2-10%. This means that the decrease in the storage modulus of cement paste with strain cannot be interpreted directly as a true value of yield stress since some links between cement particles might break for strains higher than this one.

Lei and Struble (1997) already proved that measurements made below this critical strain allow the storage modulus of cement paste to increase over time in different phases. In general, this increase has been associated with the continual formation of hydrate products, especially to the nucleation and growth of C-S-H during the dormant phase (Nachbaur *et al.*, 2001). The first phase is very short and has been referred to as the coagulation phase, while the second phase is quite lengthy and is called rigidification (Jiang, Mutin & Andre Nonat, 1995; Nonat *et al.*, 1997).

It was concluded that the macroscopic critical strain of ξ / d within the cement suspension of grains with a typical size d (10 μm) and inter particle bond ξ in the nm range is only a few hundredths of a percent. Although the degree of hydration is zero (the ratio between the hydrate product and the initial amount of the cement), the consequence of the C-S-H will always be strong at a macroscopic level since the nucleation zone of C-S-H occurs between particle grains. The first critical strain is therefore a signature of the breaking of C-S-H links between cement particles. Below this critical strain, referred to as the *rigid critical value*, the storage modulus values are very high. The largest critical strain however, involves the interactions of cement particles without being in direct contact. This ascribes a large movement of two adjacent particles within the suspension. Note that there exists several non-contact interactions within the cementitious suspensions such as Van der Waals forces, electrostatic forces (resulting from the presence of adsorbed ions on the surface of cement particles) and steric hindrance (in the case where polymers are introduced in the suspension) (Zukoski, 1995). The magnitude of these interaction forces depends on the distance between particles.

Attractive forces are generally more dominant than the repulsive forces within the suspension. Thus, extra repulsive forces from dispersant agents such as polymers must be induced within the suspension to prevent the agglomeration of particles. Due to the high-volume fraction of cement pastes, there is a percolated network of particles dominated by the colloidal attractive interactions that allows the suspension to withstand a finite amount of stress without flowing. The breaking of this network would occur only if the critical strain of a few percent is exceeded. This is related to the second critical strain within the suspension.

Rigidification of cement paste microstructure

According to Bellotto (2013), from the initial contact of cement with water, attractive inter-particle forces prevail within the colloidal system of the paste. These forces are responsible for its initial developed elasticity. Among all the available surface forces within the cement suspension (i.e. Brownian, electrostatic, hydrodynamic) due to the characteristic cement particle size (larger than 1 um), the observed attractive forces are mostly attributed to the precipitation of C-S-H gel through its high surface charge density. However, the later build-up of cement paste microstructure is not only a result of the precipitation of hydrate products.

After a physical analysis of the colloidal interactions within the cement suspension by considering all preferential factors responsible for particle flocculation such as Brownian motion (thermal agitation inducing the energy potential between particles), viscous dissipation (drag forces on the particles from the liquid phase), Roussel *et al.* (2012) suggested different stages of cement paste toward the setting. Firstly, the colloidal network percolation takes place in the first seconds straight after cement paste mixing. This is defined as *flocculation* or agglomeration of particles. Thereafter, a transient phase known as the *rigid percolation* phase follows, depending on the C-S-H nucleation. Secondly, the C-S-H nucleation strengthens the local colloidal interaction between particles and a more rigid interaction with higher energy potential is formed. This phase is referred to as the *rigidification phase.* Further increase in cement paste rigidity or macroscopic elastic modulus will depend on either the number or size of C-S-H bridges between particles. Much evidence shows that the rigidification phase is characterized by a linear increase of elastic modulus over time.

The storage modulus of cement paste increases, according to Bellotto (2013), within the dormant phase if the paste is not sheared. Otherwise, the storage modulus decreases to the initial level. Its value will depend on the magnitude of the applied shear stress and the time elapsed during the shearing process. Bellotto believed that if this process is stopped, the storage modulus should increase again with the same growth rate as previously. This phenomenon should be observed, however, if the forces responsible for the modulus growth are purely colloidal since the formed network is reversible, as discussed by Jiang *et al.* (1995).

The strength development of cement paste, referred to as *thixotropy,* is often reversible with a short time interval of observation. The irreversible scenario of this behaviour is an indication of the effect of hydration phenomenon on the cement suspension. This phenomenon contributes to the long-term evolution of cement paste properties. Jiang *et al.* (1995) stated that previous researchers have also confirmed the existence of colloidal forces of the magnitude of Van der Waals type and chemical bonds in the form of bridges between particles at pseudo contact points.

The first forces are mainly responsible for the coagulation phenomenon characterized by a structure that is mechanically reversible, whereas the second ones are bound to the rigidification of the coagulated cement particles by means of bridging contacts due to the hydrate products, resulting in an irreversible structure.

Coagulation or flocculation occurs at the very beginning after mixing once the interstitial solution becomes an electrolytic solution. This happens even before the hydrates begin forming. On the other hand, the rigidification of the microstructure is defined by a sharp increase in cohesion corresponding to the acceleration of the hydrate products. This is due to the formation of hydrates near the contact zones and could only occur with a small hydration percentage. With respect to this condition, the rigidified paste becomes more and more mechanically irreversible and the increase of cement paste strength at this stage is proportional to the quantity of precipitated hydrate.

Similarly, Kirby and Lewis (2002) also believed that the increase of the stress-bearing contacts among the fractal clusters can be related to the precipitation of C-S-H on the surface of cement particles. This strengthens the links within the network and decreases the agglomerates sizes. The microstructure development of cement paste is therefore indicated by the increase in storage modulus as a consequence of the hydrating cement particles being trapped in an ever-increasing local potential energy minimum by the interactions with neighbour particles occurring through the precipitating C-S-H. In addition, Nonat *et al.* (1997) have demonstrated the importance of calcium ions Ca^{+2} for the rigidification of cement systems as a consequence of C-S-H nucleation and growth. It was observed that the storage modulus *G'* of cement paste increases over time after some retardations. The magnitudes of *G'* in this delay zone were comparable to those of suspensions with attractive inter-particle forces and hydrates dissolution-precipitations have been significantly decreased by the use of admixture, according to Bellotto (2013). However, this increase in G' showed some dependences on the solid volume fraction within the system. He concluded that this rigidification was due to the presence of agglomerates whose elastic properties are a function of their size.

Non-contact interactions within cement microstructure

Without doubt, the rheological properties of cementitious materials depend not only on the stress history and chemical phenomena but also on various physical parameters such as the volume fraction (ϕ) of powder in the suspension (Zhou *et al.*, 1999; Flatt, 2004; Toutou & Roussel, 2007). Depending on the amount of ϕ, the cement paste might exhibit Newtonian or non-Newtonian behaviour. Roussel *et al.* (2010) conducted a meticulous analysis to demonstrate the significance of these interactions providing a deeper understanding of the non-contact interactions between the particles of cement paste. They confirmed that, as cement particles are very small, the latter

are subjected to random thermal motion, referred to as *Brownian motion*, which allows the particles to diffuse through the liquid phase. The relative magnitude of this interaction was defined by Coussot and Ancey (1999) as per Equation (2.23):

$$N_r = \frac{\phi_0}{kT} \tag{2.23}$$

Where ϕ_0 is the energy that characterized the strength of the interaction or energy potential; kT is the energy associated with the thermal agitation; with k the Boltzmann Constant; and T the absolute temperature.

Next, the energy potential can be determined as per Equation (2.24):

$$\phi_0 \cong \frac{A_0 a^*}{12H} \tag{2.24}$$

Where A_0 is the Hamaker constant (1.6x10^{-20} J for C_3S particles); a^* is the radius of curvature of the contact points between particles (500 nm); and H is the surface to surface separation distance at contact point (2-10 nm) (Flatt, 2004).

Considering all these values, it can be found that the N_r for a flocculated system is greater than 1, suggesting that the Brownian effect does not play a major role and that van der Waals attractive inter-particle forces prevail in this case. This confirms that in the cement suspension, thermal agitation is not sufficient to separate two adjacent particles that are subjected to van der Waals attractive forces.

This appears to be contradictory to the accumulated evidence on cementitious materials that demonstrates the temperature dependence of cement (Petit *et al.*, 2006). Indeed, temperature is one of the factors that activate some physico-chemical processes during hydration, of which thermal agitation would play a minor role. Nevertheless, thermal agitations allow cement particles to diffuse in the liquid phase, thus reducing the distance between particles, and allowing the van der Waals forces to dominate the repulsive forces and favour the agglomeration of particles. In other words, cement particles randomly move within the continuum media due to their Brownian energy as long as they do not approach each other closely. This random motion helps in carrying particles to their eventual position where their surrounding attraction clouds can encounter each other. This causes cement particles to flocculate and the percolation time can be shortened (Mostafa & Yahia, 2017; Mewis & Wagner, 2012), explaining why in the heavily dilute suspension (the inter-particle distance is very high) the cement does not experience any yield stress. This is

related to the volume fraction of solids in the mixture that should be over a certain value, critical packing fraction ϕ_c for the suspension to form an interaction network able to support a stress.

Previous experiments suggest that ϕ_c should be around 0.5 for uniform spherical particles (Onoda & Liniger, 1990). There exists also a dense packing fraction ϕ_m which was reported by Struble and Lei (1995) as between 0.6 and 0.7 for identical spheres; a value of 0.64 was reported by Do *et al.* (2007) for dense random packing.

Cement suspensions and rheological parameters

The critical and dense packing fractions $(\phi_c, \phi_{\max})$, two important characteristics of a cement suspension, have a substantial impact on the rheological behaviour of cement paste (Struble & Lei, 1995; Justnes & Vikan, 2005).

Different attempts have been made to correlate the rheological parameters to these packing parameters. Probably the most successful model that can predict the viscosity of a dispersed suspension based on its solid concentration is the Krieger and Dougherty model, given in Equation (2.25).

$$\frac{\eta}{\eta_c} = \left(1 - \frac{\phi}{\phi_{\max}}\right)^{-[\eta]\phi_{\max}} \tag{2.25}$$

Where, η is the apparent viscosity of the suspension; η_c is the apparent viscosity of the liquid phase; and $[\eta]$ the intrinsic viscosity that measures the effect of individual particles on the viscosity. For rigid spherical particles, it is assumed to be equal to 2.5 and a value close to 6 is allocated to cement based materials (Struble & Lei, 1995; Justnes & Vikan, 2005).

With the improvement in predictive capability of the viscosity of highly concentrated suspensions, Chong *et al.* (1971) proposed Equation (2.26) to estimate the viscosity of suspension materials:

$$\frac{\eta}{\eta_c} = \left[1 + \frac{0.75\left(\phi / \phi_{\max}\right)}{1 - \left(\phi / \phi_{\max}\right)}\right]^2 \tag{2.26}$$

From Equation (2.25) and Equation (2.26) it is possible to decrease the viscosity of the suspension at a given ϕ by increasing the ϕ_{max} . For poly-dispersed suspensions such as cement paste, this infers that adding small particles to the larger ones would enable an increase in the solid content as small particles are assumed to fill the voids between the larger particles, thereby decreasing the liquid phase content and resulting in higher value of ϕ_{max} . Do *et al.* (2007) concluded that there might be a specific amount of large and small particles in the poly-dispersed suspension for an optimum value of ϕ_{max} at which target rheological properties can be achieved.

Recently, Bentz *et al.* (2012) demonstrated through thorough experimental work that the yield stress of cementitious material depends strongly on the number of cement particles contained in a specific volume of the cement suspension 'particle density'. They observed a power law relationship between the cement particle density φ and the yield stress of the cement paste as given in Equation (2.27) and illustrated in Figure 2.19.

$$\tau_y = \alpha(\varphi - \varphi_c)^{\beta} \tag{2.27}$$

Where β is the critical percolation for yield stress defined as the slope of the particle density-yield stress relationship on log-log scale. Its value was found to be 4.5$\pm$ 0.4; α is the constant of proportionality; and φ_c the percolation threshold that was found to be zero (by fitting the experimental data with the Eqn. above), suggesting that only few cement particles are required to form a percolating network structure because of their strong tendency to agglomerate. The particle density was obtained on the PSD curve by considering the characteristic cement particle size, the specific surface area and the density of the paste.

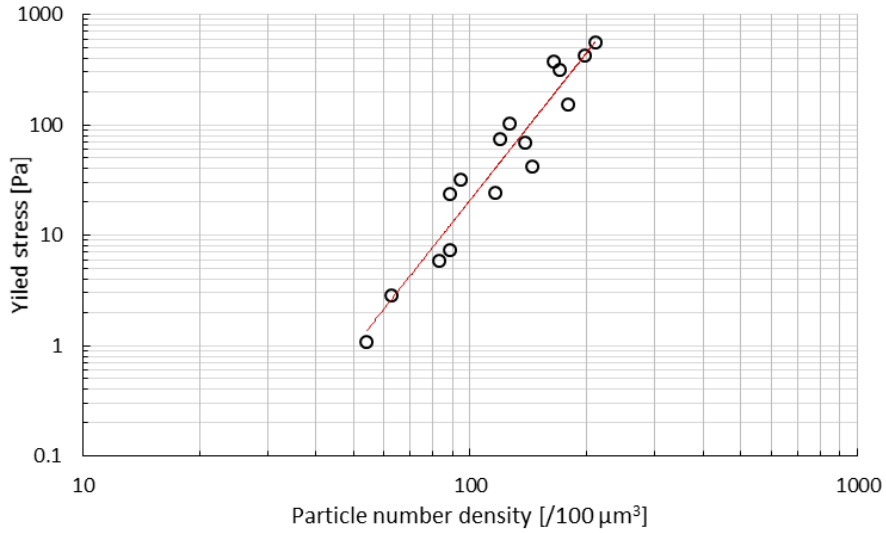

Figure 2.19: Effect of particle density of a typical cementitious material on the yield stress values (Bentz *et al.*, 2012)

Similarly, much research has been conducted with results indicating that the yield stress of suspension materials is proportional to the inter-particle forces. Flatt (2004) reported a yield stress model, in Equation (2.28), that involves the presence of these interaction forces based on the solid volume fraction, the packing density, and the size and distribution of particles.

$$\tau_y = m_1 \frac{\phi^2}{\phi_{\max}(\phi_{\max} - \phi)} \tag{2.28}$$

Where m_1 is a factor defined as a function of the volume mean particle size and its calculation can be found elsewhere in Flatt (2004). Equation (2.28) suggests that there should be a volume fraction percolation threshold ϕ_c below which the suspension will not experience a yield stress and will thus behave as a Newtonian fluid. This percolation limit was taken into account by Kashani *et al.* (2014), as per Equation (2.29):

$$\tau_y = m_1 \frac{(\phi - \phi_c)^2}{\phi_{\max}(\phi_{\max} - \phi)} \tag{2.29}$$

In conjunction with predicting the rheological properties of cement paste based on the physical characteristics of the suspension, Kashani *et al.* (2014) developed a yield stress model from both the PSD of the cementitious materials and the w/b ratio. First they transformed the Rosin-

Rammler function into a logarithmic function and then calculated the yield stress value, as proposed in Equation (2.30).

$$\tau_y = (n-0.68)[1470-3141(w/b)], n > 0.68 \quad (2.30)$$

However, the validation is critical, since its constants were determined based on the value of n obtained from experiments on cements with specific characteristics.

In many experimental works, the value of ϕ is known beforehand. Unfortunately, the determination of $\phi_{\max}$ is not always easy, especially for a poly-dispersed suspension. Many techniques have been used to estimate this value that depends on factors such as the arrangement, shape and size distribution of particles. The maximum packing $\phi_{\max}$ can either be determined directly or indirectly. The solid bed density, extrapolation from rheological data and theoretical calculations, can all be applied for this purpose. The first approach requires a graduated centrifuge tube to be used and after a centrifugation at approximately 4000 rpm for 5 min, Eq. (2.31) provides the maximum packing (Ng & Justnes, 2015):

$$\phi_{\max} = \frac{Vol_{cement}}{Vol_{(cement+water)}} \quad (2.31)$$

The volume of water and cement are calculated from the mass remaining in the residue after centrifugation.

The second approach consists of fitting the plastic or apparent viscosity data to the Krieger-Dougherty model by setting [η] to 2.5 or 6, depending on the material, and ϕ_{max} is obtained as a fitting parameter. Lately, Liu (2000) has proposed a simple model, Equation (2.32), that can be used to accurately determine ϕ_{max} of concentrated colloidal suspensions.

$$1-\eta_r^{-1/2} = a\phi + b \quad (2.32)$$

The model parameters a and b are experimentally determined based on viscosity data of the suspension at different volume fractions of solids. On the graph relating $1-\eta_r{}^{-1/2}$ to ϕ, the constants a and b are respectively the slope and the intercept of the obtained line. Finally, the

maximum packing density is found by assuming that η_r will tend to infinite when $\phi = \phi_{max}$ such as per Equation (2.33):

$$\phi_{\max} = \frac{1-b}{a} \tag{2.33}$$

The third approach involves empirical formulas, for example, which express the maximum packing of solids to the small and the large diameter of the particles $\left(d_{\min}, d_{\max}\right)$, as provided in Equation (2.34).

$$\phi_{\max} = 1 - 0.45\left(\frac{d_{\min}}{d_{\max}}\right)^{0.19} \tag{2.34}$$

2.7 Overview of cement hydration measurements

Different techniques have been used in many investigations of cementitious materials to either follow the hydration kinetics or to assess its consequences on the microstructure development of the paste. These techniques include thermodynamics, spectroscopy, microscopy and more recently, rheometry.

2.7.1 Thermodynamic

During the hydration process where cement comes in contact with water, various chemical and physical changes take place and an appreciable amount of heat is released. This amount of generated heat is used to characterize cement paste hydration kinetics. For instance, the isothermal and adiabatic calorimetry technique can be used for this purpose, a technique which allows for a continuous acquisition of data over specific periods in time. However, the isothermal calorimetry technique is preferable to the adiabatic technique, as the interpretation of the latter is complex and possesses many experimental difficulties (Prosen *et al.*, 1985).

Cement paste once exposed to a temperature sweep at a considerable rate loses weight with respect to the decomposition of constituent hydrate phases. These transformations occur at specific temperatures. Differential Scanning Calorimetry (DSC) or Differential Thermal Analysis (DTA) and Thermogravimetric Analysis (TGA) are primarily used as thermal techniques to determine and quantify these cement hydrate phases after a given curing time.

2.7.2 Spectroscopy

In this analysis category, X-ray diffraction is the most frequently used instrument for the cement hydrate phases' determination and quantification. However, this technique needs additional

methods for a full assessment of the phases since it cannot detect amorphous phase such as C-S-H (Snellings *et al.*, 2014). Nowadays, infrared and other spectroscopic instruments have been used successfully for the study of phase composition of hydrate cement systems. With most of these tools, it is possible to not only detect cement crystalline phases but also determine amorphous phases (Hughes *et al.*, 1995; Fernández Carrasco *et al.*, 2012).

There are additional spectroscopy tools used for cement pore solution investigations. Since the hydration of cement is a dissolution-precipitation process, the quantification of elements prevailing within the pore solution can produce relevant information about the solid phases' assemblages and the degree of their saturation. Atomic absorption spectroscopy (AAS) and inductively coupled plasma spectroscopy (ICP) are used for this purpose (Caruso *et al.*, 2017).

2.7.3 Microscopy

The scanning electron microscopy using backscattered electron (BSE) imaging, together with energy dispersive spectroscopy (EDS), have demonstrated over the years to have great potential for the study of cement based materials (Scrivener, 2004). This technique offers many advantages, including the possibility of having a wide range of magnifications so that features can be seen in detail and in context. The arrangement of solids in the paste and other defects within the material can be detected at low magnification, whereas the morphology of C-S-H, AFt and pores can be observed at high magnification. The Scanning Electron Microscopy (SEM) and Transmitted Electron Microscopy (TEM) are widely used for this purpose. The use and the physics behind these techniques can be found elsewhere (Scrivener, 2004).

2.7.4 Rheometry

Rheometry comprises a set of techniques that can acquire rheological data of the material under investigation. These techniques, successfully implemented in the cement industry, can be done either in dynamic or shear mode depending on the rheological properties in which the investigator is interested. However, the dynamic mode rheology, especially the oscillatory mode, is generally chosen to investigate the microstructure evolution of cement paste during hydration, while the shear mode technique is selected to characterize the flow properties of the cement paste (Nachbaur *et al.*, 2001).

2.8 Conclusion

The main purpose of this research was to investigate the effect of gypsum phases' proportions in the poly-phase cement system on microstructure level and rheological behaviour. Natural gypsum

is added to cement clinker during the grinding process. The importance of this addition was highlighted and discussed. This practice offers some benefits in terms of controlling the setting times of cement pastes. This not only implies phase transformations on microscopic levels, but also physical interactions that directly affect the rheological properties of the cement suspension.

For this reason, the manufacturing process of Portland cement, especially the grinding process and its eventual effect (due to degeneration of gypsum dihydrate to hemihydrate) on the flow behaviour of cement paste, were discussed. The phase transformations due to the presence of natural gypsum and hemihydrate during cement paste hydration were also reviewed using different approaches. Since cement rigidification does not depend exclusively on chemical interactions that take place during hydration reactions, it was thus of great importance that consequent physical interactions within the cement paste during hydration be correctly considered. This was done after a brief introduction to the fundamentals of rheology and thereafter linked to the viscoelastic and flow properties of cement pastes. The available possible measurements used to study the effect of hydration on either cement paste microstructure, pore solution or rheological behaviours were concisely presented.

Although much work pertaining to the cement hydration kinetics has been accomplished, these investigations have primarily been conducted in regard to pure phases (mono-phase cement) of synthesized clinker in diluted suspensions (Schöler *et al.*, 2017). This present experimental work examines the hydration kinetics of cement paste, considering industrial available real material at realistic water-to-cement ratio, where the effect of dissolution and precipitation mechanisms as observed in the laboratory can be linked directly to field experience. Studying the effect of calcium sulphate bearing materials on only a mono-phase cement system (i.e. C_3A phase) cannot be extrapolated in the poly-phase cement system. This is because some cement phases can be affected by the incursion of sulphate ions on their hydrate products, modifying the overall rate of hydration (Quennoz & Scrivener, 2013b).

In addition, the effect of SO_3 on some mechanical properties of cement paste not only depends on the C_3A phase, but also on the available alkali equivalent within the cement clinker (Jelenic *et al.*, 1977). Besides, it was suggested that the results obtained from the reactions of laboratory C_3A, C_4AF or any other cement phase with water alone, in the presence of calcium sulphate or calcium hydroxide, should be interpreted with more caution, due to the fact that the composition of aluminate phases in industrial clinker differs considerably from that in synthetic preparations (Newman & Choo, 2003). As a consequence, limited work has been undertaken to assess the impact and the effect of the mix proportion of calcium sulphate bearing materials (in the calcium sulphate phase) on the hydration kinetics, microstructure and variations in rheological properties

of freshly mixed cement pastes. The interaction of gypsum and clinker phases during the early cement hydration is not well-understood.

Chapter 3 Research methodology

3.1 Introduction

The effect of mix proportion of hemihydrate and natural gypsum within the cement gypsum phase was investigated on the hydration kinetics and microstructural changes that occur within the cement suspension. Since most of physical properties of cement paste are direct consequences of the physicochemical phenomena involved during cement hydration, the rheological behaviours of corresponding hydrating cement pastes were tentatively correlated to their microstructure developments and further, to the observed mechanical properties.

Within the scope of this research, the effect of hemihydrate and natural gypsum concentrations in the cement gypsum phase was simultaneously estimated on both cement paste hydration kinetics and rheokinetics. To this end, the investigations considered different approaches to more clearly understand these interactions. This current chapter presents the experimental methods and procedures, describing in detail the instrumentation used for data collection and techniques adopted to analyse the cement hydration and microstructural kinetics.

The rheometry technique was selected to assess the viscoelastic and flow properties of cement pastes, while the isothermal conduction calorimetry was used to evaluate the hydration kinetics. A thermal analysis was carried out to determine the hydrate products, while the scanning electron microscopy (SEM) in backscattered mode, together with the energy dispersive spectroscopy, assesses the microstructure of cement paste with different proportions of these calcium sulphate bearing materials within the cement gypsum phase. Mechanical properties of cement paste, such as compressive strength and setting times, were also measured to assess the potential effect of the microscopic behaviour of pastes on their macroscopic scale.

3.2 Rheokinetics measurements of cement paste

In general, for colloidal materials, it is possible for a three dimensional structure to form within the suspension at rest due to the presence of van der Waals attractive forces (Mostafa & Yahia, 2016). This aggregation can easily break into flocs when the material is subjected to a certain flow regime. For a time dependent material, such as cement paste, an additional phenomenon occurs during hydration that is accepted as irreversible, and together with the defined flocculation phenomenon, affect the fresh properties of cement-based materials. It is thus acceptable that at rest, the cement microstructure development is caused by physical interactions between particles and chemical rigidification stemming from hydration products.

The investigation of material properties requires that the rheological measurements be done independently of any specific kinematic conditions. This can be done by performing asymptotic kinematic tests which consist of adopting measuring conditions that provide asymptotic values of the material parameters determined only by the material characteristics without being affected by the amplitude of the applied load such as small amplitude oscillation (SAO). The dynamic rheometry (i.e. SAO) has been successfully used to investigate the viscoelastic properties and the time dependence of cement-based microstructures. This approach is preferred because it is a non-destructive technique. In this practice, the recovery of the internal structure is monitored by applying a small amplitude oscillatory shear (SAOS) within the linear viscoelastic domain (LVED). Within this region, the induced shear strain is lower than the critical strain value defined as the limit of the LVED. It is agreed that the material structure remains undisturbed during the measurements and the evolution of storage modulus with time can describe the structuration of cement based materials (Roussel *et al.*, 2012). Consequently, this method seems convenient, providing insight on the contribution of physical and chemical phenomena regarding the formation of the internal network during cement hydration.

3.3 Cement hydration kinetics measurements

Different techniques, such as the total chemical shrinkage and the non-evaporable water content, are available for the measurement of cement hydration kinetics. Although correlation exists between these methods in evaluating the degree of cement hydration, the isothermal calorimetry approach seems to be the most established technique to measure the overall cement hydration progress (Parrott *et al.*, 1990; Escalante-Garcia, 2003).

Isothermal calorimetry, an easy and non-invasive method suitable for cement hydration kinetics investigations,allows for continuously following the hydration reactions since the overall heat balance of cement hydration is sufficiently exothermic (Quennoz, 2011). It would have been appreciated to estimate the contribution of each cement phase to the overall hydration kinetics by executing a deconvolution of collected heat evolution profiles. But this treatment is not always easy due to various simultaneous chemical reactions within the system.

3.4 Cement hydrate phases estimation

There are a number of techniques available for the quantitative analysis of early hydrate products. Thermogravimetric analysis with differential scanning calorimetry or differential thermal analysis, x-ray diffraction and selective dissolution have all been used for this purpose (Odler & Abdul-Maula, 1984; Vedalakshmi *et al.*, 2003). However, the presence of several amorphous phases within the cement system makes the quantitative determination of the phase assemblage in

hydrated cement systems a challenging task. So it is advisable to use more than one technique for the cement phase characterization. For instance, when using thermogravimetric analysis for hydrate phase identification, due to proximity of the temperatures of thermal decompositions of hydrate phases, only some phases can be accurately quantified. Likewise, x-ray diffraction with Rietveld refinement can only quantify crystalline phases and fails to distinguish between multiple amorphous components without specific calibration prior to the measurements (Durdziński *et al.*, 2017).

3.5 Research design

An experimental approach was conducted throughout this research. Samples of cement clinker with different proportions of natural gypsum and hemihydrate were prepared in sufficient quantity for eventual testing procedures, as described in sections 3.2-3.4. This practice seemed to be more effective than preparing individual samples each time a test was required. By so doing, it was possible to establish fair comparisons between samples of either the same or different cement mix proportions since they were considered representative of batches with consistent characteristics. Therefore, validation of results between testing protocols was acceptable.

3.6 Research methodology

The following section gives details on the scope of the experimental work, an overview on the rheological methodology used for the microstructure investigation, and preliminary tests for ionic activities within suspensions as induced by the presence of calcium bearing materials. The collection of data and analysis are also presented.

3.6.1 Experimental project matrix

The experimental work was subdivided into two phases. The first phase consisted of assessing the individual effect of each calcium sulphate bearing material on the hydration kinetics of cement paste. For this purpose, natural gypsum or hemihydrate was used as set regulator at different concentrations and the rate of heat flow was measured. In addition, the hydrate products formed after 24 hours of hydration time, the compressive strength (of corresponding mortars) after 1 curing day and the setting times were also evaluated. From these results, an optimum concentration of the calcium sulphate phase within the cement was established and then used for the next phase. The latter consisted primarily of evaluating the effect of natural gypsum degenerations into hemihydrate (during a cement milling process) on the hydration and rheological kinetics of cement paste. The main experimental tasks executed during this research are illustrated in Figure 3.1.

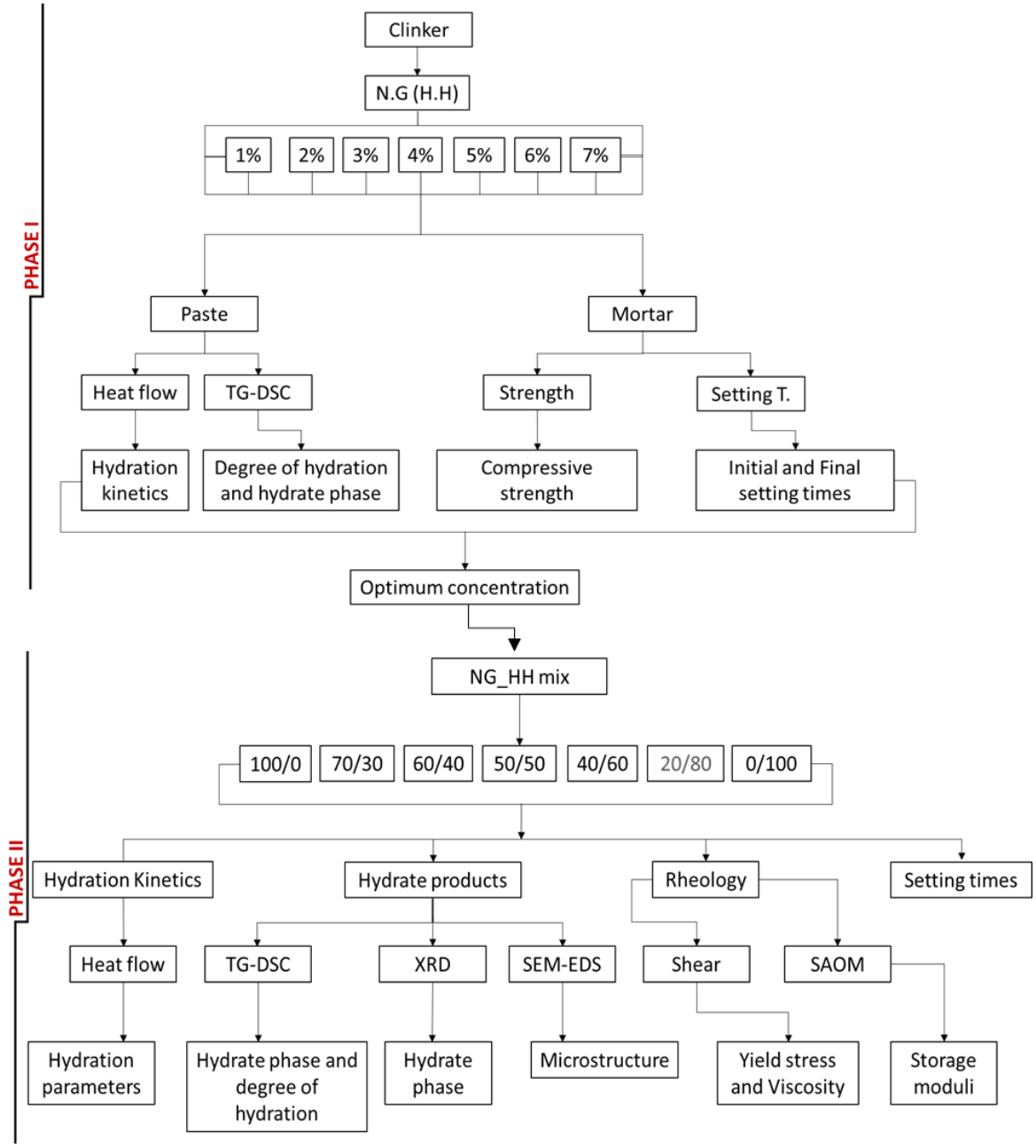

Figure 3.1: Experimental project matrix for each concentration of individual calcium bearing material (phase I) and their mix proportions (phase II)

3.6.2 Physical and chemical interactions for cement microstructure development

The development of cement paste microstructure as a result of particle agglomerations has been at the centre of many controversies. The storage modulus development is a fingerprint of the microstructure evolution since it indicates the aging process of a given system due to the increase in its relaxation time (Mutin & Nonat, 1995; Roussel *et al.*, 2012). Some researchers have attributed the early increase in storage modulus to colloidal interactions that happen during

cement hydration while others, to the interactions of C-S-H at pseudo contact points between particles (Nachbaur *et al.*, 2001).

These debates are due to some discrepancies within the current literature that define the length of hydration after which a cement particle surface is covered by C-S-H. According to Sujata and Jennings (1992), cement particles are covered by a layer of C-S-H immediately after mixing, a finding also confirmed by Roussel *et al.* (2012) who demonstrated the ability of cementitious materials to develop a coagulated particle network a few seconds after mixing. This property was attributed primarily to the nucleation of C-S-H responsible for strengthening colloidal interactions of cement particles thereby creating a rigid system. On the other hand, Lootens *et al.* (2004) reported that it requires more than an hour for cement particles to be completely covered by a C-S-H layer. They agreed that physical interactions within the cement suspension should be responsible for the early particle cohesions, as also reported by Nachbaur *et al.* (2001) and Mostafa and Yahia (2016).

Considering this, it was important to bring clarity to these disagreements when SAO is used to study cement systems' microstructure. Preliminary tests were thus conducted to verify the eventual ability of SAO techniques to detect any physical or chemical contribution of some inclusions on the cement system microstructure development. This was of great interest due to the fact that investigated cement systems had less than 8% calcium sulphate phase. At such small concentrations, it could have been difficult to depict the effect of these inclusions on the rheokinetics of cement pastes, if the technique used could only detect one of these hydration phenomena.

For this reason, inert materials such as silica fume were considered at different water/powder (w/p) ratios for physical interaction and activated by calcium hydroxide at different concentrations as sufficient sources of calcium ions within the system for chemical interactions. The coagulation was monitored by changing the inter-particle distances (w/p) and by adding calcium hydroxide in different dosages. The calcium hydroxide or portlandite used contained 98% of $Ca(OH)_2$.

In the next section, results are presented and discussed without describing the experimental protocol in detail, as presented in 3.6.4-3.6.7.

In general, the growth of storage modulus described three distinct intervals as observed by Bellotto (2013): 1) a retardation period, characterized by small magnitudes of storage modulus; followed by a rapid increase of modulus, whose magnitudes were in order of 10^5-10^7 Pa; and thereafter, a plateau is observed. The referred plateau can either be an artefact due to the

limitations of the instrumentations used or some physical (chemical) equilibrium reached within the suspension. Thus, storage moduli within this interval were not considered. It was observed that the retardation period, reflecting the coagulation or flocculation period of cement particles, was affected by the inclusion of CH within the suspension. This period seemed to take longer when there was no CH within the paste, and shorter in the presence of CH, indicating that the presence of calcium ions preferential for the precipitation of some cementitious hydrates has an effect on the agglomeration of particles, as demonstrated by Nonat *et al.* (1997). These researchers found that the coagulation of cement particles depends strongly on the calcium concentration within the suspension. Particle coagulations occurred when the calcium concentration reached 1 mmol/L and became less effective when the calcium concentration was greater than 100 mmol/L.

Likewise, the second period also appeared to be affected by the presence of CH within the suspension as the rate of this period was faster for pastes with CH as compared to those without. This could be attributed to the fact that the chemical reactions induced by the presence of CH within the suspension helped strengthen the weak bonds (from physical interactions) between particles.

It is thus clear that the microstructure development of time dependent materials such as cementitious materials can be investigated using the SAO. Additionally, it is efficient in detecting the chemical and physical contributions of some phases, regardless of their concentrations as compared to the overall system. It is also understood that the storage modulus growth is an indication of physical and chemical interactions that occur simultaneously during cement hydration.

3.6.3 Ionic activity within cement suspensions

Chemical interactions within cement suspensions are a consequence of ion transfers from available cement phases. This phenomenon was assessed beforehand to make sure that differences in terms of ionic activities as induced by the calcium sulphate phase could be noticed. The electrical conductivity technique was thus deployed as a preliminary and quick approach for this purpose. The time dependence of electrical conductivity during hydration has been used to study the early hydration reactions of different cementitious materials (Chung, 2002; Heikal *et al.*, 2006). This technique is complex and can be affected, for exemple, by w/c ratio, gypsum content, clinker fineness and admixtures (El-Enein Abo *et al.*, 1995; Tamás *et al.*, 1987).

The electrical conductivity of most cementitious materials is primarily due to the transport of ions through the pore solution medium. Within the first 10 minutes after the contact of water and

cement, calcium (Ca^{+2}) and hydroxyl (OH^{-}) ions are released into the suspension. The variation in electrical conductivity of a cement paste over time can therefore give information about the internal changes occurring within its pore solution. The precipitation of ettringite, CH and C-S-H phases are the first hydrate products that reduce the mobility of these ions through cement liquid medium (Maximilien *et al.*, 1997). These hydrates gradually fill up the capillary pores as the hydration proceeds, forming a rigid internal network with increasing strength. At this time, the electrical conductivity of cement paste decreases (Topçu *et al.*, 2012).

Figure 3.2 presents the electrical conductivity of cement with each calcium sulphate bearing material at different concentrations.

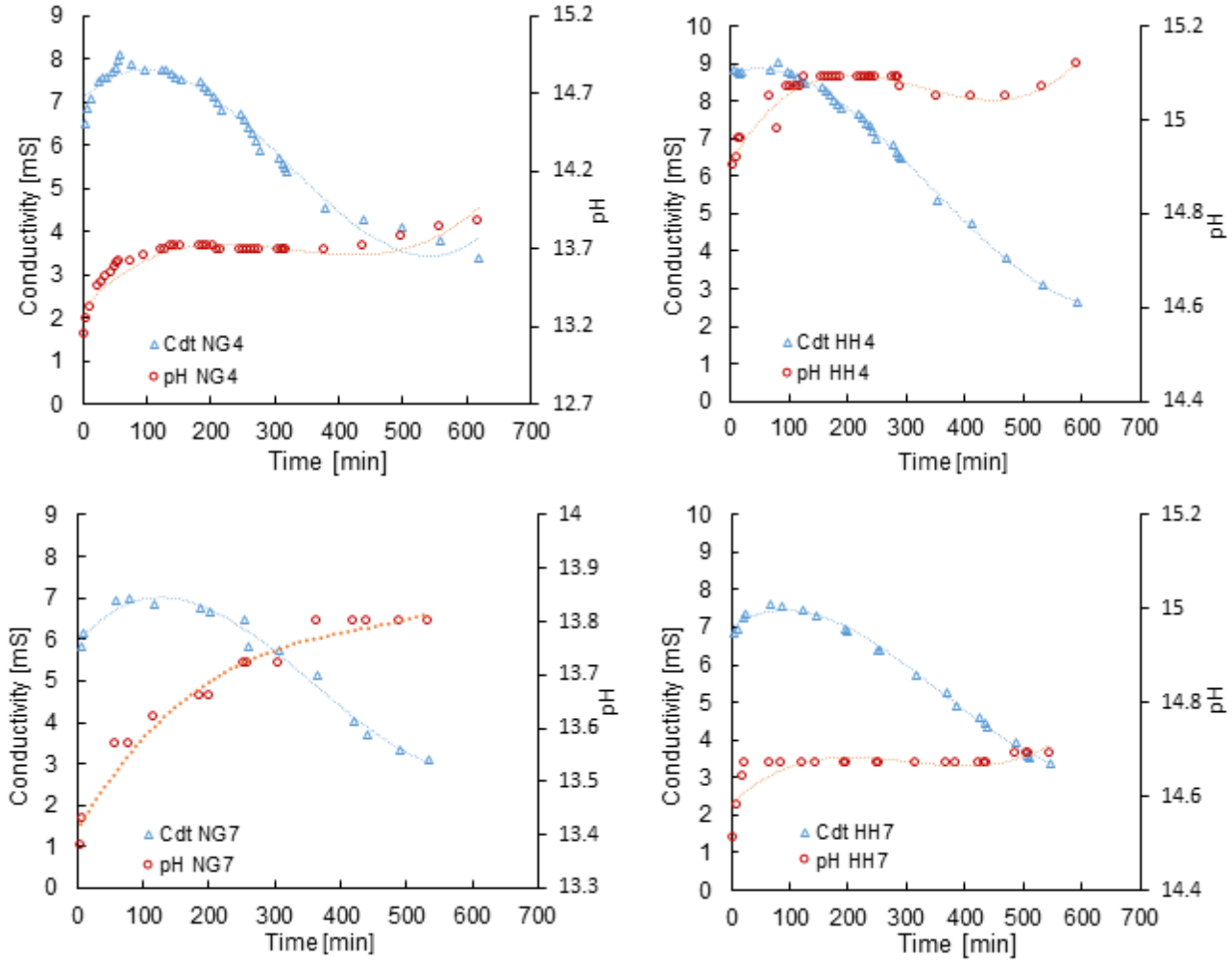

Figure 3.2: Typical electrical conductivity of cement with natural gypsum and hemihydrate at different concentrations

The early increase of the cement conductivity during hydration has been attributed by Nalet and Nonat (2016) to the dissolution of the anhydrous cement phases which release Ca^{+2}, OH^{-}, SO_4^{-2} and alkali ions and their mobility through water within the pores (El-Enein Abo *et al.*, 1995). Once

the concentration of these ions becomes high, ionic associations begin within the suspension and become rich in Ca^{+2} since the silicate phase provides half of its calcium content for C-S-H formation. The decrease in conductivity, on the other hand, has been associated with the precipitation of portlandite after a long period of supersaturation due to its slow nucleation (Maximilien *et al.*, 1997).

Cement pastes with hemihydrates at 4% concentration presented high values of conductivities as compared to the other cement pastes at any other concentration of both calcium sulphate types. This was likely due to high pH values experienced with this cement paste that favoured the hydrolysis of some cement phases enriching the suspension with ions susceptible for the formation of early hydrate products such as portlandite and ettringite.

After the pH had stabilized, around 100 minutes, the suspension experienced a decrease in sulphate ions (probably consumed for ettringite formation) and a constant concentration in calcium ions. This indicates that hydrate products precipitate by consuming the prevailing ions in the suspension resulting in a decrease in the number of ions released (Heikal *et al.*, 2006). At this stage, the large pores, or capillary pores, are filled with the yielded hydrate products, decreasing their volume fraction within the suspension (Rahimi-Aghdam *et al.*, 2017).

In general, cement pastes with natural gypsum presented lower values of electrical conductivity as compared to those with hemihydrate at equivalent concentrations of 4%. Having all cements with similar and equal phase contents, different only in calcium sulphate phase, it can be assumed that there were fewer SO_4^{-2} or Ca^{+2} ions released within the suspension with cements with natural gypsum as compared to those with hemihydrate, indicating that more sulphate ions were consumed within cement pastes with hemihydrate than those with natural gypsum.

It is evident from the observed experiments that the precipitation of early hydrate products are a consequence of the ionic activities induced by the type and the amount of gypsum phase during cement hydration.

3.6.4 Collection and analysis of data

This section presents relevant data pertaining to the rheological behaviour, and thermal and spectroscopy analysis of investigated cement paste. Their interpretations and analysis are also discussed within the scope of this research.

Flow properties: The yield stress and plastic viscosity of cement paste

Fresh properties of cement pastes, especially those related to the flow of materials, are significant in the manufacturing process, transport and placement of cementitious materials. The gypsum phase reacts with the most reactive cement phase, aluminate affecting the rheology of the whole cement matrix. It is therefore vital to assess the effect of the type and content of calcium sulphate bearing materials within the cement systems on the yield stress and the viscosity of cement paste. Dynamic yield stress and plastic viscosity values were obtained from the flow curve by extrapolating the measured data of the down curve to zero shear rate with the Bingham model. The measuring cycle time was 300 s as in work by Banfill and Saunders (1981), with a viscosity ramp of 100/150 s^{-2} for both up and down curves. The variation of stress within the specified time for up and down curve is illustrated in Figure 3.3.

A relationship between each rheological parameter (yield stress and plastic viscosity) and the corresponding mix with specified concentrations of natural gypsum or hemihydrate was then established. This allowed an evaluation of the effect of natural gypsum degeneration into hemihydrate on the flow properties of cement paste. It was critical to execute a such analysis to bring clarity on factors that affect the plastic viscosity of cement paste.

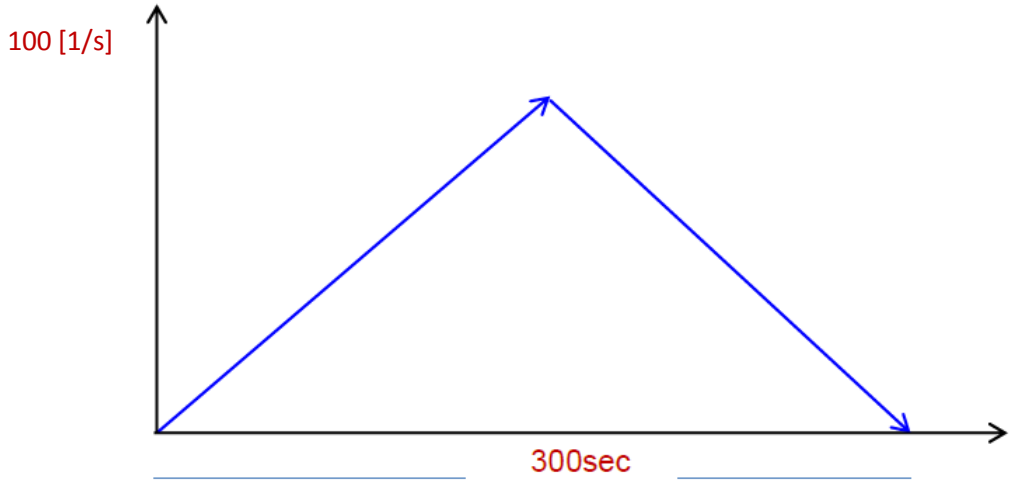

Figure 3.3: Shear rate variation within the measuring time for cement paste yield stress and plastic viscosity assessments

Viscoelastic properties: storage modulus and phase angle of cement paste

These measurements provide insight into the microstructure development of cement paste, as mentioned earlier. For this reason, the evolution of the storage modulus G' was monitored over a period of about 1 hour under a non-destructive regime defined within a linear viscoelastic domain (LVED) determined by applying a small amplitude oscillatory shear at a constant frequency of 1 Hz and an amplitude strain value of 0.06%. From the following measurements,

phase angles of corresponding cement pastes were also considered within the defined measuring time to assess the structuration of their internal networks.

The microstructure development of the cement system was assessed by estimating the internal strength rate development G'_{rate}. This rheokinetic parameter consists of calculating the ratio between the rigidification time, T^* (time at which the storage modulus reaches the maximum, $G'_{\max}$ according to the working zone of the rheometer) and $G'_{\max}$.

It was possible to evaluate the effect of hemihydrate within the gypsum phase of cements on the internal strength development of cement paste by correlating each strength rate value to the corresponding mix with specified hemihydrate concentration. Moreover, this provided an idea of the effect of hemihydrate on the workability loss of a given cement during concrete placement or casting.

Isothermal calorimetry: Heat flow rate of cement paste

The rate of cement heat evolution with time has been used to describe the chemical reactions that take place during cement hydration. Salvador *et al.* (2016) have defined a few parameters that characterize the isothermal calorimetry heat profile for cementitious materials. Although their primary goal was to analyse the effect of some accelerators in cement paste, these defined parameters can be somewhat appropriately interpreted for any cementitious mix which has been investigated using the calorimetric technique.

In this respect, the heat flow generated during the cement hydration was monitored using an isothermal TAM Air calorimeter at 20 ^{o}C and the reactivity induced within the mix was defined as illustrated in Figure 3.4. The reaction rate of the system was estimated by considering the slope of the ascending peak corresponding to the activity of the silicate and calcium sulphate phase on the heat flow curve. The energy released during cement hydration was evaluated by specifically integrating the area under the main peak of the curve. The length of the induction period comprised between the end of the pre-induction stage and the onset of the acceleration stage.

Furthermore, the degree of hydration was estimated by considering the theoretical total heat of hydration of cement under investigation and the amount of heat generated at a considered hydration time, as in research by Lawrence *et al.* (2003), Mota *et al.* (2015), and Salvador *et al.* (2016). The theoretical total heat (J) of hydration was obtained by summing the individual heat of hydration of different cement phases with their corresponding concentrations such as 510 J/g for C_3S; 260 J/g for C_2S; 1100 J/g for C_3A and 410 J/g for C_4AF.

The calcium sulphate consumption rate was estimated by comparing the initial available amount of calcium sulphate within the system and the time of the occurrence of the main peak. This was because in most cases the depletion of calcium sulphate happened at the same time as the silicate peak, as experienced by Kumar *et al.* (2012) and Thongsanitgarn *et al.* (2014) in some of their cements without admixtures.

The effect of calcium sulphate type and content on the hydration kinetics of cement was evaluated by establishing relationships between these hydration kinetic parameters and the concentration of each, or mix proportions, of the calcium sulphate phase.

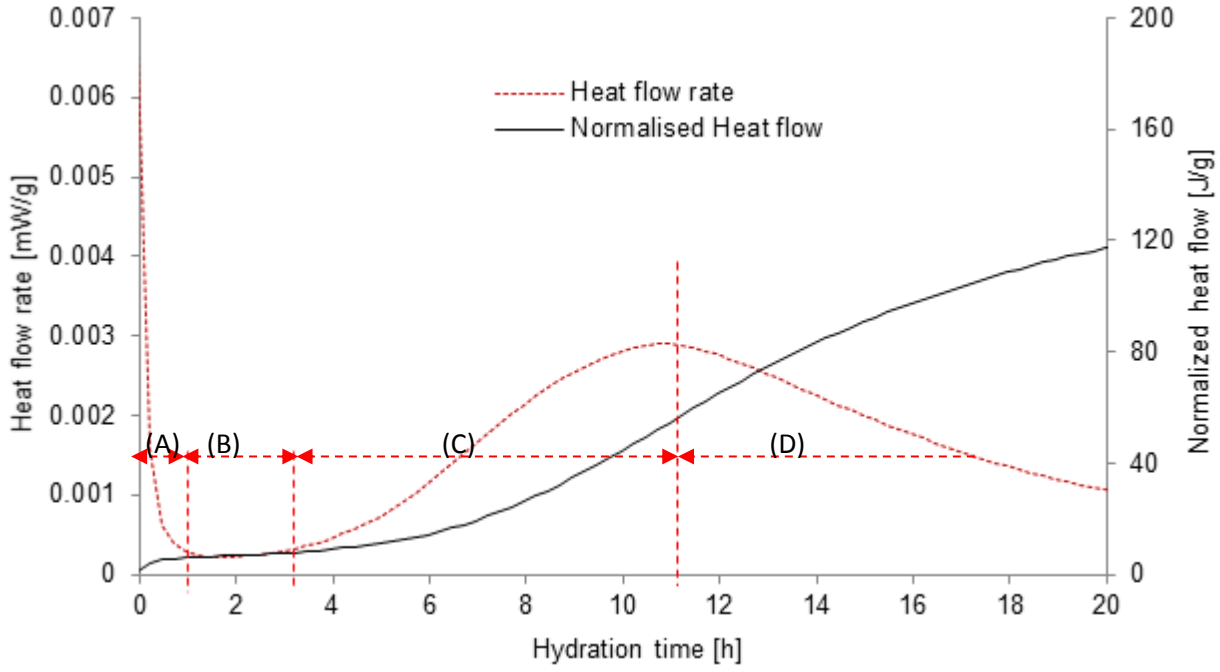

Figure 3.4: Generic heat flow rate of cement with 3% of natural gypsum: (A) pre-induction zone; (B) dormant phase; (C) acceleration zone; and (D) deceleration zone

Thermogravimetric and Differential Scanning Calorimetry: TG-DSC heat profiles

The TG-DSC profiles of stopped cement samples were used to quantify the hydrate phases and estimate the degree of hydration at specific hydration times. These profiles were collected over a dynamic heating ramp varied between 24 ^{o}C and 1000 ^{o}C, within which temperature range the thermal decomposition of hydrate phases occurs within three distinct intervals – the dehydration, the dehydroxylation and the decarbonation – as better resolved by the differential scanning calorimetry curve. Although the limiting temperatures of these regions are different from one published study to the other, those suggested by Bhatty (1986) appeared consistent and were

validated recently by Monteagudo *et al.* (2014). These regions are illustrated on a generic thermogravimetric and differential thermal (TG-DTA) heating curve, as in Figure 3.5.

The dehydration occurs between 105 ^{o}C and 430 ^{o}C and belongs to the decomposition of C-S-H and ettringite. The dehydroxylation or the decomposition of calcium hydroxide (CH) occurs between 430 ^{o}C and 530 ^{o}C, while the decarbonation is within 530 ^{o}C and 1000 ^{o}C. In particular, within the dehydration region, the ettringite thermal decomposition was considered to be tween 110 ^{o}C and 140 ^{o}C even though susceptible to ambient pressure and humidity, as reported by Meller *et al.* (2009) and Wang *et al.* (2016).

The quantification of the hydrate phase was estimated by considering the weight loss within the specified temperature region and expressed in percentage of the sample weight, as per Equation (3.1):

$$P(\%) = \frac{\Delta w \times M_{hp}^{H2O}}{M_{hp}^{H2O} - M_{hp}} \tag{3.1}$$

Where $P(\%)$ is the quantity of the hydrate phase; Δw the mass loss within the specified interval (%); M_{hp}^{H2O} is the molecular weight of the hydrate phase (g); and M_{hp} is the molecular weight of the decomposed hydrate phase after losing its crystal water (g).

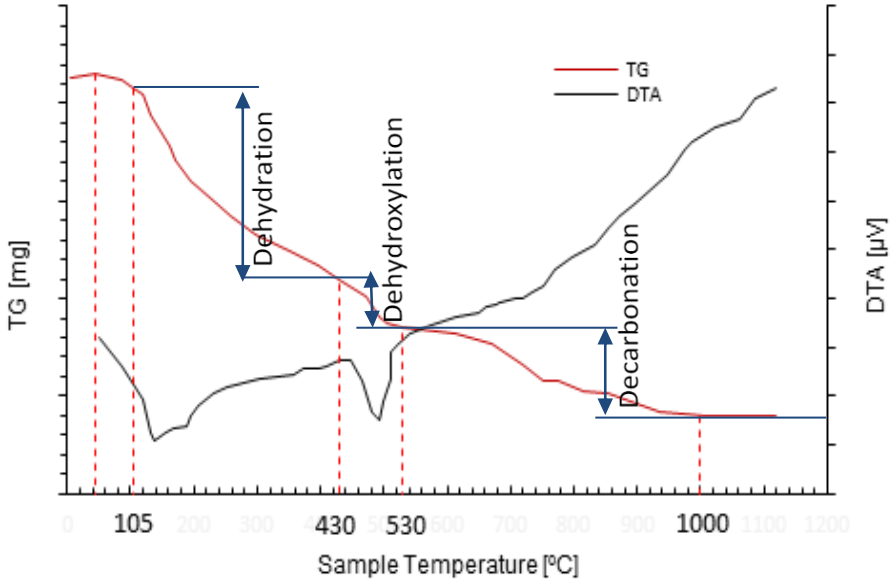

Figure 3.5: Typical thermogravimetric and differential thermal profile of cement (Monteagudo *et al.*, 2014)

The amount of calcium hydroxide formed during hydration, CH (%), can be estimated as suggested by El-Jazairi and Illston (1980) in Equation (3.2):

$$CH(\%) = 4.11\Delta W_{dx} + 1.68\Delta W_{dc} \tag{3.2}$$

Where ΔW_{dx} and ΔW_{dc} are, respectively, the weight losses of the sample for the dehydroxylation and decarbonation peaks.

The degree of hydration was assessed by considering the chemically bound water incorporated in C-S-H gel, as per Equation (3.3) suggested by Bhatty (1986).

$$\alpha = \frac{w_B}{0.24} \tag{3.3}$$

w_B is the chemically bound water expressed in percentage and obtained as per Equation (3.4)

$$W_B = \Delta W_{dh} + \Delta W_{dx} + 0.41\Delta W_{dc} \tag{3.4}$$

ΔW_{dh} the weight loss of the sample for the dehydration peak.

The values of 0.24 and 0.41 are, respectively, the maximum chemical bound water required to fully hydrate a cement particle and the conversion factor to assess the chemically bound water derived from the carbonated portlandite, equivalent to the ratio between the molecular weight of H_2O and CO_2.

The amount of ettringite and portlandite precipitated with respect to the natural gypsum substitution could then be estimated, and the effect of the hemihydrate concentration within the cement on the formation of these early hydrate products was assessed.

Scanning Electron Microscopy and Energy Dispersive Spectroscopy

SEM, though still an experimental technique, provides relevant understanding of various hydrated compounds, their relative amounts and the morphology changes undergone by cement microstructures during hydration. This information is of utmost importance as most macroscopic properties of the material can be interpreted rationally and optimized.

In this research, the cement paste microstructure was analysed using secondary and backscattered electron imaging approaches. Hydrate phases were then characterized on a map with superimposed layers of different dominant cement elements, including calcium, aluminium, silicon, iron and magnesium. Identification of these hydrates was by an energy dispersive X-ray analyser over different areas of the sample (Hu *et al.*, 2017). The acquired X-ray spectra as illustrated on the generic ED-spectra in Figure 3.6 helped obtain the atomic concentrations of each element at specific slot, and after a statistical analysis, the atomic ratio Al/Ca vs Si/Ca was plotted, as represented in Figure 3.7.

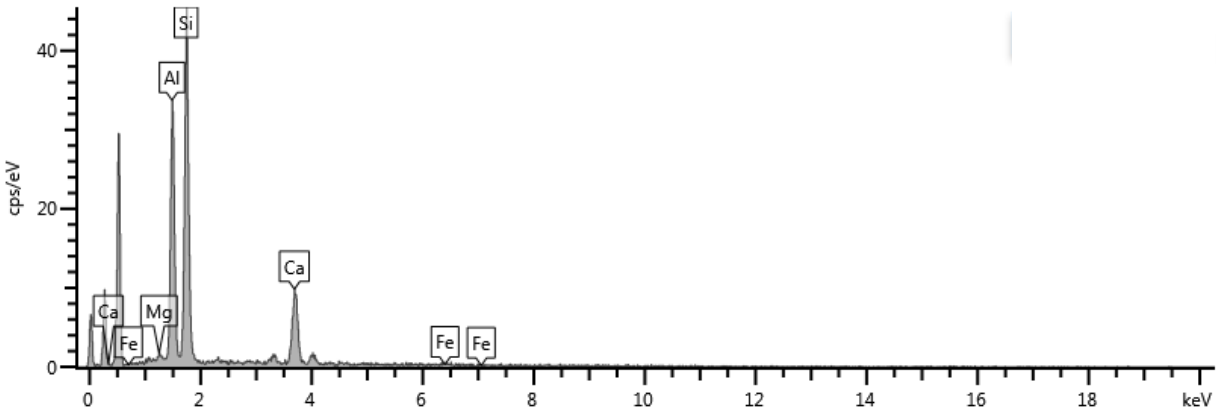

Figure 3.6: Typical energy dispersive X-ray spectra on a spot area of cement paste sample with only hemihydrate as set regulator after 1 hour of hydration time

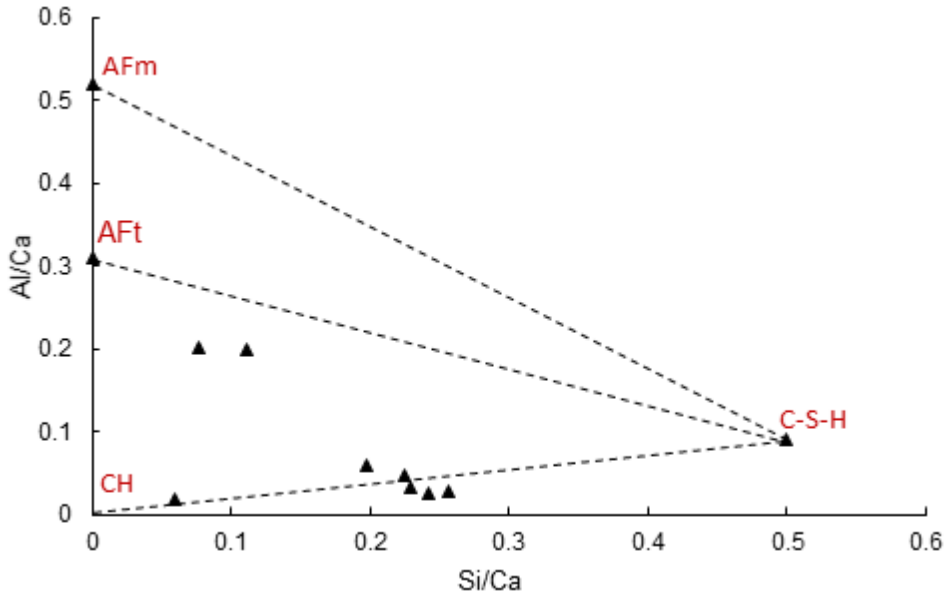

Figure 3.7: Typical atomic ratio of Si/Ca vs Al/Ca for cement paste with only hemihydrate as set regulator hydrated for 1 h

X-ray diffraction

The powder X-ray diffraction method was used to qualitatively identify hydrate and anhydrous cement phases as an integral approach to previous techniques such as TG-DSC and SEM. This technique is preferred over the in-situ XRD technique because water loss and carbonation issues during measurements are avoided. X-ray patterns of good resolution could also be obtained, since it is possible to achieve smooth surfaces during sample treatment. In addition, there is no absorption of the signal by water film that is normally formed between the wet sample and the protective material used around it to avoid evaporation and contact with the air. These can cause artefacts at realistic w/c ratios causing misguided interpretations of the results.

X-ray patterns of cement with different proportions of natural gypsum and hemihydrate were collected at different times of hydration to qualitatively evaluate the evolution of phases within the cement microstructure and the subsequent effect of the natural gypsum substitution.

Setting times and compressive strength of mortars

The primary reason calcium sulphate bearing materials are introduced in cement clinker is for controlling the setting time of cementitious materials. This is achieved by regulating the hydration of aluminate phase with the presence of calcium sulphate within the system (Strydom & Potgieter, 1999).

Initial and final setting times of different cement mixes with different types and content of calcium sulphate bearing materials were measured. Since physical properties of cementitious materials depend on changes occurring on microstructural levels (Thomas & Jennings, 2006), these results were compared to those observed on cement paste microstructures.

Compressive strengths were also measured of mortar with different types and content of calcium bearing materials cured for 24 hours. These strengths were only collected for the first phase in order to optimise for the required SO_3 concentration within the cement system. This helped to execute the experimental work pertaining to the second phase of this research, as specified in section 3.6.1.

3.6.5 Research instruments

Different apparatuses were employed to achieve the aim and objectives of this research during the experimental work. These instruments were calibrated according to specified standards before testing and serviced in accordance to manufacturer recommendations.

Rheometer

Steady shear and small oscillatory shear experiments were carried out on a shear strain rate controlled MCR 51 rheometer supplied by Anton Paar. This rheometer is fitted with a circulating water bath keeping the sample isothermally at 23 ^{o}C during all rheological measurements. The geometry used was suitable for dispersion materials such as cement pastes.

In dynamic rheometry, both the sample and shaft transducer exhibit some compliance. This is the displacement experienced by the shaft transducer and the sample, resulting from the torque applied to the transducer. During measurements, as the transducer is being deformed along with the sample, some of the applied strain deforms the sample and some the transducer, leading to errors in sample moduli which gradually increases as the sample stiffness increases. The latter defines the sample compliance that can be adjusted by either accommodating the sample dimensions or the geometry used to that of the shaft transducer. This practice is critical because it designates the operation range of the instrument, defining the maximum and minimum possible complex modulus that can be measured by each transducer using a specific geometry (Rheometric Scientific Inc, 2003).

The operating working zone of the rheometer using a roughened parallel plate of PP50/S type, a gap of 0.6 mm and for a time sweep recorded at 10 rad/s was determined by Equation (3.5).

$$G^* = \left(\frac{K_\tau}{K_\gamma} \right) C \tag{3.5}$$

Where, K_τ is the stress constant for the specific geometry; K_γ is the strain constant for the specific geometry; and C is the stiffness (the reciprocal of the instrument compliance) of the instrument. The maximum storage modulus *G'* that can safely be measured using this specific geometry was $5x10^5$ Pa. Measurements above this limit value were discarded during analysis of results.

Calorimeter

The heat flow generated during the cement hydration was monitored using an isothermal TAM Air Calorimeter at 20 ^oC. This equipment consists of eight parallel twin measurement cells with one allocated to the actual sample and the other to the reference vessel. In this work, water with the same mass as the sample (6 g) was used as reference to improve the signal-to-noise ratio and to correct measurements and temperature artefacts. The testing procedure consisted of lowering a glass ampoule containing 4.8 g of cement into the measuring position inside the calorimeter. The mixing water (w/c =0.4) 1.2 g was injected into the ampoule after a steady state was reached. To avoid losing relevant information pertaining to the first contact of water and cement, the mixing was performed using an internal stirring mechanism.

TG-DSC instrument

A Netzsch STA model TG-DSC instrument was used for thermal gravimetric analysis. This is a simultaneous thermal analyser, equipped with a data acquisition system using Nersch software, to allow the instrument to simultaneously carry out the thermal gravimetric analysis and the differential scanning calorimetry of the sample. The base line was established by using the crucible pan in aluminium. The nitrogen (N_2) flux was used as the flowing gas at 50 ml/min. The heating started at 23 ^oC at a rate of 5 K/min to allow the equipment to stabilize beforehand and to eliminate all possible defects from the setting up of the instrument. The reference sample was air and the experimental heating temperature ranged from 105-1000 ^oC.

SEM and XRD equipment

Images of stopped hydrated cement were obtained using a Zeiss Auriga field emission gun scanning electron microscope (FEG-SEM) operated at 15 kV for imaging and 20 kV for EDS analyses. All EDS analyses were completed using an Oxford Instruments X-Max solid-state silicon drift detector.

Additionally, powder diffraction data were collected on a D8 ADVANCED diffractometer from BRUKER AXS (Germany) using Cu-Kα radiation (λKα=1.5406 Å) operated in the reflection geometry in a locked coupled mode at room temperature with a LynxEye position sensitive detector. Data were collected from 5° to 90° in 2θ with a step size of 0.034° at 0.5 s/step. The X-ray tube was operated at 40 kV and 40 mA. The X-ray diffraction patterns were analysed semi-quantitatively by Rietveld analysis using the software X'Pert High Score Plus. C-S-H could not be detected due to its low degree of crystallinity.

Other equipment

Setting times were evaluated on an automatic computer-controlled Vicat needle ToniSet Expert. The instrument has up to 12 measuring stations for cement paste for setting characteristic determinations. This machine, mounted with an external thermostat to maintain the curing temperature at a constant value, has a high precision measurement of the penetration depth by incremental measuring system with a resolution of 0.05 mm. It also allows experiments to be executed under different set standards. Data were thus collected according to EN196/ASTM C 191 under 23 ± 1 °C curing temperature.

Compressive strengths were assessed on a ToniZEM compressive test machine. This equipment is a standard-compliant compressive strength test for cement and various other binding materials. It can execute experiments on mortar samples with variant geometric forms (prisms and cubes) and with different specification options. The instrument is mounted with a microprocessor and a servo-hydraulic control with an accuracy of quality class 1/EN ISO 7500-1/DIN 51220.

Particle size distribution of cement systems were measured using a Malvern Mastersizer 2000 (Malvern Instruments, UK) with the capacity to detect particles within the range of 0.02-2000 µm. Samples were under constant agitation at 2000 rpm in isopropanol as solvent.

3.6.6 Material used

An ordinary Portland cement clinker was sampled during the production process of CEM I in accordance with ASTM C150 under stable kiln operations at a local cement plant. This was crushed and ground without any form of calcium sulphate bearing material and was considered relatively pure cement clinker. Two types of calcium sulphate materials – natural gypsum (NG) and hemihydrate (HH) – were considered as a source of sulphate within the clinker. The French sand standard CEN, EN 196-1 was applied for assessing the compressive strength of cement mortars. This European sand was selected since its particle size distribution is wider allowing better particle packing, improving the connectivity of the capillary pores and leading to better availability of water necessary for ettringite formation, as suggested by Horkoss *et al.* (2016).

The chemical compositions of the cement clinker and calcium sulphate materials, as determined by XRF spectroscopy, are presented in Table 3.1.

Table 3.1: Chemical and phase composition of clinker and calcium sulphate

Compounds	clinker	NG	HH
SiO_2	23.2	0.81	1.01
Al_2O_3	5.96	0.03	0.10
Fe_2O_3	3.61	0.00	0.00
Mn_2O_3	0.38	0.08	0.08
TiO_2	0.27	0.01	0.02
CaO	62.38	42.08	40.63
MgO	1.68	0.46	0.56
P_2O_5	0.09	0.05	0.05
Cl	0.02	-	-
SO_3	0.81	44.71	52.43
K_2O	0.45	0.03	0.03
Na_2O	0.07	-	-

It is clear that the clinker had a negligible amount of SO_3 which was inevitable due to the characteristics of the kiln used for clinkering. The high amount of CaO and SO_3 and the low concentration of foreign oxides noticed in the calcium sulphate bearing materials evidenced their purity.

3.6.7 Sample preparations and measurements

Sample preparation is an important task in any experimental work, influencing the reproducibility of measurements. It is therefore required that cement samples be brought on the same reference conditions prior to testing. This can be achieved by consistency throughout measurement protocols, including material storing, sample curing, mixing and running of the equipment.

Cement powder

Cement powder was obtained by adding directly to the clinker different concentrations of either natural gypsum/hemihydrate or different mix proportions of these two materials. The prepared raw material was homogenized in a ball mill bottle for a few hours, as done by Li *et al.* (2014). Each calcium sulphate type was individually added to the clinker at concentrations ranging from 2% to 7%. In many countries, an addition of calcium sulphate bearing material of not more than 5% is advised (AENOR.UNE-EN 197-1, 2011). Therefore, amounts beyond 5% were only considered for scientific interest.

The mix proportions of natural gypsum and hemihydrate were determined based on a set concentration previously determined in the first phase based on the mechanical and chemical performance of cement mixes. These proportions were identified in terms of NG/HH nomenclatures defining an NG (natural gypsum) fraction and HH (hemihydrate) fraction within the set concentration of calcium sulphate cement phase.

The addition of these calcium sulphate bearing materials to the clinker affects the SO_3 content of the overall cement system. The total SO_3 content of the raw material was estimated using a Leco sulphur analyser. For this purpose, 0.01 to 0.1 g of the cement sample was heated to approximately 1350 °C in an induction furnace while allowing a stream of oxygen to pass through. Sulphur dioxide released from the sample was then measured by an IR detection system and the total sulphur result was provided. Table 3.2 provides theoretical and actual concentrations of SO_3 within the cement systems with respect to the initial quantity of added calcium sulphate type, whereas the corresponding SO_3 content within the mix proportion NG/HH is given in Table 3.3.

Table 3.2: Concentration of SO_3 as provided by the initially added amount of natural gypsum and hemihydrate in the clinker

	Concentration [%]	2	3	4	5	6	7
HH	Actual SO_3 [%]	1.65	2.18	2.64	3.06	3.48	3.95
	Theoretical SO_3 [%]	1.77	2.27	2.76	3.26	3.76	4.26
NG	Actual SO_3 [%]	0.1	1.64	1.72	2.11	2.70	3.51
	Theoretical SO_3 [%]	1.64	2.07	2.50	2.93	3.36	3.79

It was assumed that the slight differences of SO_3 concentrations, as determined theoretically and experimentally using the leco method, were due to human error during sampling.

Table 3.3: Total SO_3 concentration within the clinker with 4% calcium sulphate provided by the mixture of natural gypsum (NG) and hemihydrate (HH) in different proportions

NG/HH concentration	0/100	40/60	50/50	60/40	70/30	100/0
SO_3 [%]	2.89	2.56	2.97	2.46	2.69	2.38
Number of mole of sulphate	0.69	0.63	0.62	0.61	0.59	0.55

It can be noticed that at this calcium sulphate concentration (4%), the total SO_3 generated by the mix proportions of the two types of calcium sulphate bearing materials within the cement systems was within the recommended limits (2.5-3%) for commercial Portland cements (Peray, 1979; AENOR.UNE-EN 197-1, 2011). The particle size distributions of the cement mixes measured are presented in Table 3.4

Table 3.4: Particle size distribution of the clinker and cement clinker with different proportion of NG and HH at 4% calcium sulphate within the system

Sample ID/ characteristic size	d_{10}	d_{50}	d_{90}	D [3, 2]	D [4, 3]	SSA[cm^2/g]
Clinker	5.956	16.363	36.111	10.416	18.949	3840
100/0	4.858	15.81	35.182	9.471	18.234	4220
70/30	5.345	16.165	36.449	10.034	18.848	3990
60/40	5.801	16.304	36.44	10.319	19.038	3880
50/50	5.316	16.123	36.208	10.026	18.715	3990
40/60	5.186	16.361	37.193	10.011	19.159	4000
0/100	4.333	30.798	82.524	10.983	37.973	3640

Clearly, the addition of 4% calcium sulphate bearing materials to the clinker does not much affect the specific surface area of the cement systems. Also, the characteristic sizes such as d_{10}, d_{50} and d_{90} of all the cement mixes remain similar to the original clinker size except that with only hemihydrate.

Mixing cement paste and mortar

A constant w/c ratio of 0.4 was used throughout the experimental work. Cement paste was batched with a laboratory Hobart mixer using distilled water cooled to a constant temperature of 23 ± 1 ^oC. Water was first introduced to the mixer and the cement gradually added over a period of 2 min. After two consecutive resting times of approximately 2 min each, the mixing resumed for a further total mixing time of about 10 min. A portion of the fresh cement was collected for rheological measurements and stored in a water bath at 23 ± 1 ^oC for 15 minutes prior to the test. This curing time is enough for the precipitation of at least one third of the total ettringite amount (Dalas *et al.*, 2015). The other portions were cast in small plastic containers and kept in the curing room at 23 ± 1 ^oC with relative humidity of more than 90%.

Similarly, cement mortars were also mixed following the same sequences, except that sand particles were added during the procedure. For this reason, 450 g of cement (clinker with specified amount of calcium sulphate bearing material) and 1310 g of sand were considered for the mixing. Thereafter, the mortar was vibrated on a ToniVIB vibrating table according to ASTM C109 to eliminate all possible air within the system. Mortar prisms of 40 x 40 x160 mm were cast and maintained in the same conditions as for cement pastes. After a curing time of 10 hours, samples were demoulded and stored for a further 14 hours before crushing.

The hydration reaction of cement paste was stopped at different curing times by immersing the sample in isopropanol for three days. The free water within the pores was removed with a vacuum pump for several hours and then vacuum dried at 40 ^oC for 72 hours. Finally, the specimen was

dry ground for TG-DSC, SEM analysis and sulphate determination and ground with hexane for X-ray diffraction analysis with a laboratory ring mill.

3.7 Conclusion

The two major phases of this research have been presented in detail. The experimental techniques and analysis for each specific measurement were discussed. Requirements for acceptable rheological measurements were explained and their applications to cementitious materials were also introduced.

Preliminary tests were conducted to determine the eventual effect of ionic activities on the microstructure development and the verification of possible differences in cement mix performances. This was considered important due to the fact that the amount of calcium sulphate phase initially added to the clinker was insignificant as compared to that of the bulk cement system.

An experimental and comparative research design was considered during the two phases of this project. The first completed the experimental work related to the assessment of the individual effect of each calcium sulphate bearing material (natural gypsum and hemihydrate) on the hydration kinetics, and on the mechanical properties of cement systems. This provided the optimum concentration of calcium sulphate to be added to the clinker. The effect of the mix proportion of natural gypsum and hemihydrate were chosen with respect to a previously determined concentration, constituting the second phase.

Dynamic yield stress and plastic viscosity values of cement systems were obtained on flow curves using the Bingham model, while the rigidification of the cement microstructure was estimated based on the measurements of storage moduli in the oscillatory mode. The heat flow rates of cement pastes were collected on a TAM Air calorimeter and parameters for their characterizations were determined. TG-DSC heat profiles with experimental temperatures starting from 105-1000 ^{o}C were acquired on thermogravimetric analysis equipment for the quantification of early hydrate products such as ettringite and portlandite. The degree of hydration was also estimated from these profiles based on the quantity of chemically bound water and free calcium hydroxyl present in the system. Cement microstructure images were captured using a SEM-SBE approach and hydrate phases were identified using an EDS analyser based on atomic ratios of determined cement elements. XRD patterns were considered as integral techniques to the TG-DSC and SEM methods.

The preparation and mixing protocols of samples, and their experimental measurements adhered to specified standards using approved academic and industrial instruments. Challenges encountered during the execution of the experimental work, data analysis and limitations of equipment used were also discussed.

Chapter 4 Effect of natural gypsum and hemihydrate on cement paste hydration kinetics

4.1 Introduction

It was previously shown in section 2.5 that the rapid hydration of cement aluminate phase is mainly controlled by the calcium sulphate. This is generally added at the final grinding in the form of natural gypsum that can be transformed into hemihydrate due to temperatures increases within the ball mill. In fact, ready soluble sulphate ions SO_4^{-2}, from the added calcium sulphate phase, are released into the aqueous solution and react with the C_3A phase to form ettringite. This hydrate product passivates the reactivity of the aluminate phase in the presence of water, allowing the paste to remain fresh for some time.

The solubility rates of these calcium sulphate types are distinctly different, hemihydrate being more rapidly soluble than gypsum. Consequently, the hydration kinetics of cement paste with hemihydrate is expected to also be different from that with natural gypsum. The designation of the type of calcium sulphate to be used as set regulator is therefore as important as the adjustment of the calcium sulphate content within cement systems.

This section presents and discusses the results related to the use of natural gypsum/ hemihydrate as set regulators at different concentrations. The hydration kinetics and subsequent hydrate products were investigated with respect to these concentrations. The effect of these calcium bearing material types and concentrations on the mechanical properties of cement systems were also considered.

4.2 Hydration kinetics of cement systems

The hydration kinetics of these calcium bearing materials are described in the corresponding heat flow curves in Figure 4.1 Figure 4.2. The overall heat flow profiles can be found in Appendix A.

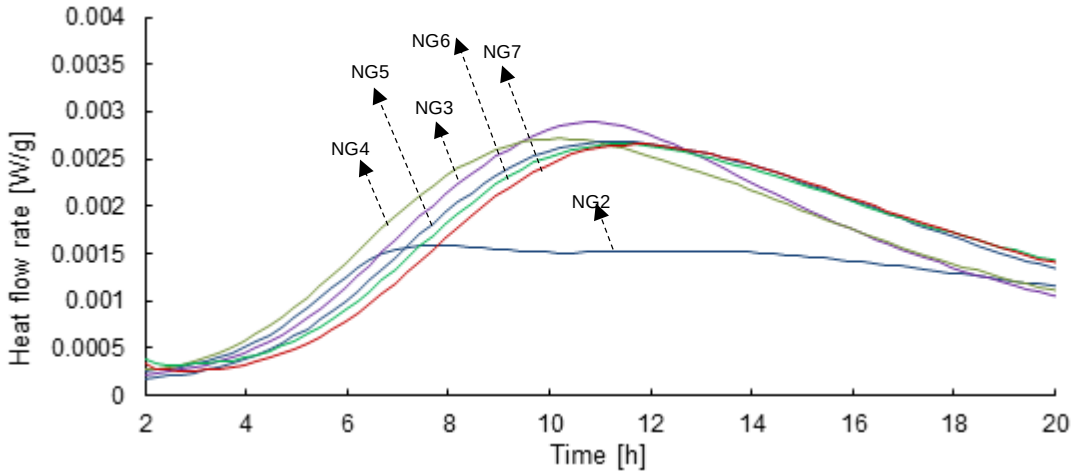

Figure 4.1: Influence of natural gypsum concentration on the hydration kinetics of cement paste

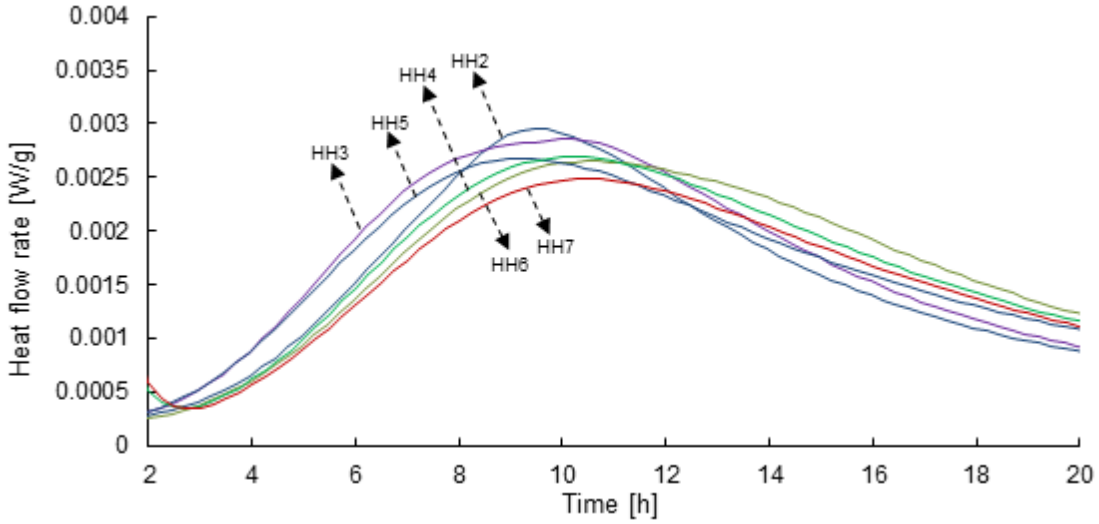

Figure 4.2: Influence of hemihydrate concentration on the hydration kinetics of cement paste

These calorimetry heat profiles describe the different stages of hydration at all calcium sulphate concentrations. The initial peaks that are well resolved on the overall profiles in Appendix A correspond to the pure dissolution of different cement compounds. Thereafter comes a period of low thermal flow defining a slow rate of hydration, referred to as the dormant phase. This, in most cases, lasted for a few minutes after the contact of water and the cement. This period was followed by a sharp increase in heat flow and reached a peak after around 12 hours of hydration.

From Figure 4.1 to Figure 4.2, it was observed that the hydration kinetics of both natural gypsum and hemihydrate tended to increase the dormant period length with the increase in their respective concentrations up to 4%, and thereafter it decreased. Also, the reaction rate during the acceleration period seemed to decrease with higher concentrations of these calcium bearing materials. Conversely, the reaction rate during the deceleration period increased with higher

concentrations of these calcium sulphates. This phenomenon could be due to the decrease in available space for eventual reactions caused by the precipitation of important amounts of early hydrate products as reported by Quennoz (2011). The cumulated heat released during the hydration of cement mixes is presented in Figure 4.3.

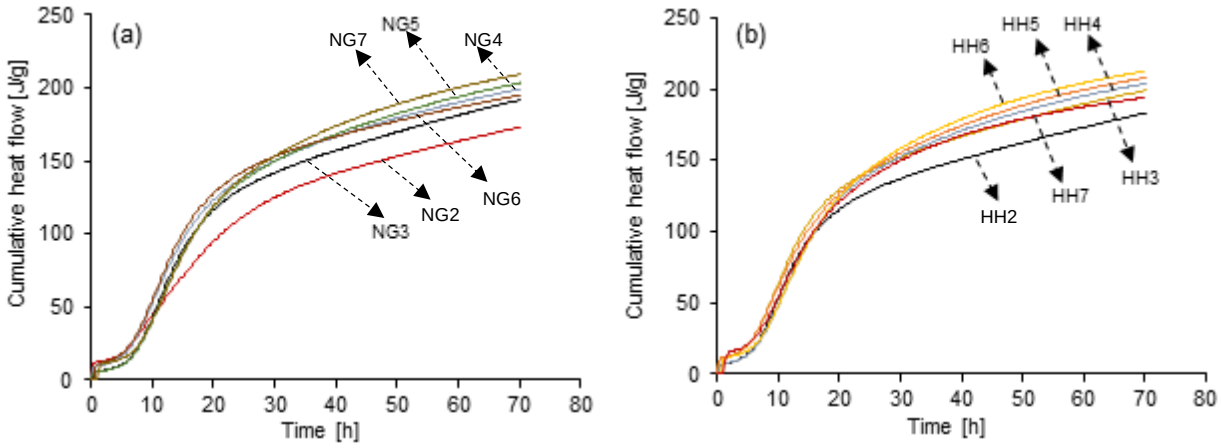

Figure 4.3: Cumulative heat flow of cement with natural gypsum (a) and hemihydrate (b) at different concentrations

It can be seen from Figure 4.3 that the total heat of hydration reactions changes with the increase in calcium sulphate concentration within the systems. For both natural gypsum and hemihydrate, at a concentration of 2%, the cumulative heat released is lower at all times of hydration and increased with increasing concentration.

From Figure 4.4 and Appendix B, it can be noticed that at equal concentrations, the reaction rate of cement clinker with hemihydrate seemed to be faster than that with natural gypsum. Correspondingly, the total heat released during the hydration was also higher in cement with HH than NG, as shown.

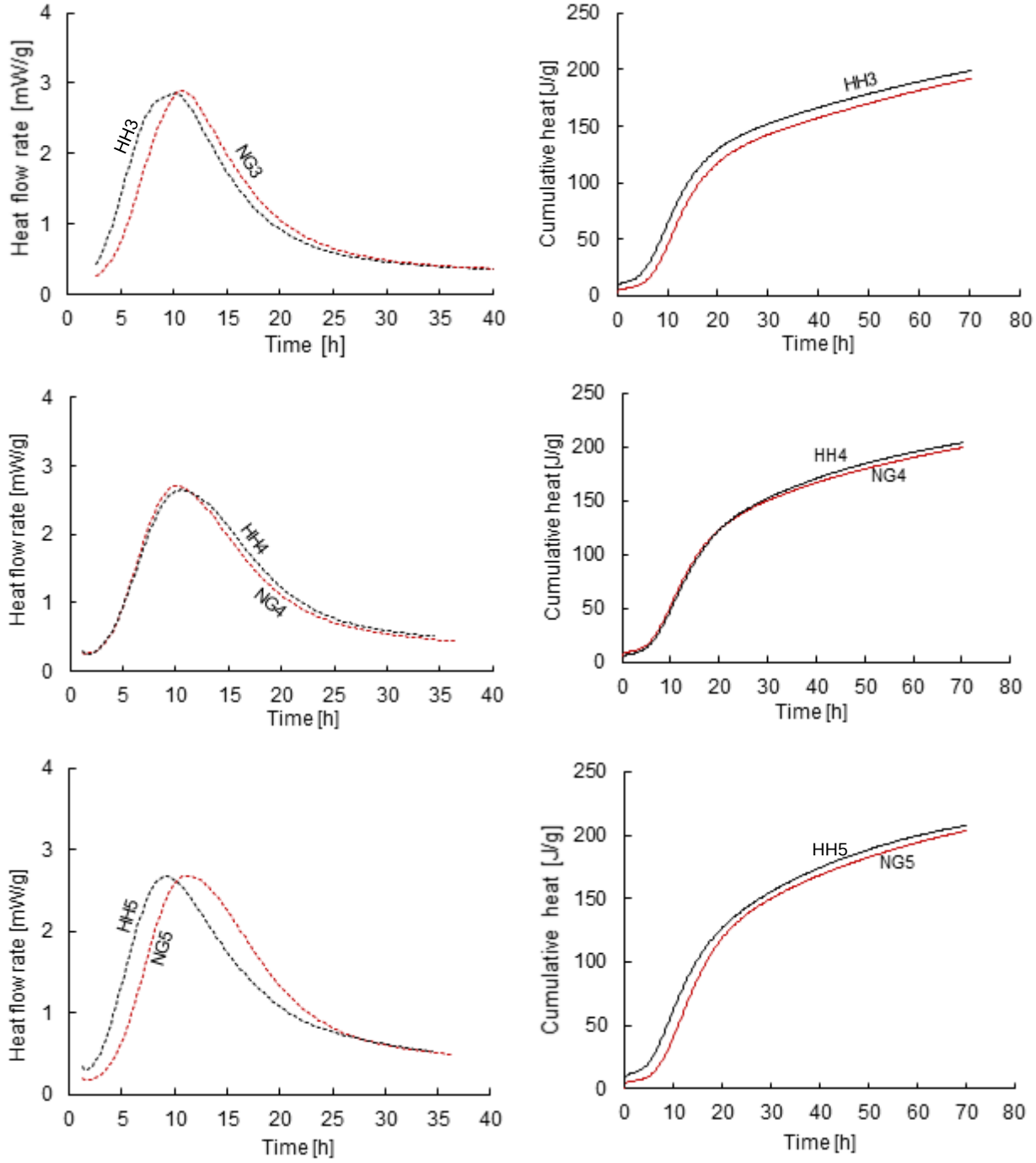

Figure 4.4: Comparison of reaction rates and cumulative heat flow of cement with hemihydrate (HH) and natural gypsum (NG) at 3%, 4% and 5% concentrations

The occurrence time of the exhothermic peak, corresponding to the depletion of calcium sulphate within the system, appeared earlier in systems with hemihydrate than those with natural gypsum except at 4% where the occurrence times were identical. However, after the calcium sulphate depletion, it was observed that the deceleration rate was higher in systems with natural gypsum.

Comparing the dormant phase length as illustrated in Figure 4.5, it can be seen that these were longer in cement systems with natural gypsum and shorter in those with hemihydrate, especially at higher concentrations.

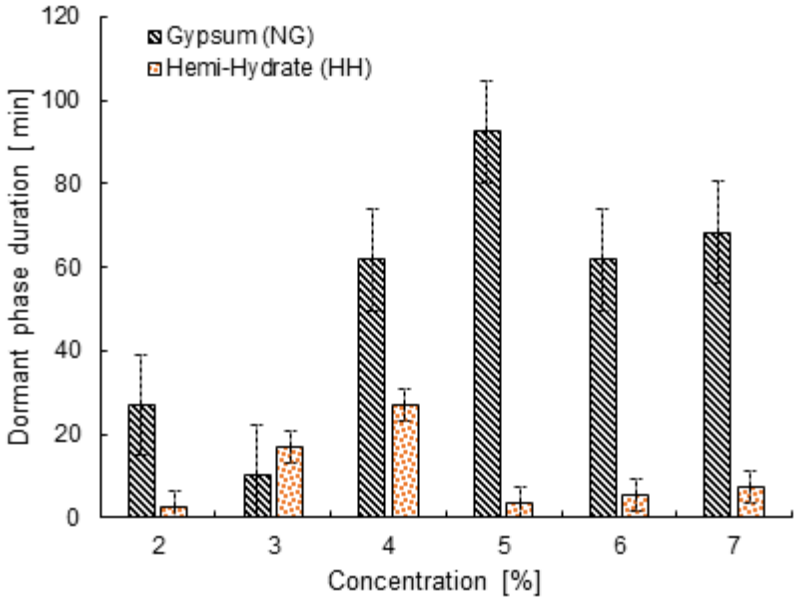

Figure 4.5: Comparison of dormant phase duration of cement systems with natural gysum and hemihydrate at different concentrations

It is undisputable that these reaction kinetics reveal information on the reactivity induced within the cement system and depend on the type and concentration of calcium sulphate bearing material used.

4.3 Reactivity induced within cement systems

The hydration process involves different reactions between cement phases. When natural gypsum was used as a source of calcium sulphate, these reactions were understood to happen at a lower speed, especially before the depletion of calcium sulphate. This was attested by the long durations of the dormant phase, the slow acceleration rate and the essential energy released during the early hydration of the cement mixes.

Considering everything equal in the cement clinker (e.g. at the same w/c ratio), the clinker phases react in the same manner. The difference in the kinetics of these cement systems can hypotheticaly therefore be attributed to the presence of calcium sulphate within the system. Due to the high solubility of hemihydrate, it can be accepted that sulphate ions would be supplied faster in the liquid phase of cement systems with hemihydrate than those with natural gypsum.

Consequently, a rapid formation of early hydrate products stemming from aluminate-sulphate interactions takes place and leads to a faster depletion of these ions within the system.

Considering the time of occurrence of the main peak and the initially added amount of calcium sulphate concentrations within the system, the consumption rate of $CaSO_4^{-2}$ ions can be estimated as explained in section 3.6.4 and represented in Figure 4.6.

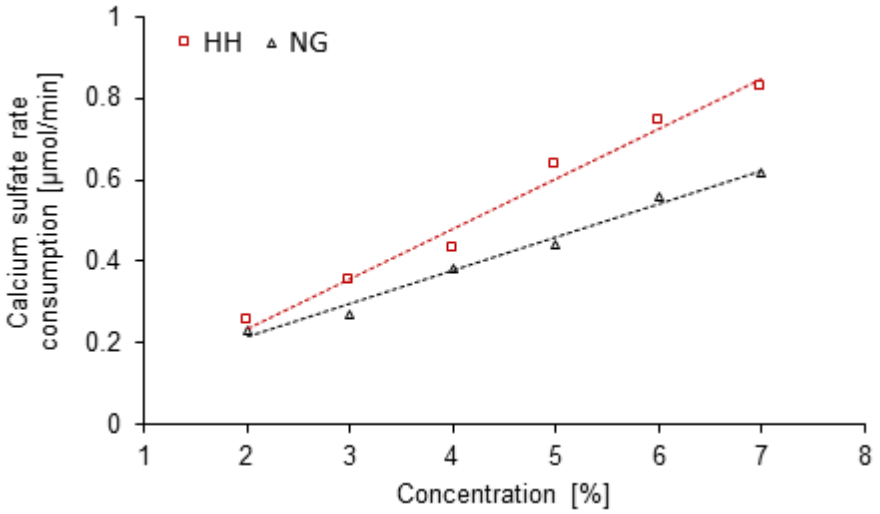

Figure 4.6: Consumption rate of calcium sulphate per gram of cement with hemihydrate (HH) and natural gypsum (NG) at different concentrations

It can be seen from Figure 4.6 that at all concentrations of cement sytems with hemihydrate experienced higher rates of calcium sulphate consumption as compared to those with natural gypsum. In addition, the consumption rate increased with the increase in the initial amount of calcium sulphate. At a concentration of 2%, these two calcium sulphate bearing materials had almost the same consumption rates of $CaSO_4^{-2}$ ions. However, Figure 4.1 and Figure 4.2 show that their respective kinetics were very different. At this concentration (2%), cement with natural gypsum exhibited a main peak with a lower amplitude and a broader width, implying a lack of necessary ions to perform essential reactions within the system. In all cases, an average value of calcium sulphate consumption rates were evaluated around 0.42 µmole/min and 0.54 µmole/min, respectively, for natural gypsum and hemihydrate. This suggested that significant amounts of ettringite would be expected to form in pastes with hemihydrate more so than those with natural gypsum.

Furthermore, the degree of hydration as presented in Figure 4.7 shows that the degree of hydration of cement systems depended on the type and concentration of calcium sulphate within the suspension. Before or at the time of the exhaustion of sulphate ions present in the liquid

phase, cement with hemihydrate had a higher degree of hydration than that with natural gypsum at all concentrations except at 4% where they were equal. After the depletion of calcium sulphate, at 24 hours of hydration, it was noticed that all cement systems experienced similar degrees of hydration, regardless of the type and concentration of calcium sulphate bearing materials used.

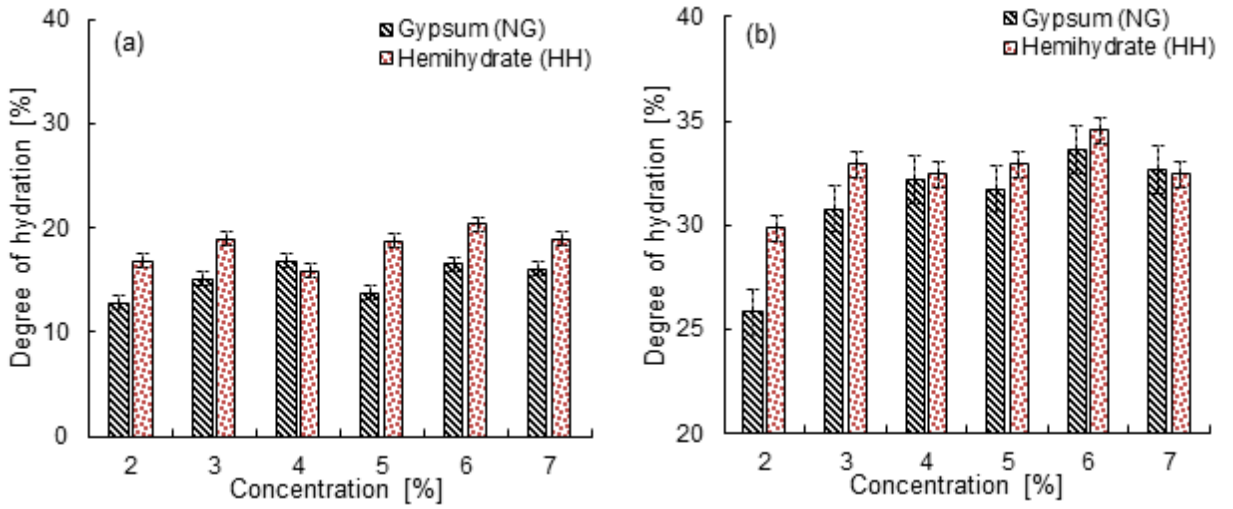

Figure 4.7: Degree of hydration of cement system with different calcium bearing material at variant concentrations (a) at the exhaustion of $CaSO_4^{-2}$; (b) after $CaSO_4^{-2}$ depletion at 24 hours

There is no doubt that these induced reactivities would influence the precipitation of early hydrate products as indicated by their respective degree of hydration, especially before the depletion of calcium sulphate, as seen in Figure 4.7 (a).

4.4 Early hydrate products: ettringite (Aft) and portlandite (CH)

The quantification of the early hydrate products was done by executing the thermogravimetric analysis, as presented in Figure 4.8. The weight losses of the cement mixes were depicted with respect to temperature ranges of cement phase decompositions as previously described in section 3.6.4 and presented in Table 4.1 and Table 4.2. It can be seen from Figure 4.8 that the weight loss corresponding to the decomposition of ettringite was not appreciable at 2% when natural gypsum was used as set regulator, likely due to the insufficient amount of calcium sulphate ions as discussed in section 4.3 and shown in Figure 4.6. Also, when comparing the weight losses within these defined temperature ranges, as presented in Table 4.1 and Table 4.2, it was noticed that cement with hemihydrate exhibited higher mass losses as compared to that with natural gypsum within the corresponding temperature range.

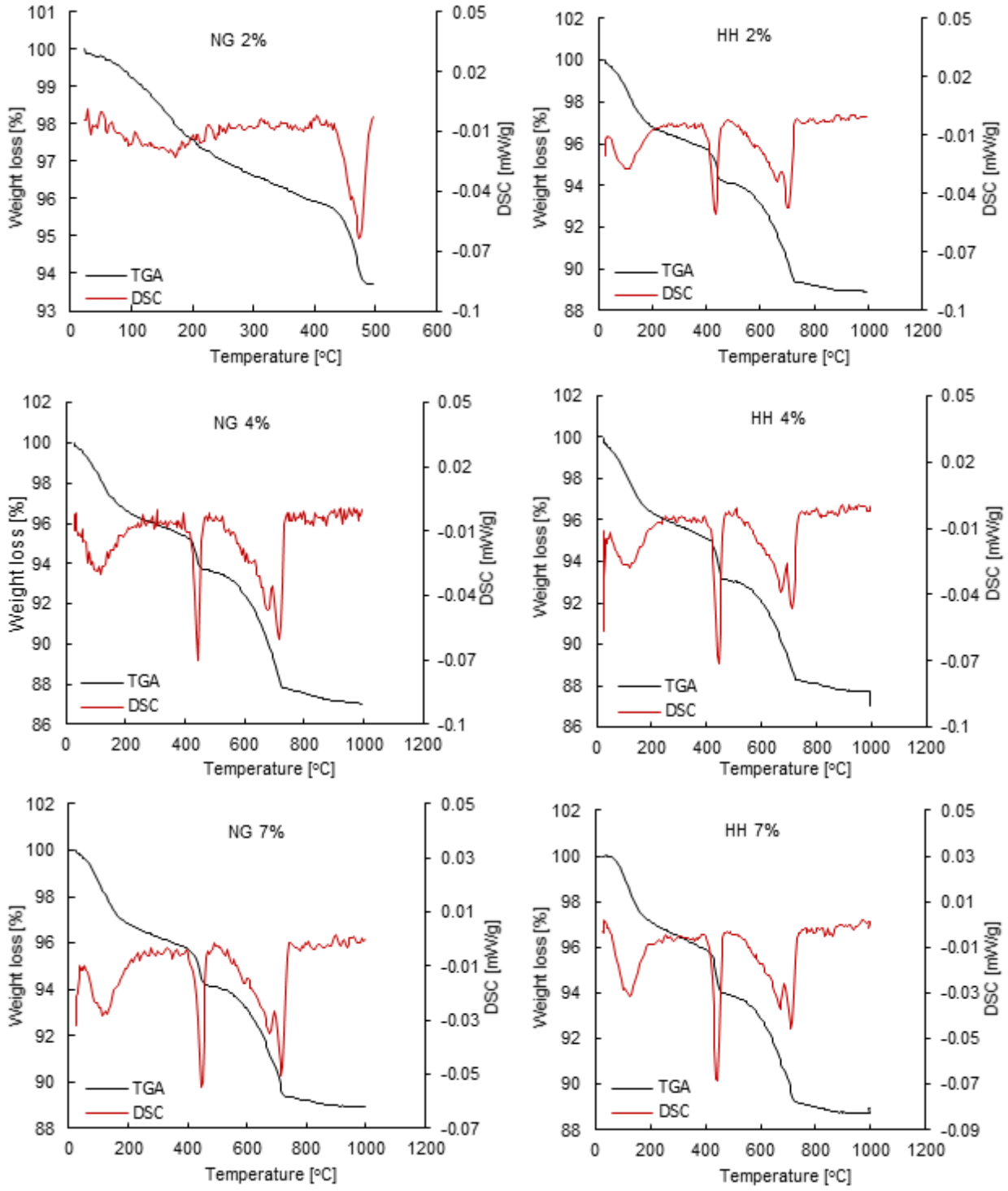

Figure 4.8: Typical thermogravimetric analysis and differential scanning calorimetry profiles after calcium sulphate depletion within cement systems with hemihydrate (HH) and natural gypsum (NG) at 2%, 4% and 7% concentrations

Table 4.1: Mass loss of cement with natural gypsum (NG) at different concentrations 2%-7% within temperature ranges of cement phase decomposition

	Temperature range [°C]				
Cement ID	25-100	100-140	140-430	430-530	530-900
NG2	0.79	0.58	2.90	2.04	3.00
NG3	0.87	0.66	2.69	1.93	5.00
NG4	1.56	0.88	2.70	1.45	5.79
NG5	1.59	0.89	2.48	1.35	4.97
NG6	1.59	0.91	2.42	1.31	5.65
NG7	1.46	0.91	2.37	1.30	4.70

Table 4.2: Mass loss of cement with hemihydrate at different concentrations 2%-7% within temperature ranges of cement phase decomposition

	Temperature range [°C]				
Cement ID	25-100	100-140	140-430	430-530	530-900
HH2	0.89	0.69	2.69	2.17	3.00
HH3	0.93	0.82	3.11	2.24	4.00
HH4	1.17	0.93	2.68	1.71	4.79
HH5	1.79	1.00	2.80	1.73	4.96
HH6	1.58	1.07	2.80	1.82	3.16
HH7	0.91	1.04	2.63	1.69	4.67

Figure 4.9 shows the amount of ettringite formed after 12 hours of hydration (corresponding to the time before the exhaustion of calcium sulphate within the cement systems) of cement with hemihydrate and natural gypsum at different concetrations, while Figure 4.10 presents their corresponding amounts of formed portlandite after the same hydration time.

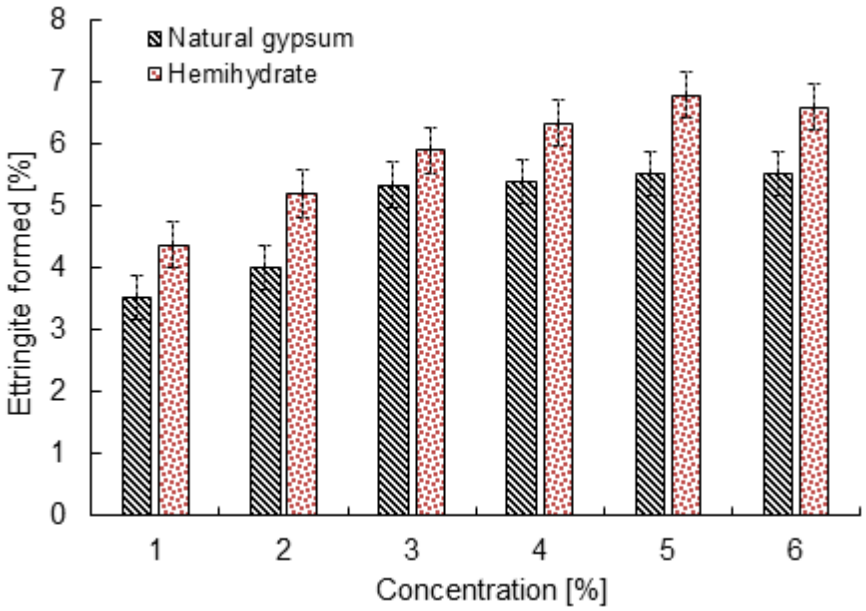

Figure 4.9: Amount of ettringite formed after 12 hours of hydration for cement clinker with different calcium sulphate types at different concentrations

It can be seen from Figure 4.9 that the quantity of ettringite formed for cement with hemihydrate was higher than that with natural gypsum. This phenomenon has also been observed by Bensted (1982) who reported a value of 8.3% more of ettringite within cement paste with hemihydrate than that with natural gypsum. Also, for both calcium sulphate bearing materials, the amount of this hydrate product increased as their concentrations increased within the cement system up to around 4%. Above this concentration, the quantity of ettringite formed remained reasonably constant within the system. In addition, the amount of portlandite precipated after 12 hours of hydration as seen in Figure 4.10, proving that cement systems with hemihydrate yielded more portlandite as compared to those with natural gypsum, especially at high calcium sulphate concentrations. However, it was observed that the amount of calcium hydroxide within the cement systems decreased with the increase in concentration of calcium sulphate bearing materials.

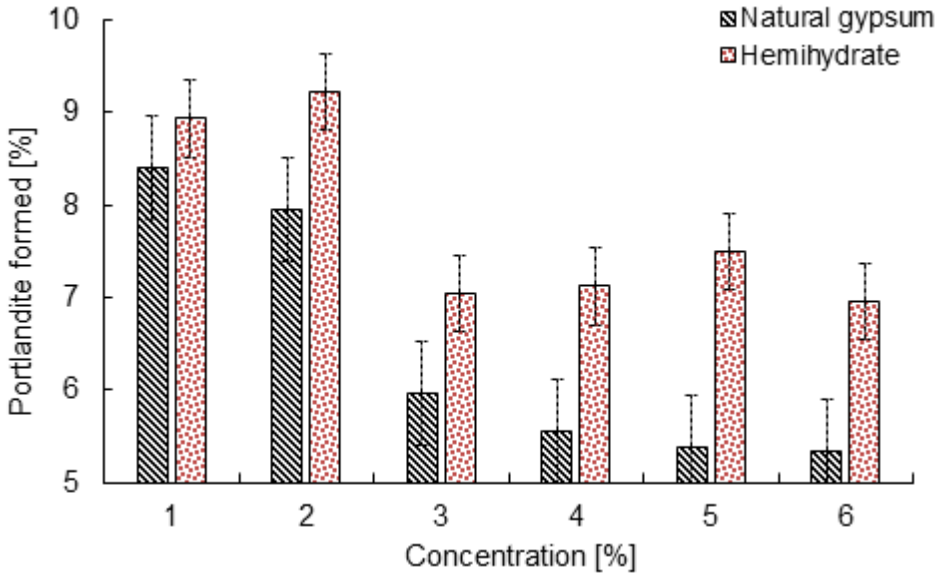

Figure 4.10: Amount of portlandite formed after 12 hours of hydration for cement clinker with different calcium sulphate types at different concentrations

This could be due to the availability of SO_4^{-2} consumed within the suspension by interacting with Ca^{+2} for the ettringite formation, as previously presented in Figure 4.6. Therefore, it could be assumed that at low concentrations of these calcium bearing materials, there was not enough SO_4^{-2} prevailing within the system. This resulted in less ettringte formation, counteracted by more precipitation of portlandite since there was enough available Ca^{+2} within the suspension. Conversely, at high calcium sulphate concentrations, more ettringite products precipitated accordingly by consuming more $CaSO_4^{-2}$ causing a low CH formation. Above the concentration of 4% for both calcium sulphate bearing materials, the amount of CH remained constant, as also observed for ettringite formation in Figure 4.9. These observations agree with those found by Clark and Brown (1999) who revealed the dependency of ettringite formation on calcium concentrations within cement suspensions.

Ettringite and portlandite are not the only hydrate products formed during the early hydration of cement pastes. For instance, Odler and Abdul-Maula (1984) have quantified different cement hydrate products within the acceleration phase of cement. Minard *et al.* (2007) have also shown the inevitable presence of hydroxy-AFm within the cement paste regardless of the amount of added gypsum. The identification of the presence of other calcium aluminate hydrate (CAH) can be done by assuming that ettringite is the only sulfoaluminate hydrate. The immediate precipitation of AFt would therefore be attributed to the consumption of all available sulphate ions within the cement system. Consequently, a linear regression relationship can be established between the cumulated heat released at the exhaustion of sulphate and the initial amount of added calcium sulphate, the slope of which expresses the enthalpy of ettringite formation while

the intercept reflects the total heat released for the initial formation of hydroxyl-AFm from aluminate grains (Pourchet *et al.*, 2009).

Figure 4.11 presents the linear relationship between the total quantity of heat released at the time of sulphate depletion and the initial amount of added sulphate estimated in terms of mmol per

$$Q = 213.7 * 3 * n_{Gypsum} + 269 \quad (4.1)$$

gram of cement with hemihydrate and natural gypsum.
It was noticed that this relationship depended on the type of calcium sulphate used, as shown in Equation (4.1) and Equation (4.2).

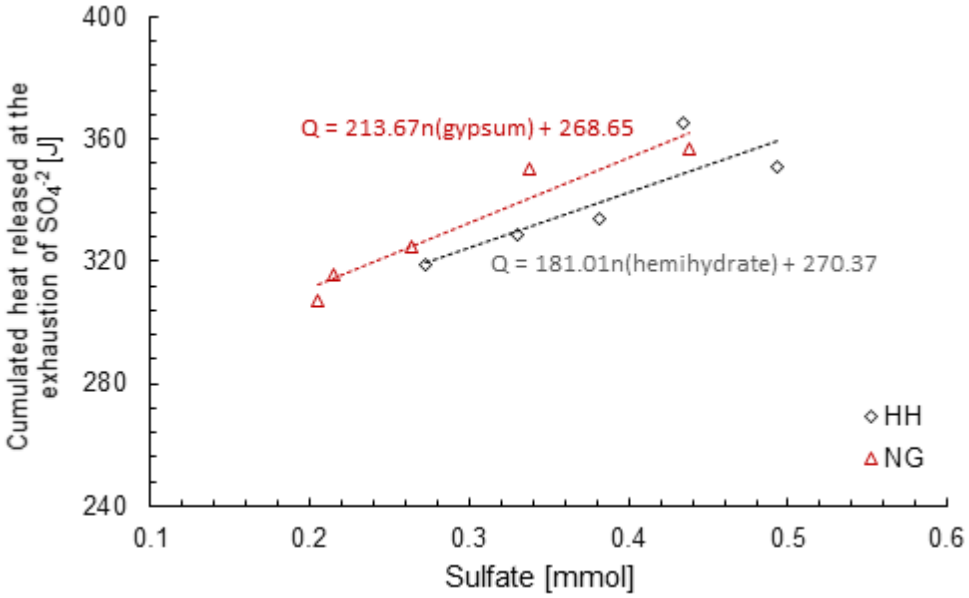

Figure 4.11: Cumulated heat flow at the time of sulphate exhaustion against the initial added quantity of sulphate per gram of cement

$$Q = 213.7 * 3 * n_{Gypsum} + 269 \quad (4.1)$$

$$Q = 181 * 3 * n_{Hemihydrate} + 270 \quad (4.2)$$

Where Q is the cumulated heat [J]; and n_i the sulphate quantity [mmol] induced by the type of calcium sulphate. The multiplier 3 is introduced to take into consideration the number of moles of sulphate required for the formation of one mole of ettringite, as per Equation (4.3).

$$Ca_3Al_2O_6 + 3CaSO_4.2H_2O + 30H_2O \rightarrow Ca_6Al_2(SO_4)_3(OH)_{12}.26H_2O \quad (4.3)$$

The slope of Equations (4.1) and (4.2) were 641 KJ and 543 KJ, equivalent respectively to the enthalpy of ettringite formation when natural gypsum and hemihydrate were used as set regulators within the cement systems. These values were in the same order of magnitude as those determined by Taylor (2003), Minard *et al.* (2007), and Pourchet *et al.* (2009) in accordance with reported thermodynamic data.

It is evident that the enthalpy of ettringite formation of cements with hemihydrate was higher than those with natural gypsum. From a thermodynamic point of view, this suggests that more ettringite is expected to be formed in the presence of hemihydrate than in the presence of natural gypsum. Ettringite particles emanating from the reaction of C_3A and hemihydrate are also less stable than those from the C_3A-natural gypsum reactions.

The higher deceleration rate of the cement systems with natural gypsum, observed in Figure 4.4 and Appendix B, can then be understood as resulting from a comparable remaining available space on C_3A grains. This allows ettringite particles to react with the remaining C_3A and yield monosulfoaluminate AFm phase, as reported by Quennoz and Scrivener (2012). This reaction generates more heat, as observed in the cement system kinetics.

The linear coefficients were almost equal and approximated to around 270 J for both types of calcium sulphate bearing materials. This value is independent of the initially added sulphate within the system and would be attributed to the heat released during the formation of calcium aluminate hydrate (CAH). A similar value (272 J) corresponding to the formation of CAH in the absence of gypsum has been observed and reported by Minard *et al.* (2007). According to these researchers, the formation of this hydrate product is controlled primarily by the surface of the aluminate phase. It is then conceivable that regardless of the type of calcium sulphate used, equal y-intercepts are observed since their corresponding clinker systems had similar phases including the aluminate phase.

Bullard *et al.* (2011) have also noticed the formation of CAH in the absence of calcium sulphate and referred to this hydrate product as a poorly crystalized aluminium hydroxide, AFm phase, described by C_2AH_8 and C_4AH_8. Within cement systems with calcium sulphate bearing materials, ettringite and hydroxyl-AFm phases are the first aluminate hydrates to precipitate. However, Pourchet *et al.* (2009) have shown that their nucleation frequencies are quite different depending on the type of calcium sulphate bearing material present within the cement system. Because AFt formations require an important amount of C_3A dissolution when natural gypsum is used as

compared to hemihydrate, hydroxyl-AFm precipitates before the formation of AFt in the presence of natural gypsum while the opposite happens in the presence of hemihydrate. This can be visualized in the SEM-BSE Figure 4.12 of a cement clinker system with natural gypsum and hemihydrate at a concentration of 4%.

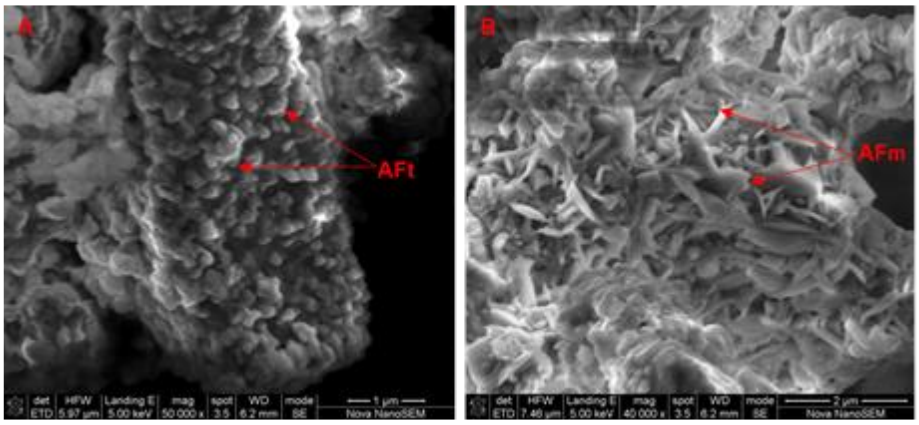

Figure 4.12: SEM-BSE of cement system hydrated for 30 min of (A) hemihydrate; and (B) natural gypsum at a concentration of 4%

Figure 4.12 shows that after 30 minutes of hydration, within cements with hemihydrate, small ettringite needles are formed on the surface of cement particles (Figure 4.12 (A)); while within those with natural gypsum, platelets of AFm dominate the cement microstructure (Figure 4.12 (B)).

4.5 Effect of calcium sulphate bearing materials on physical and mechanical properties of cement paste

Previous research has shown the importance of cement paste microstructures on its physical and mechanical properties (Thomas & Jennings, 2006). In this section, the effect of calcium sulphate types and dosage on the initial, final setting times and early compressive strengths is assessed. Figure 4.13 shows the variations in strength of mortars with hemihydrate and natural gypsum at various concentrations. Each compressive strength value was an average of six collected readings, as detailed in Appendix D.

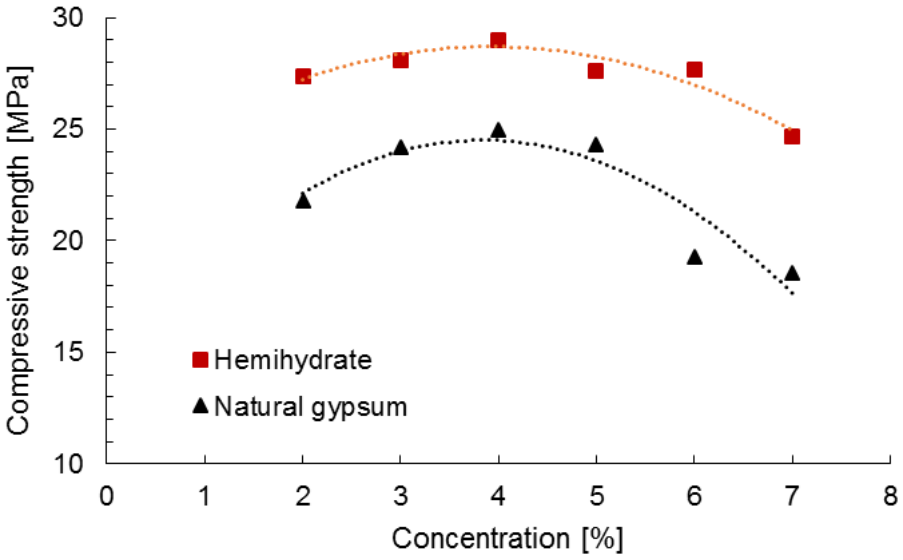

Figure 4.13: Compressive strength of cement mortar with natural gypsum and hemihydrate at different concentrations hydrated during 1 day

A quadratic relationship between the compressive strength of mortars and the concentration of both calcium sulphate bearing materials was observed. The maximum strength was obtained at a concentration of 4% for both natural gypsum and hemihydrate. Above this concentration, mortars experienced a decrease in strength that was more pronounced in the presence of natural gypsum and progressive when hemihydrate was used. In all cases, mortar prepared with hemihydrate had higher compressive strength than those with natural gypsum. The average difference in strength between the two calcium sulphate bearing materials was approximately 15%.

The strength improvement at low calcium sulphate concentrations, as observed in Figure 4.13, would probably be related to low SO_3 prevailing within the cement systems, as shown in Table 3.3, and moderate ettringite formation. The latter phenomenon could be due to the fact that cement systems with small total SO_3 contents are expected to have low SO_4^{-2} concentrations at early hydrations. Conseqently, less ettringite would precipitate, thereby availing more space for C_3S hydration. This resulted in mortar strength improvements. On the other hand, the decrease in strength at higher calcium sulphate concentrations could be attributed to important ettringite formations within the cement system due to higher total SO_3 contents. According to Zhang *et al.* (2018), the hydration process of C_3S is usually limited in cement systems with a higher quantity of ettringite which covers the unhydrated cement grains. Besides, cement microstructures experience excessive expansion as a result of this large amount of generated ettringite. This increases porosity within the system that significantly reduces its overall strength.

As a matter of fact, the hydration kinetics of cement systems as presented in Figure 4.1 and Figure 4.2 supports this hypothesis. During the acceleration period, the reaction rate of cement systems seemed to decrease with the increase in calcium sulphate concentrations. In addition, Figure 4.4 showed that the reaction rate of cement with natural gypsum was lower when compared to that with hemihydrate. This has also been observed by Quennoz (2011) who noticed that with a significant amount of sulphate ions within the suspension, the specific surface areas of the anhydrous silicate and aluminate compounds decrease. Because of a large amount of ettringite and C-S-H formed, the space available for the reaction of these cement phases also decreases, thereby affecting the reaction rate of the overall system. The phenomenon observed in Figure 4.10, showing a decrease in the amount of portlandite with the increase in calcium sulphate concentrations at the time before the exhaustion of sulphate and lower strengths of natural gypsum compared to hemihydrate, can then be explained. Figure 4.14 shows the initial and the final setting times of cement pastes with different concentrations of calcium sulphate.

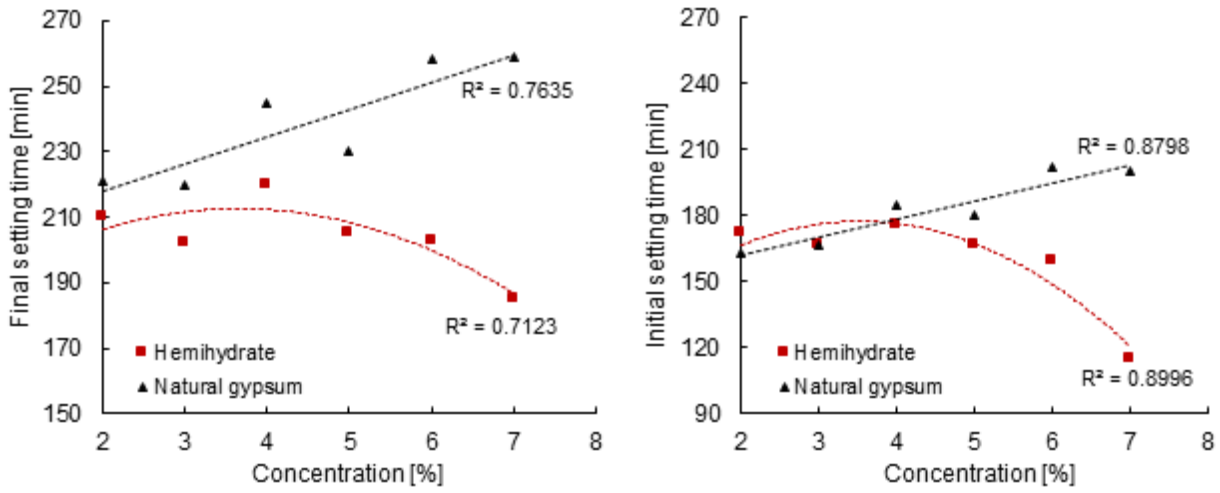

Figure 4.14: Final and Initial setting times of cement paste with natural gypsum and hemihydrate at different concentrations

In the presence of natural gypsum, the setting times of cement systems seemed to increase linearly with the increase in concentration. A quadratic relationship between the setting times and the concentration of calcium sulphate was observed when hemihydrate was used. Changing the concentration of calcium sulphate from 2% to 7% induced an increase of 15% in final setting time when natural gypsum was used, while a decrease of about 12% was estimated when hemihydrate was used as set regulator. In the same way, a 19% increase in initial setting time was noticed when natural gypsum was used, while a decrease of around 33% was observed in cement pastes with hemihydrate.

In all cases, the final setting times of systems with hemihydrate were shorter when compared to those with natural gypsum. However, at concentrations below 4%, the initial setting time of cement pastes seemed to be independent of the type and concentration of calcium bearing materials.

Cement setting is a consequence of C-S-H precipitation that strengthens the newly formed microstructure and enables the cement paste to withstand some stresses (Hildago *et al.*, 2008; Bishnoi & Scrivener, 2009; Roussel *et al.*, 2012). The kinetics and reactivity induced by the presence of these calcium sulphate bearing materials elucidate their respective setting time values.

First of all, the formation of C-S-H appeared to be favoured in systems with hemihydrate, as their hydration rate was more improved than those with natural gypsum (see Figure 4.4). Also, the dormant phase of systems with hemihydrate were shorter than those with natural gypsum (see Figure 4.5). This suggests that the onset of the acceleration period would occur earlier, justifying the shorter initial setting times obtained in systems with hemihydrate than those with natural gypsum. These observations are in agreement with those of Nelson *et al.* (1990) and Pedrajas *et al.* (2014) who noticed that cements with long induction or dormant phases experienced higher initial setting time values that improved their pumpability.

Secondly, the short final setting times in systems with hemihydrate could be due to the amount and rate of ettringite formation during hydration. Actually, the precipitation of these hydrate products allows the formation of a network structure that is able to enclose a large amount of free water necessary for the progression of hydration reactions (Zhang *et al.*, 2018). Xu *et al.* (2012) have also observed disparities in setting times of mortars with different calcium sulphate bearing materials used as set regulators, attributing these differences to the solubility of the set regulators and the formation of ettringite.

4.6 Conclusion

The influence of the type and concentration of natural gypsum and hemihydrate used as set regulators in OPC was investigated. The kinetics and reactivity induced by these calcium sulphate bearing materials were studied and correlated to the mechanical and physical properties of corresponding cement systems.

The hydration kinetics of all prepared cement systems described all four hydration stages pertaining to that of normal OPCs. In particular, cements with hemihydrate presented shorter durations of dormant periods than those with natural gypsum. The reaction rates of cement systems with hemihydrate were faster than those with natural gypsum and generally tended to

decrease with the increase with concentration. This behaviour was attributed to the unavailability of possible reaction spaces within the system due to the early precipitation of important hydrate products.

The consumption rate of calcium sulphate was higher in cement systems with hemihydrate than those with natural gypsum, with an averaged difference of 19%. Generally, this rate seemed to increase with the increase in calcium sulphate concentration. Consequently, cement with hemihydrate experienced higher degrees of hydration, especially at times corresponding to the exhaustion of sulphate ions within the system. After the depletion of sulphate, all cements had almost equal degrees of hydration.

In these events, hemihydrate systems had more ettringite and portlandite formed than that of natural gypsum. However, the amount of ettringite increased with the increase in calcium sulphate concentration to a certain extent (4%), and thereafter remained constant regardless of the dosage within the system. Conversely, the amount of portlandite decreased with the increase in calcium sulphate and also remained unchanged after 4%. These phenomena were attributed to the availability of SO_4^{-2} ions and their interactions with Ca^{+2} ions which were conditioned by the dosage of calcium sulphate within the system.

The evaluation of the enthalpy formation of these early hydrate products attested the formation of AFm phases in the cement systems. However, while this hydrate phase prevailed in systems with natural gypsum, it was not depicted in those with hemihydrate after 30 minutes of hydration as observed with the scanning electon microscopy. Additionally, the estimated energy formation of ettringite phases revealed that those generated from hemihydrate were less stable than those from natural gypsum. This implied that the phenomenon observed during the deceleration period was mostly related to the remaining hydration space on the C_3A compound after the depletion of sulphate within the system. It was also established that mechanical and physical performances of cement systems were dictated by the kinetics observed at microstructural level.

Generally, cements with hemihydrate had higher compressive strengths when compared to those with natural gypsum, with a maximum strength for both calcium sulphate bearing materials achieved at 4% concentration. This early strength development was attributed to the C_3S hydration, whose hydration space depends on the amount of ettringite formed.

In the same way, the amount of ettringite increased with the increase in calcium sulphate concentration to a certain extent (4%), and thereafter remained constant regardless of the dosage within the system. Conversely, the amount of portlandite decreased with the increase in calcium

sulphate and also remained unchanged after 4%. An increase of 15% in the final setting time for natural gypsum systems in comparison to a 12% decrease in those with hemihydrate were observed when the dosage of calcium sulfate was varied from 2% to 7%. A 19% increase and 33% decrease were noted, respectively, in the initial setting times of natural gypsum and hemihydrate systems.

This behaviour was in connection with the kinetics of the cement systems in terms of their hydration rates and dormant phase durations. The formation of a network by the generated ettringite and the solubility of the set regulators used was also suspected to be responsible for these cement physical properties.

Chapter 5 Rheokinetics of cement paste with mix proportion of natural gypsum and hemihydrate

5.1 Introduction

The previous chapter gave the scientific basis of optimum sulphate content within the cement systems. Previous research set this optimum by primarily considering the sulphate content at which the system achieves maximum compressive strength. It is understood that high sulphate content might lead to excessive formation of Aft, which can cause both the expansion and microstructure disruption of the cement paste. This decreases the overall strength development of the system. On the other hand, a low sulphate content may promote the formation of AFm phases. This consumes most of the Ca^{+2} necessary for the precipitation of CH and C-S-H phases that are responsible for cement system strength developments.

Considering this, a concentration of calcium sulphate set at 4% was therefore accepted as the optimum for both natural gypsum and hemihydrate. Not only did the cement systems achieve maximum strength at this dosage but also had similar hydration kinetics with equal degrees of hydration prior to the exhaustion of sulphate within the system.

This chapter assesses the effect of mix proportions of natural gypsum and hemihydrate at 4% calcium sulphate phase on the cement paste rheological properties. The hydration kinetics and physical performances of cement mixes were also studied. A connection between the hydration parameters (rheokinetics, hydration kinetics and physical performances) was attempted.

5.2 Effect of natural gypsum and hemihydrate on the viscoelastic properties of cement paste

The non-destructive dynamic rheometry measurements taken in small amplitude oscillatory are introduced to investigate the viscoelastic properties and the time dependence of fresh cement paste. Figure 5.1 presents the evolution of storage moduli and corresponding phase angles of cements with different proportions of natural gypsum and hemihydrate within the cement calcium sulphate phase.

The evolution of the storage modulus when monitored within the linear viscoelastic domain is a pure signature of cement microstructure development (Roussel *et al.*, 2012). The storage modulus development describes the structuration or the strength development of the newly formed network (Gauffinet-Garrault, 2012). It can be observed in Figure 5.1 that immediately after the pre-shearing, the mixtures initially experienced negligible storage modulus values with values

of angle phases around 50°. This evidenced the liquid-like state of the cement suspensions with weak bonds prevailing within the microstructure at the beginning of hydration. Generally, viscoelastic materials have phase angle values between 0°-90° with 0° describing the elastic behaviour and 90° the viscous behaviour (Eirich, 1958). Afterward, the storage modulus increases with the evolution of hydration time, indicating a gain in rigidity of the formed network likely due to the yielded hydrate products. At the same time, the phase angle decreases until it reaches a steady state.

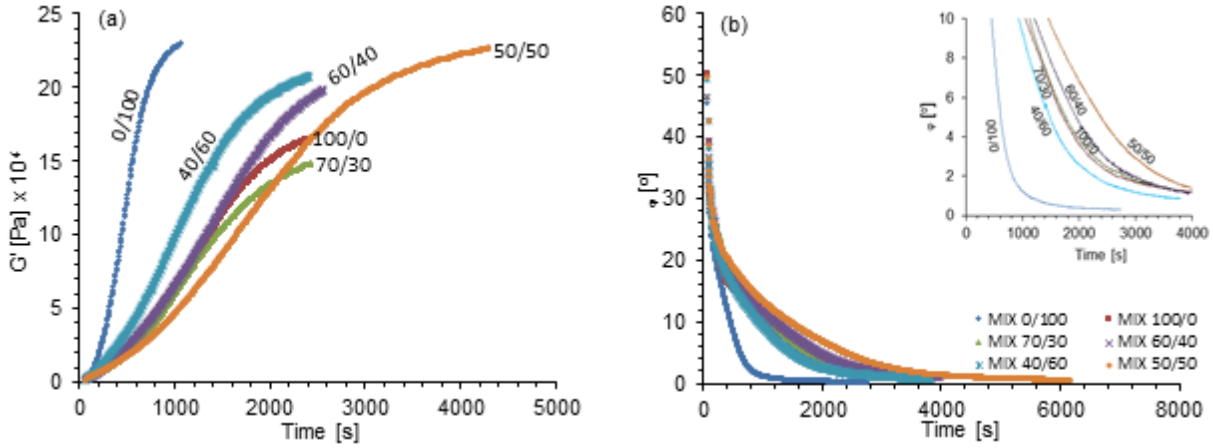

Figure 5.1: Evolution of storage modulus (a) and corresponding phase angle (b) during the early hydration of cement with different proportions of natural gypsum and hemihydrate set at 4% calcium sulphate cement content

This monotonic decrease of phase angle and increase of storage modulus reflects a gelation process, or formation of an elastic network, indicating a transition from the liquid-like state to a solid-like state. The decay rate of the phase angle, as illustrated on Figure 5.1 (b), shows that this transition generally occurs faster in mixtures with higher amount of hemihydrate fractions. In particular, cement with a 70/30 proportion of NG and HH seems to have the same decay rates as that of the 100/0 proportion. Moreover, those with 40 and 50% hemihydrate fractions experienced the lowest decay rates. This would indicate that small replacements of natural gypsum by hemihydrate do not affect the speed of this transition and become very slow at almost equal fractions. Subsequently, formation of an elastic percolated network is faster in cements with a higher amount of HH within the calcium sulphate phase and slower in those with as much hemihydrate as natural gypsum. According to Mostafa and Yahia (2017), the point in time where the phase angle reaches the lowest and steady value can be considered as the colloidal percolation time defined as the time needed for the formation of the percolated network. Figure 5.2 shows the effect of hemihydrate fractions within the cement gypsum phase on the percolation time.

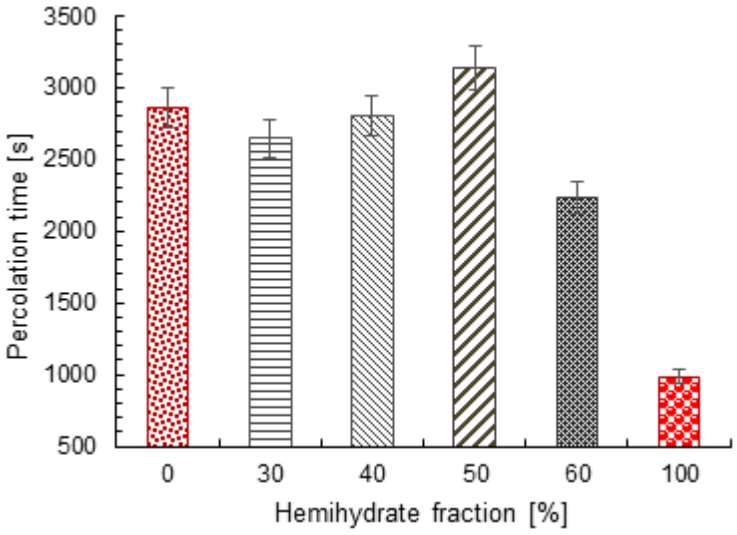

Figure 5.2: Time required for the microstructural network percolation occurrence with respect to the inclusion of hemihydrate in the gypsum phase

It was observed that the percolation time of cement with only hemihydrate was about 30% of that with only natural gypsum. Increasing the amount of hemihydrate fraction up to 50% within the gypsum phase did not show any influence on the onset of the network formation. During this stage, flocculated cement particles generally undergo numerous physical interactions within the suspension (Nachbaur *et al.*, 2001; Mostafa & Yahia, 2016) as quantified by Flatt (2004) and Roussel (2007). Since all cement mixes had similar SSA (see Table 3.4.), it can then be speculated that these reactions were promoted by the reactivity of calcium sulphate used. Consequently, the agglomeration of cement particles seemed to be hastened in the presence of hemihydrate.

This agglomeration is a result of the early cohesion between cement particles as reported in previous investigations (Sujata & Jennings, 1992; Roussel *et al.*, 2012) and responsible for the initial elasticity within the formed particle network. The increase in storage modulus has been considered the footprint of this phenomenon, referred to as the rigidification of cement microstructure (Nonat *et al.*, 1997; Kirby & Lewis, 2002; Bellotto, 2013). The increase in storage modulus, as illustrated in Figure 5.1, indicates the rigidification of the cement microstructures. In particular, a linear relationship was established between the maximum storage value G'_{max} and the concentration of hemihydrate within the cement gypsum phase. A gradual increase in G'_{max} was observed when increasing the concentration of hemihydrate fraction, as shown in Figure 5.3.

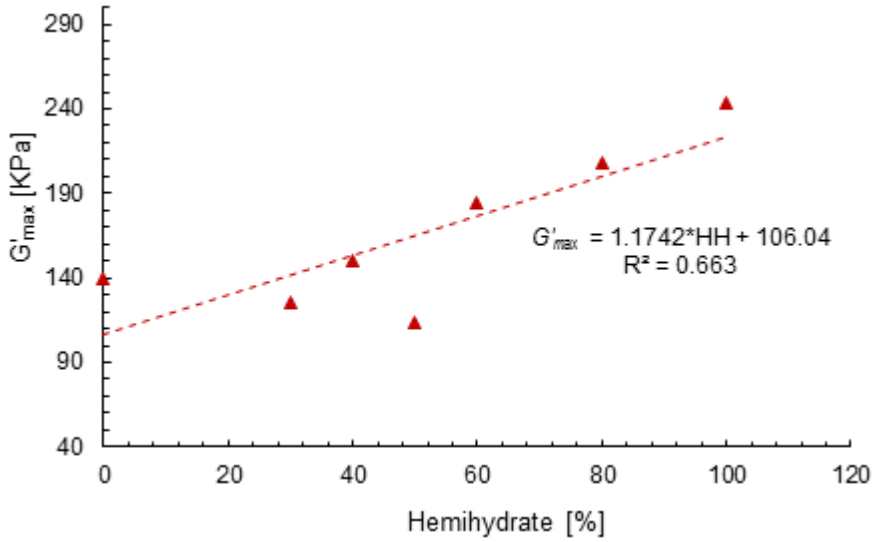

Figure 5.3: Maximum storage modulus of hydrate cement (at 20 °C) with different fractions of hemihydrate within the gypsum phase set at 4% cement content

It is more rational to compare these maximum storage moduli with respect to their corresponding characteristic times since they are achieved over different time intervals. Subsequently, the evolution of the stress-bearing capacity of the formed network can be estimated, rendering it possible to calculate the strength rate development of the pastes, as described in section 3.6.4 and presented in Figure 5.4.

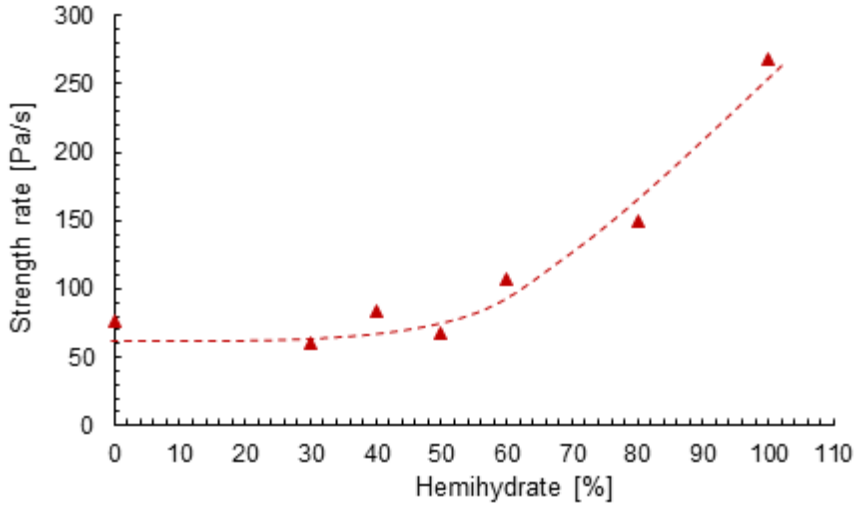

Figure 5.4: Strength rate development of cement paste with different fractions of hemihydrate within the gypsum phase set at 4% cement content

Figure 5.4 demonstrates that the strength rate development of cement increased when increasing the amount of hemihydrate fraction within the gypsum phase at concentrations above 50%. This underlined that the microstructural strength rate development could be affected from the point the

degeneration of natural gypsum to hemihydrate has exceeded 50% of transformation. Comparatively, these results corroborated with those of cement percolation time onsets which showed appreciable values only from 50% hemihydrate fraction.

5.3 Effect of natural gypsum and hemihydrate on the flow properties of cement paste

The yield stress and viscosity values of the cements were estimated from typical flow curves, as shown in Figure 5.5 It was noticed that the characterization of all down curves of hysteresis loops on flow curves could be fitted with the Bingham model. Cement systems with only hemihydrate presented higher Bingham parameters than those with pure natural gypsum. These parameters seemed to change with respect to the replacement of natural gypsum by hemihydrate in cement systems with mix proportions of these two calcium sulphate bearing materials.

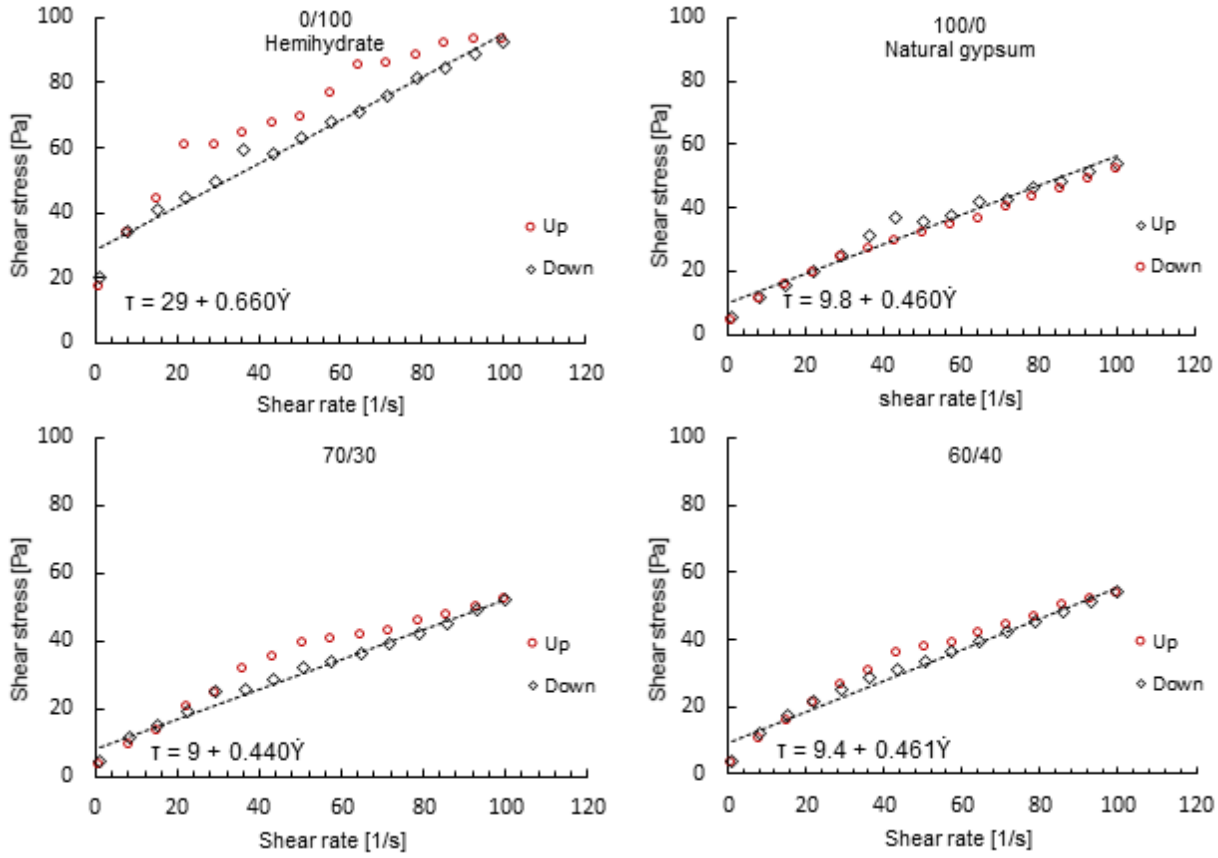

Figure 5.5: Typical flow curves of cement pastes with different proportions of natural gypsum and hemihydrate within gypsum cement phase

The effect of the presence of hemihydrate within the gypsum phase on the flow behaviour of cement paste can be seen by establishing a relationship between these obtained rheological parameters and the actual concentration of hemihydrate, as illustrated in Figure 5.6.

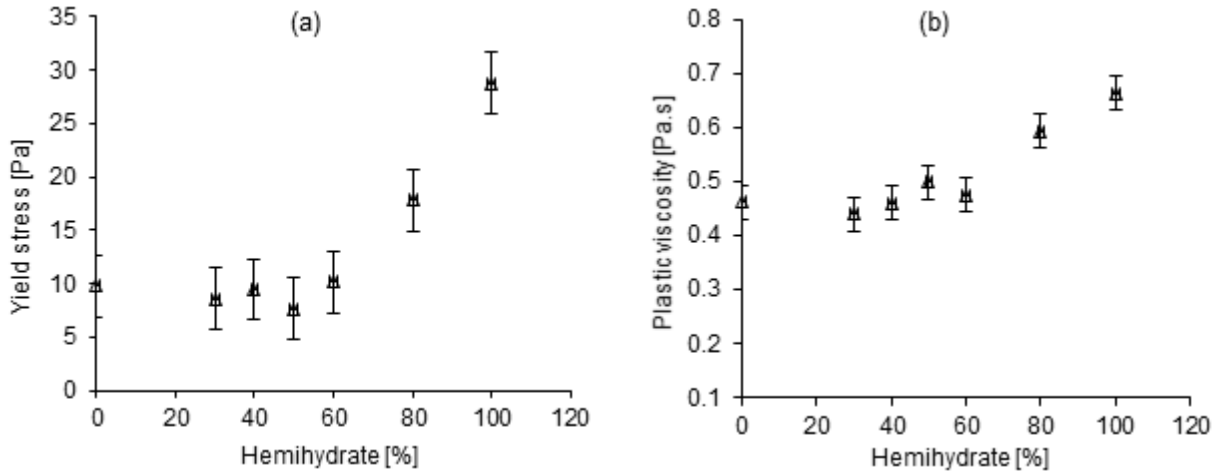

Figure 5.6: Effect of hemihydrate fraction within gypsum cement phase on (a) the yield stress and (b) plastic viscosity

It can be observed from Figure 5.6 that the presence of hemihydrate resulted in an increase in both yield stress and plastic viscosity of the cement pastes. In particular, below 50% hemihydrate fraction, yield stress values are similar to those of cement with only natural gypsum. Above this concentration, cement paste yield stress values significantly increased.

5.4 Early hydration cement products: ettringite and portlandite

The effect of the mix proportions on the quantity of ettringite and portlandite were quantified based on the results from thermogravimetric and differential scanning calorimetry (TG-DSC), as presented in Figure 5.7. These characteristic TG-DSC curves clearly show appreciable mass loss occurring between 100-140 ^{o}C for all cement pastes after one hour of hydration. This is mainly attributed to the dehydration of ettringite. Modest mass losses also occur between 170-200 ^{o}C in all cements except in those with 100% and 40% fraction of hemihydrate. This loss is mainly attributed to the dehydration of AFm (calcium hydroaluminate or monosulfate) phase (Odler & Abdul-Maula, 1984). Further mass losses are noticed between 350-530 ^{o}C corresponding to the dehydroxylation of portlandite. The decarbonation of carbonated phases are depicted from a temperature range of 600-900 ^{o}C. Table 5.1 shows these mass losses with respect to the defined temperature ranges.

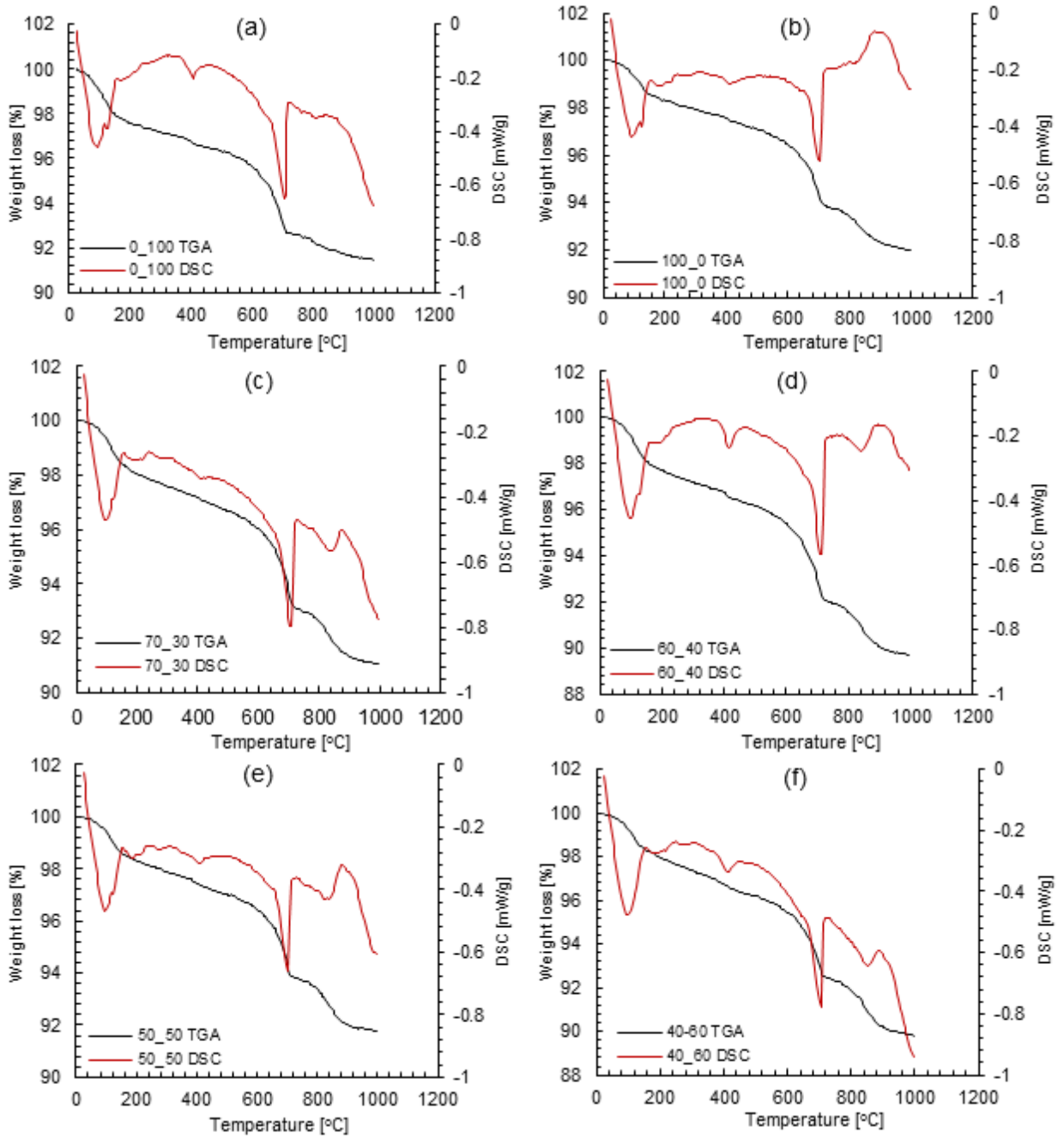

Figure 5.7: Thermogravimetric analysis and differential scanning calorimetry of one hour hydrated cement pastes with different proportions of natural gypsum and hemihydrate within the gypsum phase set at 4%: (a) cement with hemihydrate 0/100; (b) cement with natural gypsum 100/0; (c) cement with 70/30 proportion; (d) cement with 60/40 proportion; (e) cement with 50/50 proportion; and (f) cement with 40/60

Table 5.1: Mass loss of 1 hour hydrated cement with mix proportions of natural gypsum and hemihydrate within the calcium phase set at 4%

	Temperature range [°C]				
Cement ID	25-100	100-140	140-430	430-530	530-900
100/0	1.06	0.89	1.47	0.38	4.72
70/30	0.75	0.76	1.47	0.50	5.46
60/40	0.94	0.89	1.70	0.49	6.27
50/50	0.66	0.67	1.40	0.36	5.16
40/60	0.83	0.73	1.93	0.50	6.20
0/100	0.69	0.66	1.26	0.46	4.93

From these mass losses, the quantity of ettringite and portlandite precipited after one hour of hydration can be estimated, as described in section 3.6.4. Figure 5.8 shows the amount of these early hydrate products.

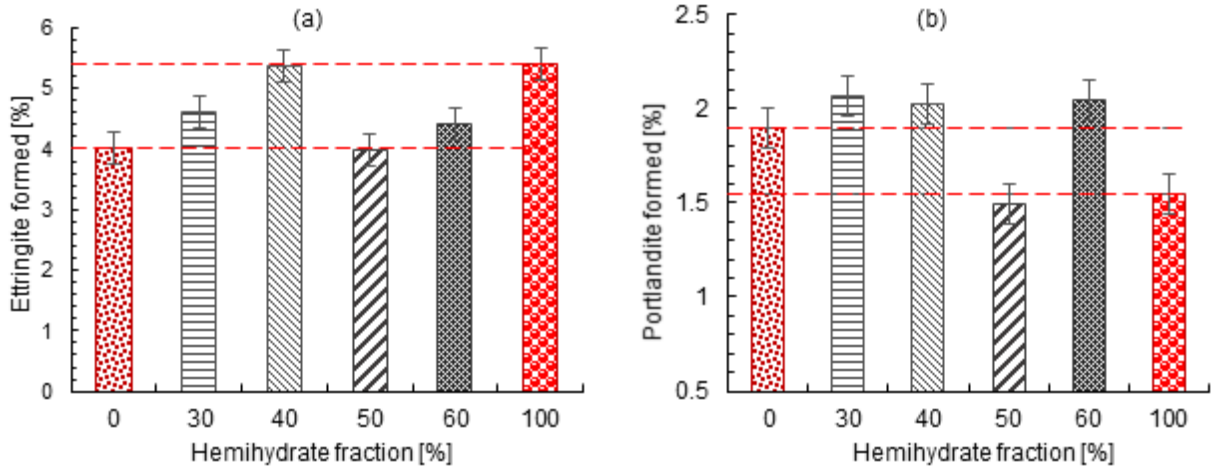

Figure 5.8: Amount of hydrate products precipitated after 1 hour of cement hydration with different fractions of hemihydrate within the gypsum phase set at 4%: (a) ettringite and (b) portlandite

After one hour of hydration, it can be observed that increasing the hemihydrate fraction within the cement system resulted in an increase in the amount of formed hydrate products. The amount of the formed ettringite varied between 4% and 5.5% and that of portlandite between 1.5% and 2%. It was also noticed that more ettringite precipitated in the systems with only hemihydrate than those with only natural gypsum. The latter had the same amount of ettringite formed when mixed with hemihydrate at equal proportion.

In such heterogeneous systems, it is difficult to explain the parameters controlling the rate of ettringite precipitation for the mix proportions that resulted in distinct amounts of formed ettringite. This has been a challenge for numerous researchers (Pourchet *et al.*, 2009). The area of the reaction interface and the departure from equilibrium of the limiting reactions such as C_3A dissolution and ettringite precipitation have been hypothesized as major parameters of ettringite formation rate (Minard *et al.*, 2007). According to this hypothesis, about 30% of the C_3A consumption is due to early AFm precipitation that significantly decreases the C_3A surface area within the system. Subsequently, the amount of ettringite formed also decreases. It can therefore be assumed that the AFm phase was absent in cement mixes that generated higher amounts of ettringite phases. This argument is in agreement with the investigations of Pourchet *et al.* (2009) who described the absence of the AFm phase in C_3A-$CaSO_4$ systems with hemihydrate as the source of calcium sulphate. In addition, the rate of calcium sulphate consumption within the suspension can also be at the origin of these differences in hydrate product formations. Figure 5.9 presents the calcium sulphate consumption rates as previously estimated in section 4.3 with reference to the heat flow curves given in Appendix A.

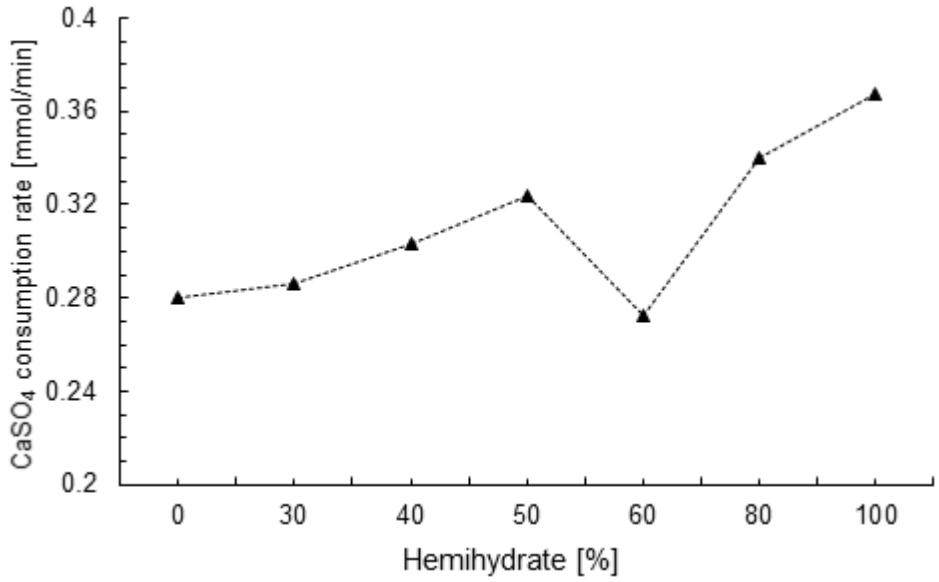

Figure 5.9: Calcium sulphate consumption rate per gram of cement with different proportions of natural gypsum and hemihydrate within the 4% calcium sulphate cement phase

It is evident that the consumption rate of calcium sulphate in cement systems increased with the increase in hemihydrate fraction, except at 60%. Since the ettringite formation depends on the hemihydrate fraction within the system, it can ultimately be understood that the amount of ettringite formed depends on both calcium sulphate consumption rates and the availability of reaction space on the aluminate phase.

5.4.1 Ettringite and cement paste rheological properties

The increase in yield stress during the induction period of cement paste has also been reported by Lei and Struble (1997) and was attributed to the accumulation of a gel between cement grains. This gel is responsible for the increase in the force that holds together the network particles and has been identified as crystalline ettringite. The yield stress of a cement system corresponds to the strength or energy required to break down a network of interacting cement particles. It is thus conceivable that the strength rate development (see Figure 5.4) of cement paste mixes follow a similar trend as for their corresponding yield stress. The early strength development of a cement system, identified by the increase in storage modulus, is initially due to the colloidal interactions between particles. These weak bonds are strengthened by the precipitation of hydrate products at pseudo contact points within the network (Nachbaur *et al.*, 2001; Roussel *et al.*, 2012).

Flatt and Bowen (2006) have shown that cement yield stress depends largely on the structure and strength of this internal network that is generally influenced by the solid volume fraction, particle size and the maximum packing. On the other hand, contrary to non-Brownian and non-colloidal particles, cement paste viscosity depends on the surface-to-surface separating distance between cement grains imposed by these attractive van der Waals forces (Hot *et al.*, 2014).

Shi *et al.* (2016) have found that ettringite improves the rigidification by filling the spaces within the cement structure. Gauffinet-Garrault (2011 determined that the formation of ettringite can indirectly affect the interparticle forces by changing the mechanical efficiency of C-S-H. Also, sulphate ions that are not consumed for the ettringite formation can be adsorbed on C-S-H layers, modifying the growth of this cement phase (Garrault-Gauffinet & Nonat, 1999). Within this context, modifications in the cement paste rheological behaviour are expected if the sulphate source affects the amount and morphology of hydrate products, changing the solid volume packing density of the system.

Assuming the densities of cement, ettringite and portlandite to be respectively 3.15 g/cm^3, 1.80 and 2.40, the variations in solid volume due to those of ettringite and portlandite can be estimated to be 2% and 0.5%, respectively. At such variations, the solid volume fraction of ettringite could expectedly affect the rheological behaviour of the suspension. There was, however, no correlation determined between these solid volume fractions and the observed rheological parameters of the corresponding cement paste. These observations are in agreement with those reported by Bonen and Sarkar (1995) who also found no correlation between the amount of ettringite formed and the rheological properties of cement paste. The essence of these flow properties could then be due to the ettringite morphology.

5.4.2 Ettringite and cement paste microstructure

The map images of one hour hydrated cement pastes with different proportions of hemihydrate and natural gypsum are shown in Figure 5.10. Ettringite is the main hydrate product. In the presence of hemihydrate, the cement microstructure appeared dense as compared to that with natural gypsum.

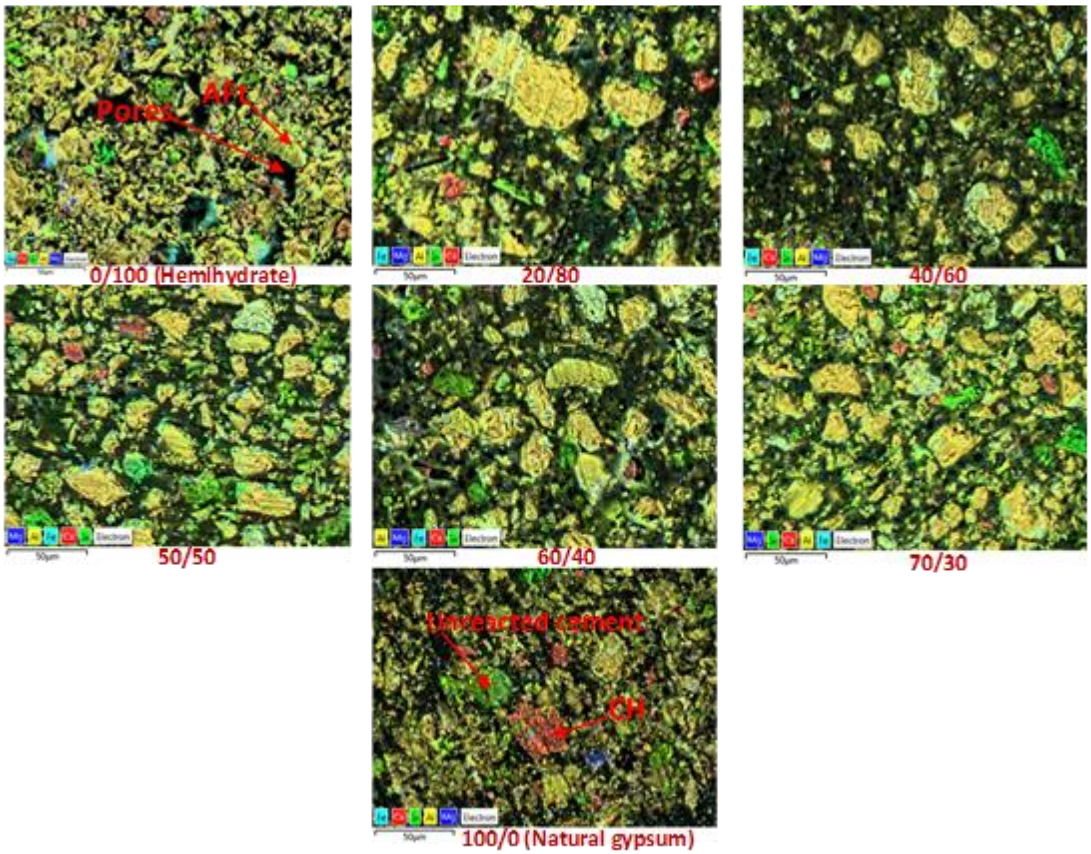

Figure 5.10: SEM-BSE images of mixes with different proportions of natural gypsum and hemihydrate within the gypsum cement phase hydrate sfter 1 hour of hydration

Looking at the XRD patterns in Figure 5.11, it can be seen that after one hour of hydration, portlandite could not be depicted, likely a result of insignificant amounts or of the morphology of portlandite that was still amorphous at this time of hydration.

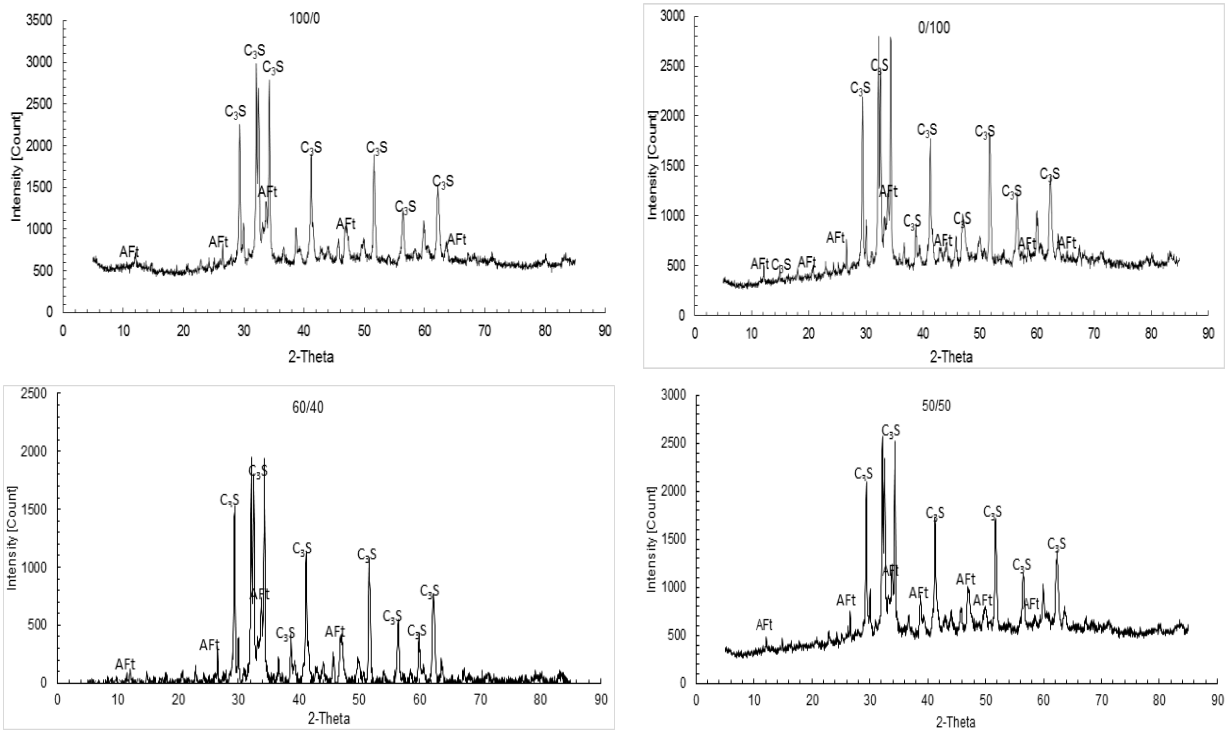

Figure 5.11: Typical x-ray difraction patterns of one hour hydrated cement with different proportion of natural gypsum and hemihydrate within 4% cement calcium sulphate phase

The portlandite phase was detected only after the depletion of calcium sulphate (around 12 hours of hydration) as shown in Appendix F. Additionally, the silicate phase was also noticed within cements microstructure, confirming the presence of unhydrous cement particles as shown in Figure 5.10.

The morphology of ettringite was considered and indirectly estimated by measuring the paste compaction. Pastes with different proportions of natural gypsum and hemihydrate were prepared with distilled water at w/c: 0.5. After mixing, the paste was kept in a sealed container at room temperature for 1 hour, allowing sufficient precipitation of ettringite. Thereafter, the paste was mixed and 1.5 mL was collected, placed in a specified tube and transferred to the centrifuge. The centrifuge was run at 5000 rpm for 10 minutes. The liquid on top was removed and weighed on an electronic balance. This was preferred to measuring the height of cement due to the fact that after centrifuging, the paste was not evenly spread around the circumference of the bottle. The solid volume fraction of the consolidated suspension which corresponds to the packing density of the suspension was then computed. Figure 5.12 presents the effect of the hemihydrate fraction on the paste packing density expressed as a percentage.

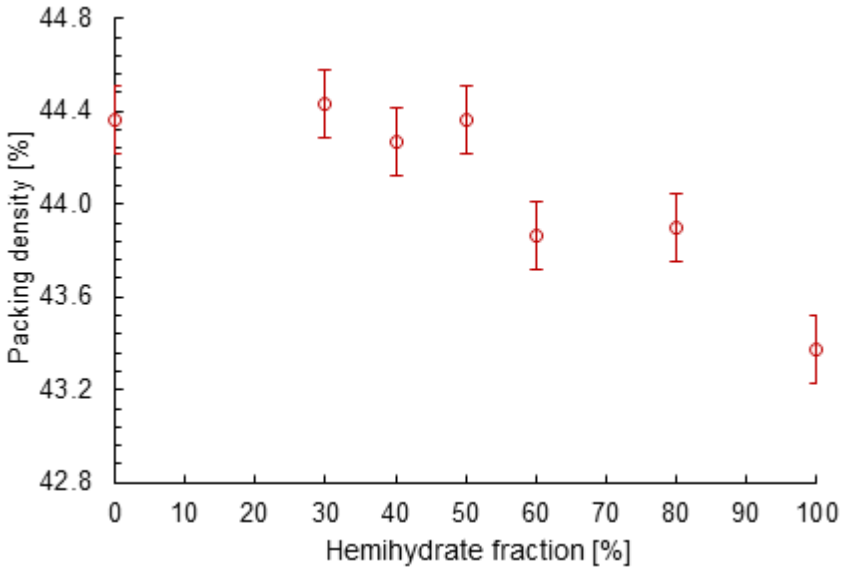

Figure 5.12: Effect of hemihydrate fraction within cement gypsum phase on cement paste packing

It can be seen that the packing density of the suspension was almost the same up to 50% hemihydrate fraction and thereafter decreased with the increase in hemihydrate concentration, suggesting that the paste was more compacted when natural gypsum was solely used or dehydrated into hemihydrate up to 50%. Beyond this concentration, the packing density decreased from 44.4% to 43.4%, indicating a less compacted paste.

These maximum packing measurements suggest that the increase of hemihydrate fraction alters the packing of the suspension. Considering that the particle size distribution of cement particles remains almost unchanged during 1 hour of hydration, the only factor that might affect the packing density of the suspension would then be the shape of the particles. Interestingly, the ettringite morphology as observed on the SEM-BSE images in Figure 5.13 explains the packing changes (see Figure 5.12).

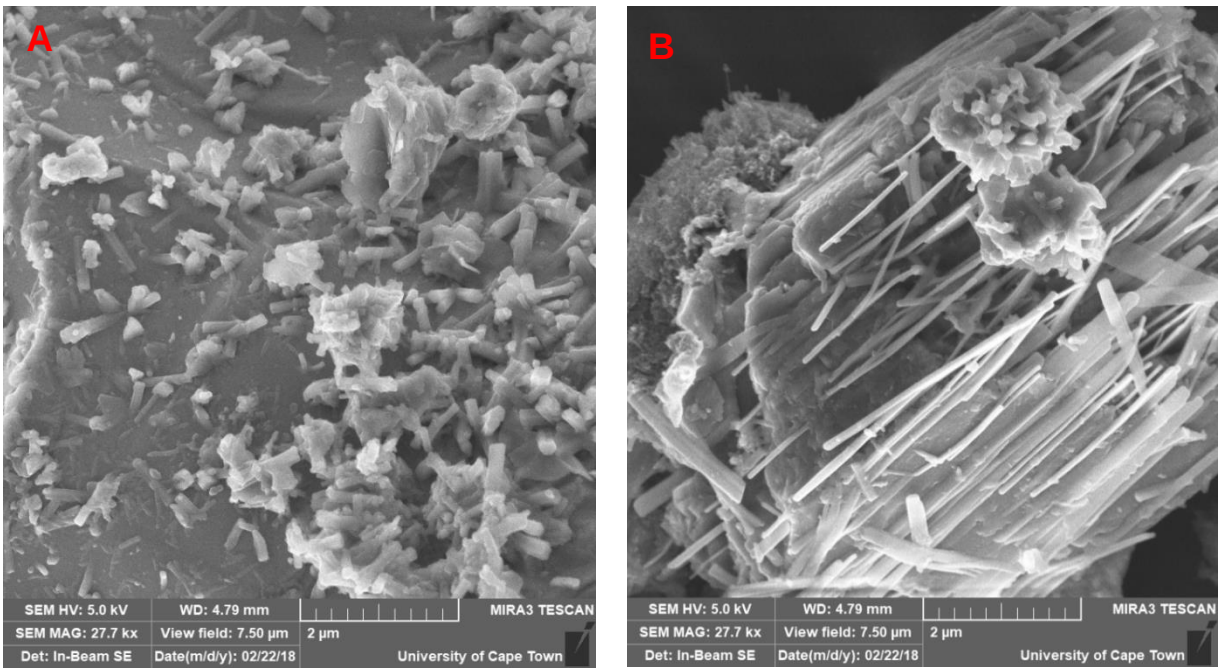

Figure 5.13: SEM-BSE images of cement surface hydrated for 1 hour and prepared with (A) natural gypsum and (B) hemihydrate

From Figure 5.13 it was observed that elongated rod-like ettringite hydrates prevailed at the surface of cement grains when hemihydrate was used, while short rod like ettringite hydrates were seen in the presence of natural gypsum. Similar phenomena pertaining to ettringite morpholy changes resulting from aluminate and calcium sulphate interactions in different cement systems have also been reported by Prince *et al.* (2003) and Pourchet *et al.* (2009).

Previously, other research has demonstrated that particles with regular shapes and flat surfaces locally arrange themselves better than those with irregular shapes (Cumberland & Crawford, 1987; German, 1989; Aste & Weaire, 2000). When a long rod is inserted into a packing of particles and if it is not small enough to occupy the space between particles, the overall packing density of the system decreases accordingly. In such an event, the decrease in packing density with the increase in hemihydrate fraction within the cement systems is then understood and attributed to the elongated shape of ettringite formed. As a consequence, it can tentatively be assumed that at concentrations below 50% hemihydrate, spherical or stubby rod shaped ettringite prevails within the suspension, and above this concentration, long elongated ettringite dominates.

It is now evident that rheological properties of fresh cement paste seem to be controlled more by the morphology than the available amount of ettringite triggered by the presence of high concentration of hemihydrate within the suspension. These observations would explain the

decrease of the packing density which results in the increase of both yield stress and viscosity as the hemihydrate fraction increases.

5.5 Effect of mix proportion of natural gypsum and hemihydrate on the initial and final setting times

Physical properties of most cementitious materials depend on the changes that occur in the cement paste microstructure (Thomas & Jennings, 2006). As was previously shown, calcium sulphate is primarily introduced within the clinker to regulate the hydration of the aluminate phase for controlling cements settings (Strydom & Potgieter, 1999). This depends on the source of the calcium sulphate (Roller, 1934; Zhang *et al.*, 1996; Shi *et al.*, 2016).

The setting times of cement clinker with different proportions of natural gypsum and hemihydrate were thus measured and presented in Figure 5.14. It can be seen that both the initial and final setting times decreased as the amount of hemihydrate fraction increased, except at 60% hemihydrate concentration. Interestingly, the trend of these setting times corroborated with that of the calcium sulphate consumption rate that generally influences the formation of ettringite. It was therefore noticed that the faster the calcium sulphate consumption, the shorter the setting times. This is in agreement with the investigations of Colombo *et al.* (2017) who found that the enhancement of ettringite formation reduces the setting time by suppling additional nucleation surfaces within the system. This would finally confirm the dependence of the macroscopic behaviour on the degree of microstructure build-up of cement paste, as reported by Mostafa and Yahia (2017).

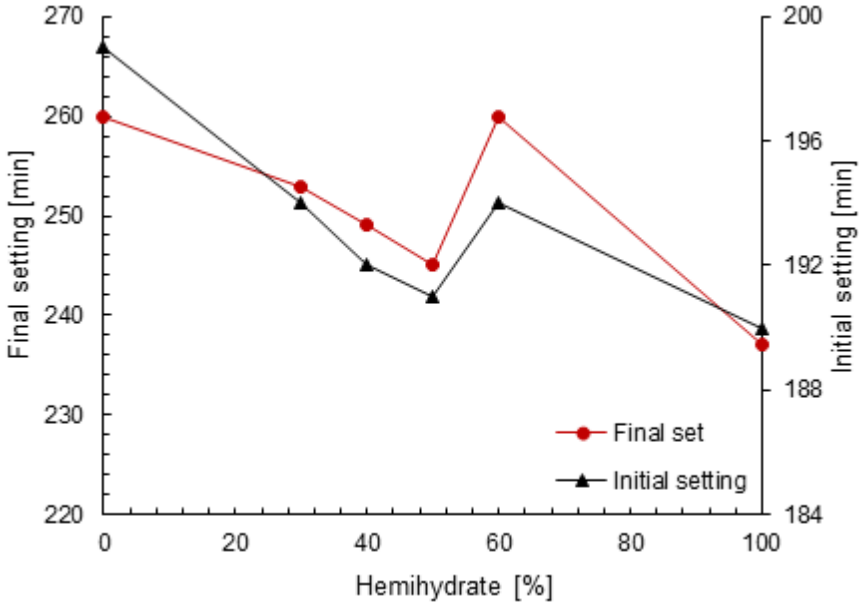

Figure 5.14: Initial and final setting times of cement with different hemihydrate fractions with the gypsum phase set at 4% cement content

5.6 Conclusion

The impact of hemihydrate content stemming from the degeneration of natural gypsum on the rheokinetics of cement paste was investigated. The storage modulus development and the decay rate of the phase angle of different cement mixes with different proportions of these two calcium bearing materials indicated that the speed of transition of the cement matrix from liquid-like to solid-like state was not affected at small hemihydrate fractions and slowed at an equal fraction (50/50) of natural gypsum and hemihydrate. Increasing the amount of hemihydrate fraction hastened the rigidity of the newly formed cement network. A linear relationship was found between the maximum storage modulus and the hemihydrate fractions, while the strength rate development of the newly formed network seemed to be affected at higher hemihydrate fractions.

The dynamic yield stress of mixes were comparable to their corresponding strength rate developments. Cements with up to 50% hemihydrate fraction had similar flow properties as those with only natural gypsum.

More ettringite formation was observed in cements with only hemihydrate as compared to those with only natural gypsum, and the amount was higher than that of portlandite in all one hour hydrated cements. The precipitation of ettringite appeared to depend on the calcium sulphate consumption and available nucleation sites on the aluminate phase. These nucleation sites can be reduced by the early precipitation of the AFm phase that was imminent in all the mixes except in those with only hemihydrate.

It was shown that besides the amount of ettringite precipitated, ettringite morphology plays a major role in controlling the packing properties and consequently the plastic viscosity of fresh cement pastes. This could be attributed to the change in the sulphate availability depending on the presence of hemihydrate fractions within the gypsum phase.

Rheological properties were more pronounced when the concentration of hemihydrate exceeded 50%. Large changes in yield stress values and variation in plastic viscosity values of approximately 50% were recorded. In all cases, dynamic yield stress values of cement mixes were comparable to their corresponding microstructure strength development rate. Furthermore, physical properties of cement pastes, especially the initial and final setting times, depended on the formation of ettringite (dictated by the sulphate consumption rate) within the system.

Chapter 6 Conclusions and recommendations

The present experimental work examined the hydration kinetics of cement paste, considering real industrially available materials at a realistic water-to-cement ratio, where the effect of dissolution and precipitation mechanisms as observed in the laboratory can be linked directly to the field experience. This chapter presents a summary of the work conducted with regard to the findings of the investigations, followed by recommendations for future research.

6.1 Effect of natural gypsum and hemihydrate on the hydration kinetics

The hydration kinetics of cement pastes were assessed by measuring the heat flow rate curves collected on a TAM Air calorimeter and characterized with respect to parameters suggested for cement thermal analysis. It was observed that regardless of the amount and type of calcium bearing material used, all cement mixes described the usual hydration process of a normal ordinary Portland cement. The dormant periods of cements with hemihydrate were shorter than those with natural gypsum. The reaction rates of cement systems with hemihydrate were faster than those with natural gypsum while tending to increase with the increase in their concentrations. likely due to the unavailability of reaction spaces within the system as a significant amount of hydrate products precipitated at early stage of hydration. Furthermore, it was noticed that the consumption rate of calcium sulphate was higher in cement systems with hemihydrate than those with natural gypsum, leading to higher degrees of hydration in systems with hemihydrate. After the depletion of sulphate within the suspension, all cements had almost an equal degree of hydration.

6.2 Effect of natural gypsum and hemihydrate on the microstructure

Early cement hydrate products were evaluated on a TG-DSC. Corresponding heat profiles with experimental temperatures starting from 105-1000 ^{o}C were acquired and, considering the thermal decomposition of hydrate products, ettringite and portlandite phases, were estimated. Cement microstructures were analysed using a SEM-BSE approach and hydrate phases were identified using an EDS analyser based on atomic ratio.

More ettringite and portlandite were observed in cement systems with hemihydrate than those with natural gypsum. The amount of ettringite increased with the increase in calcium sulphate concentration up to 4%, while thereafter it remained constant regardless of the dosage. Conversely, the amount of portlandite decreased with the increase of calcium sulphate and also remained unchanged after 4%. These phenomena were attributed to the availability of SO_4^{-2} ions and their interactions with Ca^{+2} ions which were conditioned by the concentration of calcium

sulphate within the system. In addition, the SEM images and the evaluation of the enthalpy of formation of these early hydrate products attested the formation of AFm phases mainly in cement systems with natural gypsum. Ettringite phases generated from hemihydrate seemed to be less stable than those from natural gypsum.

6.3 Effect of hemihydrate and natural gypsum on the mechanical and physical properties of cement

Mechanical and physical properties of cement systems were dictated by the kinetics observed at microstructural level. Generally, the compressive strength of cements with hemihydrate was higher than those with natural gypsum. The maximum strength for both natural gypsum and hemihydrate was achieved at 4% concentration. This early strength development was attributed to the hydration of the silicate phase where the hydration space depends on the amount of ettringite formed.

Similarly, the setting times of natural gypsum systems increased linearly with the concentration of their dosages, whereas a quadratic relationship was observed for those with hemihydrate. The setting times of hemihydrate systems were shorter than those with natural gypsum except the initial setting times that were equal at concentrations below 4%. An increase of 15% in the final setting time for natural gypsum systems in comparison to 12% decrease for those with hemihydrate were noticed when the dosage of calcium sulphate varied from 2% to 7%. A 19% increase and 33% decrease were noticed, respectively, in the initial setting times of natural gypsum and hemihydrate system when varying the calcium sulphate within the same ranges. This behaviour was related to the hydration rates and dormant phase durations of corresponding cement systems.

6.4 Effect of mix proportion of natural gypsum and hemihydrate on the rheokinetics of cement paste

During the grinding process, the natural gypsum used may dehydrate to hemihydrate depending on the mill ambient temperature. The presence and amount of hemihydrate within the cement system may involve different chemical and physical mechanisms during cement hydration due to their respective mineral characteristics. These phenomena can affect the hydration of the aluminate phase and consequently the rheological properties of the fresh cement paste. This section investigated the impact of the partial dehydration of natural gypsum to hemihydrate on the rheokinetics of cement paste. To this end, different proportions of natural gypsum and hemihydrate were considered within the 4% calcium sulphate cement phase as previously determined.

Dynamic yield stress and plastic viscosity values of cement systems were obtained from flow curves using the Bingham model, while the rigidification of the cement microstructure was estimated based on the measurements of storage moduli in the oscillatory mode. The storage modulus development and the decay rate of the phase angle of various cement mixes with different proportions of natural gypsum and hemihydrate indicated that the transition speed of the cement matrix from liquid-like to solid-like state was not affected at small hemihydrate fractions and slowed at equal fractions. The rigidification rate of the newly formed cement structure increased with the increase in the amount of hemihydrate fraction and was more pronounced at higher hemihydrate fractions. In all cases, the dynamic yield stress values of cement mixes were comparable to their corresponding microstructure strength rate developments. Rheological properties were more pronounced when the concentration of hemihydrate exceeded 50%. Large changes in yield stress values and variation in plastic viscosity values of approximately 50% were recorded. Cements with up to 50% hemihydrate fraction had similar flow properties to those with only natural gypsum.

6.5 Effect of ettringite morphology on the flow properties of cement paste

It was important to establish the cause of these observed rheological properties due to the presence of hemihydrate within the cement system. Different techniques were used to investigate the microstructure of the cement mixes. SEM-BSE images of cements with only hemihydrate and natural gypsum were collected and maximum packing densities of suspensions were evaluated. The number of early hydrate products increased with the increase in the hemihydrate fraction. More ettringite precipitated in cement systems with only hemihydrate than those with only natural gypsum. The latter had the same amount of ettringite formed when mixed with hemihydrate at equal proportions. The amount of formed ettringite varied between 4% and 5.5% and that of portlandite between 1.5% and 2%. At such variations, the solid volume fraction of ettringite could expectedly affect the rheological behaviour of the suspension. However, there was no correlation established between these solid volume fractions and the observed rheological parameters of the corresponding cement paste.

With reference to the behaviour observed in the rheological parameters of cement mixes, the packing density of cement suspensions remained almost the same up to 50% hemihydrate concentration, and thereafter decreased with the increase in concentration. This underlined that the paste was more compact when only natural gypsum was used or dehydrated into hemihydrate up to 50%. This behaviour was related to the ettringite morphology changes observed in the cement systems. Elongated rod-like ettringite hydrates at the surface of cement grains in the presence of hemihydrate were responisible for the packing density decrease especially at higher hemihydrate concentrations. This resulted in pastes with higher yield stress and plastic viscosity

values. On the other hand, the higher maximum packing density achieved in the presence of natural gypsum up to 50% degeneration was due to short rod like ettringite hydrates as revealed by the SEM images. This resulted in pastes with lower yield stress and viscosity values. It was thus concluded that rheological properties of fresh cement pastes are more controlled by the ettringite morphology than the available amount of ettringite triggered by the presence of high concentrations of hemihydrate.

6.6 Recommendations for further research

This study has investigated the effect of different calcium sulphate bearing materials in terms of their concentrations and mix proportions on the hydration and rheological kinetics of cement paste. The partial dehydration of natural gypsum was simulated by replacing its initial amount with a well-defined portion of hemihydrate within the cement system. In practice, this degeneration is a function of the mill grinding ambient temperatures. Knowing the effect of the degeneration of natural gypsum into hemihydrate, it would be interesting to relate these partial dehydrations to different mill grinding temperatures in order to optimize operational temperatures with reference to a target rheological behaviour.

As it is difficult to control the availability or sulphate consumptions within cement suspensions for concrete rheological purposes, it would be recommended that practical and effective ways for changing the ettringite morphology be investigated by incorporating intercalating polymers.
It could be interesting to conduct a similar investigation by introducing commercially available supperlasticizers within the cement matrixes which would allow the evaluation of the effect of calcium sulphate consumption on the hydration kinetics and estimation of the effect of superplasticizer on ettringite morphology changes.

References

AENOR.UNE-EN 197-1, E.S. 2011. *Cement - Part 1: Composition, Specifications and Conformity Criteria for Common Cements.*

Aïtcin, P.-C. & Flatt, R.J. 2016. *Science and technology of concrete admixtures*. Cambridge UK: Elsevier.

Aste, T. & Weaire, D. 2000. *The Pursuit of Perfect Packing*. Bristol: Institute of Physics.

Ataie, F.F. & Riding, K.A. 2016. Influence of agricultural residue ash on early cement hydration and chemical admixtures adsorption. *Construction and Building Materials*, 106: 274-281.

Baldino, N., Gabriele, D., Lupi, F.R., Seta, L. & Zinno, R. 2014. Rheological behaviour of fresh cement pastes: Influence of synthetic zeolites, limestone and silica fume. *Cement and Concrete Research*, 63: 38-45.

Banfill, P.F.G. & Saunders, D. 1981. On the viscometer examination of cement pastes. *Cement and Concrete Research*, 11: 363-370.

Baran, T. & Pichniarczyk, P. 2017. Correlation factor between heat of hydration and compressive strength of common cement. *Construction and Building Materials*, 150: 321-332.

Barnes, H.A., Hutton, J.F. & Walters, K. 1989. *An introduction to rheology*. Amsterdam: Elsevier.

Barnes, P. & Bensted, J. 2002. *Structure and performance of cements*. CRC Press.

Bellmann, F., Sowoidnich, T., Ludwig, H.-M. & Damidot, D. 2015. Dissolution rates during the early hydration of tricalcium silicate. *Cement and Concrete Research*, 72: 108-116.

Bellotto, M. 2013. Cement paste prior to setting: A rheological approach. *Cement and Concrete Research*, 52: 161-168.

Bensted, J. 1982. Effect of the clinker-gypsum grinding temperature upon early hydration of Portland cement. *Cement and Concrete Research*, 12: 341-348.

Bentz, D.P., Ferraris, C.F., Galler, M.A., Hansen, A.S. & Guynn, J.M. 2012. Influence of particle size distributions on yield stress and viscosity of cement–fly ash pastes. *Cement and Concrete Research*, 42(2): 404-409.

Bhanumathidas, N. & Kalidas, N. 2004. Dual role of gypsum: set retarder and strength accelerator. *Indian Concrete J*, 78(3): 1-4.

Bhatty, J.I. 1986. Hydration versus strength in a Portland cement developed from domestic mineral wastes—a comparative study. *Thermochimica acta*, 106: 93-103.

Bishnoi, S. 2008. *Vector modelling of hydrating cement microstructure and kinetics*. Citeseer.

Bishnoi, S. & Scrivener, K.L. 2009. Studying nucleation and growth kinetics of alite hydration using μic. *Cement and Concrete Research*, 39(10): 849-860.

Bisschop, J. & Kurlov, A. 2013. A flow-through method for measuring the dissolution rate of alite and Portland cement clinker. *Cement and Concrete Research*, 51: 47-56.

Blezard, R.G. 1998. The history of calcareous cements. *Lea's chemistry of cement and concrete*, 4: 1-23.

Bobby, S.S. & Singamneni, S. 2014. Influence of Moisture in the Gypsum Moulds Made by 3D Printing. *Procedia Engineering*, 97: 1618-1625.

Bonen, D. & Sarkar, S.L. 1995. The superplasticizer adsorption capacity of cement pastes, pore solution composition, and parameters affecting flow loss. *Cement and Concrete Research*, 25(7): 1423-1434.

Bullard, J.W., Jennings, H.M., Livingston, R.A., Nonat, A., Scherer, G.W., Schweitzer, J.S., Scrivener, K.L. & Thomas, J.J. 2011. Mechanisms of cement hydration. *Cement and Concrete Research*, 41(12): 1208-1223.

Burgos-Cara, A., Putnis, C.V., Rodriguez-Navarro, C. & Ruiz-Agudo, E. 2016. Hydration effects on gypsum dissolution revealed by in situ nanoscale Atomic Force Microscopy observations. *Geochimica et Cosmochimica Acta*.

Camarini, G. & De Milito, J.A. 2011. Gypsum hemihydrate–cement blends to improve renderings durability. *Construction and Building Materials*, 25(11): 4121-4125.

Caruso, F., Mantellato, S., Palacios, M. & Flatt, R.J. 2017. ICP-OES method for the characterization of cement pore solutions and their modification by polycarboxylate-based superplasticizers. *Cement and Concrete Research*, 91: 52-60.

Chhabra, R.P. & Richardson, J.F. 1999. *Non-Newtonian flow in the process industries*. Butterworth-Heinemann Oxford.

Ching, S.H., Bansal, N. & Bhandari, B. 2016. Rheology of emulsion-filled alginate microgel suspensions. *Food Research International*, 80: 50-60.

Chong, J.S., Christiansen, E.B. & Baer, A.D. 1971. Rheology of concentrated suspensions. *Journal of applied polymer science*, 15(8): 2007-2021.

Chung, D.D.L. 2002. Electrical conduction behaviour of cement-matrix composites. *Journal of Materials Engineering and Performance*, 11(2): 194-204.

Ciach, T.. & Swenson, E.. 1971. Morphology and microstructure of hydrating Portland cement and its constituents. *Cement and Concrete Research*, 1: 143-158.

Clark, B.A. & Brown, P.W. 1999. Formation of ettringite from monosubstituted calcium sulfoaluminate hydrate and gypsum. *Journal of the American Ceramic Society*, 82(10): 2900-2905.

Colombo, A., Geiker, M.R., Justnes, H., Lauten, R.A. & De Weerdt, K. 2017. On the effect of calcium lignosulfonate on the rheology and setting time of cement paste. *Cement and Concrete Research*, 100: 435-444.

Constantinides, G. & Ulm, F.-J. 2004. The effect of two types of C-S-H on the elasticity of cement-based materials: Results from nanoindentation and micromechanical modeling. *Cement and Concrete Research*, 34(1): 67-80.

Contrafatto, L., Cuomo, M. & Gazzo, S. 2016. A concrete homogenisation technique at meso-scale level accounting for damaging behaviour of cement paste and aggregates. *Computers & Structures*, 173: 1-18.

Coussot, P. & Ancey, C. 1999. Rheophysical classification of concentrated suspensions and granular pastes. *Physical Review E*, 59(4): 4445.

Cumberland, D. & Crawford, R. 1987. *The packing of particles*. Amsterdam: Elsevier.

Dalas, F., Pourchet, S., Rinaldi, D., Nonat, A., Sabio, S. & Mosquet, M. 2015. Modification of the rate of formation and surface area of ettringite by polycarboxylate ether superplasticizers during early C3A–CaSO4 hydration. *Cement and Concrete Research*, 69: 105-113.

Danner, T., Justnes, H., Geiker, M. & Lauten, R.A. 2016. Early hydration of C3A–gypsum pastes with Ca- and Na-lignosulfonate. *Cement and Concrete Research*, 79: 333-343.

D'Ayala, D. & Fodde, E. eds. 2008. *Structural analysis of historic constructions: preserving safety and significance; proceedings of the Sixth International Conference on Structural Analysis of Historic Construction, 2-4 July, Bath, United Kingdom*. Boca Raton, Fla.: CRC Press.

Do, T.-A., Hargreaves, J.M., Wolf, B., Hort, J. & Mitchell, J.R. 2007. Impact of particle size distribution on rheological and textural properties of chocolate models with reduced fat content. *Journal of food science*, 72(9): E541-E552.

Dunn, J., Oliver, K., Nguyen, G. & Sills, I. 1987. The quantitative determination of hydrated calcium sulphates in cement by DSC. *Thermochimica acta*, 121: 181-191.

Durdziński, P.T., Haha, M.B., Zajac, M. & Scrivener, K.L. 2017. Phase assemblage of composite cements. *Cement and Concrete Research*, 99: 172-182.

Eirich, F.R. 1958. *Rheology: Theory and Applications*. New York: Academic Press.

El-Enein Abo, S.., Kotkata, M.., Hanna, G.., Saad, M. & Abd El Razek, M. 1995. Electrical conductivity of concrete containing silica fume. *Cement and Concrete Research*, 25(8): 1615-1620.

El-Jazairi, B. & Illston, J.M. 1980. The hydration of cement paste using the semi-isothermal method of derivative thermogravimetry. *Cement and Concrete Research*, 10(3): 361-366.

Engelsen, C.J. 2009. *Quality improvers in cement making–State of the art*. Norway: Concrete Innovation Center.

Eriksson, R., Pajari, H. & Rosenholm, J.B. 2009. Shear modulus of colloidal suspensions: Comparing experiments with theory. *Journal of Colloid and Interface Science*, 332(1): 104-112.

Escalante-Garcia, J.I. 2003. Nonevaporable water from neat OPC and replacement materials in composite cements hydrated at different temperatures. *Cement and Concrete Research*, 33(11): 1883-1888.

Fathi, M.S. 2012. *Introduction to cement.*

Ferguson, J. & Kemblowski, Z. 1991. *Applied fluid rheology*. Springer Netherlands.

Fernández Carrasco, L., Torrens Martín, D., Morales, L.M. & Martínez Ramírez, S. 2012. *Infrared spectroscopy in the analysis of building and construction materials*. InTech.

Flatt, R. 2004. Towards a prediction of superplasticized concrete rheology. *Materials and Structures*, 37: 289-300.

Flatt, R.J. 2004. Dispersion forces in cement suspensions. *Cement and Concrete Research*, 34(3): 399-408.

Flatt, R.J. & Bowen, P. 2006. Yodel: A Yield Stress Model for Suspensions. *Journal of the American Ceramic Society*, 89(4): 1244-1256.

Fonseca, P.C. & Jennings, H.M. 2010. The effect of drying on early-age morphology of C–S–H as observed in environmental SEM. *Cement and Concrete Research*, 40(12): 1673-1680.

Gao, T., Shen, L., Shen, M., Chen, F., Liu, L. & Gao, L. 2015. Analysis on differences of carbon dioxide emission from cement production and their major determinants. *Journal of Cleaner Production*, 103: 160-170.

García-Maté, M., De la Torre, A.G., León-Reina, L., Losilla, E.R., Aranda, M.A.G. & Santacruz, I. 2015. Effect of calcium sulphate source on the hydration of calcium sulfoaluminate eco-cement. *Cement and Concrete Composites*, 55: 53-61.

Garrault, S., Behr, T. & Nonat, A. 2006. Formation of the C−S−H Layer during Early Hydration of Tricalcium Silicate Grains with Different Sizes. *The Journal of Physical Chemistry B*, 110(1): 270-275.

Garrault-Gauffinet, S. & Nonat, A. 1999. Experimental investigation of calcium silicate hydrate (CSH) nucleation. *Journal of crystal growth*, 200(3-4): 565-574.

Garrault-Gauffinet, S. 2012. The rheology of cement during setting. In *Understanding the rheology of concrete*. Cambridge UK: Wodhead Publishing: 96-113.

German, R.M. 1989. *Particle packing characteristics*. Princeton: Metal Powder Industry Federation.

Goñi, S., Frias, M., Vegas, I., García, R. & de la Villa, R.V. 2012. Quantitative correlations among textural characteristics of C–S–H gel and mechanical properties: Case of ternary Portland cements containing activated paper sludge and fly ash. *Cement and Concrete Composites*, 34(8): 911-916.

Hall, C. 2009. *Cement and concrete material: materials fundamentals + mix design.*

Han, C.D. 2007. *Rheology and processing of polymeric materials*. Oxford ; New York: Oxford University Press.

Hanehara, S. & Yamada, K. 2008. Rheology and early age properties of cement systems. *Cement and Concrete Research*, 38(2): 175-195.

Havlica, J., Roztockà, D. & Sahu, S. 1993. Hydration kinetics of calcium aluminate phases in the presence of various ratios of Calcium and sulphate ions in liquid phase. *Cement and Concrete Research*, 23: 294-300.

Heikal, M., Morsy, M.S. & Aiad, I. 2006. Effect of polycarboxylate superplasticizer on hydration characteristics of cement pastes containing silica fume. *Ceramics Silikáty*, 50(1): 5.

Hesse, C., Goetz-Neunhoeffer, F. & Neubauer, J. 2011. A new approach in quantitative in-situ XRD of cement pastes: Correlation of heat flow curves with early hydration reactions. *Cement and Concrete Research*, 41(1): 123-128.

Hewlett, P.C. 2001. *Lea's Chemistry of Cement and Concrete*. 4th ed. Oxford: Elsevier.

Hildago, J., Struble, L., Leslies, J. & Chun-Tao, C. 2008. Correlation between paste and concrete flow behaviour. *Material Journal*, 105: 281-288.

Hot, J., Bessaies-Bey, H., Brumaud, C., Duc, M., Castella, C. & Roussel, N. 2014. Adsorbing polymers and viscosity of cement pastes. *Cement and concrete research*, 63: 12-19.

Hu, C., Gao, Y., Chen, B., Zhang, Y. & Li, Z. 2016. Estimation of the poroelastic properties of calcium-silicate-hydrate (C-S-H) gel. *Materials & Design*, 92: 107-113.

Hu, C., Hou, D. & Li, Z. 2017. Micro-mechanical properties of calcium sulfoaluminate cement and the correlation with microstructures. *Cement and Concrete Composites*, 80: 10-16.

Hughes, T.L., Methyen, C.M., Jones, T.G.., Pelham, S.E., Fletcher, P. & Hall, C. 1995. Determining Cement Composition by Fourier Transform Infrared Spectroscopy. *Advanced Cement Based Materials*, 2: 91-104.

Ishak, S.A. & Hashim, H. 2015. Low carbon measures for cement plant – a review. *Journal of Cleaner Production*, 103: 260-274.

Jankovic, A., Valery, W. & Davis, E. 2004. Cement grinding optimisation. *Minerals Engineering*, 17(11): 1075-1081.

Jelenic, I., Panovic, A., Halle, R. & Gracesa, T. 1977. Effect of gypsum on the hydration and strength development of commercial Portland cements containing alkali sulfates. *Cement and Concrete Research*, 7: 239-246.

Jennings, H.M. 2008. Refinements to colloid model of C-S-H in cement: CM-II. *Cement and Concrete Research*, 38(3): 275-289.

Jennings, H.M. & Thomas, J. *Burning in a kiln-formation of cement clinker*. *Northenwestern.edu/cement/index.html*.

Jiang, S.., Mutin, J. & Nonat, A. 1995. Studies on mechanism and physico-chemical parameters at the origin of the cement setting. I the fundamental processes involved during the cement setting. *Cement and Concrete Research*, 25(4): 779-789.

Jiang, S., Mutin, J. & Nonat, Andre. 1995. Study on mechanism and physico-chemical parameters at the origin of the cement setting- The fundamental processes involved during the cement setting. *Cement and Concrete Research*, 25(4): 779-789.

Joergensen, S.W. 2016. *Cement grinding-Vertical roller mills versus ball mills.*

Jolicoeur, C. & Simard, M.-A. 1998. Chemical admixture- cement interactions: phenomenology and physico-chemical concepts. *Cement and Concrete Composites*, 20: 87-101.

Juilland, P., Gallucci, E., Flatt, R. & Scrivener, K. 2010. Dissolution theory applied to the induction period in alite hydration. *Cement and Concrete Research*, 40(6): 831-844.

Justnes, H. & Vikan, H. 2005. Viscosity of cement slurries as a function of solids content. *Ann. Trans. Nordic Rheology Soc*, 13: 75-82.

Kamali, M. & Ghahremaninezhad, A. 2016. An investigation into the hydration and microstructure of cement pastes modified with glass powders. *Construction and Building Materials*, 112: 915-924.

Kashani, A., San Nicolas, R., Qiao, G.G., van Deventer, J.S.J. & Provis, J.L. 2014. Modelling the yield stress of ternary cement-slag-fly ash pastes based on particle size distribution. *Powder Technology*, 266: 203-209.

Kirby, G.H. & Lewis, J.A. 2002. Rheological Property Evolution in Concentrated Cement-Polyelectrolyte Suspensions. *Journal of the American Ceramic Society*, 85(12): 2989-2994.

Kumar, M., Singh, S.K. & Singh, N.P. 2012. Heat evolution during the hydration of Portland cement in the presence of fly ash, calcium hydroxide and super plasticizer. *Thermochimica Acta*, 548: 27-32.

Lagosz, A. & Malolepszy, J. 2003. Tricalcium aluminate hydration in the presence of calcium sulphite hemihydrate. *Cement and concrete research*, 33(3): 333-339.

Lawrence, P., Cyr, M. & Ringot, E. 2003. Mineral admixtures in mortars. *Cement and Concrete Research*, 33(12): 1939-1947.

Lei, W.-G. & Struble, L.J. 1997. Microstructure and flow behaviour of fresh cement paste. *Journal of the American Ceramic Society*, 80(8): 2021-2028.

Lewry, A.J. & Williamson, J. 1994. The setting of gypsum plaster. *Journal of materials science*, 29(20): 5279-5284.

Li, X., Xu, W., Wang, S., Tang, M. & Shen, X. 2014. Effect of SO3 and MgO on Portland cement clinker: Formation of clinker phases and alite polymorphism. *Construction and Building Materials*, 58: 182-192.

Lin, B. & Zhang, Z. 2016. Carbon emissions in China's cement industry: A sector and policy analysis. *Renewable and Sustainable Energy Reviews*, 58: 1387-1394.

Liu, D.-M. 2000. Particle packing and rheological property of highly-concentrated ceramic suspensions: ϕ_m determination and viscosity prediction. *Journal of materials science*, 35: 5503-5507.

Liu, S., Wang, L., Gao, Y., Yu, B. & Tang, W. 2015. Influence of fineness on hydration kinetics of supersulfated cement. *Thermochimica Acta*, 605: 37-42.

Lootens, D., Hébraud, P., Lécolier, E. & Van Damme, H. 2004. Gelation, shear-thinning and shear-thickening in cement slurries. *Oil & gas science and technology*, 59(1): 31-40.

López, A., Tobes, J.M., Giaccio, G. & Zerbino, R. 2009. Advantages of mortar-based design for coloured self-compacting concrete. *Cement and Concrete Composites*, 31(10): 754-761.

Lucas, A. 1933. Ancient Egyptian materials and Industries about 1350 BC. *Analyst*, 58(692): 654-664.

Ludwig, H.-M. & Zhang, W. 2015. Research review of cement clinker chemistry. *Cement and Concrete Research*, 78: 24-37.

Ma, H., Hou, D. & Li, Z. 2015. Two-scale modeling of transport properties of cement paste: Formation factor, electrical conductivity and chloride diffusivity. *Computational Materials Science*, 110: 270-280.

Ma, S., Li, W., Zhang, S., Hu, Y. & Shen, X. 2015. Study on the hydration and microstructure of Portland cement containing diethanol-isopropanolamine. *Cement and Concrete Research*, 67: 122-130.

Macphee, D.E. & Lachowski, E.E. 2003. Cement Components and Their Phase. *Lea's chemistry of cement and concrete*: 95.

Maksoud, M.A. & Ashour, A. 1981. Heat of hydration as a method for determining the composition of calcined gypsum. *Thermochimica Acta*, 46(3): 303-308.

Maloney, C.E. & Lemaître, A. 2006. Amorphous systems in athermal, quasistatic shear. *Physical Review E*, 74(1).

Mardani-Aghabaglou, A., Boyacı, O.C., Hosseinnezhad, H., Felekoğlu, B. & Ramyar, K. 2016. Effect of gypsum type on properties of cementitious materials containing high range water reducing admixture. *Cement and Concrete Composites*, 68: 15-26.

Maximilien, S., Péra, J. & Chabannet, M. 1997. Study of the reactivity of clinkers by means of the conductometric test. *Cement and concrete research*, 27(1): 63-73.

Meller, N., Kyritsis, K. & Hall, C. 2009. The hydrothermal decomposition of calcium monosulfoaluminate 14-hydrate to katoite hydrogarnet and β-anhydrite: An in-situ synchrotron X-ray diffraction study. *Journal of Solid State Chemistry*, 182(10): 2743-2747.

Mewis, J. & Wagner, N.J. 2012. *Suspension rheology.*

Mezger, T.G. 2006. *The rheology handbook: for users of rotational and oscillatory rheometers*. Vincentz Network GmbH & Co KG.

Minard, H., Garrault, S., Regnaud, L. & Nonat, A. 2007. Mechanisms and parameters controlling the tricalcium aluminate reactivity in the presence of gypsum. *Cement and Concrete Research*, 37(10): 1418-1426.

Monteagudo, S.M., Moragues, A., Gálvez, J.C., Casati, M.J. & Reyes, E. 2014. The degree of hydration assessment of blended cement pastes by differential thermal and thermogravimetric analysis. Morphological evolution of the solid phases. *Thermochimica Acta*, 592: 37-51.

Mostafa, A.M. & Yahia, A. 2016. New approach to assess build-up of cement-based suspensions. *Cement and Concrete Research*, 85: 174-182.

Mostafa, A.M. & Yahia, A. 2017. Physico-chemical kinetics of structural build-up of neat cement-based suspensions. *Cement and Concrete Research*, 97: 11-27.

Mota, B., Matschei, T. & Scrivener, K. 2015. The influence of sodium salts and gypsum on alite hydration. *Cement and Concrete Research*, 75: 53-65.

Nachbaur, L., Mutin, J.C. & Choplin, L. 2001. Dynamic mode rheology of cement and tricalcium silicate paste from mixing to setting. *Cement and Concrete Research*, 31: 183-192.

Nalet, C. & Nonat, A. 2016. Impacts of hexitols on the hydration of a tricalcium aluminate-calcium sulphate mixture. *Cement and Concrete Research*, 89: 177-186.

Nehdi, M. & Al Martini, S. 2009. Estimating time and temperature dependent yield stress of cement paste using oscillatory rheology and genetic algorithms. *Cement and Concrete Research*, 39(11): 1007-1016.

Nelson, E.B., Baret, J.-F. & Michaux, M. 1990. 3 Cement Additives and Mechanisms of Action. *elsevier*, (28): 3-37.

Newman, J. & Choo, B.S. eds. 2003. *Advanced concrete technology*. Amsterdam; Boston: Elsevier Butterworth-Heinemann.

Ng, S. & Justnes, H. 2015. Influence of dispersing agents on the rheology and early heat of hydration of blended cements with high loading of calcined marl. *Cement and Concrete Composites*, 60: 123-134.

Nonat, A., Mutin, J. & Jiang, S. 1997. physico-chemical parameters determining hydration and particle interactions during setting of silicate cements. *Solid State Ionics*, 101(103): 923-930.

Nowack, T. 2015. *Cement Grinding-an overview & improvement possibility.*

Odler, I. 1998. Hydration, setting and hardening of Portland cement. *LEA's Chemistry of Cement and Concrete*, 4: 241-297.

Odler, I. & Abdul-Maula, S. 1984. Possibilities of quantitative determination of the AFt-(ettringite) and AFm-(monosulphate) phases in hydrated cement pastes. *Cement and Concrete Research*, 14(1): 133-141.

Onoda, G.Y. & Liniger, E.G. 1990. Random loose packings of uniform spheres and the dilatancy onset. *Physical Review Letters*, 64(22): 2727.

Pan, Z., Lou, Y., Yang, G., Ni, X., Chen, M., Xu, H., Miao, X., Liu, J., Hu, C. & Huang, Q. 2013. Preparation of calcium sulphate dihydrate and calcium sulphate hemihydrate with controllable crystal morphology by using ethanol additive. *Ceramics International*, 39(5): 5495-5502.

Papageorgiou, A., Tzouvalas, G. & Tsimas, S. 2005. Use of inorganic setting retarders in cement industry. *Cement and Concrete Composites*, 27(2): 183-189.

Parrott, L.J., Geiker, M., Gutteridge, W.A. & Killoh, D. 1990. Monitoring Portland cement hydration: comparison of methods. *Cement and Concrete Research*, 20(6): 919-926.

Patent granted by James Parker. 1811. Specification of the Patent Granted to James Parker, of Northfleet, in the country of Kent, Gentleman; for Cement or Terras to be used in Aquatic and other buildings and stucco-work. *Belfast Monthly Magazine*, 6(34): 401-402.

Pedrajas, C., Rahhal, V. & Talero, R. 2014. Determination of characteristic rheological parameters in Portland cement pastes. *Construction and Building Materials*, 51: 484-491.

Peray, K.E. 1979. *Cement Manufacturer's Handbook*. New York: Chemical Publishing Co., Inc.

Petit, J.-Y., Khayat, K.H. & Wirquin, E. 2006. Coupled effect of time and temperature on variations of yield value of highly flowable mortar. *Cement and concrete research*, 36(5): 832-841.

Potgieter, J.H. 2012. An Overview of Cement production: How "green" and sustainable is the industry? *Environmental Management and Sustainable Development*, 1(2): 14-37.

Pourchet, S., Regnaud, L., Perez, J.P. & Nonat, A. 2009. Early C3A hydration in the presence of different kinds of calcium sulphate. *Cement and Concrete Research*, 39(11): 989-996.

Powers, T.C. 1958. Structure and physical properties of hardened Portland cement paste. *Journal of the American Ceramic Society*, 41(1): 1-6.

Prince, W., Espagne, M. & Aïtcin, P.-C. 2003. Ettringite formation: A crucial step in cement superplasticizer compatibility. *Cement and Concrete Research*, 33(5): 635-641.

Prosen, E.J., Brown, P.W., Frohnsdorff, G. & Davis, F. 1985. A multichambered microcalorimeter for the investigation of cement hydration. *Cement and Concrete Research*, 15: 703-710.

Quennoz, A. 2011. *Hydration of C3A with Calcium Sulfate Alone and in the Presence of Calcium Silicate*. Doctoral thesis. Ecole Polytechnique Federale de Lausanne.

Quennoz, A. & Scrivener, K.L. 2012. Hydration of C3A–gypsum systems. *Cement and Concrete Research*, 42(7): 1032-1041.

Quennoz, A. & Scrivener, K.L. 2013. Interactions between alite and C3A-gypsum hydrations in model cements. *Cement and Concrete Research*, 44: 46-54.

Radwan, M.M. & Heikal, M. 2005. Hydration characteristics of tricalcium aluminate phase in mixes containing β-hemihydate and phosphogypsum. *Cement and Concrete Research*, 35(8): 1601-1608.

Rahimi-Aghdam, S., Bažant, Z.P. & Abdolhosseini Qomi, M.J. 2017. Cement hydration from hours to centuries controlled by diffusion through barrier shells of C-S-H. *Journal of the Mechanics and Physics of Solids*, 99: 211-224.

Reid, H. 1877. *The science and art of the manufacture of Portland cement*. London: ICE Publishing.

Rheometric Scientific Inc. 2003. *Rheometrics series user manual.*

Richardson, I. 2000. The nature of the hydration products in hardened cement pastes. *Cement and Concrete Composites*, 22: 97-173.

Roller, P.S. 1934. The Setting of Portland Cement. *Industrial and Engineering Chemistry*, 26(6): 669-677.

Rossen, J.E., Lothenbach, B. & Scrivener, K.L. 2015. Composition of C-S-H in pastes with increasing levels of silica fume addition. *Cement and Concrete Research*, 75: 14-22.

Roussel, N. 2007. A Theoretical Frame to Study Stability of Fresh Concrete. *Materials and Structures*, 39(1): 81-91.

Roussel, N., Lemaître, A., Flatt, R.J. & Coussot, P. 2010. Steady state flow of cement suspensions: A micromechanical state of the art. *Cement and Concrete Research*, 40(1): 77-84.

Roussel, N., Ovarlez, G., Garrault, S. & Brumaud, C. 2012. The origins of thixotropy of fresh cement pastes. *Cement and Concrete Research*, 42(1): 148-157.

Salah, B. *Portland cement.*

Salas, D.A., Ramirez, A.D., Rodríguez, C.R., Petroche, D.M., Boero, A.J. & Duque-Rivera, J. 2016. Environmental impacts, life cycle assessment and potential improvement measures for cement production: a literature review. *Journal of Cleaner Production*, 113: 114-122.

Saleh Ahari, R., Erdem, T.K. & Ramyar, K. 2015. Time-dependent rheological characteristics of self-consolidating concrete containing various mineral admixtures. *Construction and Building Materials*, 88: 134-142.

Salvador, R.P., Cavalaro, S.H.P., Cincotto, M.A. & Figueiredo, A.D. de. 2016. Parameters controlling early age hydration of cement pastes containing accelerators for sprayed concrete. *Cement and Concrete Research*, 89: 230-248.

Schöler, A., Lothenbach, B., Winnefeld, F., Haha, M.B., Zajac, M. & Ludwig, H.-M. 2017. Early hydration of SCM-blended Portland cements: A pore solution and isothermal calorimetry study. *Cement and Concrete Research*, 93: 71-82.

Scholtzová, E., Kucková, L., Kožíšek, J. & Tunega, D. 2015. Structural and spectroscopic characterization of ettringite mineral–combined DFT and experimental study. *Journal of Molecular Structure*, 1100: 215-224.

Scrivener, K.L. 2004. Backscattered electron imaging of cementitious microstructures: understanding and quantification. *Cement and Concrete Composites*, 26(8): 935-945.

Scrivener, K.L., Juilland, P. & Monteiro, P.J.M. 2015. Advances in understanding hydration of Portland cement. *Cement and Concrete Research*, 78: 38-56.

Shafeek, A.M., Salah, H., Shehata, N. & Saddek, A.B. 2017. The impact of cooling water types on the cement clinker properties. *Egyptian Journal of Petroleum,* 27(3):277-284.

Shi, C., Zhang, G., He, T. & Li, Y. 2016. Effects of superplasticizers on the stability and morphology of ettringite. *Construction and Building Materials*, 112: 261-266.

Singh, M. 2000. Influence of blended gypsum on the properties of Portland cement and Portland slag cement. *Cement and concrete research*, 30(8): 1185-1188.

Singh, N.B. & Middendorf, B. 2007. Calcium sulphate hemihydrate hydration leading to gypsum crystallization. *Progress in Crystal Growth and Characterization of Materials*, 53(1): 57-77.

Smallwood, T.B. & Wall, C.D. 1981. The quantitative determination of hydrated calcium sulphates in cement by use of self-generating atmosphere thermogravimetry. *Talanta*, 28(4): 265-267.

Snellings, R., Salze, A. & Scrivener, K.L. 2014. Use of X-ray diffraction to quantify amorphous supplementary cementitious materials in anhydrous and hydrated blended cements. *Cement and Concrete Research*, 64: 89-98.

Stafford, F.N., Viquez, M.D., Labrincha, J. & Hotza, D. 2015. Advances and Challenges for the Co-processing in Latin American Cement Industry. *Procedia Materials Science*, 9: 571-577.

Struble, L.J. & Lei, W.-G. 1995. Rheological changes associated with setting of cement paste. *Advanced Cement Based Materials*, 2(6): 224-230.

Strydom, C.A. & Potgieter, J.H. 1999. Dehydration behaviour of a natural gypsum and a phosphogypsum during milling. *Thermochimica acta*, 332(1): 89-96.

Stutzman, P. 2004. Scanning electron microscopy imaging of hydraulic cement microstructure. *Cement and Concrete Composites*, 26(8): 957-966.

Sujata, K. & Jennings, H.M. 1992. Formation of a protective layer during the hydration of cement. *Journal of the American Ceramic Society*, 75(6): 1669-1673.

Sun, Z., Voigt, T. & Shah, S.P. 2006. Rheometric and ultrasonic investigations of viscoelastic properties of fresh Portland cement pastes. *Cement and Concrete Research*, 36(2): 278-287.

Svinning, K., Høskuldsson, A. & Justnes, H. 2008. Prediction of compressive strength up to 28days from microstructure of Portland cement. *Cement and Concrete Composites*, 30(2): 138-151.

Tamás, F.D., Farkas, E., Vörös, M. & Roy, D.M. 1987. Low-frequency electrical conductivity of cement, clinker and clinker mineral pastes. *Cement and Concrete Research*, 17(2): 340-348.

Tattersall, G.H. & Banfill, P.F.G. 1983. *Rheology of Fresh Concrete*. london: Pitman Advanced Publishing Program.

Taylor, H.F.W. 2003. *Cement chemistry*. 2. ed., repr. London: Telford Publ.

Tennis, P.D. & Jennings, H.M. 2000. A model for two types of calcium silicate hydrate in the microstructure of Portland cement pastes. *Cement and Concrete Research*, 30(6): 855-863.

The Cement Grinding Office. 2016. cement mill heat balance.

Thomas, J.J. & Jennings, H.M. 2006. A colloidal interpretation of chemical aging of the C-S-H gel and its effects on the properties of cement paste. *Cement and Concrete Research*, 36(1): 30-38.

Thongsanitgarn, P., Wongkeo, W., Chaipanich, A. & Poon, C.S. 2014. Heat of hydration of Portland high-calcium fly ash cement incorporating limestone powder: Effect of limestone particle size. *Construction and Building Materials*, 66: 410-417.

Thurston, A. 1938. Parker's 'Roman' Cement. *Transactions of the Newcomen Society*, 19(1): 193-206.

Topçu, İ.B., Uygunoğlu, T. & Hocaoğlu, İ. 2012. Electrical conductivity of setting cement paste with different mineral admixtures. *Construction and Building Materials*, 28(1): 414-420.

Toutou, Z. & Roussel, N. 2007. Multi Scale Experimental Study of Concrete Rheology: From Water Scale to Gravel Scale. *Materials and Structures*, 39(2): 189-199.

Trapote-Barreira, A., Cama, J. & Soler, J.M. 2014. Dissolution kinetics of C-S-H gel: Flow-through experiments. *Physics and Chemistry of the Earth, Parts A/B/C*, 70-71: 17-31.

Tzouvalas, G., Dermatas, N. & Tsimas, S. 2004. Alternative calcium sulphate-bearing materials as cement retarders: part I. Anhydrite. *Cement and concrete research*, 34(11): 2113-2118.

Tzouvalas, G., Rantis, G. & Tsimas, S. 2004. Alternative calcium-sulphate-bearing materials as cement retarders: Part II. FGD gypsum. *Cement and Concrete Research*, 34(11): 2119-2125.

UNIDO & MITI. 1994. cement industry.

Vargas, J. & Halog, A. 2015. Effective carbon emission reductions from using upgraded fly ash in the cement industry. *Journal of Cleaner Production*, 103: 948-959.

Vedalakshmi, R., Raj, A.S., Srinivasan, S. & Babu, K.G. 2003. Quantification of hydrated cement products of blended cements in low and medium strength concrete using TG and DTA technique. *Thermochimica Acta*, 407(1): 49-60.

Vikan, H., Justnes, H., Winnefeld, F. & Figi, R. 2007. Correlating cement characteristics with rheology of paste. *Cement and Concrete Research*, 37(11): 1502-1511.

Wallevik, O.H. & Wallevik, J.E. 2011. Rheology as a tool in concrete science: The use of rheographs and workability boxes. *Cement and Concrete Research*, 41(12): 1279-1288.

Wang, Y., Zhu, B., Li, X. & Chen, P. 2016. Effect of dispersants on the hydrate morphologies of spinel-containing calcium aluminate cement and on the properties of refractory castables. *Ceramics International*, 42(1, Part A): 711-720.

Whorlow, R.. 1992. *Rheological techniques*. 2nd, Illustrated ed. University of Michigan: Ellis Horwood Limited.

Xu, L., Wang, P. & Zhang, G. 2012. Formation of ettringite in Portland cement/calcium aluminate cement/calcium sulphate ternary system hydrates at lower temperatures. *Construction and Building Materials*, 31: 347-352.

Yu, Q.L. & Brouwers, H.J.H. 2011. Microstructure and mechanical properties of β-hemihydrate produced gypsum: An insight from its hydration process. *Construction and Building Materials*, 25(7): 3149-3157.

Zhang, H., Zhongsou, L. & Tong, D. 1996. Influence of the type of calcium sulphate on the strenght and hydration of Portland cement under initial steam-curing condition. *Cement and Concrete Research*, 26(10): 1505-1511.

Zhang, M.-H., Sisomphon, K., Ng, T.S. & Sun, D.J. 2010. Effect of superplasticizers on workability retention and initial setting time of cement pastes. *Construction and Building Materials*, 24(9): 1700-1707.

Zhang, S., Xu, X., Memon, S.A., Dong, Z., Li, D. & Cui, H. 2018. Effect of calcium sulphate type and dosage on properties of calcium aluminate cement-based self-leveling mortar. *Construction and Building Materials*, 167: 253-262.

Zhou, P., Wu, H. & Xia, Y. 2016. Influence of synthetic polymers on the mechanical properties of hardened β-calcium sulphate hemihydrate plasters. *Journal of Industrial and Engineering Chemistry*, 33: 355-361.

Zhou, Z., Solomon, M.J., Scales, P.J. & Boger, D.V. 1999. The yield stress of concentrated flocculated suspensions of size distributed particles. *Journal of Rheology*, 43(3): 651-671.

Zukoski, C.F. 1995. Particles and suspensions in chemical engineering: accomplishments and prospects. *Chemical Engineering Science*, 50(24): 4073-4079.

Appendices

Appendix A. Heat flow rate profiles

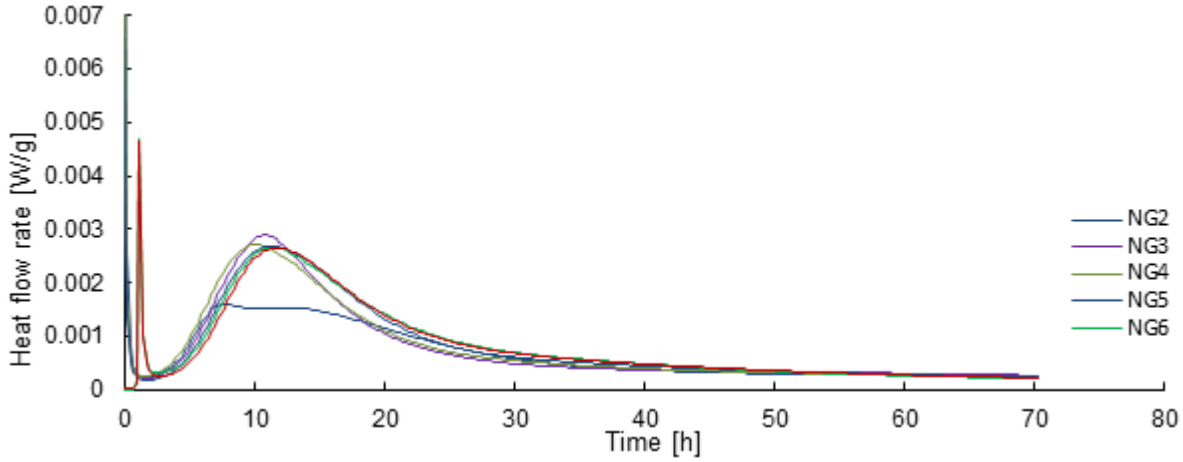

Figure A.1: Heat flow rate of cement paste with different concentrations of natural gypsum

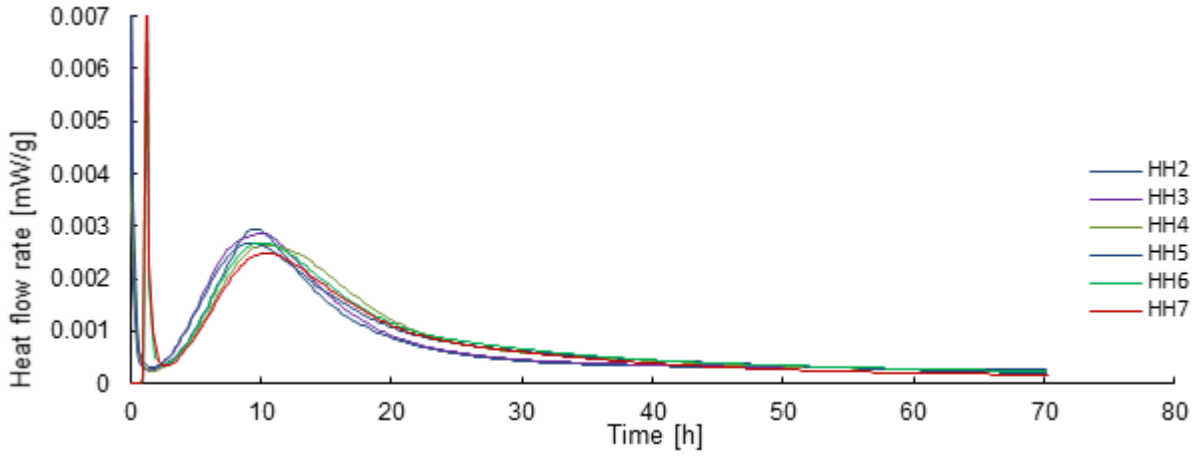

Figure A.2: Heat flow rate of cement paste with different concentrations of hemihydrate

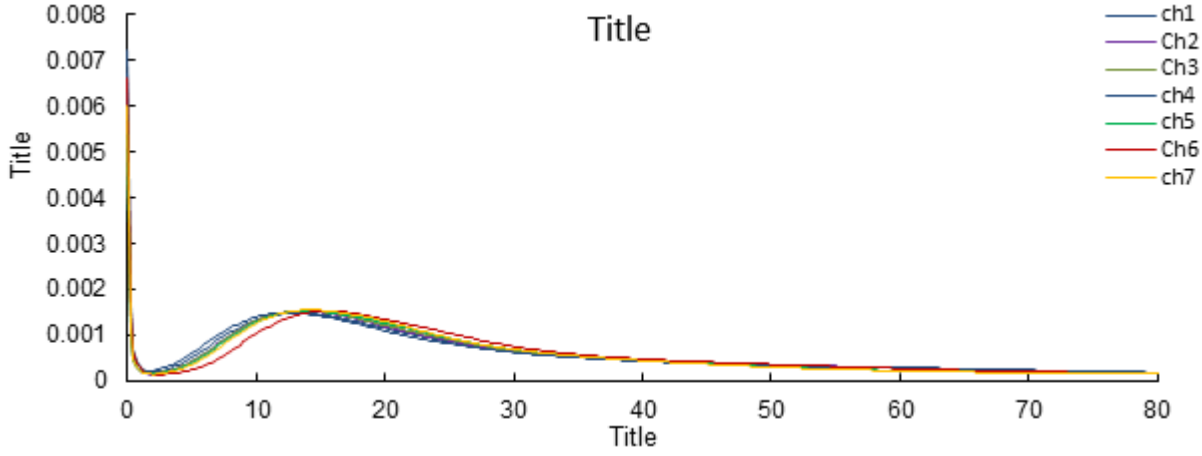

Figure A.3: Heat flow rate of cement paste with different proportions of natural gypsum and hemihydrate at 4% calcium sulphate cement phase

Appendix B. Reaction rate and total heat of reaction

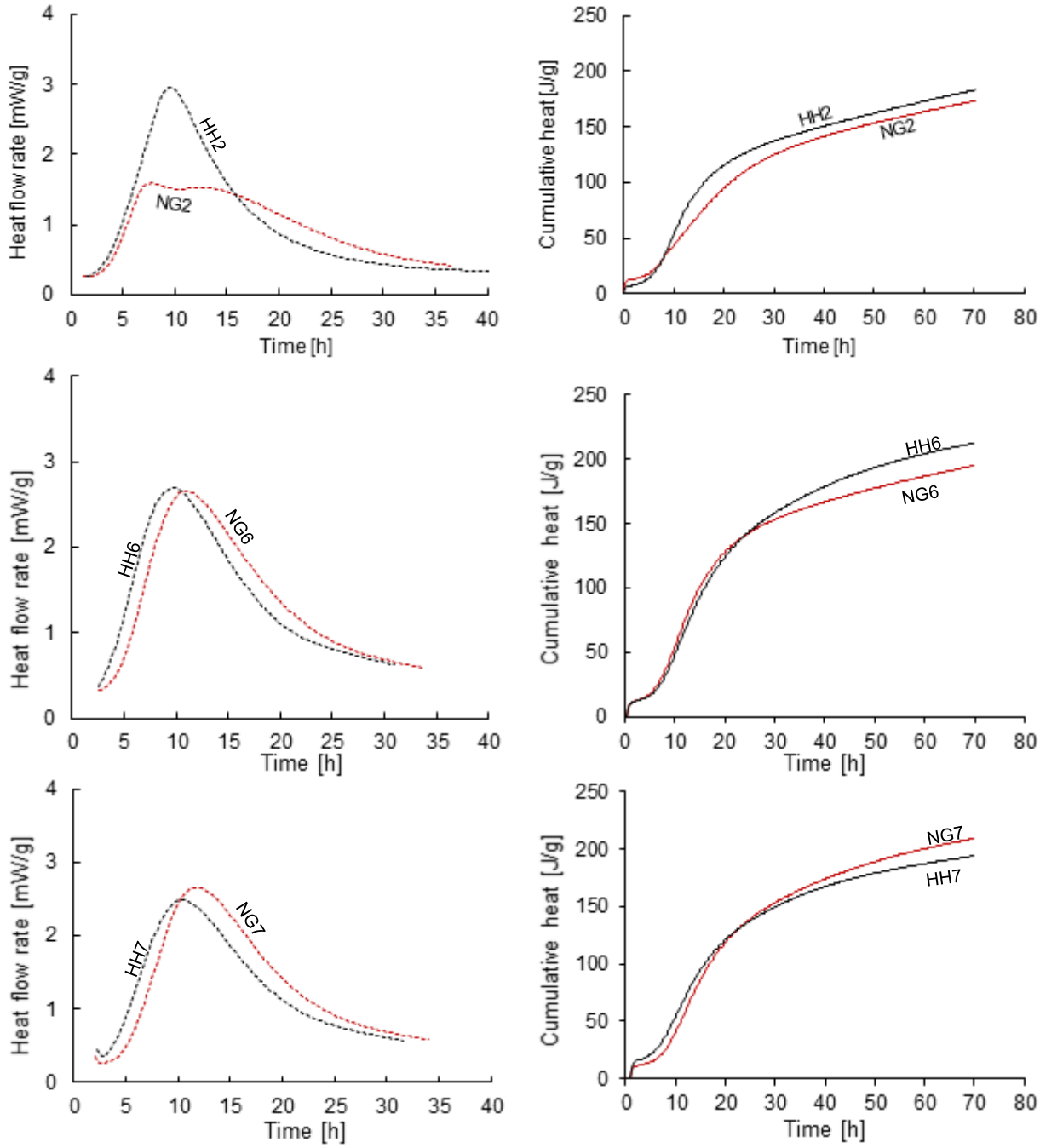

Figure B.1: Comparison of reaction rate and cumulative heat flow of cement with hemihydrate (HH) and natural gypsum (NG) at 2%, 6% and 7%

Appendix C. Thermogravimetric analysis and differential scanning calorimetric

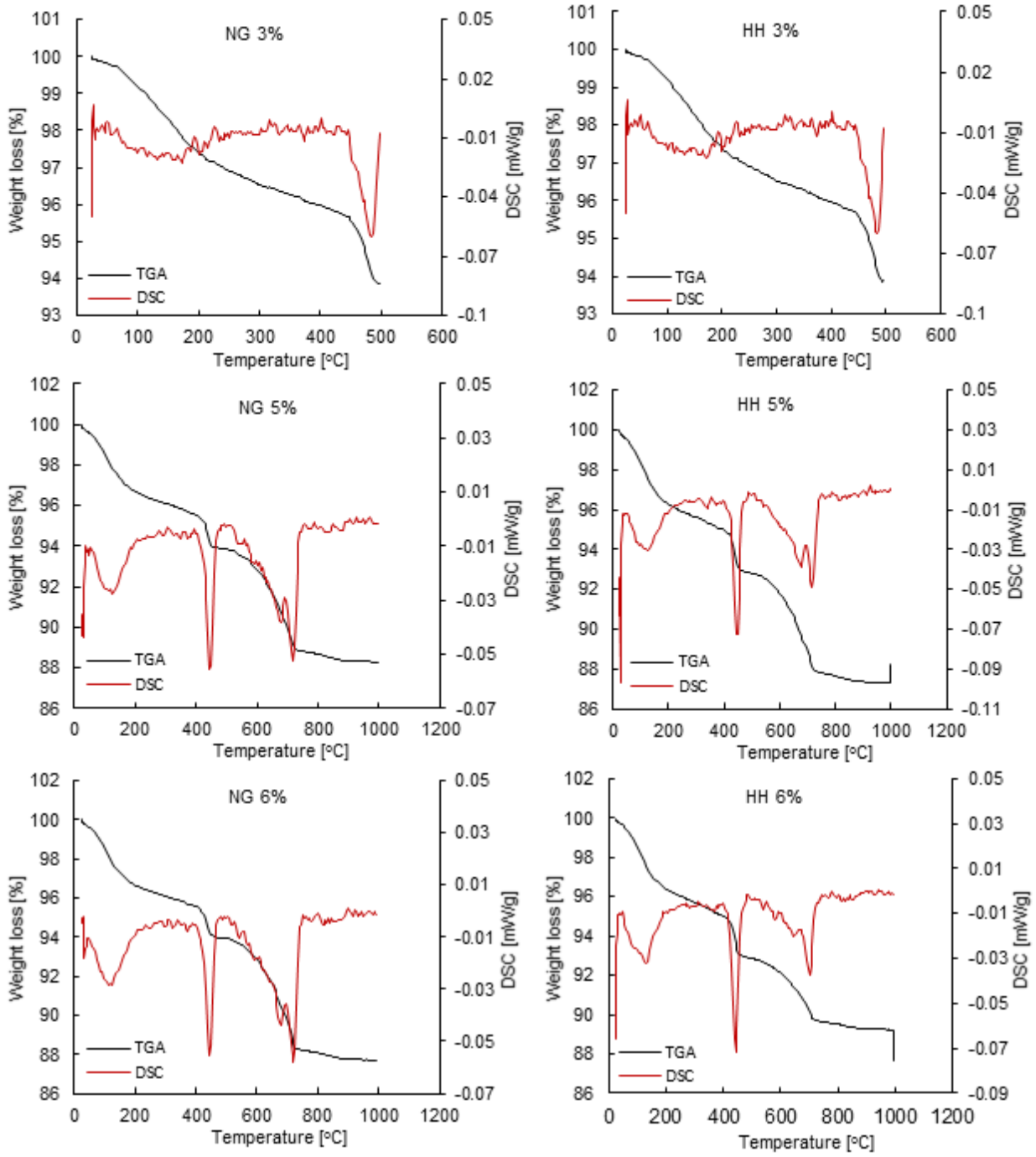

Figure C.1: Typical thermogravimetric analysis and differential scanning calorimetry profiles after calcium sulphate depletion within cement systems with hemihydrate (HH) and natural gypsum (NG) at 3%, 5% and 6%

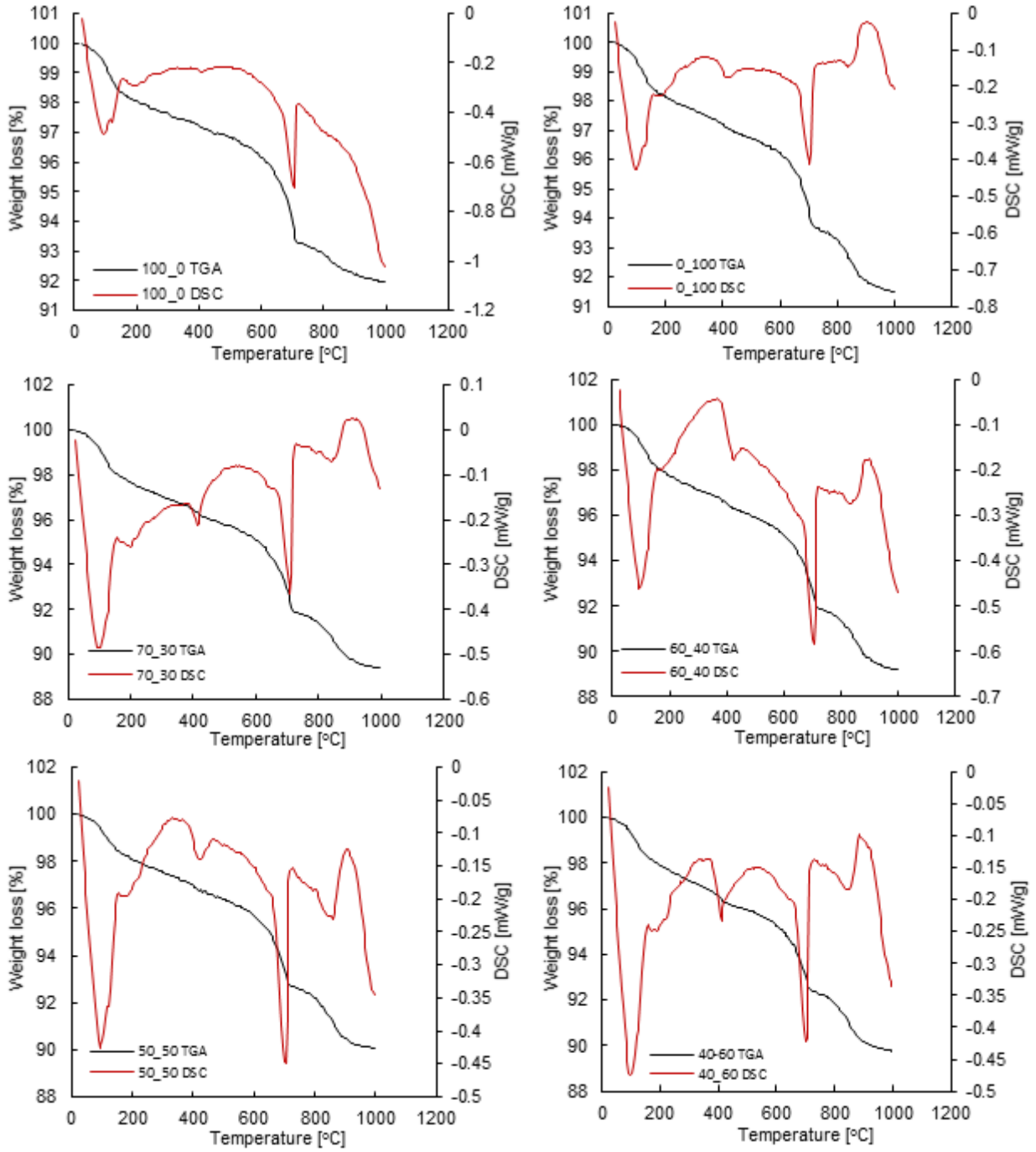

Figure C.2: Thermogravimetric analysis and differential scanning calorimetry profiles of 4 hours hydrated cement with different proportion of hemihydrate and natural gypsum within the calcium sulphate phase set at 4% concentration

Appendix D. Compressive strength readings of cement mortar

Table 6.1: 1 day compressive strength of cement mortar with natural gypsum and hemihydrate at different concentrations

		Mass [g]			Reading [MPa]						Average
	Dosage[%]	A	B	C	1	2	3	4	5	6	[MPa]
Hemihydrate	2	587.1	586.8	585.1	27.6	27.2	27.6	26.8	28.1	26.9	27.4
	3	588.6	588.8	587.9	22.8	22.4	22.3	23.1	24.7	24.5	28.1
	4	591.2	589.8	587.6	29.3	28.4	29.6	29.2	28.2	29.4	29.0
	5	593.9	601.3	600.1	27.3	26.9	27.6	27.7	28.2	28.1	27.6
	6	589.9	588	585.8	27.7	27.4	28.2	27.3	27.3	28.3	27.7
	7	589.5	593.9	594.4	24.8	24.9	25.2	24.3	25.6	23.3	24.7
Natural gypsum	Dosage[%]	Mass [g]			Reading [MPa]						Average
	2	591.3	592.3	589.7	22.1	22.1	21.2	22.1	21.8	21.6	21.8
	3	597.8	598	594.6	24.8	24.9	23.6	23.6	24.6	23.6	24.2
	4	5981.5	586.1	583.7	23	23.6	24	25.5	24.7	25.1	25.0
	5	582.4	584.8	588.5	25	24.4	25.4	24.4	24.7	25.8	24.3
	6	583.1	585.5	586.8	14.4	15.92	18.9	19.3	18.65	18.61	19.3
	7	588	585	586.5	17.81	18.11	17.9	19.4	18.75	19.4	18.6

Appendix E. Flow curves of cement pastes

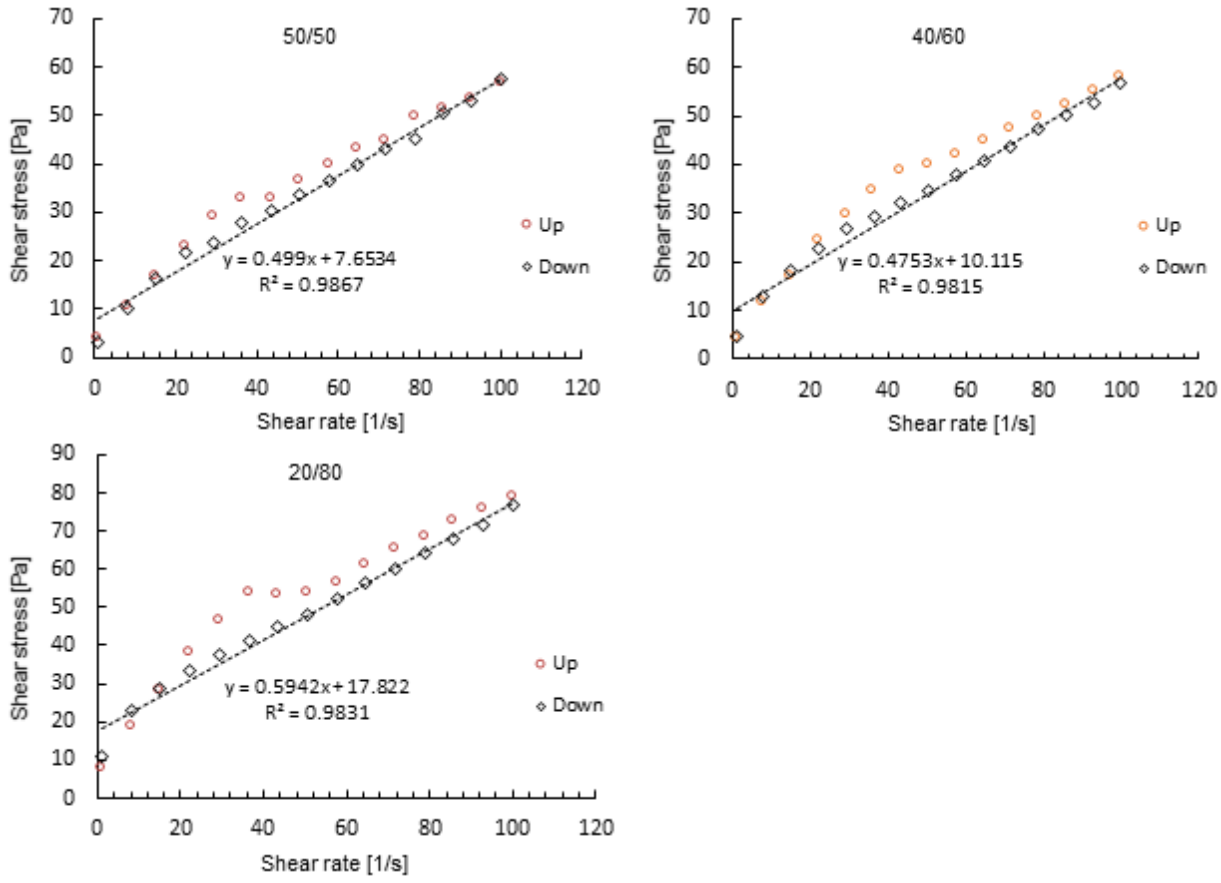

Figure E.1: Rheological parameters fitted by Bingham model of cement pastes with different natural and hemihydrate proportions within the calcium sulphate cement phase set at 4%

Appendix F. X-ray diffraction patterns of hydrated cement paste

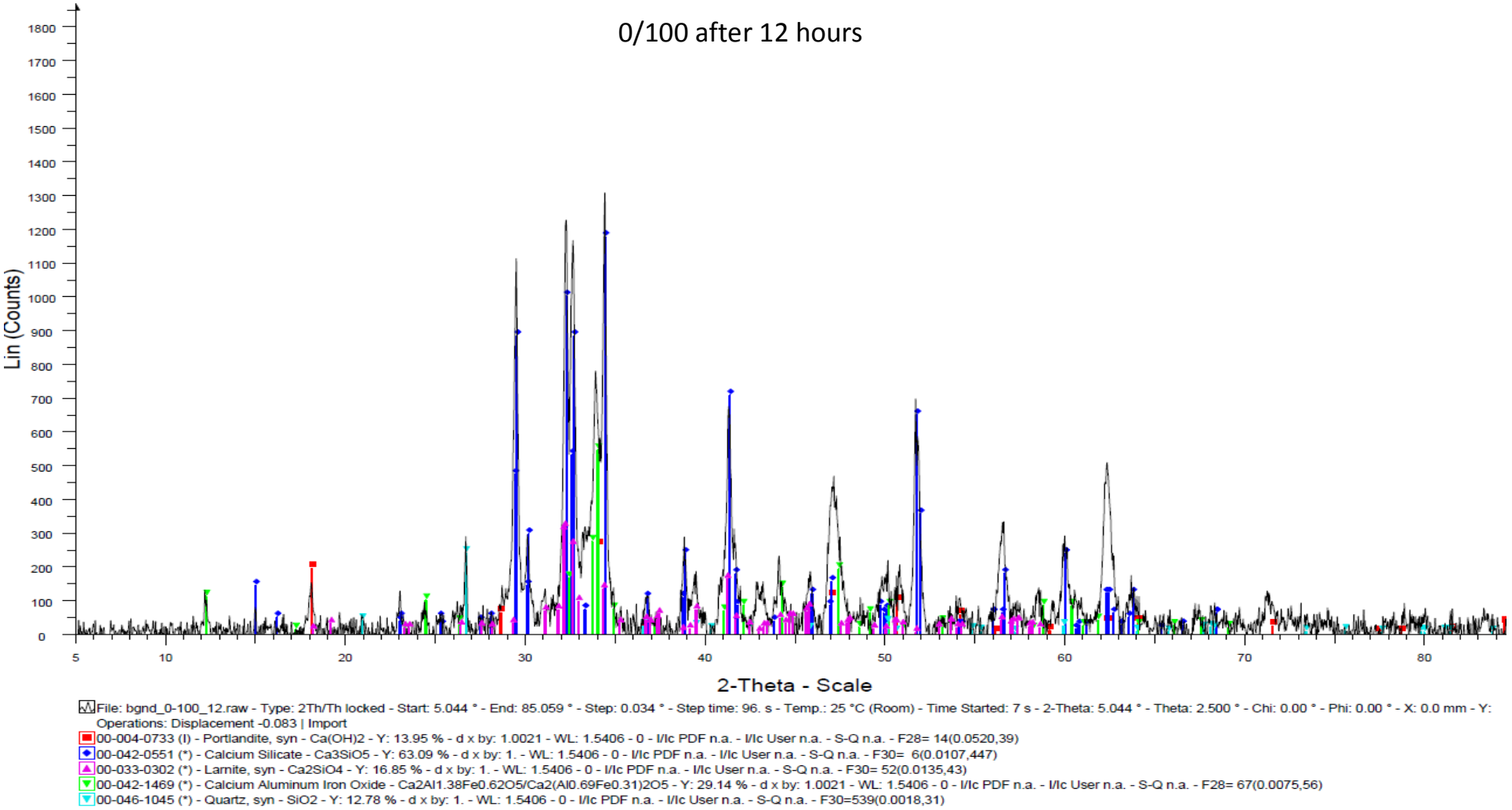

100/0 after 12 hours

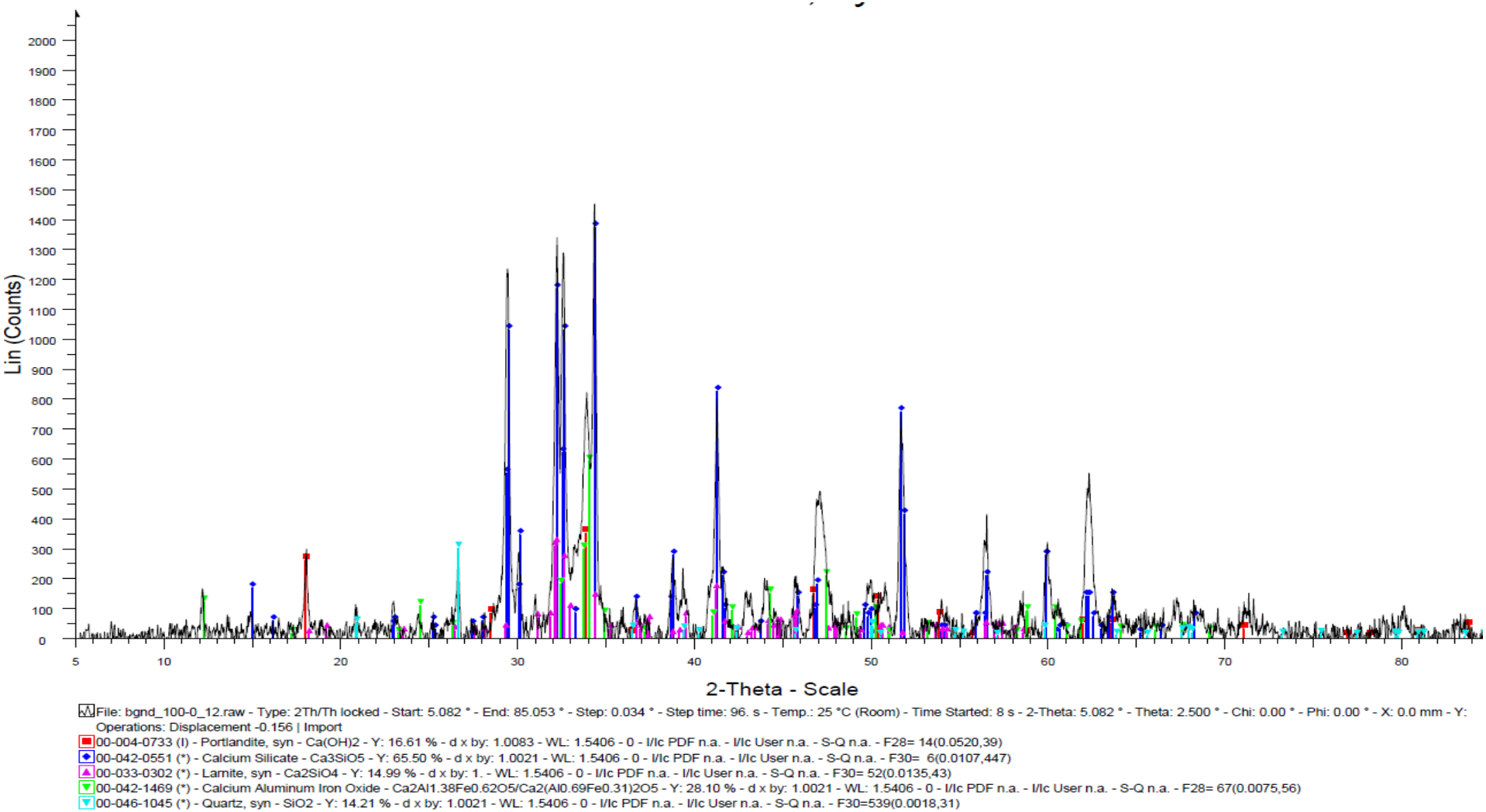

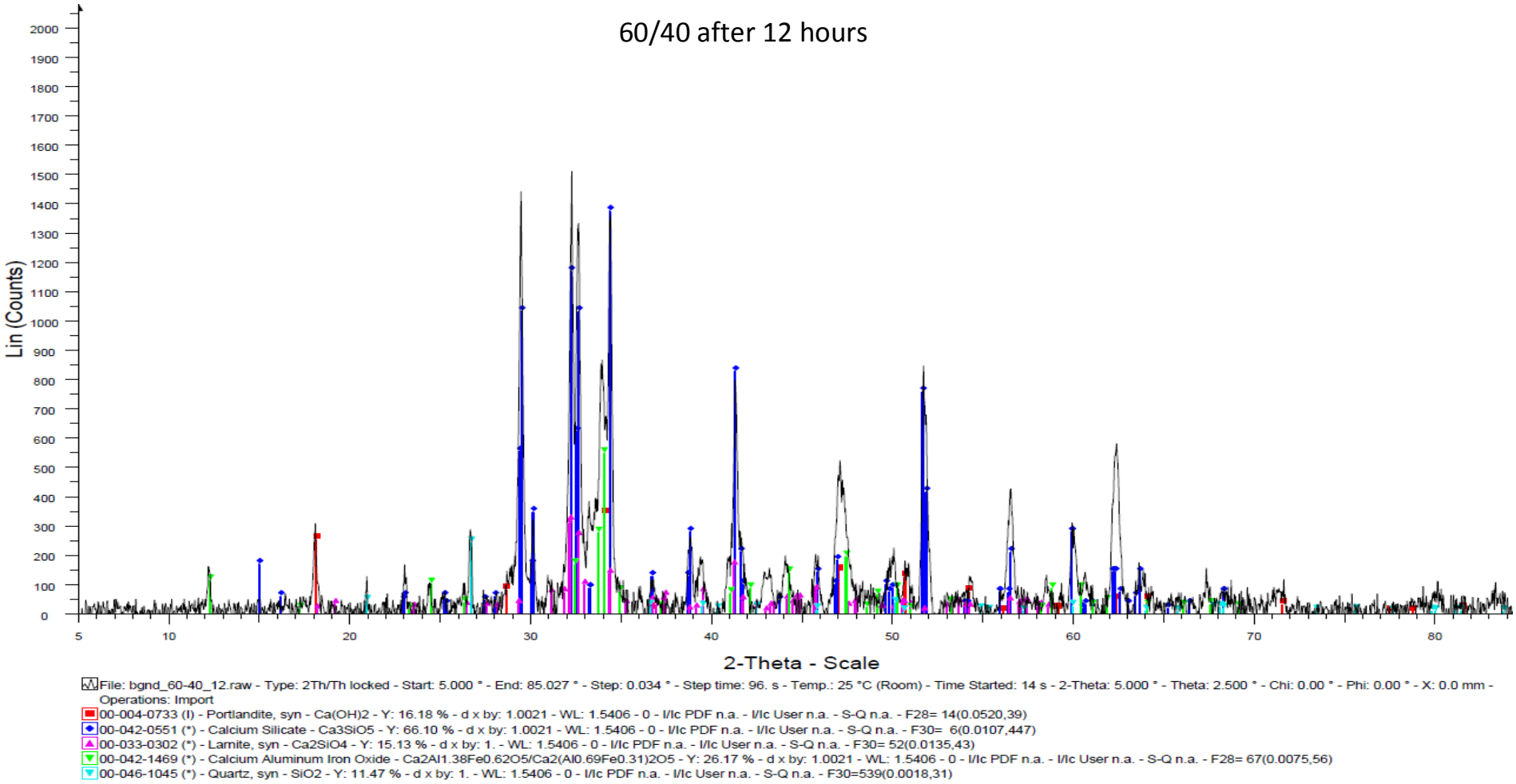
60/40 after 12 hours
Lin (Counts)
2-Theta - Scale
File: bgnd_60-40_12.raw - Type: 2Th/Th locked - Start: 5.000 ° - End: 85.027 ° - Step: 0.034 ° - Step time: 96. s - Temp.: 25 °C (Room) - Time Started: 14 s - 2-Theta: 5.000 ° - Theta: 2.500 ° - Chi: 0.00 ° - Phi: 0.00 ° - X: 0.0 mm - Operations: Import
00-004-0733 (I) - Portlandite, syn - Ca(OH)2 - Y: 16.18 % - d x by: 1.0021 - WL: 1.5406 - 0 - I/Ic PDF n.a. - I/Ic User n.a. - S-Q n.a. - F28= 14(0.0520,39)
00-042-0551 (*) - Calcium Silicate - Ca3SiO5 - Y: 66.10 % - d x by: 1.0021 - WL: 1.5406 - 0 - I/Ic PDF n.a. - I/Ic User n.a. - S-Q n.a. - F30= 6(0.0107,447)
00-033-0302 (*) - Larnite, syn - Ca2SiO4 - Y: 15.13 % - d x by: 1. - WL: 1.5406 - 0 - I/Ic PDF n.a. - I/Ic User n.a. - S-Q n.a. - F30= 52(0.0135,43)
00-042-1469 (*) - Calcium Aluminum Iron Oxide - Ca2Al1.38Fe0.62O5/Ca2(Al0.69Fe0.31)2O5 - Y: 26.17 % - d x by: 1.0021 - WL: 1.5406 - 0 - I/Ic PDF n.a. - I/Ic User n.a. - S-Q n.a. - F28= 67(0.0075,56)
00-046-1045 (*) - Quartz, syn - SiO2 - Y: 11.47 % - d x by: 1. - WL: 1.5406 - 0 - I/Ic PDF n.a. - I/Ic User n.a. - S-Q n.a. - F30=539(0.0018,31)

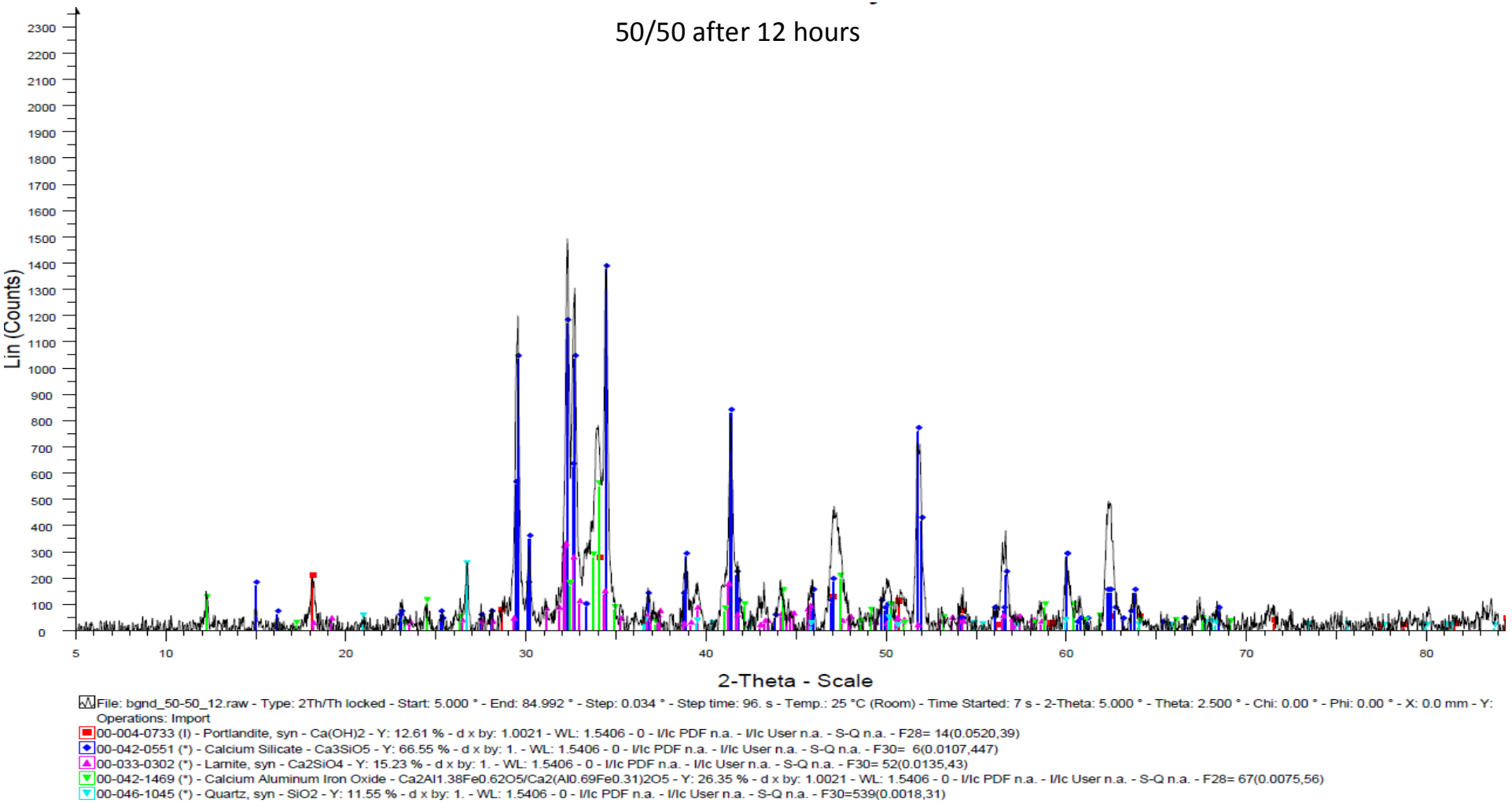
50/50 after 12 hours
Lin (Counts)
2-Theta - Scale
File: bgnd_50-50_12.raw - Type: 2Th/Th locked - Start: 5.000 ° - End: 84.992 ° - Step: 0.034 ° - Step time: 96. s - Temp.: 25 °C (Room) - Time Started: 7 s - 2-Theta: 5.000 ° - Theta: 2.500 ° - Chi: 0.00 ° - Phi: 0.00 ° - X: 0.0 mm - Y:
Operations: Import
00-004-0733 (I) - Portlandite, syn - Ca(OH)2 - Y: 12.61 % - d x by: 1.0021 - WL: 1.5406 - 0 - I/Ic PDF n.a. - I/Ic User n.a. - S-Q n.a. - F28= 14(0.0520,39)
00-042-0551 (*) - Calcium Silicate - Ca3SiO5 - Y: 66.55 % - d x by: 1. - WL: 1.5406 - 0 - I/Ic PDF n.a. - I/Ic User n.a. - S-Q n.a. - F30= 6(0.0107,447)
00-033-0302 (*) - Larnite, syn - Ca2SiO4 - Y: 15.23 % - d x by: 1. - WL: 1.5406 - 0 - I/Ic PDF n.a. - I/Ic User n.a. - S-Q n.a. - F30= 52(0.0135,43)
00-042-1469 (*) - Calcium Aluminum Iron Oxide - Ca2Al1.38Fe0.62O5/Ca2(Al0.69Fe0.31)2O5 - Y: 26.35 % - d x by: 1.0021 - WL: 1.5406 - 0 - I/Ic PDF n.a. - I/Ic User n.a. - S-Q n.a. - F28= 67(0.0075,56)
00-046-1045 (*) - Quartz, syn - SiO2 - Y: 11.55 % - d x by: 1. - WL: 1.5406 - 0 - I/Ic PDF n.a. - I/Ic User n.a. - S-Q n.a. - F30=539(0.0018,31)

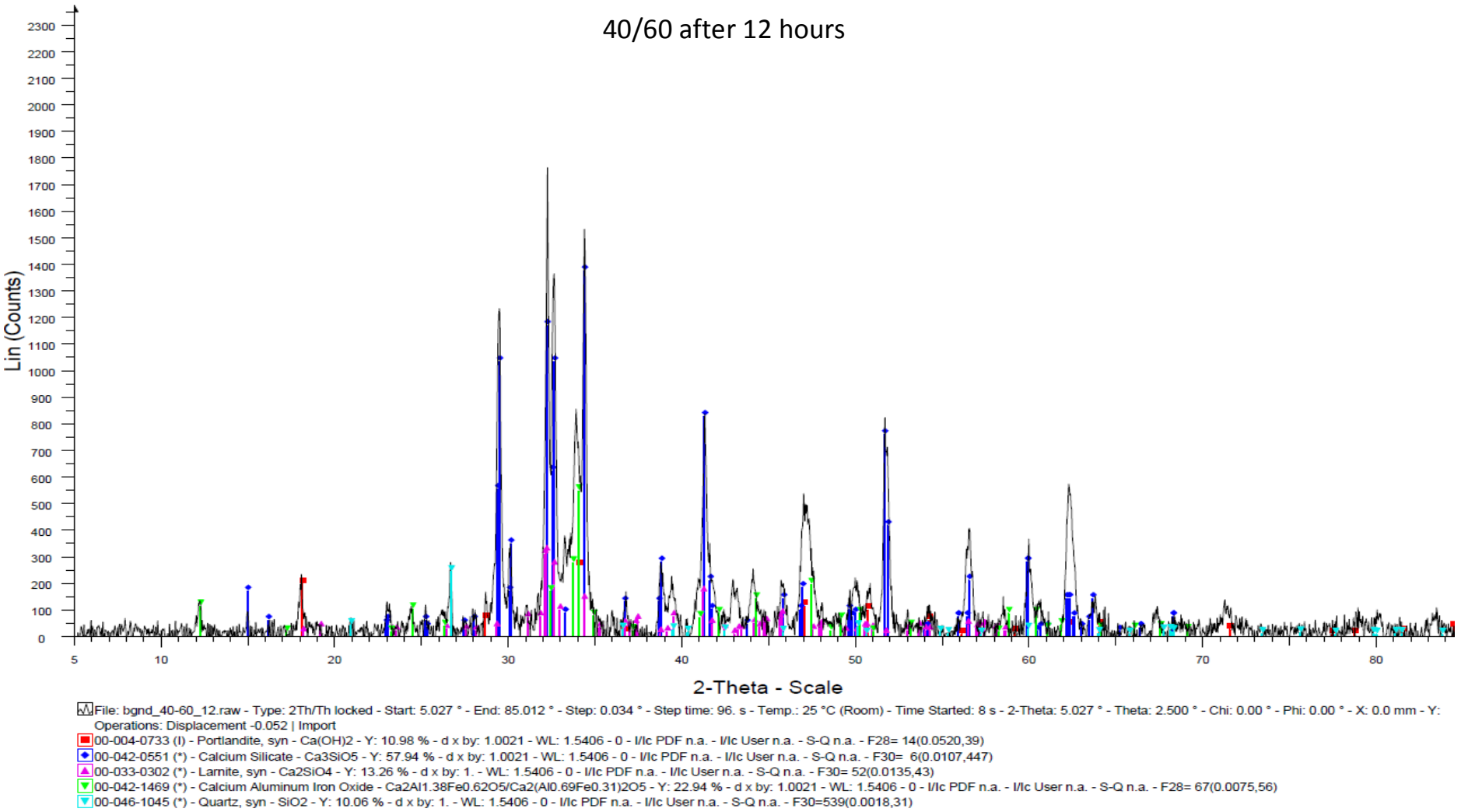
40/60 after 12 hours
Lin (Counts)
2-Theta - Scale
File: bgnd_40-60_12.raw - Type: 2Th/Th locked - Start: 5.027 ° - End: 85.012 ° - Step: 0.034 ° - Step time: 96. s - Temp.: 25 °C (Room) - Time Started: 8 s - 2-Theta: 5.027 ° - Theta: 2.500 ° - Chi: 0.00 ° - Phi: 0.00 ° - X: 0.0 mm - Y:
Operations: Displacement -0.052 | Import
00-004-0733 (I) - Portlandite, syn - Ca(OH)2 - Y: 10.98 % - d x by: 1.0021 - WL: 1.5406 - 0 - I/Ic PDF n.a. - I/Ic User n.a. - S-Q n.a. - F28= 14(0.0520,39)
00-042-0551 (*) - Calcium Silicate - Ca3SiO5 - Y: 57.94 % - d x by: 1.0021 - WL: 1.5406 - 0 - I/Ic PDF n.a. - I/Ic User n.a. - S-Q n.a. - F30= 6(0.0107,447)
00-033-0302 (*) - Larnite, syn - Ca2SiO4 - Y: 13.26 % - d x by: 1. - WL: 1.5406 - 0 - I/Ic PDF n.a. - I/Ic User n.a. - S-Q n.a. - F30= 52(0.0135,43)
00-042-1469 (*) - Calcium Aluminum Iron Oxide - Ca2Al1.38Fe0.62O5/Ca2(Al0.69Fe0.31)2O5 - Y: 22.94 % - d x by: 1.0021 - WL: 1.5406 - 0 - I/Ic PDF n.a. - I/Ic User n.a. - S-Q n.a. - F28= 67(0.0075,56)
00-046-1045 (*) - Quartz, syn - SiO2 - Y: 10.06 % - d x by: 1. - WL: 1.5406 - 0 - I/Ic PDF n.a. - I/Ic User n.a. - S-Q n.a. - F30=539(0.0018,31)

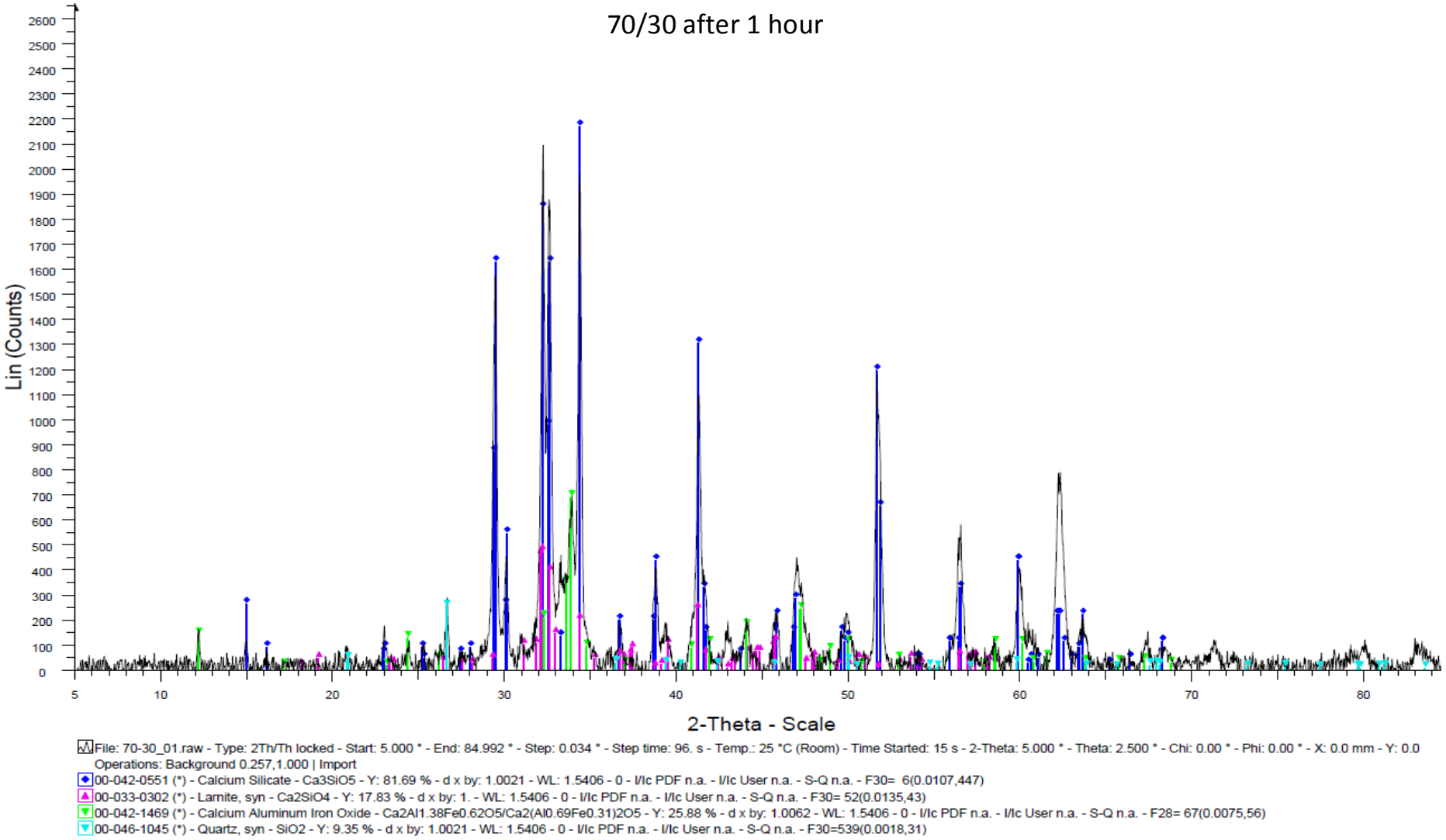
70/30 after 1 hour
Lin (Counts)
2-Theta - Scale
File: 70-30_01.raw - Type: 2Th/Th locked - Start: 5.000 ° - End: 84.992 ° - Step: 0.034 ° - Step time: 96. s - Temp.: 25 °C (Room) - Time Started: 15 s - 2-Theta: 5.000 ° - Theta: 2.500 ° - Chi: 0.00 ° - Phi: 0.00 ° - X: 0.0 mm - Y: 0.0
Operations: Background 0.257,1.000 | Import
00-042-0551 (*) - Calcium Silicate - Ca3SiO5 - Y: 81.69 % - d x by: 1.0021 - WL: 1.5406 - 0 - I/Ic PDF n.a. - I/Ic User n.a. - S-Q n.a. - F30= 6(0.0107,447)
00-033-0302 (*) - Larnite, syn - Ca2SiO4 - Y: 17.83 % - d x by: 1. - WL: 1.5406 - 0 - I/Ic PDF n.a. - I/Ic User n.a. - S-Q n.a. - F30= 52(0.0135,43)
00-042-1469 (*) - Calcium Aluminum Iron Oxide - Ca2Al1.38Fe0.62O5/Ca2(Al0.69Fe0.31)2O5 - Y: 25.88 % - d x by: 1.0062 - WL: 1.5406 - 0 - I/Ic PDF n.a. - I/Ic User n.a. - S-Q n.a. - F28= 67(0.0075,56)
00-046-1045 (*) - Quartz, syn - SiO2 - Y: 9.35 % - d x by: 1.0021 - WL: 1.5406 - 0 - I/Ic PDF n.a. - I/Ic User n.a. - S-Q n.a. - F30=539(0.0018,31)

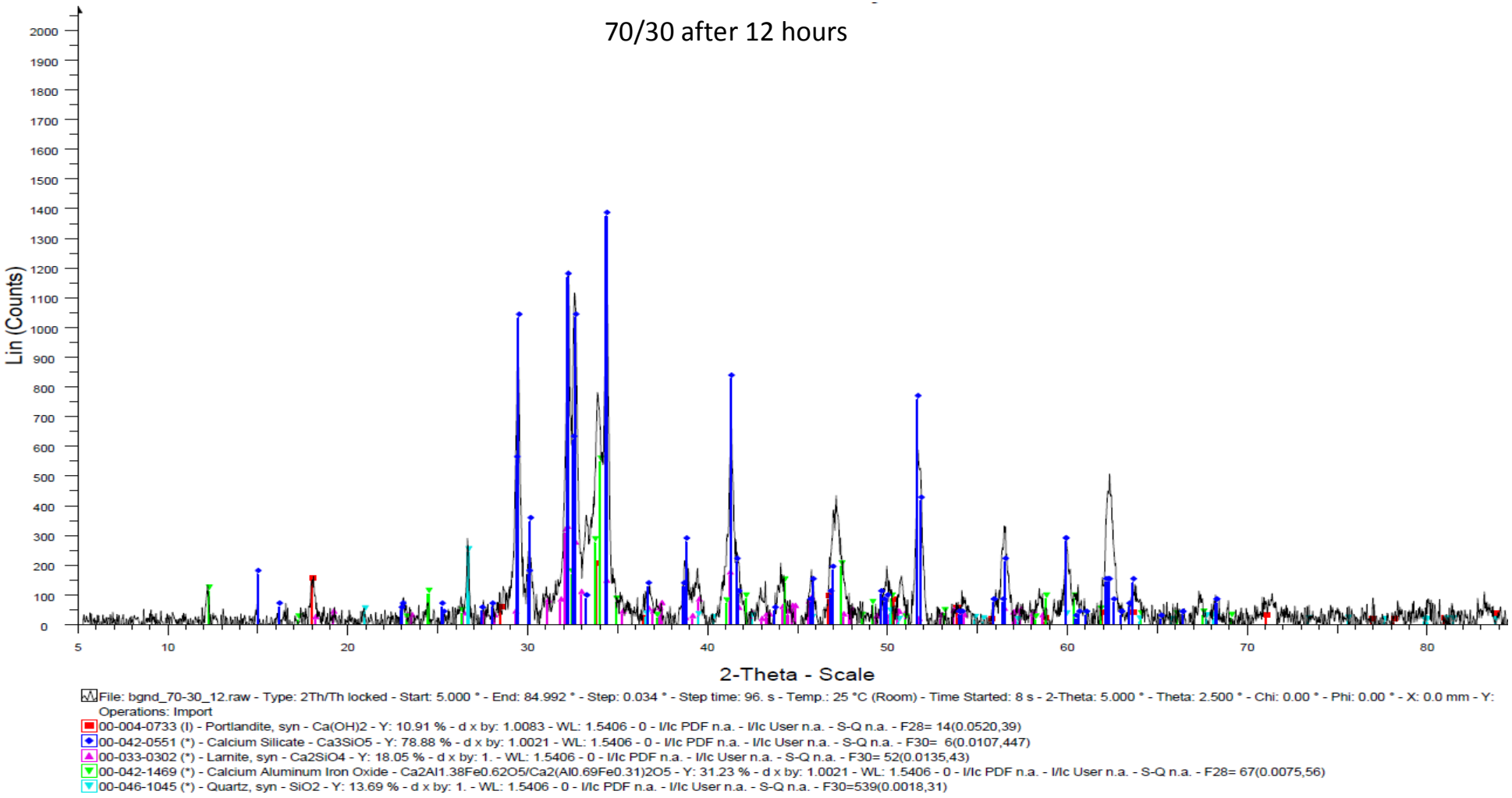
70/30 after 12 hours
Lin (Counts)
2-Theta - Scale
File: bgnd_70-30_12.raw - Type: 2Th/Th locked - Start: 5.000 ° - End: 84.992 ° - Step: 0.034 ° - Step time: 96. s - Temp.: 25 °C (Room) - Time Started: 8 s - 2-Theta: 5.000 ° - Theta: 2.500 ° - Chi: 0.00 ° - Phi: 0.00 ° - X: 0.0 mm - Y:
Operations: Import
00-004-0733 (I) - Portlandite, syn - Ca(OH)2 - Y: 10.91 % - d x by: 1.0083 - WL: 1.5406 - 0 - I/Ic PDF n.a. - I/Ic User n.a. - S-Q n.a. - F28= 14(0.0520,39)
00-042-0551 (*) - Calcium Silicate - Ca3SiO5 - Y: 78.88 % - d x by: 1.0021 - WL: 1.5406 - 0 - I/Ic PDF n.a. - I/Ic User n.a. - S-Q n.a. - F30= 6(0.0107,447)
00-033-0302 (*) - Larnite, syn - Ca2SiO4 - Y: 18.05 % - d x by: 1. - WL: 1.5406 - 0 - I/Ic PDF n.a. - I/Ic User n.a. - S-Q n.a. - F30= 52(0.0135,43)
00-042-1469 (*) - Calcium Aluminum Iron Oxide - Ca2Al1.38Fe0.62O5/Ca2(Al0.69Fe0.31)2O5 - Y: 31.23 % - d x by: 1.0021 - WL: 1.5406 - 0 - I/Ic PDF n.a. - I/Ic User n.a. - S-Q n.a. - F28= 67(0.0075,56)
00-046-1045 (*) - Quartz, syn - SiO2 - Y: 13.69 % - d x by: 1. - WL: 1.5406 - 0 - I/Ic PDF n.a. - I/Ic User n.a. - S-Q n.a. - F30=539(0.0018,31)

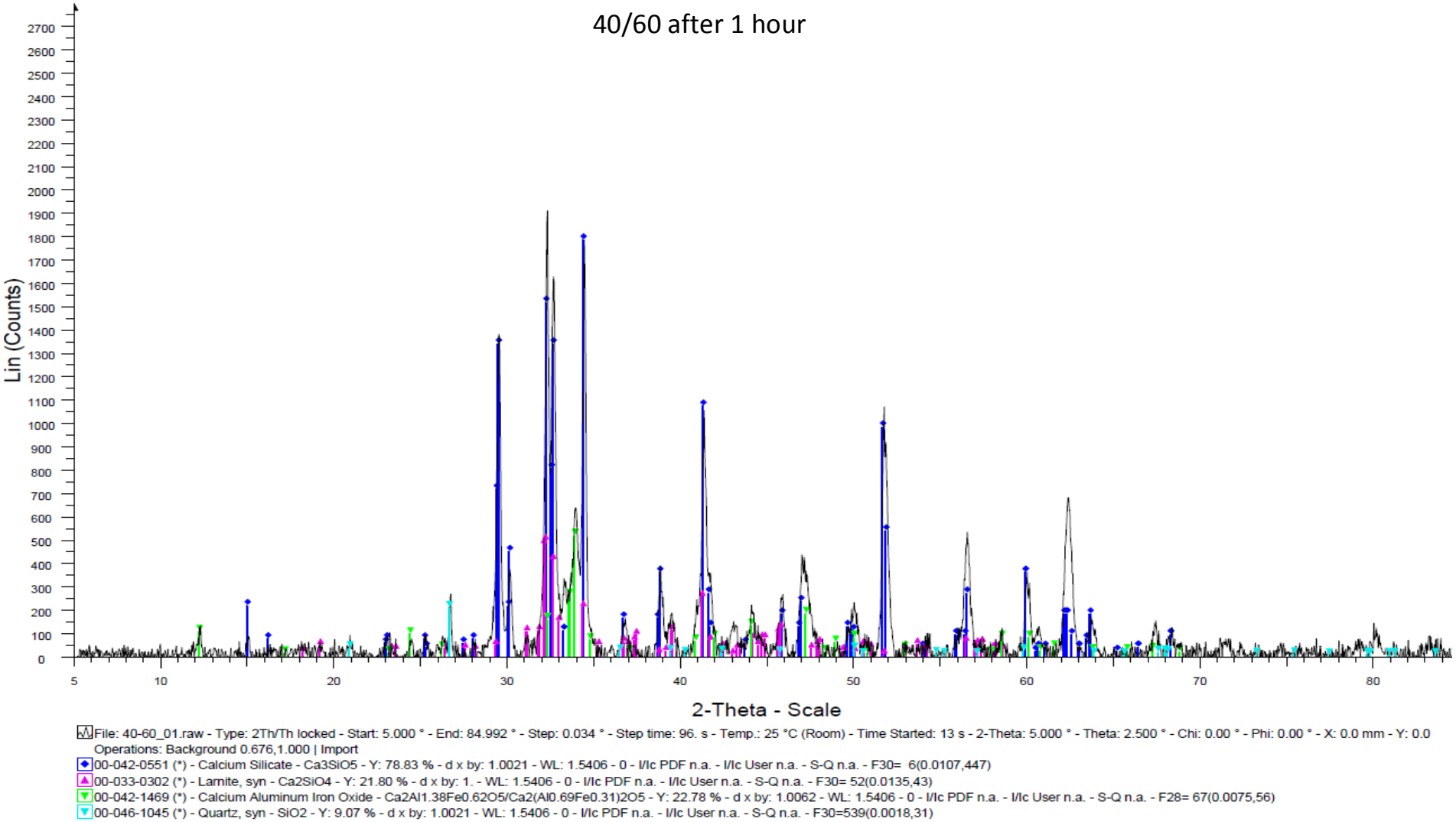
40/60 after 1 hour
Lin (Counts)
2-Theta - Scale
File: 40-60_01.raw - Type: 2Th/Th locked - Start: 5.000 ° - End: 84.992 ° - Step: 0.034 ° - Step time: 96. s - Temp.: 25 °C (Room) - Time Started: 13 s - 2-Theta: 5.000 ° - Theta: 2.500 ° - Chi: 0.00 ° - Phi: 0.00 ° - X: 0.0 mm - Y: 0.0
Operations: Background 0.676,1.000 | Import
00-042-0551 (*) - Calcium Silicate - Ca3SiO5 - Y: 78.83 % - d x by: 1.0021 - WL: 1.5406 - 0 - I/Ic PDF n.a. - I/Ic User n.a. - S-Q n.a. - F30= 6(0.0107,447)
00-033-0302 (*) - Larnite, syn - Ca2SiO4 - Y: 21.80 % - d x by: 1. - WL: 1.5406 - 0 - I/Ic PDF n.a. - I/Ic User n.a. - S-Q n.a. - F30= 52(0.0135,43)
00-042-1469 (*) - Calcium Aluminum Iron Oxide - Ca2Al1.38Fe0.62O5/Ca2(Al0.69Fe0.31)2O5 - Y: 22.78 % - d x by: 1.0062 - WL: 1.5406 - 0 - I/Ic PDF n.a. - I/Ic User n.a. - S-Q n.a. - F28= 67(0.0075,56)
00-046-1045 (*) - Quartz, syn - SiO2 - Y: 9.07 % - d x by: 1.0021 - WL: 1.5406 - 0 - I/Ic PDF n.a. - I/Ic User n.a. - S-Q n.a. - F30=539(0.0018,31)

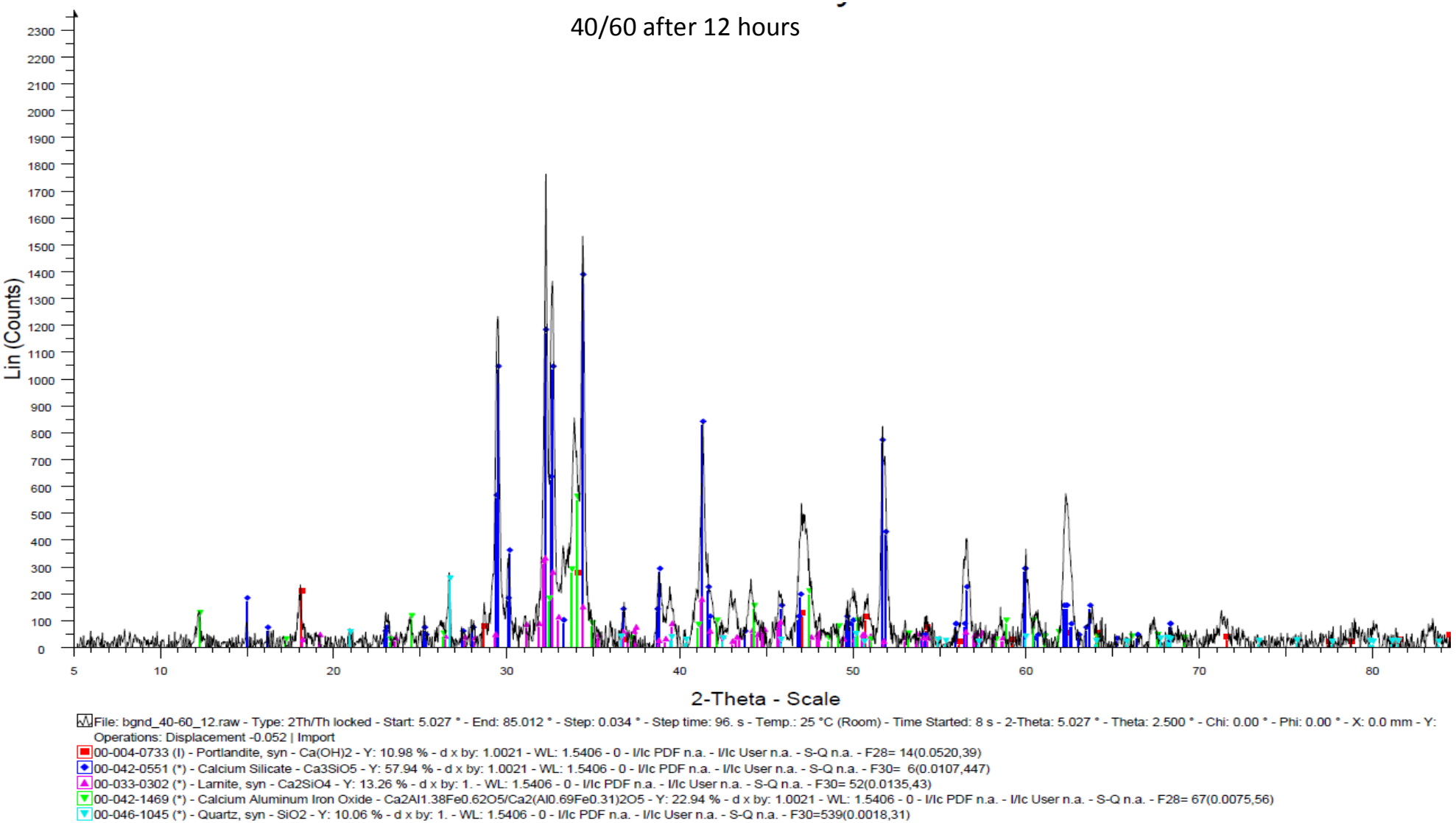
40/60 after 12 hours
Lin (Counts)
2-Theta - Scale
File: bgnd_40-60_12.raw - Type: 2Th/Th locked - Start: 5.027 ° - End: 85.012 ° - Step: 0.034 ° - Step time: 96. s - Temp.: 25 °C (Room) - Time Started: 8 s - 2-Theta: 5.027 ° - Theta: 2.500 ° - Chi: 0.00 ° - Phi: 0.00 ° - X: 0.0 mm - Y:
Operations: Displacement -0.052 | Import
00-004-0733 (I) - Portlandite, syn - Ca(OH)2 - Y: 10.98 % - d x by: 1.0021 - WL: 1.5406 - 0 - I/Ic PDF n.a. - I/Ic User n.a. - S-Q n.a. - F28= 14(0.0520,39)
00-042-0551 (*) - Calcium Silicate - Ca3SiO5 - Y: 57.94 % - d x by: 1.0021 - WL: 1.5406 - 0 - I/Ic PDF n.a. - I/Ic User n.a. - S-Q n.a. - F30= 6(0.0107,447)
00-033-0302 (*) - Larnite, syn - Ca2SiO4 - Y: 13.26 % - d x by: 1. - WL: 1.5406 - 0 - I/Ic PDF n.a. - I/Ic User n.a. - S-Q n.a. - F30= 52(0.0135,43)
00-042-1469 (*) - Calcium Aluminum Iron Oxide - Ca2Al1.38Fe0.62O5/Ca2(Al0.69Fe0.31)2O5 - Y: 22.94 % - d x by: 1.0021 - WL: 1.5406 - 0 - I/Ic PDF n.a. - I/Ic User n.a. - S-Q n.a. - F28= 67(0.0075,56)
00-046-1045 (*) - Quartz, syn - SiO2 - Y: 10.06 % - d x by: 1. - WL: 1.5406 - 0 - I/Ic PDF n.a. - I/Ic User n.a. - S-Q n.a. - F30=539(0.0018,31)